Linearized Saint-Venant Equations in Various Forms with Lateral Inflow in a Channel of Finite Length

by

Shiva Kandpal

DEPARTMENT OF MATHEMATICS

INDIAN INSTITUTE OF TECHNOLOGY GUWAHATI

GUWAHATI-781039, INDIA

April, 2024

Linearized Saint-Venant Equations in Various Forms with Lateral Inflow in a Channel of Finite Length

A Thesis submitted
in partial fulfillment of the requirements
for the degree of

DOCTOR OF PHILOSOPHY

by

Shiva Kandpal

(Roll No: 186123102)

DEPARTMENT OF MATHEMATICS

INDIAN INSTITUTE OF TECHNOLOGY GUWAHATI

GUWAHATI-781039, INDIA

April, 2024

Dedicated to

my mother Smt. Madhubala Kandpal

and

my father Shri Mohan Chandra Kandpal

Declaration

I do hereby declare that this thesis entitled **Linearized Saint-Venant Equations in Various Forms with Lateral Inflow in a Channel of Finite Length** is a presentation of my original research work done under the supervision of **Dr. Swaroop Nandan Bora**, Professor, Department of Mathematics, Indian Institute of Technology Guwahati for the award of the degree of Doctor of Philosophy and this work has not been submitted elsewhere for a degree.

April, 2024

Shiva Kandpal
Roll No. 186123102
Department of Mathematics
Indian Institute of Technology Guwahati

Certificate

It is to certify that the work contained in this thesis entitled **Linearized Saint-Venant Equations in Various Forms with Lateral Inflow in a Channel of Finite Length** has been carried out by **Shiva Kandpal**, a student in the Department of Mathematics, Indian Institute of Technology Guwahati, under my supervision for the award of the degree of Doctor of Philosophy and this work has not been submitted elsewhere for a degree.

April, 2024

Dr. Swaroop Nandan Bora
Professor
Department of Mathematics
Indian Institute of Technology Guwahati

Acknowledgements

I am deeply grateful to the individuals who have contributed to the completion of this thesis and helped me in this journey in their own ways. Their support, encouragement, and guidance have been instrumental in my academic achievements.

First and foremost, I express my deepest gratitude to my esteemed supervisor, Prof. Swaroop Nandan Bora, whose wisdom, patience, and unwavering support have been the cornerstone of this research. The trajectory of this thesis has been formed by his perceptive criticism, direction, and tireless support, all of which have nourished my development as a researcher. Without his faith in me, this journey would not have been possible.

I am also thankful to esteemed members of my Doctoral Committee, Prof. Rajen Kumar Sinha, Prof. Natesan Srinivasan, Dr. Sweta Tiwari for their invaluable insights, constructive criticism, and scholarly contributions. Their varied viewpoints and combined experience have enhanced the depth of this work.

My heartfelt gratitude is extended to Indian Institute of Technology Guwahati for offering the tools, space, and academic atmosphere required to support research and education. The implementation of this study has been made possible by the institutional support. I am also grateful to the Ministry of Education, Government of India for the financial assistance provided.

I owe sincere gratitude towards my father Shri Mohan Chandra Kandpal and my mother Smt. Madhubala Kandpal for always being my pillars of strength, for cheering me on every step of the way, and for instilling in me the importance of education and lifelong learning. This achievement is as much yours as it is mine, and I dedicate this thesis to you with all my love and gratitude. To my siblings Hema and Om, thank you for your unconditional support, understanding, and encouragement throughout this journey. My gratitude also goes out to my extended family for their love, encouragement, and support.

I owe Dr. Sreeja Pekkat a debt of gratitude for lending me her generous time and knowledge, which have surely improved the caliber and scope of my research. I am also grateful for the rigorous journal peer review process, which has helped refine the quality and rigor of this research. The constructive feedback received from anonymous reviewers has been instrumental in strengthening the validity and clarity of the findings presented in this thesis.

I want to thank my seniors, Dr. Sunanda Saha, Dr. Kuldeep Singh Yadav, Dr. Koushik Kanti Barman, Dr. Naresh Kumar, whose mentorship have been invaluable in my Ph.D. journey. I also thank my friends, Dr. Papi Ray, Khyodeno, Dr. Gauranga Pradhan, Dr. Raman Kumar, Dr. Matap Shankar, Sunil, Mahesh, Shilpi, Abhijit, Gaurav, Gurinder, who made my experience in IIT Guwahati a memorable one.

I would like to express my heartfelt gratitude to my dear friends Indira, Pooja, Aditya, Reema, and Akanksha, whose steady support and encouragement sustained me throughout this academic journey. Your presence in my life has been a constant source of strength and inspiration.

Last but not the least, I want to express my sincere gratitude to everyone who has already been acknowledged as well as to others whose contributions were perhaps not made clear but are nonetheless very much appreciated.

April, 2024 **Shiva Kandpal**

Abstract

Investigation of open channel flows includes the study of routing in rivers and channels. The study of channel routing allows us to examine the change in the behavior of the flow discharge and the flow depth along the length of the channel by observing the change in the shape of the hydrograph as the mass moves down the slope. The values of the flow discharge or the flow depth are recorded at different gauging stations along the channel, and these values are used as the boundary conditions for the study of the flow in the channel. Saint-Venant equations are popularly used to represent the flow in a channel in mathematical form. These equations are derived by using the concept of conservation of mass and momentum. The assumptions for the Saint-Venant equations are that the flow is considered one-directional; the slope of the bed is small, the pressure distribution is hydrostatic, the flow is gradually varied, etc. These solutions predict the flow discharge and the flow depth in overland flows, floods, and irrigation canals.

A model governed by the full Saint-Venant equations is also known as the dynamic wave model. The diffusive wave model is a simplified form of the dynamic wave model which ignores the impact of the inertial forces and can provide results as close as the dynamic wave model. This thesis focuses on finding the analytical solutions for the linearized Saint-Venant equations or their simplified forms subject to different lateral inflows in a channel of finite length. Ignoring the downstream boundary is a common practice that reduces the mathematical complexity of the problem to be solved analytically. However, ignoring the downstream boundary is not always appropriate. It can be implemented for very long rivers or channels, but in a channel of short length, the downstream boundary significantly alters the flow behavior. This is why we focus on working with channels of finite length. The boundary conditions in this study are considered in one of the following forms: a flow-discharge hydrograph, a flow-depth hydrograph, and a stage-discharge relationship. In most of the problems, the solution is presented for both the unknowns: the

flow discharge and the flow depth. The results are presented in the form of convolution. The lateral inflow is considered in one of the following forms:

- uniformly distributed throughout the length of the channel,
- concentrated at a location (e.g., tributary of negligible width that can be considered as a concentrated source),
- uniformly distributed between any two locations along the length of the channel (e.g., any tributary of significant width).

The first problem looks at the solution for the complete linearized Saint-Venant equations in a finite length channel with a uniformly distributed lateral inflow along the length of the channel. Since the response functions corresponding to the upstream and downstream boundaries are already present, the behavior of the lateral channel response function is explored. The solution is presented for the flow discharge only. The behavior of the flow discharge is studied for different parameters controlling the flow, like bed slope, channel width, reference flow discharge, and roughness coefficients. Furthermore, a comparison with the already existing results corresponding to the semi-infinite channel is shown by plotting hydrographs. To study the effect of a space- and time-dependent lateral inflow, the diffusive wave model, also known as the non-inertia wave model, is considered. For the rest of the problems, the lateral inflow is considered either to be concentrated at a location or uniformly distributed between any two locations along the length of the channel. The solutions are presented for the flow discharge and the flow depth. The results are compared with the analytical solutions for the semi-infinite channels available in the literature. For the second and third problems, a flow-depth hydrograph is considered as the downstream boundary with two types of upstream boundary conditions: a flow-discharge hydrograph and a flow-depth hydrograph. The distinction in the problems is as per the type of lateral inflow considered. The first problem of these two focuses on the behavior of the flow discharge and the flow depth corresponding to a concentrated lateral inflow while the second one accounts for a uniformly distributed lateral inflow between any two locations. The behavior of the unknowns is thoroughly discussed for both types of upstream boundary conditions and for different values of the Péclet number along the length of the channel. The difference in their behavior corresponding to different types of upstream boundary condition is also highlighted.

For the fourth problem, only one upstream boundary is considered in terms of a flow-depth hydrograph, and a flow-discharge hydrograph is imposed at the downstream end. The behavior of the flow discharge and the flow depth is studied at different locations of the channel for different parameters like the Péclet number and the locations of the lateral inflow. The results are compared with the corresponding semi-infinite channel responses. The effect of the flow-discharge-based downstream boundary is found to be different from that of a flow-depth-based downstream boundary. For the fifth and sixth problems, a stage-discharge relationship is considered as the downstream boundary with two types of upstream boundary conditions: a flow-discharge hydrograph and a flow-depth hydrograph. The distinction in the problems is as per the type of lateral inflow considered. For these two problems, the effect of the downstream boundary is controlled by a feedback parameter. The fifth problem focuses on the results corresponding to a concentrated lateral inflow. The behavior of the response functions for the flow discharge and the flow depth is thoroughly studied for different concentrated lateral inflows, different values of the Péclet number, and the feedback parameter. The results are also compared with the corresponding semi-infinite channel responses. In the sixth problem, the considered lateral inflow is uniformly distributed between any two locations, and the behavior of the response functions of the flow discharge and the flow depth is studied along the entire channel corresponding to different values of the Péclet number and the feedback parameter. The backwater effect of the lateral inflow is also shown for the flow discharge and the flow depth.

Contents

List of Figures

CHAPTER 1

Introduction

1.1 Preface

A *fluid* is known as a substance whose molecules are loosely packed, which means that the force of attraction between its molecules is not strong enough to keep it in a particular shape. It is a substance that continuously deforms under a small amount of shear or tangential stress. This makes the rate of deformation of a fluid an exciting study. *Fluid mechanics* is the study of a fluid at rest and also of its behavior under the application of various types of forces. Fluid mechanics is mainly focused on the combined behavior of the molecules of a fluid instead of the individual behavior of a molecule. To study the physics behind the motion of a fluid, fundamental concepts like *conservation of mass, momentum, and energy* are used. The mathematical representation of these concepts requires an application of differential calculus. However, differential calculus cannot be applied directly to a fluid in motion because properties like velocity, density, or mass are not continuous since the molecule distribution for a fluid in motion is not smooth enough. To deal with this, the concept of *continuum* is used, which translates to a continuous medium. This means that all the properties of a fluid, like density, velocity, and mass, are continuous enough that we can study the combined physical behavior of a fluid under motion or at rest.

Fluids can be categorized in various ways under some basic properties. A fluid is called a *Newtonian fluid* when the relation between the stress and the deformation rate (strain) is linear (e.g., water, air, alcohol, etc.). The category which does not hold the Newtonian properties (e.g., paint, blood, etc.) is called a *non-Newtonian fluid.* If the volume of a fluid changes significantly under the application of external forces or normal compressive forces, then the flow is termed as a *compressible fluid flow*. The normal compressive stress at rest is called the *hydrostatic pressure* for a fluid. When the change in normal compressive forces does not significantly change the volume, the resulting flow is called an *incompressible fluid flow*, e.g., the flow of water. The property of a fluid due to which it offers resistance to its flow is called *viscosity*. If the viscosity is negligible, the flow is called an *inviscid flow*, and when it cannot be ignored, the flow is termed as a *viscous flow*. If the fluid flow is random and its properties can change randomly with space and time, the flow is called a *turbulent flow*; otherwise, it is called a *laminar flow*. To study the dynamics of the flow, some idealization of fluid properties is often required. An *ideal fluid* is the one which experiences no shear stress implying that the viscosity of the fluid is zero. This assumption is often made for water. Although water is not an ideal fluid, it does have negligible viscosity, which makes the ideal fluid assumption for water flow an acceptable one. Ideal fluid, as the name suggests, is an idealization of a real fluid. A fluid which experiences the shear stress, that is, possessing positive viscosity, is called a *real fluid*. Most of the fluids around us are real fluids.

The motion of a fluid can be described in one of the following ways: a *Lagrangian* approach and an *Eulerian* approach. In the Lagrangian approach, the motion of the fluid is described by following the path of each and every particle in the flow. A particle is specified by its location at a given time. For any other instant of time, the position of a particle is defined as a function of time and its initially specified location. However, in fluid mechanics, it is quite difficult to follow the path of a single particle. For the Eulerian approach, the behavior of the fluid flow is observed at a location. Various particles passing through a particular location can be easily observed by using this approach. All the hydrodynamic properties are functions of space and time. Due to this property, the Eulerian approach, or control volume approach, is considered more useful in fluid mechanics where the flow can be described at each location as a function of time. The governing laws of a fluid flow are described by using a control volume approach. A *control volume* is a specific region of space which is selected for the study where the fluid enters and leaves. To analyze a control volume, three laws always hold true: *conservation of mass*, *conservation of momentum*, and *conservation of energy*. The conservation of mass states that the total mass entering the control volume is equal to the mass exiting the control volume plus the mass stored within the control volume. The conservation of momentum is based on Newton's second law of motion. It states that the rate of change of momentum of a system is equal to the sum of the external forces acting on the body. The conservation of energy states that the net energy supplied to a system is equal to the increase in energy of the system plus the energy that leaves the system.

In general, the law of conservation of mass in a fluid leads to an equation called the *equation of continuity* expressed as

$$\frac{\partial \rho}{\partial t} + \nabla.(\rho \vec{V}) = 0, \tag{1.1}$$

where $\vec{V}$ is the velocity of the fluid and ρ is the density of the fluid. For an incompressible, inviscid fluid, the above equation of continuity reduces to

$$\nabla.\vec{V} = 0. \tag{1.2}$$

With respect to the conservation of momentum, there are two types of forces acting on a control volume: the surface forces (e.g., pressure and shear stress) and the volume forces (e.g., gravity) applied at the center of mass of the control volume. It leads to an equation called the *equation of motion* given by

$$\frac{\partial (\rho \vec{V})}{\partial t} + (\vec{V}.\nabla)(\rho \vec{V}) = \rho \vec{F}_v - \nabla P + \vec{F}_{visc}, \tag{1.3}$$

where $\vec{F}_v$ is the resultant of volume forces (per unit volume), $\vec{F}_{visc}$ is the resultant of viscous forces (per unit volume), and P is the hydrodynamic pressure. For an incompressible, inviscid fluid, where the gravity ($\vec{g}$) and pressure forces are considered to act on the fluid, the above equation of motion reduces to

$$\frac{\partial \vec{V}}{\partial t} + (\vec{V}.\nabla)\vec{V} = \vec{g} - \frac{1}{\rho}\nabla P. \tag{1.4}$$

A streamline is an imaginary line in the fluid flow which is everywhere tangent to the fluid velocity vector. The interpretation of conservation of mechanical energy was first described by Daniel Bernoulli in 1738. If the fluid is inviscid with constant density and the flow is steady, *Bernoulli's equation* along a streamline states that the sum of the kinetic energy, potential energy, and flow energy per unit weight remains conserved as it is transmitted from one point to another in the flow field along a streamline. In the mathematical form, for a fluid flow in the xyz-plane, Bernoulli's equation is represented in the following way:

$$\frac{P}{\rho} + gz + \frac{v^2}{2} = \text{constant}, \tag{1.5}$$

where v is the velocity along the streamline. Here, P/ρ represents the flow work per unit mass of the flowing fluid, gz and $v^2/2$ can be considered as the potential energy and the kinetic energy, respectively, per unit.

The next section introduces the concepts of an open channel flow and includes all the essential elements relevant to this thesis.

1.2 Open channel flow

Fluids get transported from one location to another through natural or artificial structures. Rivers are one of the leading transporters of water on the earth. They can be termed as a fundamental building block to human civilization. The widespread network of waterways on the surface of the earth resembles the blood flow system in the human body, and so does the task they fulfill. The rivers carry a range of discharges, from completely vanishing in some small streams in the summer to the yearly floods in the rainy season. In hydrology terminology, river flow comes under the category of open channel flow. An *open channel flow* is the one in which the liquid flows with a free surface. In most of the cases, this liquid is water, and the air above the flow is at rest due to which the pressure at the free surface is the standard atmospheric pressure. Some other examples of open channel flow include the flows in irrigation canals, sewers, and natural streams. The main factor in the analysis of the open channel flow is to know the location of the free surface, which changes in response to any perturbation to the flow. The other category is a closed conduit flow with no free surface, e.g., *pipe flow*. The study of open channel flows is dependent on various geometric parameters of the channel like roughness, width, and slope of the bed; and some properties of the flowing fluid like density and viscosity. The behavior of the flow is studied with respect to the parameters like discharge, depth, velocity, and cross-sectional area. There are different criteria to classify open channels: based on the shape of the channel - *prismatic* or *non-prismatic*; types of boundaries - *rigid* or *mobile*. The flow in an open channel can also be categorized as follows: *steady* or *unsteady*, *uniform* or *non-uniform*, *gradually varied* or *rapidly varied*, etc. A typical sketch of a one-directional open channel flow is given in Fig. 1.1. In this figure, Q is the flow discharge, h is the flow depth, d is the channel depth, z_0 is the elevation of the channel from the bottom, and x is the direction of the flow.

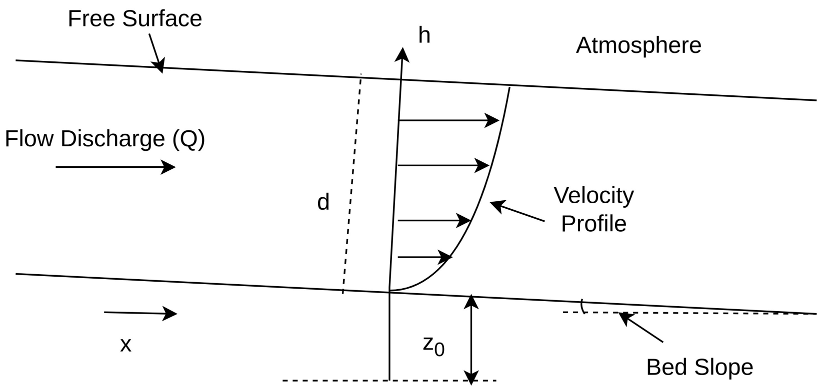

Figure 1.1: A typical sketch of an open channel flow

For engineering applications, the study of the behavior of the flow parameters like the flow discharge and the flow depth along the length of the channel is predominant. These computations determine the flow-surface elevations along the length of the channel for a specified flow discharge. The flow discharge and the flow depth data are required for the planning and design of open channels to assess the effects of various engineering works and channel modifications. For example, a dam-like structure at the downstream end increases the flow depth level at the upstream locations to the downstream end, and it is necessary to know the flow depth and the flow discharge in the upstream area to determine the magnitude of flooding. The computation of the flow depth or the flow velocity of a flood wave as it propagates in a body of water is called *flood routing*. This water body could be a river, an artificial channel, a stream, etc. The various ways to handle flood routing can be classified into two categories: *hydrologic* routing and *hydraulic* routing. The hydrologic method is primarily based on the conservation of mass, and the storage in the channel is related to the inflow and outflow discharge of the channel. The hydraulic methods are mathematically more complex, based on the conservation of mass and momentum equations. Linsley et al. [31] explained two categories of flood wave. In the first case, the flood wave is fast rising, which is frequent in the channel of a steep slope, and the flow is governed by acceleration and momentum. In the second case, the flood wave is slowly rising, and the friction force imposed by the channel or stream is the dominant force that alters the behavior of the flood wave. It moves along the flow direction; if a downstream boundary is present, the wave moves back in the upstream direction after the interaction with the structure imposed at the downstream end.

The following section briefly describes some basic definitions, terminology, and governing equations related to the open channel flows. The information related to the Saint-Venant equations and the relevant simplified forms is provided in detail.

1.3 Definitions and governing equations

1.3.1 Types of channels

The classification of open channels based on their shapes and sizes goes as follows:

- **Prismatic/Non-prismatic channel:** A fixed cross-sectional shape and size with a constant bottom slope is called a *prismatic channel*, e.g., artificial channels, irrigation canals, etc. As the name suggests, a channel with a varying cross-sectional shape and size is called a *non-prismatic channel*, e.g., rivers, streams, etc.

- **Rigid/Mobile boundary channel:** A channel with a fixed boundary such that its shape and roughness magnitude do not change is called a *rigid boundary channel*. A channel where the boundary gets deformed, like in a river is called a *mobile boundary channel*.

1.3.2 Types of flows

The classification of flows in an open channel is as follows:

- **Steady/Unsteady flow:** A flow in which the flow velocity does not change with time is called a *steady flow*, and a flow in which the flow velocity does change with time is called an *unsteady flow*. Most of the flows in our surroundings fall in the category of unsteady flows since the surface of water continuously changes due to different applied forces. In contrast, a steady flow is an idealization of an unsteady flow which allows convenient but feasible modeling.

- **Uniform/Non-uniform flow:** A flow in which the flow velocity does not change along the length of the channel is called a *uniform flow* whereas when the flow velocity changes along the length of the channel, it is called a *non-uniform flow*.

- **Gradually/Rapidly varied flow:** A flow in which the change in the water surface elevation is gradual is called a *gradually varied flow*, and the case where the flow depth changes significantly over a shorter length of the channel is called a *rapidly varied flow*.

- **Critical/Sub-critical/Super-critical flow:** A flow is called *critical* if the flow velocity is equal to the velocity of a gravity wave having a small amplitude. A change in the flow depth may produce a gravity wave. If the flow velocity is less than the critical flow velocity, then the flow is called *sub-critical*, and if the flow velocity is greater than the critical flow velocity, then the flow is called *super-critical*. Another criterion to classify flows into critical, sub-critical or super-critical is described in the next subsection.

1.3.3 Some hydrology-related definitions and formulas

- **Response function:** The response of a linear system for any particular type of input is called a *response function*.

  1. *Impulse response function:* The output of a linear system to a unit amount of input given instantaneously is called an impulse response function.
  2. *Step response function:* The output of a linear system to a unit-step input that goes from 0 to 1 at time 0 and then remains the same after that, is called a step response function.
  3. *Pulse response function:* The output of a linear system to a unit pulse input of unit amount for a fixed duration is called a pulse response function.

- **Hydrograph:** A plot of the flow discharge or the flow depth against time is called a *hydrograph*. This is the most useful tool that helps in assessing the behavior of the flow discharge and the flow depth at different locations of a channel. Additionally, the flow information at the boundaries of a channel are often available in the form of hydrographs. When displaying water level readings and forecasts visually in a single image, hydrographs can be considered a useful tool. Hydrographs provide vital information to all water users and channel building designers. An annual update of the hydrographs of all streams being measured is usually published by the governments of majority of countries.

  The *unit hydrograph* is the unit pulse response function of a linear hydrologic system. It was first proposed by Sherman [29] in 1932. It is defined as a direct runoff hydrograph resulting from one unit (one inch or one cm) of constant intensity uniform rainfall occurring over the entire watershed. Based on the principles of superposition and proportionality, the unit hydrograph concept is derived from the theory of linear systems. The unit hydrograph is considered unique for a given watershed and invariable with respect to time. Unit hydrographs are applicable when channel conditions remain the same. In hydrology, the step response function is usually called the *S-hydrograph*, and the impulse response function is called the *instantaneous unit hydrograph*, which is the hypothetical response to a unit depth of excess rainfall deposited instantaneously on the watershed surface.

- **Rating curve:** It is a relation between the flow discharge and the flow depth given at a particular channel location. It is also known as a *stage-discharge relationship*. The flow discharge is given as a function of the flow depth. When this relation is used as a boundary condition, the linearized form of the relation is expressed in terms of a *feedback parameter*, which ultimately controls the effect of the downstream boundary.

- **Lateral inflow:** The flow through which fluid is added from the sides of the channel to the main flow is called a *lateral inflow*. This encompasses cases like a tributary joining the channel, rain falling along the length of the river reach, etc.

- **Chezy's formula:** This resistance formula was derived by an engineer named Antoine Chezy in the year 1769 for uniform flows, which gives a relation between the mean flow velocity V and the slope S_0 of the bed. This formula is given by

$$V = C\sqrt{RS_0}, \tag{1.6}$$

  where R is called the *hydraulic radius* defined as A/P, which is the ratio of the *cross-sectional area* A and the *wetted perimeter* P. The wetted perimeter is the portion of the surface of the channel at a particular cross-section that is in contact with the flow within the channel. C is called the *Chezy's coefficient* which depends on the nature of the surface of the channel and the flow therein, and its dimension is $[L^{1/2}T^{-1}]$.

- **Manning's formula:** A flow resistance formula was proposed for uniform channels by an engineer named Robert Manning in the year 1889 as an alternative to Chezy's formula given in Eq. (1.6). It is given by

$$V = \frac{1}{n} R^{2/3} S_0^{1/2}, \tag{1.7}$$

where the new notation n is the *Manning's coefficient* with the dimension $[L^{-1/3}T]$. The values of n for different channel flows are usually selected from the table provided by Robert Manning [48]. The use of Manning's formula is more frequent than Chezy's formula.

However, it may be noted that the friction formulas are not limited to these two only. The friction formula for a particular open channel flow can be derived by using the Darcy-Weisbach equation, which is used to calculate the head loss due to wall friction. More details of the applicability range of various friction formulas can be found in [4].

- **Friction slope:** The rate of energy loss along the length of the channel is called *friction slope* which is denoted by S_f. The friction slope is dependent on the type of friction law assumed for the study (e.g., Manning's or Chezy's formula), the shape and roughness of the cross-section, the flow discharge at the cross-section, and the area of the cross-section. Usually, the friction slope can be written as a function of the flow discharge and the area of the cross-section.

- **Froude number:** It is a dimensionless quantity defined as the ratio of the inertial force to the gravitational force, and denoted by F. The flow in an open channel can be categorized as sub-critical for $F < 1$ and super-critical for $F > 1$. The flow is considered critical if $F = 1$. The Froude number is a function of the flow discharge and the cross-sectional area of a channel.

- **Péclet number:** It is a dimensionless quantity that gives a relation among the length of the channel, the wave celerity, and the diffusivity coefficient. This is mainly used for the diffusive wave model where the Péclet number signifies the role of the downstream boundary. The relation can be written as $P_e = \dfrac{CL}{D}$, where L is the length of the channel, C is the wave celerity, and D is the diffusivity coefficient. The Péclet number usually quantifies the influence of downstream disturbances on the flow within the channel. The greater is the Péclet number, the lesser is this influence. To understand this, it is sufficient to consider that high values of the Péclet number are associated with high values of celerity C (the flow is able to wash disturbances out of the channel), high values of the channel length L (the downstream disturbances are produced far from the upstream end), and low diffusivity D (the diffusive model reduces to the kinematic model in which the downstream boundary is not taken into account).

- **Backwater effect:** An interaction between the flood wave and the downstream boundary can lead to variations in the flow discharge and the water surface profile in the upstream direction. This behavior is known as the backwater effect. This commonly occurs at the locations closer to the downstream end of a river, mostly near the mouth of the river. It is an important phenomenon that presents a severe threat to lakes, tributaries, and downstream areas. The backwater effect of the river needs to be taken into consideration while designing river structures like dams, weirs, etc.

1.3.4 Saint-Venant equations

Saint-Venant equations consist of two quasi-linear, first-order partial different equations derived by using the concepts of conservation of mass and momentum. A J C Barre de-Saint Venant first derived these equations in 1871 [11] for an unsteady, gradually varied flow. These equations were derived explicitly for open channels. To describe the flow at a particular cross-section, the information on any two variables, flow depth and flow discharge or flow depth and flow velocity, is necessary. The assumptions involved in deriving these equations are as follows:

- The flow is considered one-directional since the change in velocity components along the vertical and transverse directions are usually small and negligible compared with the change in the velocity along the flow direction. Due to this, the change along the vertical and transverse directions is ignored.
- The pressure distribution is hydrostatic, which is a valid assumption if the streamlines do not have sharp curvatures.
- The channel bed slope is small so that the flow depths measured normal to the channel bottom or measured vertically are approximately the same.
- The flow velocity over the entire channel cross-section is uniform.
- The channel is prismatic. For some cases, the varying cross-section or bottom slope can be considered by approximating the channel using prismatic reaches.

- The energy losses in an unsteady flow are usually estimated by using the steady-state resistance formulas, such as the Manning's or Chezy's formula, i.e., energy losses for a given flow velocity during unsteady flow are the same as those during the steady flow. Therefore, it is a usual practice to evaluate the friction slope by using either Eq. (1.6) or Eq. (1.7).

The first equation appearing in the Saint-Venant equations is the equation of continuity, which is given by

$$\frac{\partial Q}{\partial x} + b\frac{\partial h}{\partial t} = 0. \tag{1.8}$$

It can also be written as

$$A\frac{\partial V}{\partial x} + V\frac{\partial A}{\partial x} + b\frac{\partial h}{\partial t} = 0, \tag{1.9}$$

using the relation $Q = AV$. Here, x is the space variable along the length of the channel, t is the time variable, Q is the flow discharge, A is the cross-sectional area, h is the flow depth, V is the flow velocity, and b is the top width of the channel at a depth h given as $\partial A/\partial h$.

The second equation is the equation of motion, which can be written as

$$\frac{\partial h}{\partial x} + \frac{V}{g}\frac{\partial V}{\partial x} + \frac{1}{g}\frac{\partial V}{\partial t} = S_0 - S_f, \tag{1.10}$$

where g is the gravitational constant. In the left-hand side of Eq. (1.10), the first term represents the pressure gradient, the second represents the convective acceleration, and the third represents the local acceleration. There are different ways to express the Saint-Venant equations, with some popular ones listed below:

Considering flow discharge Q and flow depth h as the dependent variables:

$$\frac{\partial Q}{\partial x} + b\frac{\partial h}{\partial t} = 0, \tag{1.11a}$$

$$\frac{\partial Q}{\partial t} + \frac{\partial}{\partial x}\left(\frac{Q^2}{A}\right) + gA\frac{\partial h}{\partial x} = gA(S_0 - S_f). \tag{1.11b}$$

Considering flow discharge Q and cross-sectional area A as the dependent variables:

$$\frac{\partial Q}{\partial x} + \frac{\partial A}{\partial t} = 0, \tag{1.12a}$$

$$\frac{\partial Q}{\partial t} + \frac{2Q}{A}\frac{\partial Q}{\partial x} + (1 - F^2)\frac{gA}{b}\frac{\partial A}{\partial x} = gA(S_0 - S_f). \tag{1.12b}$$

Considering flow velocity V and cross-sectional area A as the dependent variables:

$$\frac{\partial A}{\partial t} + V\frac{\partial A}{\partial x} + A\frac{\partial V}{\partial x} = 0, \tag{1.13a}$$

$$\frac{\partial V}{\partial t} + V\frac{\partial V}{\partial x} + \frac{g}{b}\frac{\partial A}{\partial x} = gA(S_0 - S_f). \tag{1.13b}$$

When the equation of motion is kept in the form as above, the Saint-Venant equations are also known as the *dynamic wave model*. The equation of motion leads to various approximations of the Saint-Venant equations giving rise to some simplified models which are based on the magnitude of the forces acting on the flow in the channel. An approximate model produces satisfactory results if the assumptions used to simplify it are valid, which means that discarding the ignored term from the governing equations is justified for the cases where the approximate model is applied. These simplified models have the advantage that they require less information with respect to the properties of the channel for their application in comparison with the full Saint-Venant equations. The known approximate models are as follows:

Kinematic wave model: Kinematic wave approximation of the system given in Eq. (1.11) was first explained by Lighthill and Whitham [30] in 1955. The kinematic wave theory applies to a long and flat channel where the friction slope is almost the same as the bed slope. The magnitude of all the other terms in the equation of motion is almost negligible, and it gets converted to

$$S_0 = S_f. \tag{1.14}$$

In the cases where this model is applicable, one can directly evaluate flow discharge as a function of A by using Manning's or Chezy's formula. Since all the forces are considered negligible, the flow surface does not change along the length of the channel. The name of this model is such because it is mainly based on the equation of continuity, and it approximates the equation of motion with a uniform flow condition. This model can accommodate the upstream boundary condition and lateral inflow, but it cannot assess the effect of the downstream boundary condition.

Diffusive wave model: The diffusive wave approximation is the one where the effect of the inertial forces is negligible compared to the other forces in action. This leads to neglecting the convective and local acceleration terms from the equation of motion, and it gets reduced to

$$\frac{\partial h}{\partial x} = S_0 - S_f. \tag{1.15}$$

Taking Eq. (1.15) into account, this model becomes the simplest form of the Saint-Venant equations, which can incorporate the effect of the downstream boundary condition. This model is also known as the non-inertia wave model [55].

Gravity wave model: For this approximation, friction and gravity terms are neglected; however, the effects of inertial forces and pressure are considered. Subsequently, the equation of motion reduces to

$$\frac{\partial h}{\partial x} + \frac{V}{g}\frac{\partial V}{\partial x} + \frac{1}{g}\frac{\partial V}{\partial t} = 0. \tag{1.16}$$

Quasi-steady dynamic wave model: This approximation is obtained by ignoring the local acceleration term from the equation of motion, which leads to

$$\frac{\partial h}{\partial x} + \frac{V}{g}\frac{\partial V}{\partial x} = S_0 - S_f. \tag{1.17}$$

Among all these simplified models of the Saint-Venant equations, the kinematic and the diffusive wave models are the most widely used ones. They are frequently used for overland flows and channel routing.

1.4 Used mathematical tools

Method of variation of parameters: It is a method used to solve a non-homogeneous ordinary differential equation where the solution corresponding to the non-homogeneous part of the equation is solved with the help of the solution of the homogeneous part of the equation.

Method of undetermined coefficients: It is another method used to solve a non-homogeneous ordinary differential equation where the solution for the non-homogeneous part of the equation is guessed based on the function present as the non-homogeneous term of the differential equation.

Laplace transform: The Laplace transform $\overline{f}$ of a function $f : [0, \infty) \to \mathbb{R}$ is defined as

$$\overline{f}(s) = \mathcal{L}\{f(t)\} = \int_0^\infty \exp(-st) f(t) \mathrm{d}t, \tag{1.18}$$

where $\mathcal{L}$ is the Laplace transform operator. This integral exists for a piece-wise continuous function and a function of exponential order. A function is said to be of exponential order if $\exists$ constants $M > 0$, $T > 0$, and $c_1 \in \mathbb{R}$ such that

$$|f(t)| \leq M \exp(c_1 t) \text{ for } t > T. \tag{1.19}$$

The Laplace inverse for the function $\overline{f}$ is defined as follows:

$$f(t) = \mathcal{L}^{-1}\{\overline{f}(s)\} = \frac{1}{2\pi \mathrm{i}} \int_\gamma \exp(st) \overline{f}(s) \mathrm{d}s, \tag{1.20}$$

where $\mathcal{L}^{-1}$ is the inverse Laplace operator, γ is a line parallel to the imaginary axis and all singularities of the function $\overline{f}$ lie to the left of this line. This result is known as *Laplace inversion theorem* or *Bromwich integral*.

To solve a partial differential equation for an unknown $U(x,t)$ by using the Laplace transform, we need to apply it to $U(x,t)$ as well as to its derivatives. The Laplace transform is usually applied with respect to the variable t, which mostly means time, whose values vary from 0 to ∞. The Laplace transform of a function $U(x,t)$ of two variables with respect to the variable t, and for each fixed value of x, can be defined as

$$\overline{U}(x,s) = \mathcal{L}\{U(x,t)\} = \int_0^\infty \exp(-st)U(x,t)\mathrm{d}t. \tag{1.21}$$

The Laplace transform formulas for its derivatives, up to the second-order, are as follows:

$$\mathcal{L}\left\{\frac{\partial U(x,t)}{\partial t}\right\} = s\,\overline{U}(x,s) - U(x,0), \tag{1.22}$$

$$\mathcal{L}\left\{\frac{\partial^2 U(x,t)}{\partial t^2}\right\} = s^2\,\overline{U}(x,s) - sU(x,0) - \left.\frac{\partial U}{\partial t}\right|_{(x,0)}, \tag{1.23}$$

$$\mathcal{L}\left\{\frac{\partial U(x,t)}{\partial x}\right\} = \frac{\mathrm{d}\overline{U}(x,s)}{\mathrm{d}x}, \tag{1.24}$$

$$\mathcal{L}\left\{\frac{\partial^2 U(x,t)}{\partial x^2}\right\} = \frac{\mathrm{d}^2\overline{U}(x,s)}{\mathrm{d}x^2}, \tag{1.25}$$

$$\mathcal{L}\left\{\frac{\partial^2 U(x,t)}{\partial x \partial t}\right\} = \frac{\mathrm{d}}{\mathrm{d}x}\mathcal{L}\left\{\frac{\partial U(x,t)}{\partial t}\right\} = \frac{\mathrm{d}}{\mathrm{d}x}\left(s\overline{U}(x,s) - U(x,0)\right). \tag{1.26}$$

Some Laplace inverse properties for two Laplace transformable functions $f(t)$ and $g(t)$ that have been used in this thesis are given below [1, 15]:

$$\mathcal{L}^{-1}\{\overline{f}(s-a)\} = \exp(at)f(t), \tag{1.27}$$

$$\mathcal{L}^{-1}\{\exp(-as)\overline{f}(s)\} = f(t-a)\mathrm{u}(t-a), \text{ where } a > 0, \tag{1.28}$$

$$\mathcal{L}^{-1}\{\exp(-k\sqrt{s^2-a^2}) - \exp(-ks)\} = \frac{ak}{\sqrt{t^2-k^2}}\mathrm{I}_1(a\sqrt{t^2-k^2})\mathrm{u}(t-k), \text{ where } k > 0, \tag{1.29}$$

$$\mathcal{L}^{-1}\{\overline{f}(s)\overline{g}(s)\} = f(t) \circledast g(t), \tag{1.30}$$

$$\mathcal{L}^{-1}\left(\frac{\overline{f}(s)}{s}\right) = \int_0^t f(\tau)\mathrm{d}\tau, \tag{1.31}$$

where $\mathrm{u}(.)$ is the unit-step function, $\mathrm{I}_1(.)$ is the modified Bessel function of first kind of order 1, and $\circledast$ is the convolution operator which is defined for two Laplace transformable function in the following way:

$$f(t) \circledast g(t) = \int_0^t f(\tau)g(t-\tau)\mathrm{d}\tau. \tag{1.32}$$

Residue theorem: The integral in Eq. (1.20) can be evaluated by using the *residue theorem* stated below:

$$f(t) = \sum_{k=0} \mathrm{Res}\left(\exp(st)\overline{f}(s); s = s_k\right), \tag{1.33}$$

where s_k are the poles of the function $\overline{f}(s)$. The residue for $\exp(st)\overline{f}(s)$ corresponding to a pole s_0 of order m is defined as

$$\mathrm{Res}\Big(\exp(st)\overline{f}(s), s = s_0\Big) = \frac{1}{(m-1)!}\lim_{s\to s_0}\frac{\mathrm{d}^{\mathrm{m}-1}}{\mathrm{d}s^{m-1}}\left((s-s_0)^m \exp(st)\overline{f}(s)\right). \tag{1.34}$$

One important aspect while evaluating the Bromwich integral to find the Laplace inverse, where the poles are the only singularities of the function, is that the Jordan's lemma is usually required to be used. In this context, the attribute of the Jordan's lemma that, for a function f, it must be true that $f(z) \to 0$ as $|z| \to \infty$, should be satisfied.

Perturbation technique: It is one of the most useful tools for solving nonlinear differential equations. Using perturbation, the unknown variable is linearized around some function, which is comparatively easier to handle. The unknown variable can be linearized around a steady, uniform condition for the flow in an open channel. The linearized forms of the unknowns Q and A can be written as

$$Q(x,t) = Q_0 + Q_1(x,t) + \text{ higher-order terms}, \tag{1.35a}$$

$$A(x,t) = A_0 + A_1(x,t) + \text{ higher-order terms}, \tag{1.35b}$$

where Q_0 and A_0 represent the values of the flow discharge and the cross-sectional area, respectively, for the steady uniform flow condition; Q_1 and A_1 are the first-order increments in the flow discharge and cross-sectional area, respectively, with the higher-order terms ignored. In this text, this linearization theory is used for a gradually varied flow, where the magnitude of the reference condition is much higher than its first-order increments. A similar linearization technique is used if the unknown variables are changed. In this thesis, most problems are solved by using the linearization process on the flow discharge and the flow depth.

1.5 Brief literature survey

Our thesis is mainly based on what de Saint Venant [11] initiated by introducing a system of two first-order partial differential equations to study the one-dimensional, gradually varied, unsteady flow in an open channel. These equations are mathematical descriptions of the conservation of mass and momentum. Due to the nonlinear momentum equation, an analytical solution of the complete Saint-Venant equations (SVEs) is still unavailable. However, some idealizations have led to feasible solutions obtained by different researchers. Dooge and Napiórkowski [16] studied the effect of the upstream and the downstream boundary conditions in the absence of any lateral inflow and derived the upstream and downstream response functions for the linearized SVEs in a finite length channel. They showed that the effect of the downstream boundary gets transmitted in the upstream direction. The solution was presented for one unknown variable which could be used for the flow discharge and the cross-sectional area. Later, Napiórkowski [41] presented the linearized solution of the SVEs for the general case of a channel of arbitrary shape and for any friction law. Tsai and Yen [52] presented a detailed analysis on the effect of the upstream and the downstream boundaries for all the simplified forms of the SVEs in a finite length channel. They also ignored the effect of any lateral inflow and the presented solution could be used for both the flow discharge and the cross-sectional area. Using the upstream and the downstream response functions, they exhibited the similarity and distinction among all the approximations of the SVEs in terms of their mathematical properties and physical characteristics. In the direction of the development of the solution of the full SVEs with the inclusion of the lateral inflow, Moramarco et al. [37] derived an analytical solution by considering a uniformly distributed lateral inflow for the linearized SVEs in a semi-infinite channel. The solution methodology is similar to the one followed by Dooge and Napiórkowski [16]. Although the result obtained by them is limited to a semi-infinite channel only, they did emphasize on the importance of the selection of reference flow discharge for different slopes. They performed an error analysis with respect to the selection of the reference flow discharge for channels with different slopes and widths.

The solution for the linearized SVEs has also been explored with the use of Green's function method. Brutsaert [3] used the Chezy's and Manning's formulas to calculate Green's function of the linearized SVEs, or their responses to an impulsive source term. Starting from an initial uniform state, the solution of the linearized model in a semi-infinite channel was presented with a prescribed time-varying flow rate in the upstream portion based on the analytical expression of Green's function. Ridolfi et al. [43] also presented an analytical solution for the linearized SVEs in a semi-infinite channel of rectangular cross-section by using Green's function method. They showed the existence of three simple linear waves whose interaction determined all the evolutions of the solution. They also showed the role of the Froude number for both sub-critical and super-critical cases. Di

Cristo et al. [13] extended the methodology of Ridolfi et al. [43] to find a solution of the linearized SVEs by using Green's function in laminar and turbulent flows with the incorporation of the Darcy-Weisbach friction law, which is valid for the Newtonian fluids in both laminar and turbulent flows.

The linearization technique mentioned in Eq. (1.35) has been used for all such problems where the reference conditions represented by a uniform steady condition are assumed to be known. Litrico and Fromion [33] extended this methodology by considering a steady non-uniform condition as the reference condition. In this case, the reference condition for the flow discharge was steady and uniform; however, the reference condition for the flow depth or the cross-sectional area was steady but non-uniform. Litrico and Fromion [34, 32] derived the solution for the SVEs in a finite length channel by linearizing the unknown variables around a steady non-uniform condition. They approximated the backwater curve induced by the downstream boundary with the employment of a step-wise linear function. For the upstream part which corresponds to the uniform part of the flow, the backwater curve was considered as a line parallel to the channel bed. For the downstream part, which corresponds to the non-uniform part of the flow, the backwater curve was approximated as a line tangent to the real curve at the downstream end. Munier et al. [40] extended this methodology and derived the solution of the SVEs in a finite length channel by using the moment matching method. Huang and Lee [24, 25] presented an improved quasi-linear method which replaced the linear method used to derive the response functions for the upstream and downstream boundary, originally presented by Dooge et al. [17]. They presented the results for different types of downstream boundary conditions by considering a time-varying reference flow discharge and the reference hydraulic quantities according to the Manning's formula and the cross-sectional shape. This led to precision in describing the flow response to the flood prediction. Furthermore, Huang [23] used the neural network algorithm to expand the applicability of this model in natural channels having an irregular cross-section and which can be affected by the unsteady inflow, lateral flow, and the variation of the tide level.

Coming to the simplified models of the SVEs, Tsai [50] provided the applicability of the kinematic wave, non-inertia wave, and quasi-steady dynamic wave approximations to the dynamic wave model for an unsteady flow routing by studying the propagation of a sinusoidal perturbation to the steady gradually varying flow. She provided a justification of the situation when the approximate model can be used in place of the full SVEs. It was shown that the downstream boundary could significantly alter the wave propagation in a channel flow, and due to this, the importance of the downstream boundary needs to be taken into account while selecting the approximate models of the full SVEs. Tsai [51] also carried out a linear stability analysis to investigate the propagation of flood waves in the spatially varying channel flow in a mild-sloped river. For this, the reference flow was considered to be steady. From this analysis, the non-inertia wave and quasi-steady dynamic wave were found to be more capable of accounting for the downstream backwater effect in modeling floods for a mild-sloped river among all the other simplified models of the SVEs. Exploring the analytical solutions developed for the diffusive or non-inertia wave model, Hayami [22] was the first one who presented an analytical solution for the diffusive wave model in a semi-infinite channel without the inclusion of the lateral inflow. He solved the diffusive wave equations and presented the solution for the flow depth. Subsequently, Moussa [38] solved Hayami's model by including a uniformly distributed lateral inflow with the application of the Laplace transform. He presented the solution for the flow discharge and attempted the inverse problem of finding the lateral inflow in the channel for a given outflow hydrograph. Both these solutions were derived for semi-infinite channels, implying the effect of the downstream boundary being completely ignored. This is mathematically represented by considering the dependent variable at the downstream end to be zero. Mizumara [36] presented an analytical solution corresponding to the nonlinear diffusive wave model without any lateral inflow and downstream boundary. The linearization method used by him is based on the assumption that the product of two dependent variables is equal to the summation of the two dependent variables. Through comparisons with linearized diffusive wave model and the dynamic wave model, he concluded that the linearized diffusive wave model is applicable in river flows only if the change in the flow depth caused by flood is small. However, the linearized diffusive wave model was found to be inaccurate when a flood significantly altered the flow depth. In the direction of finding the results for a finite length channel, an analytical solution for the flow depth was presented by Tingsanchali and Manandhar [49] with the consideration of the backwater effect of the downstream boundary and the impact of a lateral inflow in a finite length channel with the flow depth given at the upstream and downstream ends. They also validated the results by showing comparison with the flow depth data of a flood condition for a reach of Lower Mun River in Northeast Thailand. The comparisons were found to be satisfactory, showing the effectiveness of the analytical solution to simulate real flood data. Fan and Li [19] presented an analytical solution for the flow discharge in finite and semi-infinite channels by using the techniques of the separation of variables and the Laplace transform with a concentrated and a uniformly distributed lateral inflow when the flow discharge was given at the two ends. These results analyze well the effect of concentrated and distributed lateral inflow on the flow discharge but cannot be used for different combinations of upstream and downstream boundaries. All these analytical solutions have been presented for the Dirichlet-type boundary condition where the value of the unknown is known at the two ends of the channel.

Cimorelli et al. [7] derived an analytical solution for the linearized diffusive wave model in terms of both flow discharge and flow depth in the Laplace transform and time domains, considering a uniformly distributed lateral inflow and two different types of downstream boundaries, namely a stage-discharge relationship and a time-dependent flow depth. The downstream boundary was controlled by the feedback parameter. They compared the finite length channel responses with the available semi-infinite channel responses for different values of the Péclet number and the feedback parameter, and showed the applicability range of the semi-infinite channel to be used for the approximation of the finite channel results. In continuation of this work, Cimorelli et al. [6] proposed a flow-depth-based analytical solution for the linearized diffusive wave model by considering a stage-hydrograph at the upstream end. They used a uniform distribution of the lateral inflow throughout the channel in their formulation. A comparison of the experimental data of Rashid and Chaudhry [35] with the upstream response of the flow depth was also presented. It showed the correctness of the finite channel responses to simulate real flows when a flow-depth hydrograph was given at the upstream end and a stage-discharge relationship was imposed at the downstream end. They also provided a comparison establishing that the finite channel responses were more appropriate in comparison with the semi-infinite channel responses to simulate that experimental data. They further presented the comparison with the available results for semi-infinite channels. They studied the behavior of the flow depth and flow discharge for different values of Péclet numbers and feedback parameters.

The Laplace transform technique is the most common and popular technique for solving time-dependent problems. However, the inversion of the function from the Laplace domain is not always possible. Due to this, some semi-analytical approaches have been considered to solve the equations with the Laplace inverse obtained by using appropriate numerical techniques. In this direction, Chung et al. [5] presented an analytical solution for the linearized diffusive wave model in the Laplace transform domain with a constant flow depth and a stage-discharge relationship employed at the downstream end. They ignored the effect of any lateral inflow, and used the numerical inverse Laplace transform to find the solution. Kazezyilmaz-Alhan and Medina [27] presented a semi-analytical solution for the diffusive wave model with constant wave celerity and hydraulic diffusivity and applied it to overland flow problems. They used the Stehfest algorithm to find the Laplace inverse of the flow depth. They further developed an algorithm by using the MacCormack explicit finite difference method to solve the kinematic and diffusive wave governing equations for both overland and open channel flow. Kazezyilmaz-Alhan [26] improved this method by using the De Hoog algorithm instead of the Stehfest algorithm. Instead of constant wave celerity and hydraulic diffusivity, the solution was presented for variable wave celerity and hydraulic diffusivity. They also compared the performances of the Stehfest and the De Hoog algorithms. Cimorelli et al. [8] presented an analytical solution for a cascade of diffusive channels in the Laplace transform domain. They considered a stage-discharge relationship at the downstream end with a stage hydrograph or a flow-discharge hydrograph at the upstream end. The time domain expressions for the dependent variables were obtained by using the Crump algorithm, which gives a Fourier series approximation of the Laplace inversion integral. They compared some parts of their results with the experiment performed by Rashid and Chaudhry [35]. Nazari and Seo [42] presented two quasi-analytical methods for solving the one-dimensional linear diffusive wave model with a lateral inflow for finite channels and applied them to different routing problems. They presented the solution for the flow discharge only.

Concerning the finding of numerical solutions for such type of problems which includes lateral inflows as well, several research works are available in the literature (Moussa and Bocquillon [39], Singh et al. [47], Wang et al. [53], Wang et al. [54], etc.). Franchini and Todini [21] provided an unconditionally stable scheme to solve the diffusive wave model, which included a uniformly distributed lateral inflow as well as the flow discharge loss due to side weirs or overflow of the flow discharge over levees. This can be applied to artificial channels. Numerical works focused on alluvial channels and meandering rivers, which take into account the effect of the downstream boundary and spatial variation of lateral inflow, are also present in the literature (Crosato [9], Zhang and Duan [56], Duró et al. [18]). In a similar direction, Kefayati et al. [28] presented a numerical scheme to simulate mud and debris flows. Di Cristo et al. [14] presented an investigation concerning the applicability of the kinematic, diffusive, and quasi-dynamic wave models on the shallow mud-flows. They emphasized on the fact that the criteria developed for flows in turbulent conditions cannot be directly applied to mud-flows because the flow rheology can affect the characteristics of the propagating flood waves. Di Cristo et al. [12] also numerically investigated the conditions of the applicability of the nonlinear diffusive wave model for the prediction of mud-flows. There is a reasonable advancement in the development of numerical methods for this model (Savant et al. [46], Fenton [20], Sarkhosh et al. [45]). However, explicit closed-form analytical solutions may be preferred over numerical results to study issues such as error analysis, inference on how parameters affect the dependent variables, and when solutions at a particular location are needed quickly by avoiding lengthy integration at all grid points. In this context, there is still significant interest among researchers in taking up such problems analytically.

1.6 Motivation

The flow dynamics along a channel length are affected by many factors. The lateral inflow can significantly alter the flow dynamics along the channel length. This lateral inflow can be present in any form and at any location along the channel. The analytical solutions for the SVEs in a semi-infinite channel, which are derived by ignoring the effect of the downstream boundary, are still in use for assessing the flow behavior in a channel of finite length. This possibly cannot provide an accurate prediction of the flow behavior since it ignores the downstream boundary effect, which can highly influence the behavior of the flow in the channel. Another issue which came to our notice is that the information of the flow data is not always available at the gauging stations in the desired forms. In river flow, the information of the flow discharge and the flow depth both are usually required for better management of the water resources, flood prediction, water quality management, navigation and transportation purposes, and research purposes as well. The flow data is required at different locations of the channel no matter what type of upstream and downstream boundary conditions are present. This has immensely motivated us to make an attempt to derive closed-form solutions for the flow discharge and the flow depth which can help understand in clear terms the influence of different types of lateral inflow and different types of boundary condition on them. A theoretical study centered around the effect of the lateral inflow in a finite length channel can be significantly helpful in understanding the behavior of the flow under different circumstances.

Having extensively gone through a large number of works including those in the previous section, we realize that there is still a reasonable amount of scope left to derive and analyze analytical solutions of the SVEs corresponding to different types of lateral inflow in channels of finite length. In addition, most of the earlier results correspond to the Dirichlet-type boundary condition and are either presented for the flow discharge or the flow depth. Physically, the data at two ends of a channel are not always available in the desired way. To tackle this, in this thesis, we consider different combinations of boundary conditions so that these analytical solutions could be used for any case as per the availability of the data at the gauging stations. Further, the analytical solutions are presented for the flow discharge as well as the flow depth for most of the problems discussed in this thesis. The spatial variation of the lateral inflow has also not been explored enough, and to deal with this, the solution for the diffusive wave model corresponding to a concentrated lateral inflow and a uniformly distributed lateral inflow between any two locations along the length of the channel is presented. We strongly feel that all the problems considered in this thesis are physically relevant. To the best of our knowledge, the solutions for these types of problems have not been presented earlier, and hopefully, this study will shed some light on these unexplored topics.

1.7 Outline of the thesis

This thesis consists of 6 chapters. The present chapter introduces the topic and discusses the fundamental governing equations and the tools to be used in the following chapters. It also provides a brief survey of most of the main works available in the literature and relevant to the current research study. *Chapter 2–Chapter 5* provide the discussion for the six investigated problems, and *Chapter 6* summarizes the obtained results with a glance into the future scope of the current research work. In these problems, three types of lateral inflows are considered: (i) a uniformly distributed lateral inflow, (ii) a lateral inflow concentrated at a location, and (iii) a lateral inflow distributed between any two locations. The upstream and downstream boundaries are considered in one of the following forms: a flow-discharge hydrograph, a flow-depth hydrograph, and a stage-discharge relationship. The nonlinear problem in each chapter is linearized around some reference conditions, and the Laplace transform is used to find the analytical solutions.

In *Chapter 2*, the solution for the flow discharge is presented which corresponds to the full linearized Saint-Venant equations by considering a uniformly distributed lateral inflow along the channel length for a finite length rectangular channel. The flow discharge due to the lateral inflow is presented as the convolution of two functions: the lateral inflow distributed along the channel length and the lateral channel response function. The solution is obtained by using the Laplace transform, and the inverse of the Laplace domain function is obtained by using the already available Laplace inverses. The behavior of the lateral channel response function is studied for different cases of the reference flow discharge, channel width, Manning's roughness coefficient, and bottom slope. The results are compared with the existing semi-infinite channel results by using hydrographs.

The analytical solutions for the linearized diffusive wave model represented by a simultaneous system of two first-order partial differential equations focused on spatial variation of the lateral inflow in a finite channel are presented in *Chapter 3*. Two upstream boundaries are considered here: a flow-discharge hydrograph and a flow-depth hydrograph, while the downstream boundary is subject to a flow-depth hydrograph. The lateral inflow is considered in the form of either a concentrated lateral inflow or a uniformly distributed lateral inflow between any two locations along the length of the channel. This leads to two distinct problems as per the type of the lateral inflow considered. The first of these problems discusses the effect of the concentrated lateral inflow, whereas the other one focuses on the effect of the uniformly distributed lateral inflow between any two locations of the channel. The solution corresponding to the lateral inflow distributed between two locations can also include a lateral inflow distributed along the length of the channel. The unit-step responses are also derived corresponding to the presented impulse responses for all the problems corresponding to the diffusive wave model. The behavior of the flow discharge and the flow depth is discussed for the entire channel for different values of the Péclet number and different locations of the lateral inflow. The effect of the concentrated and uniformly distributed lateral inflows at different locations of the channel is thoroughly studied and also compared with the semi-infinite channel results wherever possible.

In *Chapter 4*, an analytical solution to the diffusive wave model is presented by obtaining the solution for two unknowns in the flow discharge and the flow depth. The upstream boundary is considered as a flow-depth hydrograph while the downstream boundary is considered as a flow-discharge hydrograph. Two different lateral inflows are considered: a concentrated lateral inflow and a uniformly distributed lateral inflow between any two locations along the channel length. The unit-step responses are derived to analyze the behavior of the responses of the flow discharge and the flow depth to different types of lateral inflows and boundary conditions. The flow properties are analyzed for different values of the Péclet number and for different locations of the lateral inflow. Some of the responses are compared with the corresponding semi-infinite channel responses wherever possible.

An analytical solution for the diffusive wave model with a stage-discharge relationship imposed at the downstream end is discussed in *Chapter 5*. A flow-depth hydrograph or a flow-discharge is taken as the upstream boundary. The downstream boundary is controlled by a coefficient called the feedback parameter. The problem is discussed for two types of lateral inflows: a concentrated lateral inflow and a uniformly distributed lateral inflow between any two locations along the channel length. This leads to two distinct problems as per the type of lateral inflow considered. The focus is on analyzing the impact of the lateral inflow on the flow discharge and the flow depth. The first of these problems discusses the effect of the concentrated lateral inflow whereas the other one focuses on the effect of the uniformly distributed lateral inflow between any two locations of the channel. For the first one, the unit-step responses corresponding to the concentrated lateral inflow are compared with the corresponding results of a semi-infinite channel. The behavior of the flow discharge and the flow depth is studied for different values of the Péclet number and the feedback parameter, and for different locations of the lateral inflow for both the problems. For the other problem, the behavior of the flow discharge and the flow depth is also discussed for both types of upstream boundaries for large times, and the similarity and distinction in their behavior corresponding to both types of upstream boundaries are discussed.

CHAPTER 2

Analytical solution for linearized Saint-Venant equations with a uniformly distributed lateral inflow in a finite rectangular channel

The analytical solution for the flow discharge corresponding to linearized full Saint-Venant equations by considering a uniformly distributed lateral inflow along the channel length for a finite length rectangular channel is obtained. The flow discharge due to the lateral inflow is presented as the convolution of two functions: a lateral inflow distributed along the channel length and the lateral channel response function. The behavior of the lateral channel response function for different cases of the reference flow discharge, channel width, Manning's roughness coefficient, and bottom slope is shown.

2.1 Mathematical description

2.1.1 Governing equations and other assumptions

We consider the one-dimensional SVEs in their conservative form which include both mass and momentum conservation equations for a simple rectangular channel as described by (following [37])

$$\frac{\partial Q}{\partial x} + \frac{\partial A}{\partial t} = q_l(t), \tag{2.1}$$

$$\frac{\partial Q}{\partial t} + \left(\frac{2Q}{A}\right)\frac{\partial Q}{\partial x} + (1-F^2)\frac{gA}{b}\frac{\partial A}{\partial x} = gA(S_0 - S_f), \tag{2.2}$$

where Q is the flow discharge, A is the cross-section area, q_l is the lateral inflow, b is the top surface width, g is the gravitational constant, S_0 is the bed slope, x and t are the space and time variables, respectively, F is the Froude number given by $F^2 = Q^2 b/gA^3$, and S_f is the friction slope which can be evaluated by Manning's formula as (same as the one given in Eq. (1.7) in *Chapter 1, Section 1.3*)

$$S_f = \frac{(Q/A)^2 n^2}{R^{4/3}}.$$

The schematic diagram for a one-dimensional flow in a rectangular channel of length L is given in Fig. 2.1. Following Napiórkowski [41], Eq. (2.2) is linearized by expressing Q

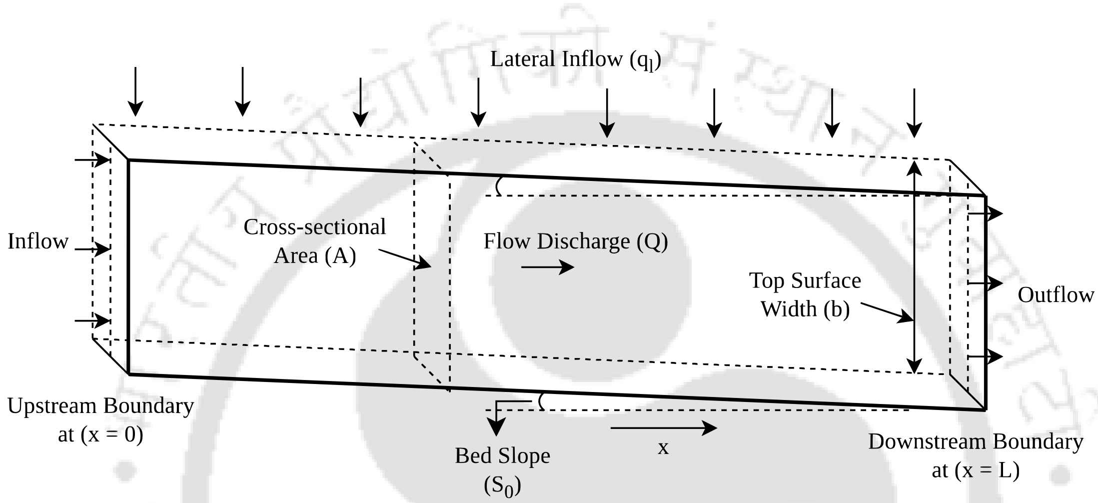

Figure 2.1: Schematic diagram for flow in a rectangular channel

and A, respectively, as (they are the same as Eq. (1.35))

$$Q(x,t) = Q_0 + Q_1(x,t) + \text{higher-order terms}, \tag{2.3}$$
$$A(x,t) = A_0 + A_1(x,t) + \text{higher-order terms}, \tag{2.4}$$

with (Q_0, A_0) representing the steady uniform condition of the flow, (Q_1, A_1) the first-order increments in the flow discharge and the cross-section area, respectively. The Taylor's series expansion for S_f for a non-uniform flow condition around a steady uniform condition represented by (Q_0, A_0) gives

$$S_f - S_0 \approx \frac{\partial S_f}{\partial Q} Q_1 + \frac{\partial S_f}{\partial A} A_1, \tag{2.5}$$

where $\partial S_f/\partial Q$ and $\partial S_f/\partial A$ are evaluated at the reference values Q_0 and A_0. Using Eqs. (2.3)–(2.5) in Eqs. (2.1) and (2.2), we get

$$\frac{\partial Q_1}{\partial x} + \frac{\partial A_1}{\partial t} = q_l(t), \tag{2.6}$$
$$\frac{\partial Q_1}{\partial t} + 2V_0 \frac{\partial Q_1}{\partial x} + (1 - F_0{}^2)\frac{gA_0}{b}\frac{\partial A_1}{\partial x} = -gA_0 \left(\frac{\partial S_f}{\partial Q} Q_1 + \frac{\partial S_f}{\partial A} A_1 \right), \tag{2.7}$$

$$\text{where } V_0 = \frac{Q_0}{A_0}; \quad F_0 = \frac{Q_0^2 b}{g{A_0}^3} = \frac{V_0}{\sqrt{gy_0}}; \quad \frac{\partial S_f}{\partial Q} = 2\frac{S_0}{Q_0}; \quad \frac{\partial S_f}{\partial A} = -2c\frac{S_0}{Q_0}.$$

Here, V_0 is the linearized reference value of the flow velocity, F_0 is the linearized reference value of F, y_0 is linearized reference value of the flow depth, c is the kinematic wave speed [30] which is related to V_0 through the relation $c^* = c/V_0$. In addition to the regular assumptions for the SVEs, it is further assumed that the flow is sub-critical (i.e., $F_0 < 1$). Differentiating Eq. (2.6) with respect to x and Eq. (2.7) with respect to t, and then combining them, the following equation is obtained:

$$-\frac{\partial^2 Q_1}{\partial t^2} - 2V_0\frac{\partial^2 Q_1}{\partial x \partial t} + (1 - {F_0}^2)gy_0\frac{\partial^2 Q_1}{\partial x^2} - gA_0\frac{\partial S_f}{\partial Q}\frac{\partial Q_1}{\partial t} + gA_0\frac{\partial S_f}{\partial A}\frac{\partial Q_1}{\partial x} = gA_0\frac{\partial S_f}{\partial A}q_l. \tag{2.8}$$

Equation (2.8) can be perceived as the linearized dynamic wave equation which governs the propagation of shallow water waves. We now present a solution to this equation satisfying initial and boundary conditions as follows:

$$Q_1(x,0) = Q_1(0,0) + q_l(0)x, \qquad \frac{\partial Q_1}{\partial t}(x,0) = 0,$$

$$Q_1(0,t) = Q_u(t), \qquad Q_1(L,t) = Q_d(t).$$

2.2 Proposed method and analytical solution

Laplace transform has been found to be the most popular method used by many researchers, e.g., [16, 37, 41, 52] to solve any form of the SVEs. We apply the Laplace transform to Eq. (2.8) with respect to the variable t, and this results in a second-order non-homogeneous ordinary differential equation as follows:

$$\begin{aligned}(1 - {F_0}^2)gy_0\frac{\mathrm{d}^2\overline{Q}_1}{\mathrm{d}x^2} + \left(gA_0\frac{\partial S_f}{\partial A} - 2V_0 s\right)\frac{\mathrm{d}\overline{Q}_1}{\mathrm{d}x} - \left(sgA_0\frac{\partial S_f}{\partial Q} + s^2\right)\overline{Q}_1 = \\ gA_0\frac{\partial S_f}{\partial A}\overline{q_l} - \left[2V_0 q_l(0) + s(Q_1(0,0) + q_l(0)x) + gA_0\frac{\partial S_f}{\partial Q}(Q_1(0,0) + q_l(0)x)\right],\end{aligned} \tag{2.9}$$

where $\overline{Q}_1(x,s)$ and $\overline{q_l}(s)$ are the Laplace transforms of $Q_1(x,t)$ and $q_l(t)$, respectively. The transformed boundary conditions are obtained as

$$\overline{Q}_1(0,s) = \overline{Q}_u(s) \quad \text{and} \quad \overline{Q}_1(L,s) = \overline{Q}_d(s). \tag{2.10}$$

The solution corresponding to the homogeneous part of Eq. (2.9) is

$$\overline{Q}_1(x,s) = c_1(s)\exp(\alpha_1(s)x) + c_2(s)\exp(\alpha_2(s)x). \tag{2.11}$$

Here $\alpha_1(s)$ and $\alpha_2(s)$ are the roots of the auxiliary equation corresponding to Eq. (2.9) given by

$$\alpha_{1,2}(s) = a_1 s + a_2 \pm \sqrt{a_3 s^2 + a_4 s + a_5},$$

where

$$a_1 = \frac{V_0}{gy_0(1-F_0{}^2)}; \qquad a_2 = \frac{cS_0}{(1-F_0{}^2)V_0 y_0}; \qquad a_3 = \frac{V_0{}^2 + (1-F_0{}^2)gy_0}{(1-F_0{}^2)^2 g^2 y_0{}^2};$$

$$a_4 = \frac{2S_0(cV_0 + (1-F_0{}^2)gy_0)}{(1-F_0{}^2)^2 y_0{}^2 g V_0}; \qquad a_5 = \frac{S_0{}^2 c^2}{(1-F_0{}^2)^2 V_0{}^2 y_0{}^2}.$$

The method of undetermined coefficients is employed to evaluate the particular integral for the non-homogeneous component of Eq. (2.9). By considering $\overline{Q}_1(x,s) = (l_1 + l_2 x)$, where l_1 and l_2 are the associated coefficients, and by using this as the particular integral of Eq. (2.9), we get l_1 and l_2 as

$$l_1 = \frac{-gA_0\dfrac{\partial S_f}{\partial A}\overline{q_l} + 2V_0 q_l(0) + \left(gA_0\dfrac{\partial S_f}{\partial Q} + s\right)Q_1(0,0) + X_1(s)l_2}{X_2(s)}, \tag{2.12}$$

$$\text{with} \qquad l_2 = \frac{sq_l(0) + gA_0 q_l(0)\dfrac{\partial S_f}{\partial Q}}{X_2(s)}, \tag{2.13}$$

$$\text{where} \qquad X_1(s) = gA_0\frac{\partial S_f}{\partial A} - 2V_0 s, \qquad X_2(s) = s^2 + sgA_0\frac{\partial S_f}{\partial Q}.$$

The general solution of $\overline{Q}_1(x,s)$ can be written as

$$\overline{Q}_1(x,s) = c_1(s)\exp(\alpha_1(s)x) + c_2(s)\exp(\alpha_2(s)x) + l_1 + l_2 x. \tag{2.14}$$

From here onward, we write $\alpha_1(s)$ and $\alpha_2(s)$ simply as α_1 and α_2, respectively, for convenience. We solve for $c_1(s)$ and $c_2(s)$ by using the transformed boundary conditions given in Eq. (2.10), and rewrite the general solution given in Eq. (2.14) as

$$\begin{aligned}\overline{Q}_1(x,s) = {}& \frac{\overline{Q}_u(s)\exp(\alpha_2 L) - \overline{Q}_d(s)}{\exp(\alpha_2 L) - \exp(\alpha_1 L)}\exp(\alpha_1 x) + \frac{\overline{Q}_d(s) - \overline{Q}_u(s)\exp(\alpha_1 L)}{\exp(\alpha_2 L) - \exp(\alpha_1 L)}\exp(\alpha_2 x) \\ & + l_1\left(\frac{1-\exp(\alpha_2 L)}{\exp(\alpha_2 L) - \exp(\alpha_1 L)}\exp(\alpha_1 x) - \frac{1-\exp(\alpha_1 L)}{\exp(\alpha_2 L) - \exp(\alpha_1 L)}\exp(\alpha_2 x) + 1\right)\end{aligned}$$

$$+ l_2 \left(\frac{L\left(\exp(\alpha_1 x) - \exp(\alpha_2 x)\right)}{\exp(\alpha_2 L) - \exp(\alpha_1 L)} + x \right). \tag{2.15}$$

If it is assumed that $q_l(0) = 0$ and $Q_1(0,0) = 0$, it implies that no perturbation exists for the reference flow discharge Q_0 before the application of the input. Then, the expressions for l_1 and l_2 reduce to

$$l_1 = \frac{-gA_0 \dfrac{\partial S_f}{\partial A} \overline{q_l}}{s^2 + sgA_0 \dfrac{\partial S_f}{\partial Q}}, \qquad l_2 = 0.$$

Subsequently, the general solution takes the form

$$\overline{Q}_1(x,s) = \frac{\overline{Q}_u(s)\exp(\alpha_2 L) - \overline{Q}_d(s)}{\exp(\alpha_2 L) - \exp(\alpha_1 L)} \exp(\alpha_1 x) + \frac{\overline{Q}_d(s) - \overline{Q}_u(s)\exp(\alpha_1 L)}{\exp(\alpha_2 L) - \exp(\alpha_1 L)} \exp(\alpha_2 x)$$
$$+ \left[\frac{(1-\exp(\alpha_1 L))\exp(\alpha_2 x)}{\exp(\alpha_2 L) - \exp(\alpha_1 L)} - \frac{(1-\exp(\alpha_2 L))\exp(\alpha_1 x)}{\exp(\alpha_2 L) - \exp(\alpha_1 L)} - 1 \right] \frac{gA_0 \dfrac{\partial S_f}{\partial A} \overline{q_l}}{s^2 + sgA_0 \dfrac{\partial S_f}{\partial Q}}. \tag{2.16}$$

2.2.1 Inverse transformation

The inverse of $\overline{Q}_1(x,s)$ in Eq. (2.16) can be written as

$$Q_1(x,t) = Q_u(t) \circledast h_u(x,t) + Q_d(t) \circledast h_d(x,t) + q_l(t) \circledast h_{lat}(x,t), \tag{2.17}$$

where $\circledast$ represents the convolution of two Laplace transformable functions; h_u is the upstream boundary response function, h_d is the downstream boundary response function and their expressions have already been found by Dooge and Napiórkowski [16] without the inclusion of any lateral inflow. The last term in Eq. (2.17) represents the flow discharge obtained due to the consideration of the uniformly distributed lateral inflow. This term can be added to the solution obtained by Dooge and Napiórkowski [16] to obtain the complete solution. Focusing on the contribution of the lateral inflow, and denoting the roots by α_1, $\alpha_2 = k_1(s) \pm \sqrt{k_2(s)}$ with $k_1(s) = a_1 s + a_2$ and $k_2(s) = a_3 s^2 + a_4 s + a_5$, we get the expression for $\overline{h}_{lat}(x,s)$ with the help of Eq. (2.16) as

$$\overline{h}_{lat}(x,s) = 2c^* gS_0 \left\{ \frac{\exp(-(k_1(s) + \sqrt{k_2(s)})L) - 1}{\left(1 - \exp(-2L\sqrt{k_2(s)})\right)(s^2 + \beta s)} \exp\left(k_1(s)x - \sqrt{k_2(s)}x\right) \right.$$
$$\left. - \frac{\exp(-(k_1(s) + \sqrt{k_2(s)})L) - \exp(-2L\sqrt{k_2(s)})}{\left(1 - \exp(-2L\sqrt{k_2(s)})\right)(s^2 + \beta s)} \exp\left(k_1(s)x + \sqrt{k_2(s)}x\right) + \frac{1}{s^2 + \beta s} \right\}, \tag{2.18}$$

$$\text{where} \quad \beta = gA_0 \frac{\partial S_f}{\partial Q} = 2g\frac{S_0}{V_0}, \qquad gA_0 \frac{\partial S_f}{\partial A} = gA_0 \left(-2c\frac{S_0}{Q_0}\right) = -2c^* gS_0. \tag{2.19}$$

Moramarco et al. [37] had further simplified Eq. (2.16) by assuming a semi-infinite channel (i.e., $L \to \infty$) and considering $Q_u(t) = Q_d(t) = 0$. Here, a finite length channel is considered and the standard formulas for inverse Laplace transform given in Eqs. (1.27)−(1.30) in *Chapter 1, Section 1.4* are used. To find the inverse of $\overline{h}_{lat}(x,s)$, it is split into three parts as follows:

$$\overline{h}_{lat}(x,s) = 2c^* gS_0\left\{\overline{f}_1(x,s) + \overline{f}_2(x,s) - \overline{f}_3(x,s)\right\}, \tag{2.20}$$

where

$$\overline{f}_1(x,s) = \frac{1}{s^2+\beta s}, \tag{2.21}$$

$$\overline{f}_2(x,s) = \frac{\exp(-(k_1(s)+\sqrt{k_2(s)})L)-1}{1-\exp(-2L\sqrt{k_2(s)})}\exp\left(k_1(s)x - \sqrt{k_2(s)}x\right)\frac{1}{s^2+\beta s}, \tag{2.22}$$

$$\overline{f}_3(x,s) = \frac{\exp(-(k_1(s)+\sqrt{k_2(s)})L)-\exp(-2L\sqrt{k_2(s)})}{\left(1-\exp(-2L\sqrt{k_2(s)})\right)(s^2+\beta s)}\exp\left(k_1(s)x + \sqrt{k_2(s)}x\right). \tag{2.23}$$

Now, we can write

$$h_{lat}(x,t) = 2c^* gS_0\left\{\mathcal{L}^{-1}\{\overline{f}_1(x,s)\} + \mathcal{L}^{-1}\{\overline{f}_2(x,s)\} - \mathcal{L}^{-1}\{\overline{f}_3(x,s)\}\right\}, \tag{2.24}$$

$$\text{with } \mathcal{L}^{-1}\{\overline{f}_1(x,s)\} = \mathcal{L}^{-1}\left\{\frac{1}{\beta}\left(\frac{1}{s} - \frac{1}{s+\beta}\right)\right\} = \frac{1}{\beta}(1-\exp(-\beta t)). \tag{2.25}$$

The other two terms require further simplification. Therefore, $\overline{f}_2(x,s)$ and $\overline{f}_3(x,s)$ are rewritten in the following way:

$$\begin{aligned}
\overline{f}_2(x,s) &= \frac{1}{s^2+\beta s}\Big\{\exp\left(-k_1(s)(L-x)\right)\exp\left(-(L+x)\sqrt{k_2(s)}\right) \\
&\quad - \exp\left(\left(k_1(s) - \sqrt{k_2(s)}\right)x\right)\Big\}\sum_{m=0}^{\infty}\exp\left(-2mL\sqrt{k_2(s)}\right) \\
&= \sum_{m=0}^{\infty}\exp\left(-k_1(s)(L-x)\right)\exp\left(-(2mL+L+x)\sqrt{k_2(s)}\right)\frac{1}{s^2+\beta s} \\
&\quad - \sum_{m=0}^{\infty}\exp\left(k_1(s)x\right)\exp\left(-(2mL+x)\sqrt{k_2(s)}\right)\frac{1}{s^2+\beta s} \\
&= \sum_{m=0}^{\infty}(\overline{h}_1)_m(x,s) - \sum_{m=0}^{\infty}(\overline{h}_2)_m(x,s) = \overline{h}_1(x,s) - \overline{h}_2(x,s),
\end{aligned} \tag{2.26}$$

with

$$\begin{aligned}\mathcal{L}^{-1}\{\overline{f}_2(x,s)\} &= \mathcal{L}^{-1}\{\overline{h}_1(x,s)\} - \mathcal{L}^{-1}\{\overline{h}_2(x,s)\} \\ &= \sum_{m=0}^{\infty}\mathcal{L}^{-1}\{(\overline{h}_1)_m(x,s)\} - \sum_{m=0}^{\infty}\mathcal{L}^{-1}\{(\overline{h}_2)_m(x,s)\}, \qquad (2.27)\end{aligned}$$

where

$$\begin{aligned}&\mathcal{L}^{-1}\{(\overline{h}_1)_m(x,s)\} = \frac{1}{\beta}\left(1-\exp\left(-\beta t\right)\right) \circledast \left(\exp\left\{-(L-x)\left(a_2 - \frac{a_1 a_4}{2a_3}\right) - \frac{a_4 t}{2a_3}\right\}\right. \\ &\times \frac{\gamma\sqrt{a_3}(2mL+L+x)}{\sqrt{(t-a_1(L-x))^2 - a_3(2mL+L+x)^2}}\mathrm{I}_1\left(\gamma\sqrt{(t-a_1(L-x))^2 - a_3(2mL+L+x)^2}\right) \\ &\left.\times\,\mathrm{u}\big[t-(a_1(L-x)+\sqrt{a_3}(2mL+L+x))\big]\right) + \frac{1}{\beta}\exp\left(-a_2(L-x) - (2mL+L+x)\frac{a_4}{2\sqrt{a_3}}\right) \\ &\qquad\times\left\{1-\exp\big\{-\beta\big(t-(a_1(L-x)+\sqrt{a_3}(2mL+L+x))\big)\big\}\right\} \\ &\qquad\qquad\times\,\mathrm{u}\big[t-(a_1(L-x)+\sqrt{a_3}(2mL+L+x))\big], \qquad (2.28)\end{aligned}$$

and

$$\begin{aligned}&\mathcal{L}^{-1}\{(\overline{h}_2)_m(x,s)\} = \left(\exp\left\{\left(a_2 - \frac{a_1 a_4}{2a_3}\right)x - \frac{a_4 t}{2a_3}\right\}\frac{\gamma\sqrt{a_3}(2mL+x)}{\sqrt{(t+a_1 x)^2 - a_3(2mL+x)^2}}\right. \\ &\left.\times\,\mathrm{I}_1\left(\gamma\sqrt{(t+a_1x)^2 - a_3(2mL+x)^2}\right)\mathrm{u}[t-(\sqrt{a_3}(2mL+x)-a_1x)]\right) \circledast \frac{1}{\beta}(1-\exp\left(-\beta t\right)) \\ &\quad + \frac{1}{\beta}\exp\left(a_2 x - (2mL+x)\frac{a_4}{2\sqrt{a_3}}\right)\left\{1-\exp\{-\beta(t-(\sqrt{a_3}(2mL+x)-a_1x))\}\right\} \\ &\qquad\qquad\times\,\mathrm{u}\big[t-(\sqrt{a_3}(2mL+x)-a_1x)\big], \qquad (2.29)\end{aligned}$$

with $\gamma = \sqrt{\left(\frac{a_4}{2a_3}\right)^2 - \frac{a_5}{a_3}}$.

Similarly, we get

$$\begin{aligned}\overline{f}_3(x,s) &= \sum_{m=0}^{\infty}\exp(-k_1(s)(L-x))\exp\left(-(2mL+L-x)\sqrt{k_2(s)}\right)\frac{1}{s^2+\beta s} \\ &\quad - \sum_{m=0}^{\infty}\exp(k_1(s)x)\exp\left(-(2mL+2L-x)\sqrt{k_2(s)}\right)\frac{1}{s^2+\beta s} \\ &= \sum_{m=0}^{\infty}(\overline{h}_3)_m(x,s) - \sum_{m=0}^{\infty}(\overline{h}_4)_m(x,s) = \overline{h}_3(x,s) - \overline{h}_4(x,s), \qquad (2.30)\end{aligned}$$

with

$$\begin{aligned}\mathcal{L}^{-1}\{\overline{f}_3(x,s)\} &= \mathcal{L}^{-1}\{\overline{h}_3(x,s)\} - \mathcal{L}^{-1}\{\overline{h}_4(x,s)\}\\ &= \sum_{m=0}^{\infty}\mathcal{L}^{-1}\{(\overline{h}_3)_m(x,s)\} - \sum_{m=0}^{\infty}\mathcal{L}^{-1}\{(\overline{h}_4)_m(x,s)\},\end{aligned} \tag{2.31}$$

where

$$\begin{aligned}&\mathcal{L}^{-1}\{(\overline{h}_3)_m(x,s)\} = \frac{1}{\beta}(1-\exp(-\beta t)) \circledast \left(\exp\left\{-(L-x)\left(a_2 - \frac{a_1 a_4}{2a_3}\right) - \frac{a_4 t}{2a_3}\right\}\right.\\ &\times \frac{\gamma\sqrt{a_3}(2mL+L-x)}{\sqrt{(t-a_1(L-x))^2 - a_3(2mL+L-x)^2}}\mathrm{I}_1\left(\gamma\sqrt{(t-a_1(L-x))^2 - a_3(2mL+L-x)^2}\right)\\ &\left.\times\, \mathrm{u}[t-(\sqrt{a_3}(2mL+L-x)+a_1(L-x))]\right) + \frac{1}{\beta}\exp\left(-a_2(L-x) - (2mL+L-x)\frac{a_4}{2\sqrt{a_3}}\right)\\ &\qquad\times\left\{1-\exp\{-\beta(t-(\sqrt{a_3}(2mL+L-x)+a_1(L-x)))\}\right\}\\ &\qquad\qquad\times\, \mathrm{u}\big[t-(\sqrt{a_3}(2mL+L-x)+a_1(L-x))\big],\end{aligned} \tag{2.32}$$

and

$$\begin{aligned}&\mathcal{L}^{-1}\{(\overline{h}_4)_m(x,s)\} = \frac{1}{\beta}(1-\exp(-\beta t)) \circledast \left(\exp\left\{\left(a_2 - \frac{a_1 a_4}{2a_3}\right)x - \frac{a_4 t}{2a_3}\right\}\right.\\ &\quad\times \frac{\gamma\sqrt{a_3}(2mL+2L-x)}{\sqrt{(t+a_1 x)^2 - a_3(2mL+2L-x)^2}}\mathrm{I}_1\left(\gamma\sqrt{(t+a_1 x)^2 - a_3(2mL+2L-x)^2}\right)\\ &\quad\left.\times\, \mathrm{u}[t-(\sqrt{a_3}(2mL+2L-x)-a_1 x)]\right) + \frac{1}{\beta}\exp\left(a_2 x - (2mL+2L-x)\frac{a_4}{2\sqrt{a_3}}\right)\\ &\times\left\{1-\exp\{-\beta(t-(\sqrt{a_3}(2mL+2L-x)-a_1 x))\}\right\}\mathrm{u}\big[t-(\sqrt{a_3}(2mL+2L-x)-a_1 x)\big].\end{aligned} \tag{2.33}$$

For the details of the derivation of the inverse, one may refer to Appendix A. The functions $\mathcal{L}^{-1}\{\overline{f}_1(x,s)\}$, $\mathcal{L}^{-1}\{\overline{f}_2(x,s)\}$, and $\mathcal{L}^{-1}\{\overline{f}_3(x,s)\}$ in Eq. (2.24) contain β in the denominator. Taking β out and still using the same terminology for the remaining functions, we get $(2c^* g S_0)/\beta = c$, which converts Eq. (2.24) into

$$h_{lat}(x,t) = c\Big\{\mathcal{L}^{-1}\{\overline{f}_1(x,s)\} + \mathcal{L}^{-1}\{\overline{f}_2(x,s)\} - \mathcal{L}^{-1}\{\overline{f}_3(x,s)\}\Big\}. \tag{2.34}$$

Setting the upstream and downstream boundary values of the flow discharge as the reference discharge, for a unit impulse input at time $t = 0$ distributed uniformly along the length of the channel, the interpretation for the lateral channel response function can be given as the total flow discharge obtained at a particular location x in a channel of length L at some time $t > 0$ corresponding to this impulse input.

2.3 Results and discussion

It is to be noted that our results involve calculations of series summations of terms from $m = 0$ to ∞. The time duration considered here is from 0 to 300 minutes. As it can be observed, unit step function and exponential function are present in almost all the terms of $h_{lat}(x,t)$. The summation index m is present in the argument of the unit step functions and exponential functions. As m increases, for this choice of the time interval, most of the terms in the series reduce to zero. If one wants to evaluate the solution for a different time interval, the same issue will surface. After a while, most of the terms in the series summation will become zero because of the unit step functions. The presence of the exponential function with negative argument also decays the value of the response function. For any time t along with given values of the physical characteristics, the evaluation of the response function is possible at any location x of the channel. The physical parameters used here are given next. For the whole study, the upstream and downstream boundary values are set the same as the reference flow discharge which allows us to take zero boundary condition for the perturbed quantity, i.e., $Q_u(t) = Q_d(t) = 0$.

The objective is to study the behavior of the lateral channel response function and to plot hydrographs for a lateral inflow with the input taken from Moramarco et al. [37]. By considering some fixed parameter values such as $S_0 = 0.0002$, $n = 0.04\ m^{-1/3}s$, $b = 20\ m$, and $Q_m = 0.6752\ m^3s^{-1}$, we present the lateral channel response function. To use the discrete convolution in place of the continuous one, we use a time step of $\delta t = 30\ s$, since smaller time steps give more accurate values of the discrete convolution (Wang et al. [54]). Here m stands for meter and s stands for second†. To calculate the final solution, it is required to know the reference values of the flow discharge, velocity, cross-section area and Froude number in advance. As this solution is for a sub-critical flow only, there is a requirement to pick values while keeping $F_0 < 1$. Either F_0 and V_0 can be chosen first and then be used to evaluate Q_0 and A_0 or it can be done the other way around, i.e., first choosing Q_0 and A_0 and then calculating F_0 and V_0. Here, Q_0 is taken as the mean flow discharge of the lateral inflow input and then A_0 is calculated by using Manning's formula, with the assumption of a steady uniform flow:

$$Q_0 = \frac{1}{n} A_0 R^{2/3} \sqrt{S_0}, \tag{2.35}$$

where R is the hydraulic radius with $R = A_0/P$. Here P is the wetted perimeter, which,

†These are not to be confused with the summation index m and Laplace transform variable s used elsewhere.

for a rectangular channel is

$$P = \frac{A_0}{b + 2\frac{A_0}{b}}. \tag{2.36}$$

We study the behavior of the lateral channel response function at different locations of the channel for different parameters like reference flow discharge, Manning's roughness coefficient, channel length, width and bottom slope of the channel. This is achieved by plotting lateral channel response function against time corresponding to different values of a specific parameter as per the requirement. We also compare the present hydrographs with one of the hydrographs plotted in [37]. The obtained results are presented next.

2.3.1 Behavior of lateral channel response function (h_{lat}) at a fixed location for different channel length L

The observation regarding the limitation of the work of Moramarco et al. [37] is that they presented the solution for semi-infinite channels only, and this result fails to work for channels of smaller length where the downstream boundary condition can have a significant effect on the flow discharge at different locations. In the process of considering a channel as a semi-infinite one, the effect of the downstream boundary was ignored. Although taking $L \to \infty$ simplified the process of calculating the inverse but it overestimated the flow discharge corresponding to the uniformly distributed lateral inflow at different locations. For a channel of finite length, their result seems not useful since it gives the same result for every location x of the channel, no matter what channel length is considered.

In Fig. 2.2, the response function for the flow discharge is plotted at location $x = 990\ m$ for different values of L with some fixed values of the parameters. For comparison, $h_{lat}(x,t)$ from Eq. (2.34) and the corresponding part of the analytical solution from Moramarco et al. [37] are plotted for different channel lengths. As can be observed in Fig. 2.2, the response function taken from [37] is the same for $x = 990\ m$, no matter what channel length is considered. For $L = 1500\ m$, the response function at $x = 990\ m$ approaches zero sooner as compared to larger values of L. This may have happened because the downstream boundary value is set the same as Q_0 and the distance between x and the downstream boundary is small. The response function at $x = 990\ m$ for $L = 3000\ m$ is almost the same as that of Moramarco et al. [37] which means that, for $x = 990\ m$, the downstream boundary can be ignored. We can further say that, for the considered parameters, any channel length less than 3000 m affects the hydrographs plotted at $x = 990\ m$ or upstream to this location. Therefore, the result presented here is expected to produce more feasible values in estimating the outflow for channels of smaller lengths than the one in [37].

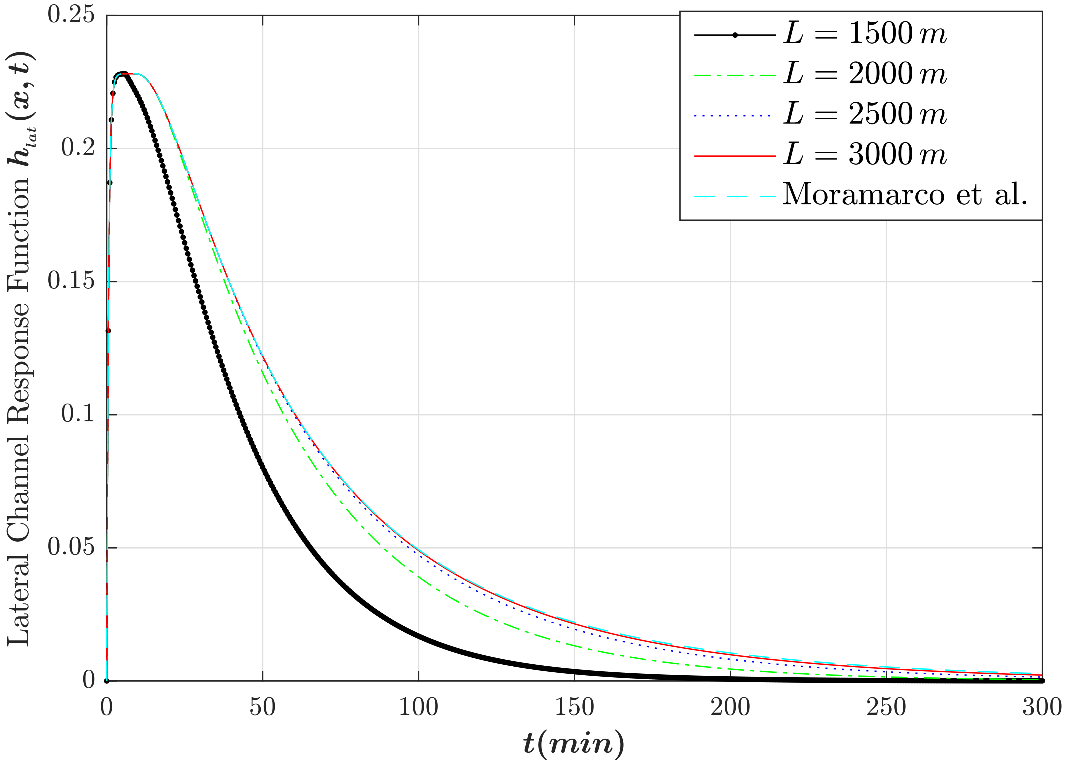

Figure 2.2: Lateral channel response function for $x = 990\ m$, $Q_0 = Q_m$, $S_0 = 0.0002$, $b = 20\ m$, $n = 0.04\ m^{-1/3}s$ with $Q_u(t) = Q_d(t) = 0$

2.3.2 Behavior of $h_{lat}(x,t)$ at different locations of the channel for different values of base flow Q_0

To understand the effect of Q_0, the response function for the flow discharge is plotted in Fig. 2.3, at different locations of the channel for different values of Q_0 by fixing other parameters for a channel length $L = 1000\ m$. For Fig. 2.3, we consider four locations of the channel, viz., $x = 10\,, 400\,, 600$ and $990\ m$. It can be observed that different choice of the base flow has a significant effect on the response function which reaches its maximum very quickly, and then there is a sudden decline in that maximum. For the locations closer to the upstream boundary (i.e., for $x = 10\ m$) and downstream boundary (i.e., for $x = 990\ m$), it is observed that smaller the value of Q_0, higher is the maximum of the response function. As the reference flow discharge decreases, the response function reduces in such a way that it approaches zero at a later time as compared to the higher values of the reference flow discharge. This may have happened because the flow discharge at the upstream and downstream end is set the same as the reference flow discharge. For a location near the mid portion of the channel, this behavior is completely reversed as can be seen from Fig. 2.3. For these locations, the decay in the maximum of the response function is also smoother for lower values of the base flow as compared with the higher

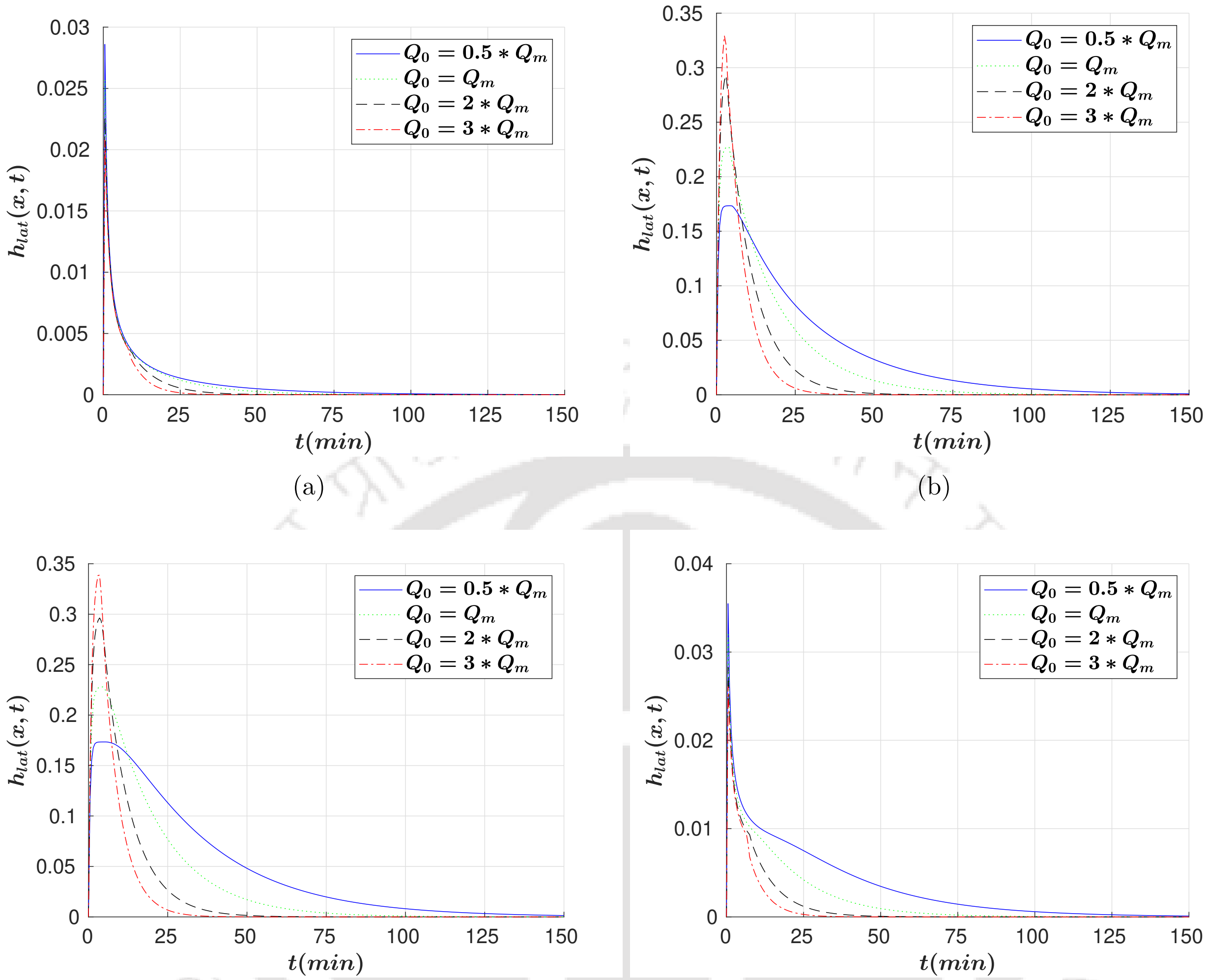

Figure 2.3: Lateral channel response function ($h_{lat}(x,t)$) at different location for (a) $x = 10\ m$, (b) $x = 400\ m$, (c) $x = 600\ m$, (d) $x = 990\ m$; with $L = 1000\ m$, $S_0 = 0.0002, Q_m = 0.6752\ m^3 s^{-1}$, $b = 20\ m$, $n = 0.04\ m^{-1/3} s$, $Q_u(t) = Q_d(t) = 0$

ones. This may have happened because the effect of the upstream and downstream boundaries is at its minimum near the mid location of the channel. Therefore, we need to choose Q_0 carefully depending upon at which location of the channel we want to observe the hydrograph.

2.3.3 Behavior of $h_{lat}(x,t)$ at different locations of the channel for different values of channel width b

To understand the effect of the channel width, the response function for the flow discharge is plotted in Fig. 2.4, at different locations of the channel for different values of b keeping the length of the channel and other parameters fixed. We show the results for four locations of the channel, viz., $x = 10\,,500\,,800$ and $990\ m$. In Fig. 2.4, we can

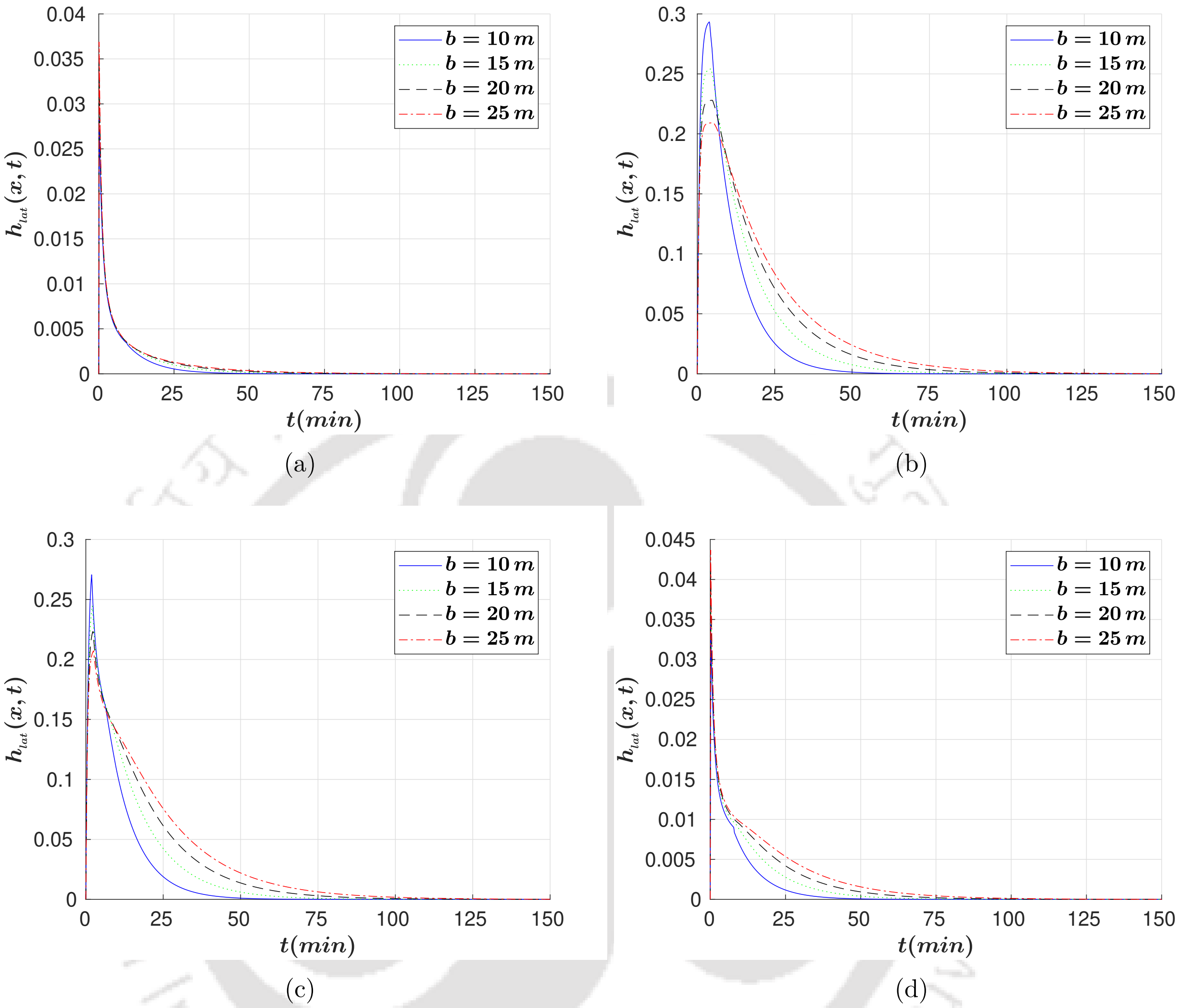

Figure 2.4: Lateral channel response function ($h_{lat}(x,t)$) at different location for (a) $x = 10\ m$, (b) $x = 500\ m$, (c) $x = 800\ m$, (d) $x = 990\ m$; with $L = 1000\ m$, $S_0 = 0.0002$, $Q_0 = 0.675\ m^3/s$, $n = 0.04\ m^{-1/3}s$, $Q_u(t) = Q_d(t) = 0$

observe that, for different values of the channel width, there is a significant effect on the response function. For locations closer to the upstream and downstream boundaries, the response function reaches its maximum instantly and drops down giving a sharp peak. The upstream and downstream boundaries set at reference flow discharge have a significant effect on the response function as it can be observed that higher the value of b, higher is the maximum of response function for $x = 10,\ 990\ m$. For $x = 10\ m$, there is not much difference in the shape of the response function for different widths, except that they have different maxima. For $x = 990\ m$, as the channel width is increased, the response function reduces slowly corresponding to higher values of the channel width. At $x = 500\ m$, the response function reaches its maximum instantly but in place of a sharp peak, a smooth peak is observed. This smoothness reduces as we go closer to the downstream end which is observed in the case of $x = 800\ m$. For the locations away from the upstream or downstream ends, the decay in the maximum of the response function is also smoother for higher values of b as compared to the lower one. In contrast to the case of $x = 10\,m,\ 990\,m$, it is observed that, corresponding to lower values of b, higher maximum of the response function appears.

2.3.4 Behavior of $h_{lat}(x,t)$ at different locations of the channel for different values of channel roughness n

To analyse the effect of Manning's roughness coefficient, the response function for the flow discharge is plotted in Fig. 2.5, at different locations of the channel for different values of n keeping the length of the channel and other parameters fixed. We take the range of n from 0.02 to 0.05 for this study. Again, we show the results for the same locations of the channel. In Fig. 2.5, we observe that, Manning's roughness coefficient has a significant effect on the response function. For the locations closer to the upstream boundary and downstream boundary, the response function reaches its maximum instantly and drops down giving a sharp peak. For $x = 10\ m$, there is not much difference in the shape of the response function for different values of n, except that they have different maxima. For other cases, only after some variation in the dropping of the maxima, for all values of n, the response function converges after a certain time. Higher the value of n, lower is the maximum of the response function. This difference in peak has a significant effect on the hydrograph generated for any choice of the uniformly distributed lateral inflow hydrograph. The shape of the response function gets distorted after the drop in the peak as we go toward the downstream boundary which is not the case for the locations near the upstream boundary. One of the reasons for this behavior is the choice of the other reference parameters. For $b > 20\ m$, this sharpness fades away. For the locations near the downstream end, if we choose a smaller value of n, then we need a higher value of b to get a smooth graph of the response function. But the pattern of the graph will certainly be different from the one corresponding to the locations far away from downstream boundary. The dominance of the downstream boundary may be the other reason behind the different patterns of the graphs for the locations closer to it.

2.3.5 Behavior of $h_{lat}(x,t)$ at different locations of the channel for different values of channel bottom slope S_0

To study the effect of S_0, we plot the response function for the flow discharge in Fig. 2.6, at different locations of the channel for different values of S_0 keeping the values of L, Q_0, and n fixed. We take the range of S_0 from 0.0001 to 0.001 for this study. Depending

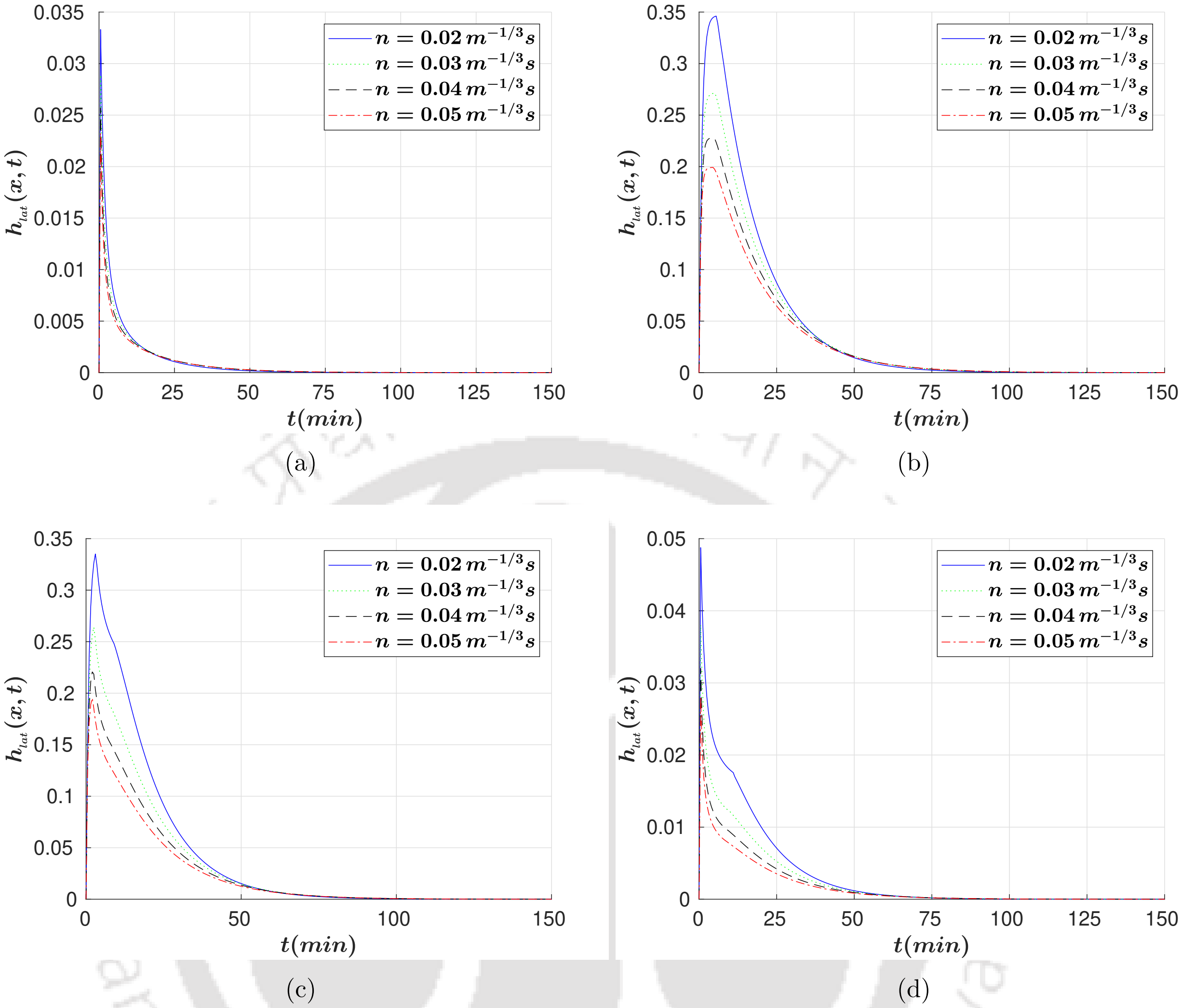

Figure 2.5: Lateral channel response function ($h_{lat}(x,t)$) at different location for (a) $x = 10\ m$, (b) $x = 500\ m$, (c) $x = 800\ m$, (d) $x = 990\ m$; with $L = 1000\ m$, $S_0 = 0.0002$, $Q_0 = 0.675\ m^3/s$, $b = 20\ m$, $Q_u(t) = Q_d(t) = 0$

on the value of S_0, we also change the width of the channel. For gentle bed slopes, a higher value of channel width can be considered but not for higher slopes. Again, we show the results for the same locations of the channel. In Fig. 2.6, we observe that changing the slope has a significant effect on the response function. For a location closer to the upstream boundary and downstream boundary, the response function reaches its maximum instantly and drops down giving a sharp peak. For $x = 10\ m$, there is not much difference in the shape of the response function for different slopes, except that they have different maxima. For all the channel locations, higher value of S_0 gives a higher maximum of the response function which achieves its highest peak in the case of $x = 500\ m$. As we move toward the downstream end, a reduction in its peak is observed. We can say that due to this behavior, we can predict the hydrograph for higher values of

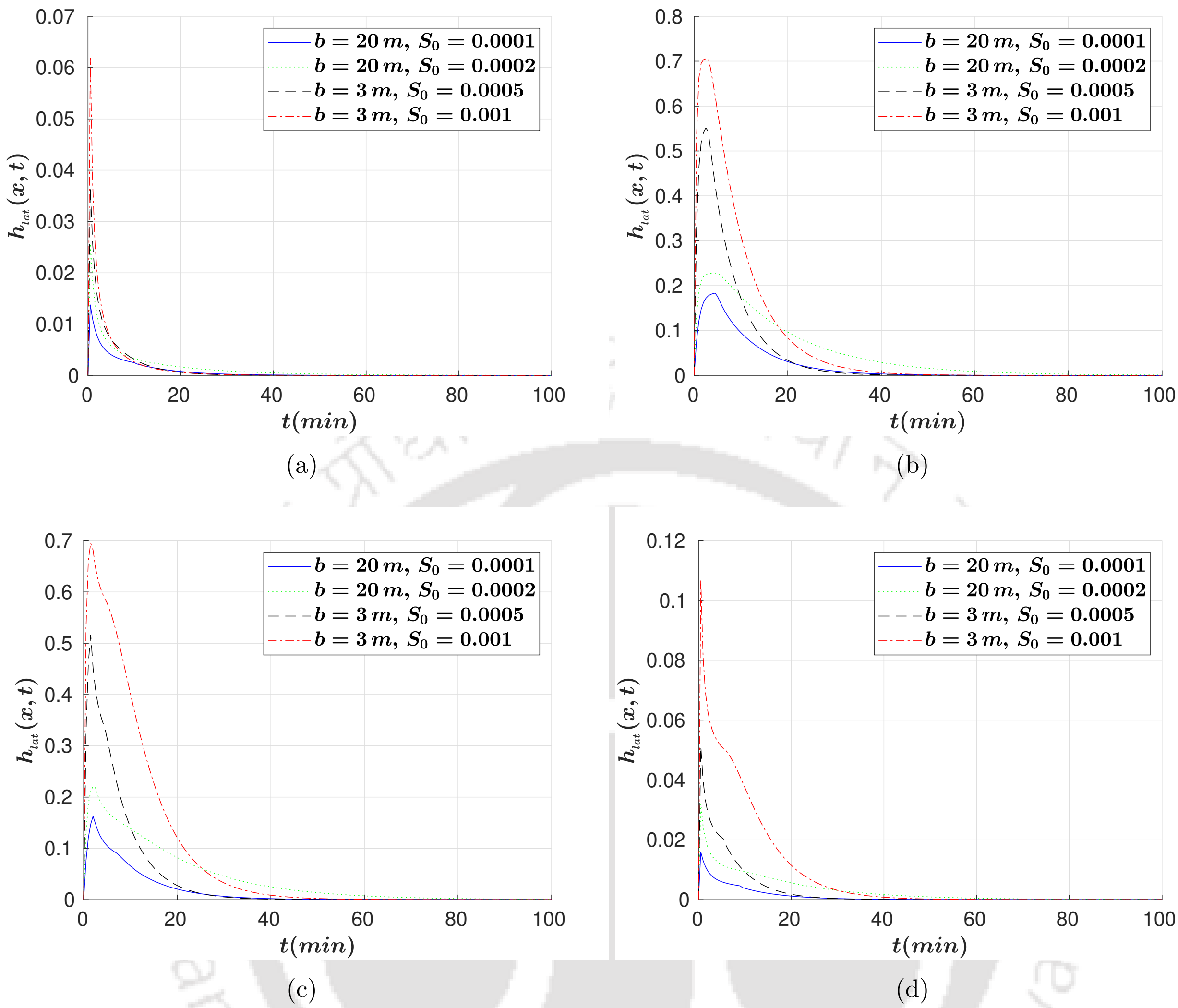

Figure 2.6: Lateral channel response function ($h_{lat}(x,t)$) at different location for (a) $x = 10\ m$, (b) $x = 500\ m$, (c) $x = 800\ m$, (d) $x = 990\ m$; with $L = 1000\ m$, $Q_0 = 0.675\ m^3/s$, $n = 0.04\ m^{-1/3}s$, $Q_u(t) = Q_d(t) = 0$

the slope in a more profound way.

2.3.6 Comparison of hydrographs at different locations for a lateral inflow input taken from Moramarco et al. [37]

To plot hydrographs at different locations, a uniformly distributed lateral inflow is considered. Let $Q_l(t)$ be the total lateral inflow hydrograph. Then, for a uniformly distributed lateral inflow along the channel reach, we can take $q_l(t) = \dfrac{Q_l}{L}\,(m^2s^{-1})$ as also considered in [38]. To calculate the flow discharge from Eq. (2.17), we apply discrete convolution on $q_l(t)$ and $h_{lat}(x,t)$ in *MATLAB*. Through Fig. 2.7, we compare our result with that of Moramarco et al. [37] at $x = 1500\ m$ for the parameters considered

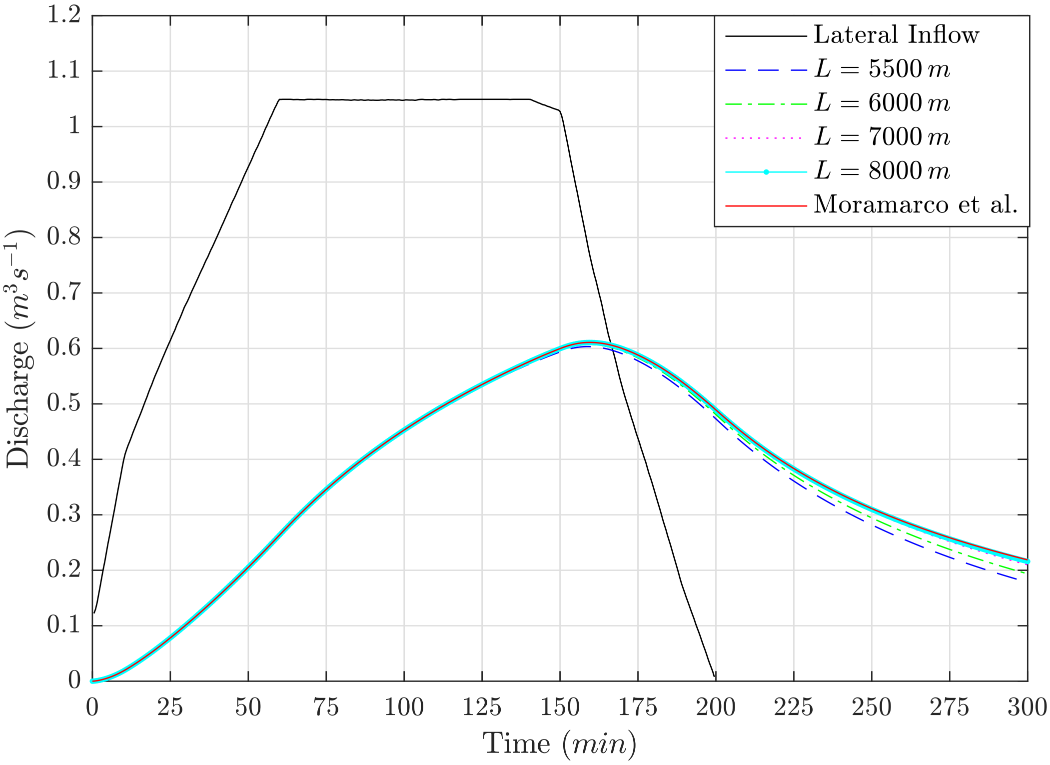

Figure 2.7: Hydrograph comparison at $x = 1500\ m$ for different channel lengths with $Q_0 = Q_m$, $S_0 = 0.0001$, $b = 10\ m$, $n = 0.05\ m^{-1/3}s$, $Q_u(t) = Q_d(t) = 0$

in [37], i.e., $Q_0 = Q_m$, $S_0 = 0.0001$, $b = 10\ m$, $n = 0.05\ m^{-1/3}s$. For comparison, we take the inflow hydrograph to be the same as the one in [37]. Their analytical solution is independent of the channel length but they considered a channel length of 1500 m for observation and plotted the hydrographs at the downstream end. We consider different lengths of the channel and observe here that, for these parameters, as we increase the length of the channel, the outflow agrees with that in [37]. Relying on the fact that their solutions work well for semi-infinite channels, this result shows, for $x = 1500\ m$, which channel lengths can actually be considered as semi-infinite ones where the effect of the downstream boundary condition can be ignored. For the flow discharge at $x = 1500\ m$ in a channel of length $L = 5000\ m$, the result obtained in [37] seems to have overestimated the outflow hydrograph. From this observation, we can infer that, for $x = 1500\ m$ or any location upstream to this location, any channel of length greater than 6000 m (approx.) can only behave like a semi-infinite channel corresponding to these parameters.

In Fig. 2.8, our result is compared with that of Moramarco et al. [37] at $x = 1500\ m$ for the parameters considered in [37], i.e., $Q_0 = Q_m$, $S_0 = 0.001$, $b = 3\ m$, $n = 0.03\ m^{-1/3}s$. We take different lengths of the channel and observe that, for these parameters, as the length of the channel is increased, the outflow agrees well with the inflow hydrograph with a shift at the time of the peak of the hydrograph. For the flow discharge at $x = 1500\ m$ in a

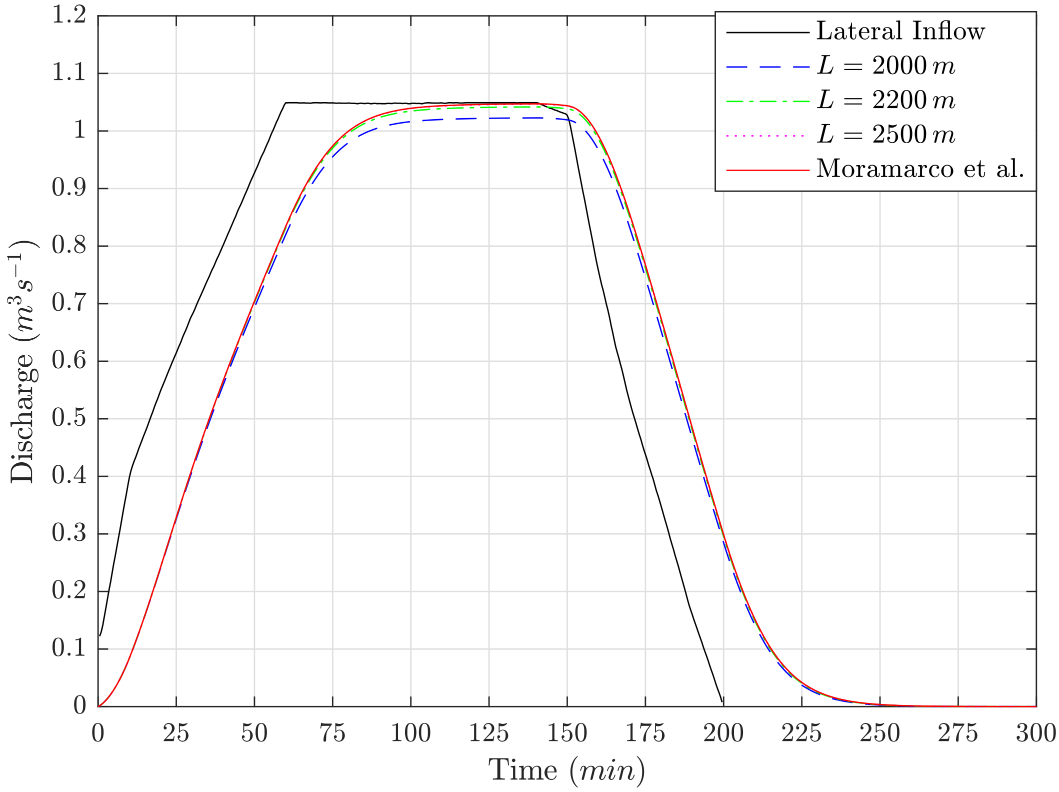

Figure 2.8: Hydrograph comparison at $x = 1500\ m$ for different channel lengths with $Q_0 = Q_m$, $S_0 = 0.001$, $b = 3\ m$, $n = 0.03\ m^{-1/3}s$, $Q_u(t) = Q_d(t) = 0$

channel of length $L = 2000\ m$, the result obtained in [37] seemed to have overestimated the outflow hydrograph. This implies that, for each distinct slope, a different interpretation of semi-infinite length channel can be given. Accordingly, for the hydrograph at $x = 1500\ m$ or for that matter, at any location upstream to this one, any length of the channel greater than or equal to 2200 m, which is much smaller in comparison with the one observed in Fig. 2.7, falls under the category of semi-infinite length for a channel corresponding to these parameters.

2.4 Conclusion

An attempt has been made to find an expression for the flow discharge obeying the linearized SVEs with a uniformly distributed lateral inflow for a finite length rectangular channel and to present the analytical solution mainly with respect to the response function. The primary focus is on the study of the effect of the lateral inflow, for which the upstream and downstream boundary values are kept as the same as the reference flow discharge. Two cases of outflow hydrograph have been discussed. For rectangular channels, this result can be combined with that of Dooge and Napiórkowski [16] to get the complete solution of the linearized SVEs with the lateral inflow and the flow discharge for non-zero upstream and downstream boundary conditions. We have emphasized on the behavior of the response function corresponding to the lateral inflow and named it "lateral channel response function" which gets affected by the presence of both the upstream as well as the downstream boundary conditions. In all the cases, the peak of the response function for $x = 500\ m$ was up to 10 times of the peak for the locations near the upstream and downstream ends. It is concluded here that this difference gives the maximum peak of the hydrograph near the mid-point location of the channel. Because the upstream and downstream boundaries were set at the reference flow discharge value, for a particular choice of lateral inflow hydrograph, a smaller peak for the locations near the ends was observed. From Figs. 2.2−2.6, it was observed that, for small length channels, the influence of the upstream and downstream boundaries on the lateral channel response function is significant which was clearly visible in the corresponding hydrographs as well. As can be observed from Figs. 2.7 and 2.8, the hydrographs changed significantly for smaller slopes. Here, the reference flow discharge was very small, and although this reference flow discharge can work fine for larger values of the slope, but for flat channels, much larger values of Q_0 are required to be considered. Therefore, in choosing the reference flow discharge, utmost care is to be taken since, for wider channels, there is a requirement of greater reference flow discharge for an accurate prediction of the hydrograph. The interpretation of semi-infinite channels also varies with respect to the considered slope of the channel. Our main observation in this respect is that the downstream boundary condition cannot always be ignored and for these cases, we observe its influence on the hydrographs plotted upstream. By comparing our results with those of Moramarco et al. [37], we have tried to provide the feasibility of the situation when it is appropriate to ignore the downstream boundary. The presented form of the analytical solution will hold for other prismatic channels as well.

CHAPTER 3

Diffusive wave model in a finite length channel with different types of lateral inflow subject to a flow-depth hydrograph at the downstream end

In this chapter, an analytical solution is presented for the linearized diffusive wave model represented by a simultaneous system of two first-order partial differential equations focused on the spatial variation of the lateral inflow in a finite channel. A concentrated lateral inflow which can represent the case of an inflow from a small-width tributary is considered through the Dirac delta function, while a uniformly distributed lateral inflow between any two locations is represented through the unit-step function. The Laplace transform method is used to solve these equations analytically. Two types of upstream boundaries are considered here: a flow-discharge hydrograph and a flow-depth hydrograph, while keeping a flow-depth hydrograph as the downstream boundary. Using unit-step responses, the effect of different boundaries and lateral inflows on the flow discharge and the flow depth is studied corresponding to different values of the Péclet number.

3.1 Mathematical formulation

3.1.1 Governing equations and the proposed method

The diffusive wave approximation of the SVEs ignores the effect of inertial forces and is described by the following equations in the unknowns Q and h [10]:

$$\frac{1}{b}\frac{\partial Q}{\partial x} + \frac{\partial h}{\partial t} = \frac{q_l}{b}, \tag{3.1}$$

$$\frac{\partial h}{\partial x} = S_0 - S_f, \tag{3.2}$$

where x and t are the independent space and time variables, respectively; $h(x,t)$ is the flow depth; $Q(x,t)$ is the flow discharge; $b(h)$ is the water surface width; $q_l(x,t)$ is the lateral inflow per unit length; S_0 is the bed slope; $S_f(Q,h)$ is the friction slope. A schematic diagram corresponding to the formulated problem is given in Fig. 3.1.

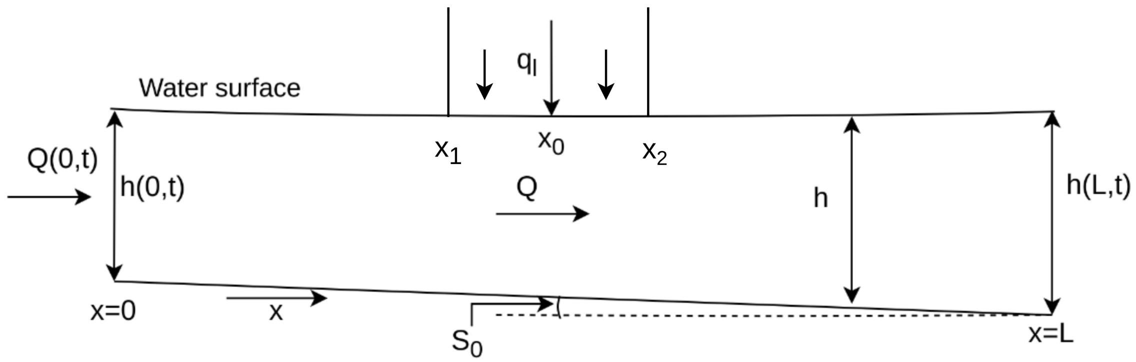

Figure 3.1: A schematic diagram for the formulated problem

Following the work of Cimorelli et al. [7], we consider a prismatic channel in order to linearize Eqs. (3.1) and (3.2). When the flow is perturbed, the unknown variables Q and h can be written as

$$Q(x,t) = Q_0 + Q_1(x,t) + \text{ higher-order terms,} \tag{3.3}$$

$$h(x,t) = h_0 + h_1(x,t) + \text{ higher-order terms,} \tag{3.4}$$

where (Q_0, h_0) are the reference values corresponding to the uniform-steady flow; (Q_1, h_1) are the first-order increments with higher-order terms being ignored. The friction slope is dependent on Q and h, and its Taylor series expansion around the point (Q_0, h_0) can be expressed as follows [16]:

$$S_f = S_f(Q_0, h_0) + \left(\frac{\partial S_f}{\partial Q}\right)_0 (Q - Q_0) + \left(\frac{\partial S_f}{\partial h}\right)_0 (h - h_0) + \text{ higher-order terms,} \tag{3.5}$$

where

$$\left(\frac{\partial S_f}{\partial Q}\right)_0 = \left.\frac{\partial S_f}{\partial Q}\right|_{(Q_0,h_0)}, \quad \left(\frac{\partial S_f}{\partial h}\right)_0 = \left.\frac{\partial S_f}{\partial h}\right|_{(Q_0,h_0)}.$$

Using Eqs. (3.3)−(3.5) in Eqs. (3.1) and (3.2), and ignoring the higher-order terms, we get

$$\frac{\partial Q_1}{\partial x} + b_0 \frac{\partial h_1}{\partial t} = q_l, \tag{3.6}$$

$$\frac{\partial h_1}{\partial x} + \left(\frac{\partial S_f}{\partial Q}\right)_0 Q_1 + \left(\frac{\partial S_f}{\partial h}\right)_0 h_1 = 0, \tag{3.7}$$

with $b_0 = b(h_0)$ as the linearized water surface width around the reference condition.

To simplify the formulation, the non-dimensional form of the variables can be considered as (Cimorelli et al. [7]):

$$t^* = t/\left(L/C_0\right), \quad x^* = x/L, \quad h^* = h_1/h_0, \quad Q^* = Q_1/Q_0, \text{ with } C_0 = -\frac{1}{b_0}\left(\frac{\partial S_f/\partial h}{\partial S_f/\partial Q}\right)_0, \tag{3.8}$$

where t^*, x^*, Q^*, h^* are the dimensionless time variable, the space variable, the flow discharge and the flow depth, respectively; L is the channel length and C_0 is the celerity of the linearized model. Using these dimensionless quantities in Eqs. (3.6) and (3.7), we get the following system:

$$\beta\frac{\partial h^*}{\partial t^*} + \frac{\partial Q^*}{\partial x^*} = q_l^*, \tag{3.9}$$

$$\frac{\partial h^*}{\partial x^*} + r_1 Q^* + r_2 h^* = 0, \tag{3.10}$$

where

$$q_l^* = q_l L/Q_0, \quad \beta = \frac{h_0}{Q_0} b_0 C_0, \quad r_1 = L\left(\frac{\partial S_f}{\partial Q}\right)_0 \frac{Q_0}{h_0}, \quad r_2 = L\left(\frac{\partial S_f}{\partial h}\right)_0. \tag{3.11}$$

Here, $q_l^*(x^*, t^*)$ is the dimensionless lateral inflow and β is the dimensionless water surface width. We assume that there is no perturbation in the flow depth and flow discharge before the application of any input, i.e., $h_1(x, 0) = 0$ and $Q_1(x, 0) = 0$. Then, applying Laplace transform on Eqs. (3.9) and (3.10), we get

$$\frac{\mathrm{d}\overline{Q^*}}{\mathrm{d}x^*} + \beta s \overline{h^*} = \overline{q_l^*}, \tag{3.12}$$

$$\frac{\mathrm{d}\overline{h^*}}{\mathrm{d}x^*} + r_1 \overline{Q^*} + r_2 \overline{h^*} = 0, \tag{3.13}$$

where $\overline{Q^*}(x^*, s)$, $\overline{h^*}(x^*, s)$, and $\overline{q_l^*}(x^*, s)$ are the Laplace transforms of $Q^*(x^*, t^*)$, $h^*(x^*, t^*)$, and $q_l^*(x^*, t^*)$, respectively. This system can also be written in the following form [7]:

$$\frac{\mathrm{d}\overline{U}(x^*, s)}{\mathrm{d}x^*} - M(s)\overline{U}(x^*, s) = R(x^*, s), \tag{3.14}$$

$$\text{where } \overline{U}(x^*,s) = \begin{bmatrix} \overline{Q^*}(x^*,s) \\ \overline{h^*}(x^*,s) \end{bmatrix}, \quad M(s) = \begin{bmatrix} 0 & -\beta s \\ -r_1 & -r_2 \end{bmatrix}, \quad R(x^*,s) = \begin{bmatrix} \overline{q_l^*}(x^*,s) \\ 0 \end{bmatrix}.$$

The solution of Eq. (3.14) is given by

$$\overline{U}(x^*,s) = \exp(M(s)x^*)\overline{U}(0,s) + \int_0^{x^*} \exp(M(s)\,(x^*-\phi))\,R(\phi,s)\mathrm{d}\phi, \tag{3.15}$$

where $\overline{U}(0,s) = \left(\overline{Q^*}(0,s)\ \overline{h^*}(0,s)\right)^T$ is the vector representing the upstream boundary condition. The entries α_{ij} of the matrix $\exp(M(s)x^*)$ were evaluated by Cimorelli et al. [7] by finding the eigenvalues and eigenvectors of the matrix $M(s)$ and these entries are as follows:

$$\alpha_{11}(x^*,s) = \exp\left(\frac{P_e x^*}{2}\right) \frac{\sqrt{Z}\cosh\left(\frac{x^*}{2}\sqrt{Z}\right) - P_e \sinh\left(\frac{x^*}{2}\sqrt{Z}\right)}{\sqrt{Z}}, \tag{3.16}$$

$$\alpha_{12}(x^*,s) = -2\beta s \exp\left(\frac{P_e x^*}{2}\right) \frac{\sinh\left(\frac{x^*}{2}\sqrt{Z}\right)}{\sqrt{Z}}, \tag{3.17}$$

$$\alpha_{21}(x^*,s) = -\frac{2P_e}{\beta} \exp\left(\frac{P_e x^*}{2}\right) \frac{\sinh\left(\frac{x^*}{2}\sqrt{Z}\right)}{\sqrt{Z}}, \tag{3.18}$$

$$\alpha_{22}(x^*,s) = \exp\left(\frac{P_e x^*}{2}\right) \frac{\sqrt{Z}\cosh\left(\frac{x^*}{2}\sqrt{Z}\right) + P_e \sinh\left(\frac{x^*}{2}\sqrt{Z}\right)}{\sqrt{Z}}, \tag{3.19}$$

with $Z = P_e^2 + 4P_e s$ where $P_e = C_0 L/D_0$ is the Péclet number; $D_0 = Q_0/(2b_0 S_0)$ is the linearized diffusivity coefficient. The significance of the Péclet number is already described in *Chapter 1, Section 1.3.*

Cimorelli et al. [7] further simplified Eq. (3.15) by replacing $\overline{q_l^*}(x^*,s)$ with $\overline{q_l^*}(s)$, and solved the given system of two ordinary differential equations. We try to use this method to study the effect of different types of lateral inflow. In many cases, the temporal and spatial components of the lateral inflow discharge $q_l(x,t)$ are independent. Consequently, we can write it as a product of two functions, i.e., $q_l(x,t) = X(x)T(t)$. Here, $X(x)$ represents the discharge distribution in space and $T(t)$ is the total discharge of the lateral inflow [19]. The non-dimensional form of $q_l(x,t)$ and the corresponding Laplace transform can be written, respectively, as

$$q_l^*(x^*,t^*) = \frac{X(x)}{1/L}\frac{T(t)}{Q_0} = X^*(x^*)T^*(t^*) \text{ and } \overline{q_l^*}(x^*,s) = X^*(x^*)\overline{T^*}(s), \tag{3.20}$$

where $\overline{T^*}(s)$ is the Laplace transform of $T^*(t^*)$.

We take up the problem for two types of lateral inflow as discussed below.

Concentrated lateral inflow: We first consider the case of a concentrated lateral inflow at some location of the channel. This can represent the cases where the lateral inflow is due to a tributary whose width is negligible in comparison with the length of the channel under study. For a concentrated lateral inflow at a location x_0, $X^*(x^*)$ can be expressed through the Dirac delta function $\delta(.)$ which satisfies the following property [44]:

$$\int_{-\infty}^{\infty} f(x^*)\delta(x^* - x_0^*)\mathrm{d}x^* = f(x_0^*), \quad \text{with} \quad \delta(x^* - x_0^*) = 0 \; \forall \; x^* \neq x_0^*, \tag{3.21}$$

for a function f. Here, x_0^* is the non-dimensional form of x_0, also called the source of the lateral inflow. Using Eqs. (3.20) and (3.21) in simplifying the integral of Eq. (3.15), we get

$$\begin{aligned}\int_0^{x^*} \exp(M(s)\,(x^* - \phi))\,R(\phi, s)\mathrm{d}\phi &= \overline{T^*}(s)\int_0^{x^*}\begin{bmatrix}\alpha_{11}(x^* - \phi, s)\delta(\phi - x_0^*)\\ \alpha_{21}(x^* - \phi, s)\delta(\phi - x_0^*)\end{bmatrix}\mathrm{d}\phi\\ &= \begin{cases}\overline{T^*}(s)\begin{bmatrix}\alpha_{11}(x^* - x_0^*, s)\\ \alpha_{21}(x^* - x_0^*, s)\end{bmatrix}, & \text{for } x^* > x_0^*,\\ 0, & \text{for } x^* < x_0^*.\end{cases}\end{aligned} \tag{3.22}$$

Finally, using Eqs. (3.15) and (3.22), we get the following form of the vector $\overline{U}(x^*, s)$:

$$\overline{U}(x^*, s) = \exp(M(s)x^*)\begin{bmatrix}\overline{Q^*}(0, s)\\ \overline{h^*}(0, s)\end{bmatrix} + \begin{bmatrix}\alpha_{11}(x^* - x_0^*, s)\overline{T^*}(s)\\ \alpha_{21}(x^* - x_0^*, s)\overline{T^*}(s)\end{bmatrix}, \quad \text{for } x^* > x_0^*, \tag{3.23a}$$

$$\overline{U}(x^*, s) = \exp(M(s)x^*)\begin{bmatrix}\overline{Q^*}(0, s)\\ \overline{h^*}(0, s)\end{bmatrix}, \quad \text{for } x^* < x_0^*. \tag{3.23b}$$

The system given in Eq. (3.23a) represents the effect of the lateral inflow concentrated at x_0^* on the subsequent downstream locations whereas the one in Eq. (3.23b) shows the effect on the locations upstream to the concentrated lateral inflow.

Distributed lateral inflow: The second type of lateral inflow is present between two locations along the length of the channel. This can represent the lateral inflow into a river from a tributary of reasonable width. We consider this lateral inflow to be uniformly distributed between locations x_1 and x_2 with x_1^* and x_2^* as the non-dimensional forms, respectively. Let the non-dimensional width of this portion be $x_2^* - x_1^*$. For this, $X^*(x^*)$ can be written as [19]

$$X^*(x^*) = \frac{\mathrm{u}(x^* - x_1^*) - \mathrm{u}(x^* - x_2^*)}{x_2^* - x_1^*} = \begin{cases}\dfrac{1}{x_2^* - x_1^*}, & \text{for } x^* \in [x_1^*, x_2^*],\\ 0, & \text{for } x^* \notin [x_1^*, x_2^*],\end{cases} \tag{3.24}$$

where u(.) is the unit-step function with $x_2^* - x_1^* \neq 0$. Using Eq. (3.24), the integral in Eq. (3.15) can be simplified as

$$\int_0^{x^*} \exp(M(s)\,(x^*-\phi))\,R(\phi,s)\mathrm{d}\phi = \frac{\overline{T^*}(s)}{x_2^*-x_1^*}\begin{cases} 0, & \text{for } 0 \le x^* < x_1^*, \\ \displaystyle\int_{x_1^*}^{x^*}\begin{pmatrix}\alpha_{11}(x^*-\phi,s)\\ \alpha_{21}(x^*-\phi,s)\end{pmatrix}\mathrm{d}\phi, & \text{for } x_1^* \le x^* < x_2^*, \\ \displaystyle\int_{x_1^*}^{x_2^*}\begin{pmatrix}\alpha_{11}(x^*-\phi,s)\\ \alpha_{21}(x^*-\phi,s)\end{pmatrix}\mathrm{d}\phi, & \text{for } x_2^* \le x^* \le 1, \end{cases}$$

$$= \begin{cases} 0, & \text{for } 0 \le x^* < x_1^* \\ \begin{pmatrix}\overline{T^*}(s)A_{11}(x^*,s)\\ \overline{T^*}(s)A_{21}(x^*,s)\end{pmatrix}, & \text{for } x^* \ge x_1^*, \end{cases} \tag{3.25}$$

with

$$A_{11}(x^*,s) = \frac{1}{s(x_2^*-x_1^*)}\exp\left(\frac{x^*-x_1^*}{2}P_e\right)\left\{\frac{P_e+2s}{\sqrt{Z}}\sinh\left(\frac{x^*-x_1^*}{2}\sqrt{Z}\right) - \cosh\left(\frac{x^*-x_1^*}{2}\sqrt{Z}\right)\right\} + \frac{1}{s(x_2^*-x_1^*)}, \quad \text{for } x_1^* \le x^* < x_2^*, \tag{3.26a}$$

$$A_{11}(x^*,s) = \frac{1}{s(x_2^*-x_1^*)}\exp\left(\frac{x^*-x_2^*}{2}P_e\right)\left\{\cosh\left(\frac{x^*-x_2^*}{2}\sqrt{Z}\right) - \frac{P_e+2s}{\sqrt{Z}}\sinh\left(\frac{x^*-x_2^*}{2}\sqrt{Z}\right)\right\} + \frac{1}{s(x_2^*-x_1^*)}\exp\left(\frac{x^*-x_1^*}{2}P_e\right)\left\{\frac{P_e+2s}{\sqrt{Z}}\sinh\left(\frac{x^*-x_1^*}{2}\sqrt{Z}\right) - \cosh\left(\frac{x^*-x_1^*}{2}\sqrt{Z}\right)\right\}, \quad \text{for } x_2^* \le x^* \le 1, \tag{3.26b}$$

$$A_{21}(x^*,s) = \frac{1}{\beta s(x_2^*-x_1^*)}\exp\left(\frac{x^*-x_1^*}{2}P_e\right)\left\{\frac{P_e}{\sqrt{Z}}\sinh\left(\frac{x^*-x_1^*}{2}\sqrt{Z}\right) - \cosh\left(\frac{x^*-x_1^*}{2}\sqrt{Z}\right)\right\} + \frac{1}{\beta s(x_2^*-x_1^*)}, \quad \text{for } x_1^* \le x^* < x_2^*, \tag{3.27a}$$

$$A_{21}(x^*,s) = \frac{1}{\beta s(x_2^*-x_1^*)}\exp\left(\frac{x^*-x_2^*}{2}P_e\right)\left\{\cosh\left(\frac{x^*-x_2^*}{2}\sqrt{Z}\right)\right.$$

$$
\begin{aligned}
& - \frac{P_e}{\sqrt{Z}} \sinh\left(\frac{x^* - x_2^*}{2}\sqrt{Z}\right)\Bigg\} \\
& + \frac{1}{\beta s(x_2^* - x_1^*)} \exp\left(\frac{x^* - x_1^*}{2} P_e\right)\Bigg\{\frac{P_e}{\sqrt{Z}} \sinh\left(\frac{x^* - x_1^*}{2}\sqrt{Z}\right) \\
& - \cosh\left(\frac{x^* - x_1^*}{2}\sqrt{Z}\right)\Bigg\}, \text{ for } x_2^* \le x^* \le 1.
\end{aligned} \tag{3.27b}
$$

Finally, using Eqs. (3.15) and (3.25), we get the following form of the vector $\overline{U}(x^*, s)$:

$$
\overline{U}(x^*, s) = \exp(M(s)x^*) \begin{bmatrix} \overline{Q^*}(0, s) \\ \overline{h^*}(0, s) \end{bmatrix} + \begin{bmatrix} A_{11}(x^*, s)\overline{T^*}(s) \\ A_{21}(x^*, s)\overline{T^*}(s) \end{bmatrix}, \qquad \text{for } x^* \ge x_1^*, \tag{3.28a}
$$

$$
\overline{U}(x^*, s) = \exp(M(s)x^*) \begin{bmatrix} \overline{Q^*}(0, s) \\ \overline{h^*}(0, s) \end{bmatrix}, \qquad \text{for } x^* < x_1^*. \tag{3.28b}
$$

The system given in Eq. (3.28a) represents the effect of the lateral inflow on locations downstream to x_1^*, whereas the one in Eq. (3.28b) shows the effect on the locations upstream to x_1^*.

3.2 Solution in the time domain

It is assumed that $Q^*(0, t^*)$, $h^*(0, t^*)$ and $h^*(1, t^*)$ as well as the corresponding Laplace transforms $\overline{Q^*}(0, s)$, $\overline{h^*}(0, s)$ and $\overline{h^*}(1, s)$ are known. In addition to this, it is assumed that x_0, x_1, x_2, and $T(t)$ are all known.

3.2.1 For the flow-discharge hydrograph at the upstream end

For this case, the upstream boundary and the downstream boundary are considered as $Q^*(0, t^*)$ and $h^*(1, t^*)$, respectively. The solutions for both types of lateral inflows are discussed next.

Concentrated lateral inflow

Using the upstream and downstream boundary conditions, $\overline{h^*}(x^*, s)$ at $x^* = 1$ can be obtained from the system given in Eq. (3.23) as

$$
\overline{h^*}(1, s) = \alpha_{21}(1, s)\overline{Q^*}(0, s) + \alpha_{22}(1, s)\overline{h^*}(0, s) + \alpha_{21}(1 - x_0^*, s)\overline{T^*}(s). \tag{3.29}
$$

Using Eq. (3.29), $\overline{h^*}(0,s)$ can be written as

$$\overline{h^*}(0,s) = \frac{\overline{h^*}(1,s)}{\alpha_{22}(1,s)} - \frac{\alpha_{21}(1,s)}{\alpha_{22}(1,s)}\overline{Q^*}(0,s) - \frac{\alpha_{21}(1-x_0^*,s)}{\alpha_{22}(1,s)}\overline{T^*}(s). \tag{3.30}$$

Subsequently, the system given in Eq. (3.23) gets converted to

$$\overline{Q^*}(x^*,s) = \overline{R}_u(x^*,s)\overline{Q^*}(0,s) + \overline{R}_d(x^*,s)\overline{h^*}(1,s) + \overline{R}_l(x^*,s)\overline{T^*}(s), \tag{3.31}$$

$$\overline{h^*}(x^*,s) = \overline{S}_u(x^*,s)\overline{Q^*}(0,s) + \overline{S}_d(x^*,s)\overline{h^*}(1,s) + \overline{S}_l(x^*,s)\overline{T^*}(s). \tag{3.32}$$

The inverses of $\overline{R}_u(x^*,s)$, $\overline{R}_d(x^*,s)$, $\overline{S}_u(x^*,s)$ and $\overline{S}_d(x^*,s)$ are already provided by Cimorelli et al. [7], and the two new terms $\overline{R}_l(x^*,s)$ and $\overline{S}_l(x^*,s)$ can be written as

$$\begin{aligned}\overline{R}_l(x^*,s) = {} & \frac{\exp\left(\frac{P_e}{2}(x^*-x_0^*)\right)}{\sqrt{Z}\cosh\left(\frac{\sqrt{Z}}{2}\right) + P_e\sinh\left(\frac{\sqrt{Z}}{2}\right)}\left\{-\frac{4P_e s}{\sqrt{Z}}\sinh\left(\frac{x_0^*}{2}\sqrt{Z}\right)\sinh\left(\frac{1-x^*}{2}\sqrt{Z}\right)\right. \\ & \left. + \sqrt{Z}\cosh\left(\frac{1+x_0^*-x^*}{2}\sqrt{Z}\right) + P_e\sinh\left(\frac{1+x_0^*-x^*}{2}\sqrt{Z}\right)\right\}, \text{ for } x^* > x_0^*,\end{aligned} \tag{3.33a}$$

$$\overline{R}_l(x^*,s) = \frac{-4P_e s\exp\left(\frac{P_e}{2}(x^*-x_0^*)\right)\sinh\left(\frac{x^*}{2}\sqrt{Z}\right)}{\sqrt{Z}\left(\sqrt{Z}\cosh\left(\frac{\sqrt{Z}}{2}\right) + P_e\sinh\left(\frac{\sqrt{Z}}{2}\right)\right)}\sinh\left(\frac{1-x_0^*}{2}\sqrt{Z}\right), \text{ for } x^* < x_0^*, \tag{3.33b}$$

and

$$\begin{aligned}\overline{S}_l(x^*,s) = {} & 2P_e\exp\left(\frac{P_e}{2}(x^*-x_0^*)\right)\sinh\left(\frac{1-x^*}{2}\sqrt{Z}\right) \\ & \times\frac{\sqrt{Z}\cosh\left(\frac{x_0^*}{2}\sqrt{Z}\right) + P_e\sinh\left(\frac{x_0^*}{2}\sqrt{Z}\right)}{\beta\sqrt{Z}\left(\sqrt{Z}\cosh\left(\frac{\sqrt{Z}}{2}\right) + P_e\sinh\left(\frac{\sqrt{Z}}{2}\right)\right)}, \text{ for } x^* > x_0^*,\end{aligned} \tag{3.34a}$$

$$\overline{S}_l(x^*,s) = 2P_e\exp\left(\frac{P_e}{2}(x^*-x_0^*)\right)\sinh\left(\frac{1-x_0^*}{2}\sqrt{Z}\right)$$

$$\times \frac{\sqrt{Z}\cosh\left(\dfrac{x^*}{2}\sqrt{Z}\right) + P_e \sinh\left(\dfrac{x^*}{2}\sqrt{Z}\right)}{\beta\sqrt{Z}\left(\sqrt{Z}\cosh\left(\dfrac{\sqrt{Z}}{2}\right) + P_e \sinh\left(\dfrac{\sqrt{Z}}{2}\right)\right)}, \text{for } x^* < x_0^*. \tag{3.34b}$$

The inverse transforms for $\overline{Q^*}(x^*, s)$ and $\overline{h^*}(x^*, s)$ can be obtained, respectively, as

$$Q^*(x^*, t^*) = R_u(x^*, t^*) \circledast Q^*(0, t^*) + R_d(x^*, t^*) \circledast h^*(1, t^*) + R_l(x^*, t^*) \circledast T^*(t^*), \tag{3.35}$$

$$h^*(x^*, t^*) = S_u(x^*, t^*) \circledast Q^*(0, t^*) + S_d(x^*, t^*) \circledast h^*(1, t^*) + S_l(x^*, t^*) \circledast T^*(t^*), \tag{3.36}$$

where $\circledast$ is the convolution operator; $R_u(x^*, t^*)$, $R_d(x^*, t^*)$, $R_l(x^*, t^*)$, $S_u(x^*, t^*)$, $S_d(x^*, t^*)$ and $S_l(x^*, t^*)$ are the inverse transforms of $\overline{R}_u(x^*, s)$, $\overline{R}_d(x^*, s)$, $\overline{R}_l(x^*, s)$, $\overline{S}_u(x^*, s)$, $\overline{S}_d(x^*, s)$ and $\overline{S}_l(x^*, s)$, respectively.

Uniformly distributed lateral inflow

Using the upstream and downstream boundary conditions, we obtain $\overline{h^*}(x^*, s)$ at $x^* = 1$ from the system given in Eq. (3.28) as

$$\overline{h^*}(1, s) = \alpha_{21}(1, s)\overline{Q^*}(0, s) + \alpha_{22}(1, s)\overline{h^*}(0, s) + A_{21}(1, s)\overline{T^*}(s). \tag{3.37}$$

Using Eq. (3.37), $\overline{h^*}(0, s)$ can be written as

$$\overline{h^*}(0, s) = \frac{\overline{h^*}(1, s)}{\alpha_{22}(1, s)} - \frac{\alpha_{21}(1, s)}{\alpha_{22}(1, s)}\overline{Q^*}(0, s) - \frac{A_{21}(1, s)}{\alpha_{22}(1, s)}\overline{T^*}(s). \tag{3.38}$$

Subsequently, the system given in Eq. (3.28) gets converted to

$$\overline{Q^*}(x^*, s) = \overline{R}_u(x^*, s)\overline{Q^*}(0, s) + \overline{R}_d(x^*, s)\overline{h^*}(1, s) + \overline{R}_{ld}(x^*, s)\overline{T^*}(s), \tag{3.39}$$

$$\overline{h^*}(x^*, s) = \overline{S}_u(x^*, s)\overline{Q^*}(0, s) + \overline{S}_d(x^*, s)\overline{h^*}(1, s) + \overline{S}_{ld}(x^*, s)\overline{T^*}(s). \tag{3.40}$$

Inverses of $\overline{R}_u(x^*, s)$, $\overline{R}_d(x^*, s)$, $\overline{S}_u(x^*, s)$ and $\overline{S}_d(x^*, s)$ are already provided by Cimorelli et al. [7], and the two new terms $\overline{R}_{ld}(x^*, s)$ and $\overline{S}_{ld}(x^*, s)$ can be written as

$$\overline{R}_{ld}(x^*, s) = \frac{2}{x_2^* - x_1^*} \frac{\sinh\left(\dfrac{x^*\sqrt{Z}}{2}\right)}{\sqrt{Z}\left(\sqrt{Z}\cosh\left(\dfrac{\sqrt{Z}}{2}\right) + P_e \sinh\left(\dfrac{\sqrt{Z}}{2}\right)\right)}$$

$$\times \left\{ \exp\left(\frac{x^* - x_2^*}{2}P_e\right)\left(\sqrt{Z}\cosh\left(\frac{1 - x_2^*}{2}\sqrt{Z}\right) - P_e \sinh\left(\frac{1 - x_2^*}{2}\sqrt{Z}\right)\right)\right.$$

$$- \exp\left(\frac{x^* - x_1^*}{2}P_e\right)\left(\sqrt{Z}\cosh\left(\frac{1-x_1^*}{2}\sqrt{Z}\right) - P_e\sinh\left(\frac{1-x_1^*}{2}\sqrt{Z}\right)\right)\Bigg\},$$

$$\text{for } 0 \le x^* < x_1^*, \tag{3.41a}$$

$$\overline{R}_{ld}(x^*, s) = \frac{2\exp\left(\frac{x^*-x_2^*}{2}P_e\right)}{x_2^* - x_1^*}\frac{\sinh\left(\frac{x^*\sqrt{Z}}{2}\right)}{\sqrt{Z}}\frac{\sqrt{Z}\cosh\left(\frac{1-x_2^*}{2}\sqrt{Z}\right) - P_e\sinh\left(\frac{1-x_2^*}{2}\sqrt{Z}\right)}{\sqrt{Z}\cosh\left(\frac{\sqrt{Z}}{2}\right) + P_e\sinh\left(\frac{\sqrt{Z}}{2}\right)}$$

$$+ \frac{1}{s\sqrt{Z}(x_2^* - x_1^*)}\frac{\exp\left(\frac{x^*-x_1^*}{2}P_e\right)}{\sqrt{Z}\cosh\left(\frac{\sqrt{Z}}{2}\right) + P_e\sinh\left(\frac{\sqrt{Z}}{2}\right)}$$

$$\times\Bigg\{\sqrt{Z}\left(P_e\sinh\left(\frac{x^*-x_1^*-1}{2}\sqrt{Z}\right) - \sqrt{Z}\cosh\left(\frac{x^*-x_1^*-1}{2}\sqrt{Z}\right)\right)$$

$$- 2s\sinh\left(\frac{x_1^*}{2}\sqrt{Z}\right)\left(\sqrt{Z}\cosh\left(\frac{x^*-1}{2}\sqrt{Z}\right) + P_e\sinh\left(\frac{x^*-1}{2}\sqrt{Z}\right)\right)\Bigg\},$$

$$+ \frac{1}{s(x_2^* - x_1^*)}, \qquad \text{for } x_1^* \le x^* < x_2^*, \tag{3.41b}$$

$$\overline{R}_{ld}(x^*, s) = \frac{1}{s\sqrt{Z}(x_2^* - x_1^*)}\frac{\exp\left(\frac{x^*-x_1^*}{2}P_e\right)}{\sqrt{Z}\cosh\left(\frac{\sqrt{Z}}{2}\right) + P_e\sinh\left(\frac{\sqrt{Z}}{2}\right)}$$

$$\times\Bigg\{\sqrt{Z}\left(P_e\sinh\left(\frac{x^*-x_1^*-1}{2}\sqrt{Z}\right) - \sqrt{Z}\cosh\left(\frac{x^*-x_1^*-1}{2}\sqrt{Z}\right)\right)$$

$$- 2s\sinh\left(\frac{x_1^*}{2}\sqrt{Z}\right)\left(\sqrt{Z}\cosh\left(\frac{x^*-1}{2}\sqrt{Z}\right) + P_e\sinh\left(\frac{x^*-1}{2}\sqrt{Z}\right)\right)\Bigg\},$$

$$- \frac{1}{s\sqrt{Z}(x_2^* - x_1^*)}\frac{\exp\left(\frac{x^*-x_2^*}{2}P_e\right)}{\sqrt{Z}\cosh\left(\frac{\sqrt{Z}}{2}\right) + P_e\sinh\left(\frac{\sqrt{Z}}{2}\right)}$$

$$\times\Bigg\{\sqrt{Z}\left(P_e\sinh\left(\frac{x^*-x_2^*-1}{2}\sqrt{Z}\right) - \sqrt{Z}\cosh\left(\frac{x^*-x_2^*-1}{2}\sqrt{Z}\right)\right)$$

$$- 2s\sinh\left(\frac{x_2^*}{2}\sqrt{Z}\right)\left(\sqrt{Z}\cosh\left(\frac{x^*-1}{2}\sqrt{Z}\right) + P_e\sinh\left(\frac{x^*-1}{2}\sqrt{Z}\right)\right)\Bigg\},$$

$$\text{for } x_2^* \le x^* \le 1, \tag{3.41c}$$

and

$$\overline{S}_{ld}(x^*,s) = -\frac{1}{\beta s(x_2^* - x_1^*)} \frac{\sqrt{Z}\cosh\left(\dfrac{x^*\sqrt{Z}}{2}\right) + P_e \sinh\left(\dfrac{x^*\sqrt{Z}}{2}\right)}{\sqrt{Z}\left(\sqrt{Z}\cosh\left(\dfrac{\sqrt{Z}}{2}\right) + P_e \sinh\left(\dfrac{\sqrt{Z}}{2}\right)\right)}$$
$$\times \left\{\exp\left(\frac{x^* - x_2^*}{2}P_e\right)\left(\sqrt{Z}\cosh\left(\frac{1-x_2^*}{2}\sqrt{Z}\right) - P_e\sinh\left(\frac{1-x_2^*}{2}\sqrt{Z}\right)\right)\right.$$
$$\left. - \exp\left(\frac{x^* - x_1^*}{2}P_e\right)\left(\sqrt{Z}\cosh\left(\frac{1-x_1^*}{2}\sqrt{Z}\right) - P_e\sinh\left(\frac{1-x_1^*}{2}\sqrt{Z}\right)\right)\right\},$$
$$\text{for } 0 \leq x^* < x_1^*, \tag{3.42a}$$

$$\overline{S}_{ld}(x^*,s) = \frac{1}{\beta s(x_2^* - x_1^*)} - \exp\left(\frac{x^* - x_2^*}{2}P_e\right)\frac{\sqrt{Z}\cosh\left(\dfrac{x^*\sqrt{Z}}{2}\right) + P_e\sinh\left(\dfrac{x^*\sqrt{Z}}{2}\right)}{\beta s\sqrt{Z}(x_2^* - x_1^*)}$$
$$\times \frac{\sqrt{Z}\cosh\left(\dfrac{1-x_2^*}{2}\sqrt{Z}\right) - P_e\sinh\left(\dfrac{1-x_2^*}{2}\sqrt{Z}\right)}{\sqrt{Z}\cosh\left(\dfrac{\sqrt{Z}}{2}\right) + P_e\sinh\left(\dfrac{\sqrt{Z}}{2}\right)}$$
$$+ \frac{2P_e\exp\left(\dfrac{x^* - x_1^*}{2}P_e\right)}{\beta s(x_2^* - x_1^*)}\frac{\sinh\left(\dfrac{x^*-1}{2}\sqrt{Z}\right)}{\sqrt{Z}}$$
$$\times \frac{\sqrt{Z}\cosh\left(\dfrac{x_1^*\sqrt{Z}}{2}\right) + (P_e + 2s)\sinh\left(\dfrac{x_1^*\sqrt{Z}}{2}\right)}{\sqrt{Z}\cosh\left(\dfrac{\sqrt{Z}}{2}\right) + P_e\sinh\left(\dfrac{\sqrt{Z}}{2}\right)}, \quad \text{for } x_1^* \leq x^* < x_2^*, \tag{3.42b}$$

$$\overline{S}_{ld}(x^*,s) = \frac{2P_e}{\beta s(x_2^* - x_1^*)}\frac{\sinh\left(\dfrac{x^*-1}{2}\sqrt{Z}\right)}{\sqrt{Z}\left(\sqrt{Z}\cosh\left(\dfrac{\sqrt{Z}}{2}\right) + P_e\sinh\left(\dfrac{\sqrt{Z}}{2}\right)\right)}$$
$$\times \left\{\exp\left(\frac{x^* - x_1^*}{2}P_e\right)\left(\sqrt{Z}\cosh\left(\frac{x_1^*\sqrt{Z}}{2}\right) + (P_e + 2s)\sinh\left(\frac{x_1^*\sqrt{Z}}{2}\right)\right)\right.$$
$$\left. - \exp\left(\frac{x^* - x_2^*}{2}P_e\right)\left(\sqrt{Z}\cosh\left(\frac{x_2^*\sqrt{Z}}{2}\right) + (P_e + 2s)\sinh\left(\frac{x_2^*\sqrt{Z}}{2}\right)\right)\right\},$$
$$\text{for } x_2^* \leq x^* \leq 1. \tag{3.42c}$$

Inverse transformation

Laplace inverses of the functions described in the previous subsection are derived here by using the *Laplace inversion theorem*. Apparently, the functions in Eqs. (3.33)−(3.34) and (3.41)−(3.42) are two-valued in the neighborhood of the point s where $Z = 0$. But all these functions give the same value for Z and $-Z$. So, these functions are all single-valued with no branch points. Subsequently, the only singularities here are the zeros of the denominators of the functions $\overline{R}_{\imath}$, $\overline{S}_{\imath}$, $\overline{R}_{\imath d}$, and $\overline{S}_{\imath d}$. The attribute of the Jordan's lemma provided in *Chapter 1, Section 1.4* also holds true for all four of these functions. As both the numerator and the denominator of these functions vanish at $s = -P_e/4$, therefore, it need not be considered as a singularity [15]. Using the similar technique as used by Cimorelli et al. [7] to find the poles of the functions in Eqs. (3.33), (3.34), 3.41), and (3.42), we need to find the roots of the following:

$$Z\cosh\left(\frac{\sqrt{Z}}{2}\right)\left\{\frac{P_e}{\sqrt{Z}}\tanh\left(\frac{\sqrt{Z}}{2}\right)+1\right\}=0. \tag{3.43}$$

The roots of Eq. (3.43) correspond only to the roots given by the quantity inside **{}**, and these are the only poles of the functions in Eqs. (3.33), (3.34), 3.41), and (3.42). Equation (3.43) has roots for the negative values of s only. Replacing s by $-r$, we get

$$\frac{P_e}{\sqrt{4P_e r - {P_e}^2}}\tan\left(\frac{1}{2}\sqrt{4P_e r - {P_e}^2}\right)+1=0, \tag{3.44}$$

by using the property $\tanh(\mathrm{i}\sqrt{x}) = \mathrm{i}\tan(\sqrt{x})$. Equation (3.44) has one root in each interval given by

$$s_{k} \in \left(\frac{P_e}{4}+\frac{(2k-1)^2\pi^2}{4P_e}\ ,\ \frac{P_e}{4}+\frac{(2k+1)^2\pi^2}{4P_e}\right), \quad \text{where} \quad k\in\mathbb{N}. \tag{3.45}$$

There are no repeated roots of Eq. (3.44) and hence, all the poles of $\overline{R}_{\imath}(x^*, s)$, $\overline{S}_{\imath}(x^*, s)$, $\overline{R}_{\imath d}(x^*, s)$, and $\overline{S}_{\imath d}(x^*, s)$ are simple poles only. Then, we use the *Residue Theorem* [2] to evaluate the integral for these functions appearing in the *Laplace inversion theorem*. Therefore, $f(t^*)$ takes the form

$$f(t^*)=\sum_{k=1}^{\infty}\mathrm{Res}\Big(\exp(st^*)\overline{f}(s)\,,\ s=s_{k}\Big)=\sum_{k=1}^{\infty}\lim_{s\to s_{k}}(s-s_{k})\exp(st^*)\overline{f}(s). \tag{3.46}$$

Now, using *Laplace inversion theorem* and Eq. (3.46), we can write

$$R_{\imath}(x^*, t^*)=\sum_{k=1}^{\infty}a_{k}(x^*)\exp(-s_{k}t^*), \tag{3.47}$$

$$S_l(x^*, t^*) = \sum_{k=1}^{\infty} b_k(x^*) \exp(-s_k t^*), \tag{3.48}$$

$$R_{ld}(x^*, t^*) = \sum_{k=1}^{\infty} a_{1k}(x^*) \exp(-s_k t^*), \tag{3.49}$$

$$S_{ld}(x^*, t^*) = \sum_{k=1}^{\infty} b_{1k}(x^*) \exp(-s_k t^*), \tag{3.50}$$

with

$$a_k(x^*) = -\frac{\exp\left(\frac{P_e}{2}(x^* - x_0^*)\right)}{(4P_e s_k + 2P_e)\cos\left(\frac{\sqrt{Z_k}}{2}\right)} \left\{ 4P_e s_k \sin\left(\frac{x_0^*}{2}\sqrt{Z_k}\right) \sin\left(\frac{1 - x^*}{2}\sqrt{Z_k}\right) \right.$$
$$\left. + P_e\sqrt{Z_k}\sin\left(\frac{1 + x_0^* - x^*}{2}\sqrt{Z_k}\right) + Z_k\cos\left(\frac{1 + x_0^* - x^*}{2}\sqrt{Z_k}\right) \right\}, \quad \text{for } x^* > x_0^*, \tag{3.51a}$$

$$a_k(x^*) = -\frac{2s_k\exp\left(\frac{P_e}{2}(x^* - x_0^*)\right)}{(2s_k + 1)\cos\left(\frac{\sqrt{Z_k}}{2}\right)} \sin\left(\frac{x^*}{2}\sqrt{Z_k}\right)\sin\left(\frac{1 - x_0^*}{2}\sqrt{Z_k}\right), \quad \text{for } x^* < x_0^*, \tag{3.51b}$$

and

$$b_k(x^*) = -\exp\left(\frac{P_e}{2}(x^* - x_0^*)\right)\sin\left(\frac{1 - x^*}{2}\sqrt{Z_k}\right)$$
$$\times \frac{\sqrt{Z_k}\cos\left(\frac{x_0^*}{2}\sqrt{Z_k}\right) + P_e\sin\left(\frac{x_0^*}{2}\sqrt{Z_k}\right)}{\beta(2s_k + 1)\cos\left(\frac{\sqrt{Z_k}}{2}\right)}, \quad \text{for } x^* > x_0^*, \tag{3.52a}$$

$$b_k(x^*) = -\exp\left(\frac{P_e}{2}(x^* - x_0^*)\right)\sin\left(\frac{1 - x_0^*}{2}\sqrt{Z_k}\right)$$
$$\times \frac{\sqrt{Z_k}\cos\left(\frac{x^*}{2}\sqrt{Z_k}\right) + P_e\sin\left(\frac{x^*}{2}\sqrt{Z_k}\right)}{\beta(2s_k + 1)\cos\left(\frac{\sqrt{Z_k}}{2}\right)}, \quad \text{for } x^* < x_0^*. \tag{3.52b}$$

Furthermore,

$$a_{1k}(x^*) = -\frac{1}{P_e(x_2^* - x_1^*)} \frac{\sin\left(\dfrac{x^*\sqrt{Z_k}}{2}\right)}{\cos\left(\dfrac{\sqrt{Z_k}}{2}\right)(1+2s_k)}$$
$$\times \left\{ \exp\left(\frac{x^* - x_2^*}{2}P_e\right)\left(\sqrt{Z_k}\cos\left(\frac{1-x_2^*}{2}\sqrt{Z_k}\right) - P_e\sin\left(\frac{1-x_2^*}{2}\sqrt{Z_k}\right)\right)\right.$$
$$\left. - \exp\left(\frac{x^* - x_1^*}{2}P_e\right)\left(\sqrt{Z_k}\cos\left(\frac{1-x_1^*}{2}\sqrt{Z_k}\right) - P_e\sin\left(\frac{1-x_1^*}{2}\sqrt{Z_k}\right)\right)\right\},$$
$$\text{for } 0 \le x^* < x_1^*, \tag{3.53a}$$

$$a_{1k}(x^*) = -\frac{\exp\left(\dfrac{x^* - x_2^*}{2}P_e\right)}{P_e(x_2^* - x_1^*)} \frac{\sin\left(\dfrac{x^*\sqrt{Z_k}}{2}\right)}{\cos\left(\dfrac{\sqrt{Z_k}}{2}\right)(1+2s_k)}$$
$$\times \left(\sqrt{Z_k}\cos\left(\frac{1-x_2^*}{2}\sqrt{Z_k}\right) - P_e\sin\left(\frac{1-x_2^*}{2}\sqrt{Z_k}\right)\right)$$
$$+ \frac{1}{s_k(x_2^* - x_1^*)} \frac{\exp\left(\dfrac{x^* - x_1^*}{2}P_e\right)}{\cos\left(\dfrac{\sqrt{Z_k}}{2}\right)(2P_e + 4P_e s_k)}$$
$$\times \left\{ \sqrt{Z_k}\left(P_e\sin\left(\frac{x^* - x_1^* - 1}{2}\sqrt{Z_k}\right) - \sqrt{Z_k}\cos\left(\frac{x^* - x_1^* - 1}{2}\sqrt{Z_k}\right)\right)\right.$$
$$\left. + 2s_k\sin\left(\frac{x_1^*}{2}\sqrt{Z_k}\right)\left(\sqrt{Z_k}\cos\left(\frac{x^*-1}{2}\sqrt{Z}\right) + P_e\sin\left(\frac{x^*-1}{2}\sqrt{Z_k}\right)\right)\right\},$$
$$\text{for } x_1^* \le x^* < x_2^*, \tag{3.53b}$$

$$a_{1k}(x^*) = \frac{1}{s_k(x_2^* - x_1^*)} \frac{\exp\left(\dfrac{x^* - x_1^*}{2}P_e\right)}{\cos\left(\dfrac{\sqrt{Z_k}}{2}\right)(2P_e + 4P_e s_k)}$$
$$\times \left\{ \sqrt{Z_k}\left(P_e\sin\left(\frac{x^* - x_1^* - 1}{2}\sqrt{Z_k}\right) - \sqrt{Z_k}\cos\left(\frac{x^* - x_1^* - 1}{2}\sqrt{Z_k}\right)\right)\right.$$
$$\left. + 2s_k\sin\left(\frac{x_1^*}{2}\sqrt{Z_k}\right)\left(\sqrt{Z_k}\cos\left(\frac{x^*-1}{2}\sqrt{Z_k}\right) + P_e\sin\left(\frac{x^*-1}{2}\sqrt{Z}\right)\right)\right\},$$

$$
\begin{aligned}
&- \frac{1}{s_k(x_2^* - x_1^*)} \frac{\exp\left(\dfrac{x^* - x_2^*}{2} P_e\right)}{\cos\left(\dfrac{\sqrt{Z_k}}{2}\right)(2P_e + 4P_e s_k)} \\
&\times \left\{ \sqrt{Z_k}\left(P_e \sin\left(\frac{x^* - x_2^* - 1}{2}\sqrt{Z_k}\right) - \sqrt{Z} \cos\left(\frac{x^* - x_2^* - 1}{2}\sqrt{Z_k}\right)\right) \right. \\
&\left. + 2s_k \sin\left(\frac{x_2^*}{2}\sqrt{Z_k}\right)\left(\sqrt{Z_k}\cos\left(\frac{x^* - 1}{2}\sqrt{Z_k}\right) + P_e \sin\left(\frac{x^* - 1}{2}\sqrt{Z_k}\right)\right)\right\}, \\
&\qquad \text{for } x_2^* \le x^* \le 1, \qquad (3.53c)
\end{aligned}
$$

$$
\begin{aligned}
b_{1k}(x^*) = &- \frac{1}{\beta s_k(x_2^* - x_1^*)} \frac{\sqrt{Z_k}\cos\left(\dfrac{x^*\sqrt{Z_k}}{2}\right) + P_e \sin\left(\dfrac{x^*\sqrt{Z_k}}{2}\right)}{\cos\left(\dfrac{\sqrt{Z_k}}{2}\right)(2P_e + 4P_e s_k)} \\
&\times \left\{ \exp\left(\frac{x^* - x_2^*}{2}P_e\right)\left(\sqrt{Z_k}\cos\left(\frac{1 - x_2^*}{2}\sqrt{Z_k}\right) - P_e \sin\left(\frac{1 - x_2^*}{2}\sqrt{Z_k}\right)\right) \right. \\
&\left. - \exp\left(\frac{x^* - x_1^*}{2}P_e\right)\left(\sqrt{Z_k}\cos\left(\frac{1 - x_1^*}{2}\sqrt{Z_k}\right) - P_e \sin\left(\frac{1 - x_1^*}{2}\sqrt{Z_k}\right)\right)\right\}, \\
&\qquad \text{for } 0 \le x^* < x_1^*, \qquad (3.54a)
\end{aligned}
$$

$$
\begin{aligned}
b_{1k}(x^*) = &- \exp\left(\frac{x^* - x_2^*}{2}P_e\right) \frac{\sqrt{Z_k}\cos\left(\dfrac{x^*\sqrt{Z_k}}{2}\right) + P_e \sin\left(\dfrac{x^*\sqrt{Z_k}}{2}\right)}{\beta s_k(x_2^* - x_1^*)} \\
&\times \frac{\sqrt{Z_k}\cos\left(\dfrac{1 - x_2^*}{2}\sqrt{Z_k}\right) - P_e \sin\left(\dfrac{1 - x_2^*}{2}\sqrt{Z_k}\right)}{\cos\left(\dfrac{\sqrt{Z_k}}{2}\right)(2P_e + 4P_e s_k)} \\
&+ \frac{\exp\left(\dfrac{x^* - x_1^*}{2}P_e\right)}{\beta s_k(x_2^* - x_1^*)} \sin\left(\frac{x^* - 1}{2}\sqrt{Z_k}\right) \\
&\times \frac{\sqrt{Z_k}\cos\left(\dfrac{x_1^*\sqrt{Z_k}}{2}\right) + (P_e - 2s_k)\sin\left(\dfrac{x_1^*\sqrt{Z_k}}{2}\right)}{\cos\left(\dfrac{\sqrt{Z_k}}{2}\right)(1 + 2s_k)}, \quad \text{for } x_1^* \le x^* < x_2^*, \qquad (3.54b)
\end{aligned}
$$

$$b_{1k}(x^*) = \frac{1}{\beta s_k(x_2^* - x_1^*)} \frac{\sin\left(\frac{x^*-1}{2}\sqrt{Z_k}\right)}{\cos\left(\frac{\sqrt{Z_k}}{2}\right)(1+2s_k)}$$
$$\times \left\{ \exp\left(\frac{x^* - x_1^*}{2}P_e\right)\left(\sqrt{Z_k}\cos\left(\frac{x_1^*\sqrt{Z_k}}{2}\right) + (P_e - 2s_k)\sin\left(\frac{x_1^*\sqrt{Z_k}}{2}\right)\right)\right.$$
$$\left. - \exp\left(\frac{x^* - x_2^*}{2}P_e\right)\left(\sqrt{Z_k}\cos\left(\frac{x_2^*\sqrt{Z_k}}{2}\right) + (P_e - 2s_k)\sin\left(\frac{x_2^*\sqrt{Z_k}}{2}\right)\right)\right\},$$
$$\text{for } x_2^* \leq x^* \leq 1, \tag{3.54c}$$

with $Z_k = 4P_e s_k - P_e^2$. The unit-step response is defined as the response of the system for a unit-step input given at initial time, i.e., u(t^*). We can get the unit-step response of the lateral inflow by the evaluation of the integral of the impulse response from 0 to t^* which can be obtained as

$$A_l(x^*, t^*) = \int_0^{t^*} R_l(x^*, \tau)\mathrm{d}\tau = \begin{cases} 1 - \displaystyle\sum_{k=1}^{\infty} \frac{a_k(x^*)\exp(-s_k t^*)}{s_k}, & \text{for } x^* > x_0^*, \\ -\displaystyle\sum_{k=1}^{\infty} \frac{a_k(x^*)\exp(-s_k t^*)}{s_k}, & \text{for } x^* < x_0^*, \end{cases} \tag{3.55}$$

$$B_l(x^*, t^*) = \int_0^{t^*} S_l(x^*, \tau)\mathrm{d}\tau = \begin{cases} \frac{1}{\beta}\{1 - \exp(P_e(x^* - 1))\} \\ -\displaystyle\sum_{k=1}^{\infty} \frac{b_k(x^*)\exp(-s_k t^*)}{s_k}, & \text{for } x^* > x_0^*, \\ \frac{1}{\beta}\{\exp(P_e(x^* - x_0^*)) - \exp(P_e(x^* - 1))\} \\ -\displaystyle\sum_{k=1}^{\infty} \frac{b_k(x^*)\exp(-s_k t^*)}{s_k}, & \text{for } x^* < x_0^*. \end{cases} \tag{3.56}$$

$$C_l(x^*, t^*) = \int_0^{t^*} R_{ld}(x^*, \tau)\mathrm{d}\tau = \begin{cases} -\displaystyle\sum_{k=1}^{\infty} \frac{a_{1k}(x^*)}{s_k}\exp(-s_k t^*), & \text{for } 0 \leq x^* < x_1^*, \\ \frac{x^* - x_1^*}{x_2^* - x_1^*} - \displaystyle\sum_{k=1}^{\infty} \frac{a_{1k}(x^*)}{s_k}\exp(-s_k t^*), & \text{for } x_1^* \leq x^* < x_2^*, \\ 1 - \displaystyle\sum_{k=1}^{\infty} \frac{a_{1k}(x^*)}{s_k}\exp(-s_k t^*), & \text{for } x_2^* \leq x^* \leq 1, \end{cases}$$
$$\tag{3.57}$$

$$D_l(x^*,t^*) = \int_0^{t^*} S_{ld}(x^*,\tau)\mathrm{d}\tau = \begin{cases} \dfrac{\exp(P_e x^*)}{\beta P_e(x_2^* - x_1^*)}\left(\exp(-P_e x_1^*) - \exp(-P_e x_2^*)\right) \\ -\dfrac{1}{\beta}\exp(P_e(x^*-1)) \\ -\displaystyle\sum_{k=1}^{\infty}\frac{b_{1k}(x^*)}{s_k}\exp\left(-s_k t^*\right), \text{ for } 0 \le x^* < x_1^*, \\ \dfrac{1 + P_e(x^* - x_1^*) - \exp(P_e(x^* - x_2^*))}{\beta P_e(x_2^* - x_1^*)} - \dfrac{\exp(P_e(x^*-1))}{\beta} \\ -\displaystyle\sum_{k=1}^{\infty}\frac{b_{1k}(x^*)}{s_k}\exp\left(-s_k t^*\right), \text{ for } x_1^* \le x^* < x_2^*, \\ \dfrac{1}{\beta}\left(1 - \exp(P_e(x^*-1))\right) \\ -\displaystyle\sum_{k=1}^{\infty}\frac{b_{1k}(x^*)}{s_k}\exp\left(-s_k t^*\right), \text{ for } x_2^* \le x^* \le 1. \end{cases} \tag{3.58}$$

These unit-step responses are derived by using the Laplace transform property given by Eq. (1.31) given in *Chapter 1, Section 1.4*.

3.2.2 For the flow-depth hydrograph at the upstream end

For this case, the upstream boundary and the downstream boundary are considered as $h^*(0,t^*)$ and $h^*(1,t^*)$, respectively. The solutions for both types of lateral inflows are discussed below.

Concentrated lateral inflow

Using the boundary conditions, we get

$$\overline{Q^*}(0,s) = \frac{\overline{h^*}(1,s)}{\alpha_{21}(1,s)} - \frac{\alpha_{22}(1,s)}{\alpha_{21}(1,s)}\overline{h^*}(0,s) - \frac{\alpha_{21}(1-x_0^*,s)}{\alpha_{21}(1,s)}\overline{T^*}(s). \tag{3.59}$$

Using Eq. (3.59), we can get the system given in Eq. (3.23) in the following form:

$$\overline{Q^*}(x^*,s) = \overline{m}_u(x^*,s)\overline{h^*}(0,s) + \overline{m}_d(x^*,s)\overline{h^*}(1,s) + \overline{m}_l(x^*,s)\overline{T^*}(s), \tag{3.60}$$
$$\overline{h^*}(x^*,s) = \overline{n}_u(x^*,s)\overline{h^*}(0,s) + \overline{n}_d(x^*,s)\overline{h^*}(1,s) + \overline{n}_l(x^*,s)\overline{T^*}(s), \tag{3.61}$$

where

$$\overline{m}_u(x^*,s) = \left(\sqrt{Z}\cosh\left(\frac{1-x^*}{2}\sqrt{Z}\right) + P_e\sinh\left(\frac{1-x^*}{2}\sqrt{Z}\right)\right)\frac{\beta}{2P_e}\frac{\exp\left(\dfrac{P_e x^*}{2}\right)}{\sinh\left(\dfrac{\sqrt{Z}}{2}\right)}, \tag{3.62}$$

$$\overline{m}_{_d}(x^*, s) = -\frac{\sqrt{Z}\cosh\left(\dfrac{x^*\sqrt{Z}}{2}\right) - P_e\sinh\left(\dfrac{x^*\sqrt{Z}}{2}\right)}{\sinh\left(\dfrac{\sqrt{Z}}{2}\right)}\frac{\beta}{2P_e}\exp\left(\frac{P_e}{2}(x^*-1)\right), \tag{3.63}$$

$$\overline{m}_{_l}(x^*, s) = \left(\sqrt{Z}\cosh\left(\frac{1-x^*}{2}\sqrt{Z}\right) + P_e\sinh\left(\frac{1-x^*}{2}\sqrt{Z}\right)\right)$$
$$\times\frac{\exp\left(\dfrac{P_e}{2}(x^*-x^*_{_0})\right)\sinh\left(\dfrac{x^*_{_0}\sqrt{Z}}{2}\right)}{\sqrt{Z}\sinh\left(\dfrac{\sqrt{Z}}{2}\right)}, \text{ for } x^* > x^*_{_0}, \tag{3.64a}$$

$$\overline{m}_{_l}(x^*, s) = \left(\sqrt{Z}\cosh\left(\frac{x^*}{2}\sqrt{Z}\right) - P_e\sinh\left(\frac{x^*}{2}\sqrt{Z}\right)\right)$$
$$\times\frac{\exp\left(\dfrac{P_e}{2}(x^*-x^*_{_0})\right)\sinh\left(\dfrac{x^*_{_0}-1}{2}\sqrt{Z}\right)}{\sqrt{Z}\sinh\left(\dfrac{\sqrt{Z}}{2}\right)}, \text{ for } x^* < x^*_{_0}, \tag{3.64b}$$

$$\overline{n}_{_u}(x^*, s) = \exp\left(\frac{P_e x^*}{2}\right)\frac{\sinh\left(\dfrac{1-x^*}{2}\sqrt{Z}\right)}{\sinh\left(\dfrac{\sqrt{Z}}{2}\right)}, \tag{3.65}$$

$$\overline{n}_{_d}(x^*, s) = \exp\left(\frac{P_e}{2}(x^*-1)\right)\frac{\sinh\left(\dfrac{x^*\sqrt{Z}}{2}\right)}{\sinh\left(\dfrac{\sqrt{Z}}{2}\right)}, \tag{3.66}$$

and

$$\overline{n}_{_l}(x^*, s) = \frac{2P_e}{\beta}\exp\left(\frac{P_e}{2}(x^*-x^*_{_0})\right)\frac{\sinh\left(\dfrac{x^*_{_0}}{2}\sqrt{Z}\right)\sinh\left(\dfrac{1-x^*}{2}\sqrt{Z}\right)}{\sqrt{Z}\sinh\left(\dfrac{\sqrt{Z}}{2}\right)}, \text{ for } x^* > x^*_{_0}, \tag{3.67a}$$

$$\overline{n}_{l}(x^*,s) = \frac{2P_e}{\beta}\exp\left(\frac{P_e}{2}(x^*-x_0^*)\right)\frac{\sinh\left(\frac{x^*}{2}\sqrt{Z}\right)\sinh\left(\frac{1-x_0^*}{2}\sqrt{Z}\right)}{\sqrt{Z}\sinh\left(\frac{\sqrt{Z}}{2}\right)}, \text{ for } x^* < x_0^*. \tag{3.67b}$$

The inverse transforms for $\overline{Q^*}(x^*,s)$ and $\overline{h^*}(x^*,s)$ can be written, respectively, as

$$Q^*(x^*,t^*) = m_u(x^*,t^*) \circledast h^*(0,t^*) + m_d(x^*,t^*) \circledast h^*(1,t^*) + m_l(x^*,t^*) \circledast T^*(t^*), \tag{3.68}$$
$$h^*(x^*,t^*) = n_u(x^*,t^*) \circledast h^*(0,t^*) + n_d(x^*,t^*) \circledast h^*(1,t^*) + n_l(x^*,t^*) \circledast T^*(t^*), \tag{3.69}$$

where $m_u(x^*,t^*)$, $m_d(x^*,t^*)$, $m_l(x^*,t^*)$, $n_u(x^*,t^*)$, $n_d(x^*,t^*)$, and $n_l(x^*,t^*)$ are the inverse transforms of $\overline{m}_u(x^*,s)$, $\overline{m}_d(x^*,s)$, $\overline{m}_l(x^*,s)$, $\overline{n}_u(x^*,s)$, $\overline{n}_d(x^*,s)$, and $\overline{n}_l(x^*,s)$, respectively.

Uniformly distributed lateral inflow

Using the boundary conditions, we get $\overline{Q^*}(0,s)$ from the system given in Eq. (3.28) as

$$\overline{Q^*}(0,s) = \frac{\overline{h^*}(1,s)}{\alpha_{21}(1,s)} - \frac{\alpha_{22}(1,s)}{\alpha_{21}(1,s)}\overline{h^*}(0,s) - \frac{A_{21}(1,s)}{\alpha_{21}(1,s)}\overline{T^*}(s). \tag{3.70}$$

Using Eq. (3.70), we can get the system given in Eq. (3.28) in the following form:

$$\overline{Q^*}(x^*,s) = \overline{m}_u(x^*,s)\overline{h^*}(0,s) + \overline{m}_d(x^*,s)\overline{h^*}(1,s) + \overline{m}_{ld}(x^*,s)\overline{T^*}(s), \tag{3.71}$$
$$\overline{h^*}(x^*,s) = \overline{n}_u(x^*,s)\overline{h^*}(0,s) + \overline{n}_d(x^*,s)\overline{h^*}(1,s) + \overline{n}_{ld}(x^*,s)\overline{T^*}(s), \tag{3.72}$$

where $\overline{m}_u(x^*,s)$, $\overline{m}_d(x^*,s)$, $\overline{n}_u(x^*,s)$, and $\overline{n}_d(x^*,s)$ are the same as the ones obtained in Eqs. (3.60) and (3.61). The new terms $\overline{m}_{ld}(x^*,s)$ and $\overline{n}_{ld}(x^*,s)$ are obtained in the following form:

$$\begin{aligned}\overline{m}_{ld}(x^*,s) = {} & \frac{1}{2P_e s(x_2^*-x_1^*)}\frac{\sqrt{Z}\cosh\left(\frac{x^*\sqrt{Z}}{2}\right) - P_e\sinh\left(\frac{x^*\sqrt{Z}}{2}\right)}{\sqrt{Z}\sinh\left(\frac{\sqrt{Z}}{2}\right)} \\ & \times\left\{\exp\left(\frac{x^*-x_2^*}{2}P_e\right)\left(\sqrt{Z}\cosh\left(\frac{1-x_2^*}{2}\sqrt{Z}\right) - P_e\sinh\left(\frac{1-x_2^*}{2}\sqrt{Z}\right)\right)\right. \\ & \left. - \exp\left(\frac{x^*-x_1^*}{2}P_e\right)\left(\sqrt{Z}\cosh\left(\frac{1-x_1^*}{2}\sqrt{Z}\right) - P_e\sinh\left(\frac{1-x_1^*}{2}\sqrt{Z}\right)\right)\right\}, \\ & \text{for } 0 \le x^* < x_1^*,\end{aligned} \tag{3.73a}$$

$$\overline{m}_{ld}(x^*,s) = \frac{\exp\left(\dfrac{x^*-x_2^*}{2}P_e\right)}{2P_e s(x_2^*-x_1^*)} \frac{\sqrt{Z}\cosh\left(\dfrac{x^*}{2}\sqrt{Z}\right) - P_e \sinh\left(\dfrac{x^*}{2}\sqrt{Z}\right)}{\sqrt{Z}\sinh\left(\dfrac{\sqrt{Z}}{2}\right)}$$
$$\times\left(\sqrt{Z}\cosh\left(\frac{1-x_2^*}{2}\sqrt{Z}\right) - P_e\sinh\left(\frac{1-x_2^*}{2}\sqrt{Z}\right)\right)$$
$$+\frac{\exp\left(\dfrac{x^*-x_1^*}{2}P_e\right)}{2P_e s(x_2^*-x_1^*)} \frac{P_e\sinh\left(\dfrac{x^*-1}{2}\sqrt{Z}\right) - \sqrt{Z}\cosh\left(\dfrac{x^*-1}{2}\sqrt{Z}\right)}{\sqrt{Z}\sinh\left(\dfrac{\sqrt{Z}}{2}\right)}$$
$$\times\left(\sqrt{Z}\cosh\left(\frac{x_1^*\sqrt{Z}}{2}\right) + P_e\sinh\left(\frac{x_1^*\sqrt{Z}}{2}\right)\right)$$
$$+\frac{1}{s(x_2^*-x_1^*)}, \qquad \text{for } x_1^* \le x^* < x_2^*, \tag{3.73b}$$

$$\overline{m}_{ld}(x^*,s) = \frac{1}{2P_e s(x_2^*-x_1^*)} \frac{P_e\sinh\left(\dfrac{x^*-1}{2}\sqrt{Z}\right) - \sqrt{Z}\cosh\left(\dfrac{x^*-1}{2}\sqrt{Z}\right)}{\sqrt{Z}\sinh\left(\dfrac{\sqrt{Z}}{2}\right)}$$
$$\times\left\{\exp\left(\frac{x^*-x_1^*}{2}P_e\right)\left(\sqrt{Z}\cosh\left(\frac{x_1^*\sqrt{Z}}{2}\right) + P_e\sinh\left(\frac{x_1^*\sqrt{Z}}{2}\right)\right)\right.$$
$$\left.-\exp\left(\frac{x^*-x_2^*}{2}P_e\right)\left(\sqrt{Z}\cosh\left(\frac{x_2^*\sqrt{Z}}{2}\right) + P_e\sinh\left(\frac{x_2^*\sqrt{Z}}{2}\right)\right)\right\},$$
$$\text{for } x_2^* \le x^* \le 1, \tag{3.73c}$$

and

$$\overline{n}_{ld}(x^*,s) = -\frac{1}{\beta s(x_2^*-x_1^*)} \frac{\sinh\left(\dfrac{x^*\sqrt{Z}}{2}\right)}{\sqrt{Z}\sinh\left(\dfrac{\sqrt{Z}}{2}\right)}$$
$$\times\left\{\exp\left(\frac{x^*-x_2^*}{2}P_e\right)\left(\sqrt{Z}\cosh\left(\frac{1-x_2^*}{2}\sqrt{Z}\right) - P_e\sinh\left(\frac{1-x_2^*}{2}\sqrt{Z}\right)\right)\right.$$
$$\left.-\exp\left(\frac{x^*-x_1^*}{2}P_e\right)\left(\sqrt{Z}\cosh\left(\frac{1-x_1^*}{2}\sqrt{Z}\right) - P_e\sinh\left(\frac{1-x_1^*}{2}\sqrt{Z}\right)\right)\right\},$$
$$\text{for } 0 \le x^* < x_1^*, \tag{3.74a}$$

$$\overline{n}_{ld}(x^*,s) = \frac{1}{\beta s(x_2^*-x_1^*)} - \frac{\exp\left(\dfrac{x^*-x_2^*}{2}P_e\right)}{\beta s(x_2^*-x_1^*)} \frac{\sinh\left(\dfrac{x^*}{2}\sqrt{Z}\right)}{\sqrt{Z}\sinh\left(\dfrac{\sqrt{Z}}{2}\right)}$$
$$\times\left(\sqrt{Z}\cosh\left(\frac{1-x_2^*}{2}\sqrt{Z}\right) - P_e\sinh\left(\frac{1-x_2^*}{2}\sqrt{Z}\right)\right)$$
$$+\frac{\exp\left(\dfrac{x^*-x_1^*}{2}P_e\right)}{\beta s(x_2^*-x_1^*)}\frac{\sinh\left(\dfrac{x^*-1}{2}\sqrt{Z}\right)}{\sqrt{Z}\sinh\left(\dfrac{\sqrt{Z}}{2}\right)}\left(\sqrt{Z}\cosh\left(\frac{x_1^*\sqrt{Z}}{2}\right)+P_e\sinh\left(\frac{x_1^*\sqrt{Z}}{2}\right)\right),$$
$$\text{for } x_1^* \le x^* < x_2^*, \tag{3.74b}$$

$$\overline{n}_{ld}(x^*,s) = \frac{1}{\beta s(x_2^*-x_1^*)}\frac{\sinh\left(\dfrac{x^*-1}{2}\sqrt{Z}\right)}{\sqrt{Z}\sinh\left(\dfrac{\sqrt{Z}}{2}\right)}$$
$$\times\left\{\exp\left(\frac{x^*-x_1^*}{2}P_e\right)\left(\sqrt{Z}\cosh\left(\frac{x_1^*\sqrt{Z}}{2}\right)+P_e\sinh\left(\frac{x_1^*\sqrt{Z}}{2}\right)\right)\right.$$
$$\left.-\exp\left(\frac{x^*-x_2^*}{2}P_e\right)\left(\sqrt{Z}\cosh\left(\frac{x_2^*\sqrt{Z}}{2}\right)+P_e\sinh\left(\frac{x_2^*\sqrt{Z}}{2}\right)\right)\right\},$$
$$\text{for } x_2^* \le x^* \le 1. \tag{3.74c}$$

The inverse transforms for $\overline{Q^*}(x^*,s)$ and $\overline{h^*}(x^*,s)$ can be written, respectively, as

$$Q^*(x^*,t^*) = m_u(x^*,t^*) \circledast h^*(0,t^*) + m_d(x^*,t^*) \circledast h^*(1,t^*) + m_{ld}(x^*,t^*) \circledast T^*(t^*), \tag{3.75}$$
$$h^*(x^*,t^*) = n_u(x^*,t^*) \circledast h^*(0,t^*) + n_d(x^*,t^*) \circledast h^*(1,t^*) + n_{ld}(x^*,t^*) \circledast T^*(t^*), \tag{3.76}$$

where $m_u(x^*,t^*)$, $m_d(x^*,t^*)$, $m_{ld}(x^*,t^*)$, $n_u(x^*,t^*)$, $n_d(x^*,t^*)$, and $n_{ld}(x^*,t^*)$ are the inverse transforms of $\overline{m}_u(x^*,s)$, $\overline{m}_d(x^*,s)$, $\overline{m}_{ld}(x^*,s)$, $\overline{n}_u(x^*,s)$, $\overline{n}_d(x^*,s)$, and $\overline{n}_{ld}(x^*,s)$, respectively.

Inverse transformation

To find the time domain expressions for the functions in Eqs. (3.62)−(3.67), (3.73) and (3.74), we again use *Laplace inversion theorem*. All these functions are single-valued with no branch points. Looking at the previous instances, it is obvious that the attribute of the Jordan's lemma given in *Chapter 1, Section 1.4* holds true. The only singularities of these functions are the roots of the denominator given by $s_k = -\left(\frac{k^2\pi^2}{P_e}+\frac{P_e}{4}\right)$ for $k \in \mathbb{N}$. No repetition of the roots of the denominator gives all poles as simple poles, and now the

Residue Theorem can be used to write

$$m_u(x^*,t^*) = \sum_{k=1}^{\infty} d_k(x^*)\exp\left(-s_k t^*\right), \quad \text{with} \tag{3.77}$$

$$d_k(x^*) = \frac{-\beta}{2P_e}\frac{\exp\left(\dfrac{P_e x^*}{2}\right)}{\dfrac{P_e}{\sqrt{Z_k}}\cos\left(\dfrac{\sqrt{Z_k}}{2}\right)}\left\{P_e\sin\left(\frac{1-x^*}{2}\sqrt{Z_k}\right) + \sqrt{Z_k}\cos\left(\frac{1-x^*}{2}\sqrt{Z_k}\right)\right\}, \tag{3.78}$$

$$m_d(x^*,t^*) = \sum_{k=1}^{\infty} e_k(x^*)\exp\left(-s_k t^*\right), \quad \text{with} \tag{3.79}$$

$$e_k(x^*) = \frac{\beta}{2P_e}\frac{\exp\left(\dfrac{P_e}{2}(x^*-1)\right)}{\dfrac{P_e}{\sqrt{Z_k}}\cos\left(\dfrac{\sqrt{Z_k}}{2}\right)}\left\{-P_e\sin\left(\frac{x^*}{2}\sqrt{Z_k}\right) + \sqrt{Z_k}\cos\left(\frac{x^*}{2}\sqrt{Z_k}\right)\right\}, \tag{3.80}$$

$$m_l(x^*,t^*) = \sum_{k=1}^{\infty} f_k(x^*)\exp\left(-s_k t^*\right), \quad \text{with} \tag{3.81}$$

$$f_k(x^*) = -\frac{\exp\left(\dfrac{P_e}{2}(x^*-x_0^*)\right)\sin\left(\dfrac{x_0^*}{2}\sqrt{Z_k}\right)}{P_e\cos\left(\dfrac{\sqrt{Z_k}}{2}\right)} \times\left\{P_e\sin\left(\frac{1-x^*}{2}\sqrt{Z_k}\right) + \sqrt{Z_k}\cos\left(\frac{1-x^*}{2}\sqrt{Z_k}\right)\right\}, \quad x^* > x_0^*, \tag{3.82a}$$

$$f_k(x^*) = \frac{\exp\left(\dfrac{P_e}{2}(x^*-x_0^*)\right)\sin\left(\dfrac{1-x_0^*}{2}\sqrt{Z_k}\right)}{P_e\cos\left(\dfrac{\sqrt{Z_k}}{2}\right)} \times\left\{P_e\sin\left(\frac{x^*}{2}\sqrt{Z_k}\right) + \sqrt{Z_k}\cos\left(\frac{x^*}{2}\sqrt{Z_k}\right)\right\}, \quad x^* < x_0^*, \tag{3.82b}$$

$$n_u(x^*,t^*) = \sum_{k=1}^{\infty} g_k(x^*)\exp\left(-s_k t^*\right), \quad \text{with} \tag{3.83}$$

$$g_k(x^*) = -\exp\left(\frac{P_e x^*}{2}\right)\frac{\sin\left(\frac{1-x^*}{2}\sqrt{Z_k}\right)}{\frac{P_e}{\sqrt{Z_k}}\cos\left(\frac{\sqrt{Z_k}}{2}\right)}, \tag{3.84}$$

$$n_d(x^*, t^*) = \sum_{k=1}^{\infty} i_k(x^*)\exp\left(-s_k t^*\right), \text{ with} \tag{3.85}$$

$$i_k(x^*) = -\exp\left(\frac{P_e}{2}(x^*-1)\right)\frac{\sin\left(\frac{x^*}{2}\sqrt{Z_k}\right)}{\frac{P_e}{\sqrt{Z_k}}\cos\left(\frac{\sqrt{Z_k}}{2}\right)}, \tag{3.86}$$

$$n_l(x^*, t^*) = \sum_{k=1}^{\infty} j_k(x^*)\exp\left(-s_k t^*\right), \quad \text{with} \tag{3.87}$$

$$j_k(x^*) = -\frac{2}{\beta}\frac{\exp\left(\frac{P_e}{2}(x^*-x_0^*)\right)\sin\left(\frac{x_0^*}{2}\sqrt{Z_k}\right)}{\cos\left(\frac{\sqrt{Z_k}}{2}\right)}\sin\left(\frac{1-x^*}{2}\sqrt{Z_k}\right), \text{ for } x^* > x_0^*, \tag{3.88a}$$

$$j_k(x^*) = -\frac{2}{\beta}\frac{\exp\left(\frac{P_e}{2}(x^*-x_0^*)\right)\sin\left(\frac{x^*}{2}\sqrt{Z_k}\right)}{\cos\left(\frac{\sqrt{Z_k}}{2}\right)}\sin\left(\frac{1-x_0^*}{2}\sqrt{Z_k}\right), \text{ for } x^* < x_0^*, \tag{3.88b}$$

$$m_{ld}(x^*, t^*) = \sum_{k=1}^{\infty} f_{1k}(x^*)\exp\left(-s_k t^*\right), \quad \text{with} \tag{3.89}$$

$$\begin{aligned} f_{1k}(x^*) = {} & \frac{1}{2P_e s_k(x_2^*-x_1^*)}\frac{\sqrt{Z_k}\cos\left(\frac{x^*\sqrt{Z_k}}{2}\right) - P_e\sin\left(\frac{x^*\sqrt{Z_k}}{2}\right)}{P_e\cos\left(\frac{\sqrt{Z_k}}{2}\right)} \\ & \times \left\{\exp\left(\frac{x^*-x_2^*}{2}P_e\right)\left(\sqrt{Z_k}\cos\left(\frac{1-x_2^*}{2}\sqrt{Z_k}\right) - P_e\sin\left(\frac{1-x_2^*}{2}\sqrt{Z_k}\right)\right)\right. \\ & \left. - \exp\left(\frac{x^*-x_1^*}{2}P_e\right)\left(\sqrt{Z_k}\cos\left(\frac{1-x_1^*}{2}\sqrt{Z_k}\right) - P_e\sin\left(\frac{1-x_1^*}{2}\sqrt{Z_k}\right)\right)\right\}, \\ & \text{for } 0 \le x^* < x_1^*, \end{aligned} \tag{3.90a}$$

$$f_{1k}(x^*) = \frac{\exp\left(\frac{x^*-x_2^*}{2}P_e\right)}{2P_e s_k(x_2^*-x_1^*)} \frac{\sqrt{Z_k}\cos\left(\frac{x^*}{2}\sqrt{Z_k}\right) - P_e\sin\left(\frac{x^*}{2}\sqrt{Z_k}\right)}{P_e\cos\left(\frac{\sqrt{Z_k}}{2}\right)}$$
$$\times\left(\sqrt{Z_k}\cos\left(\frac{1-x_2^*}{2}\sqrt{Z_k}\right) - P_e\sin\left(\frac{1-x_2^*}{2}\sqrt{Z_k}\right)\right)$$
$$+ \frac{\exp\left(\frac{x^*-x_1^*}{2}P_e\right)}{2P_e s_k(x_2^*-x_1^*)} \frac{P_e\sin\left(\frac{x^*-1}{2}\sqrt{Z_k}\right) - \sqrt{Z_k}\cos\left(\frac{x^*-1}{2}\sqrt{Z_k}\right)}{P_e\cos\left(\frac{\sqrt{Z_k}}{2}\right)}$$
$$\times\left(\sqrt{Z_k}\cos\left(\frac{x_1^*\sqrt{Z_k}}{2}\right) + P_e\sin\left(\frac{x_1^*\sqrt{Z_k}}{2}\right)\right), \quad \text{for } x_1^* \le x^* < x_2^*, \tag{3.90b}$$

$$f_{1k}(x^*) = \frac{1}{2P_e s_k(x_2^*-x_1^*)} \frac{P_e\sin\left(\frac{x^*-1}{2}\sqrt{Z_k}\right) - \sqrt{Z_k}\cos\left(\frac{x^*-1}{2}\sqrt{Z_k}\right)}{P_e\cos\left(\frac{\sqrt{Z_k}}{2}\right)}$$
$$\times\left\{\exp\left(\frac{x^*-x_1^*}{2}P_e\right)\left(\sqrt{Z_k}\cos\left(\frac{x_1^*\sqrt{Z_k}}{2}\right) + P_e\sin\left(\frac{x_1^*\sqrt{Z_k}}{2}\right)\right)\right.$$
$$\left. - \exp\left(\frac{x^*-x_2^*}{2}P_e\right)\left(\sqrt{Z_k}\cos\left(\frac{x_2^*\sqrt{Z_k}}{2}\right) + P_e\sin\left(\frac{x_2^*\sqrt{Z_k}}{2}\right)\right)\right\},$$
$$\text{for } x_2^* \le x^* \le 1, \tag{3.90c}$$

$$n_{ld}(x^*, t^*) = \sum_{k=1}^{\infty} j_{1k}(x^*)\exp(-s_k t^*), \quad \text{with} \tag{3.91}$$

$$j_{1k}(x^*) = -\frac{1}{\beta s_k(x_2^*-x_1^*)} \frac{\sin\left(\frac{x^*\sqrt{Z_k}}{2}\right)}{P_e\cos\left(\frac{\sqrt{Z_k}}{2}\right)}$$
$$\times\left\{\exp\left(\frac{x^*-x_2^*}{2}P_e\right)\left(\sqrt{Z_k}\cos\left(\frac{1-x_2^*}{2}\sqrt{Z_k}\right) - P_e\sin\left(\frac{1-x_2^*}{2}\sqrt{Z_k}\right)\right)\right.$$
$$\left. - \exp\left(\frac{x^*-x_1^*}{2}P_e\right)\left(\sqrt{Z_k}\cos\left(\frac{1-x_1^*}{2}\sqrt{Z_k}\right) - P_e\sin\left(\frac{1-x_1^*}{2}\sqrt{Z_k}\right)\right)\right\},$$
$$\text{for } 0 \le x^* < x_1^*, \tag{3.92a}$$

$$
\begin{aligned}
j_{1k}(x^*) = &-\frac{\exp\left(\dfrac{x^*-x_2^*}{2}P_e\right)}{\beta s_k(x_2^*-x_1^*)}\frac{\sin\left(\dfrac{x^*}{2}\sqrt{Z_k}\right)}{P_e\cos\left(\dfrac{\sqrt{Z_k}}{2}\right)} \\
&\times\left(\sqrt{Z_k}\cos\left(\frac{1-x_2^*}{2}\sqrt{Z_k}\right)-P_e\sin\left(\frac{1-x_2^*}{2}\sqrt{Z_k}\right)\right) \\
&+\frac{\exp\left(\dfrac{x^*-x_1^*}{2}P_e\right)}{\beta s_k(x_2^*-x_1^*)}\frac{\sin\left(\dfrac{x^*-1}{2}\sqrt{Z_k}\right)}{P_e\cos\left(\dfrac{\sqrt{Z_k}}{2}\right)}\left(\sqrt{Z_k}\cos\left(\frac{x_1^*\sqrt{Z_k}}{2}\right)+P_e\sin\left(\frac{x_1^*\sqrt{Z_k}}{2}\right)\right), \\
&\qquad\qquad\qquad\text{for } x_1^*\le x^*<x_2^*,
\end{aligned}
\tag{3.92b}
$$

$$
\begin{aligned}
j_{1k}(x^*) = &\frac{1}{\beta s_k(x_2^*-x_1^*)}\frac{\sin\left(\dfrac{x^*-1}{2}\sqrt{Z_k}\right)}{P_e\cos\left(\dfrac{\sqrt{Z_k}}{2}\right)} \\
&\times\left\{\exp\left(\frac{x^*-x_1^*}{2}P_e\right)\left(\sqrt{Z_k}\cos\left(\frac{x_1^*\sqrt{Z_k}}{2}\right)+P_e\sin\left(\frac{x_1^*\sqrt{Z_k}}{2}\right)\right)\right. \\
&\left.-\exp\left(\frac{x^*-x_2^*}{2}P_e\right)\left(\sqrt{Z_k}\cos\left(\frac{x_2^*\sqrt{Z_k}}{2}\right)+P_e\sin\left(\frac{x_2^*\sqrt{Z_k}}{2}\right)\right)\right\}, \\
&\qquad\qquad\qquad\text{for } x_2^*\le x^*\le 1.
\end{aligned}
\tag{3.92c}
$$

The unit-step responses to analyze the results are evaluated as follows:

$$
M_u(x^*,t^*)=\int_0^{t^*}m_u(x^*,\tau)\mathrm{d}\tau=\frac{\beta}{1-\exp(-P_e)}-\sum_{k=1}^{\infty}\frac{d_k(x^*)\exp(-s_kt^*)}{s_k},
\tag{3.93}
$$

$$
M_d(x^*,t^*)=\int_0^{t^*}m_d(x^*,\tau)\mathrm{d}\tau=\frac{\beta}{1-\exp(P_e)}-\sum_{k=1}^{\infty}\frac{e_k(x^*)\exp(-s_kt^*)}{s_k},
\tag{3.94}
$$

$$
M_l(x^*,t^*)=\int_0^{t^*}m_l(x^*,\tau)\mathrm{d}\tau=\begin{cases}\dfrac{1-\exp(-P_ex_0^*)}{1-\exp(-P_e)} \\ -\displaystyle\sum_{k=1}^{\infty}\frac{f_k(x^*)\exp(-s_kt^*)}{s_k}, & \text{for } x^*>x_0^*, \\ \dfrac{\exp(-P_e)-\exp(-P_ex_0^*)}{1-\exp(-P_e)} \\ -\displaystyle\sum_{k=1}^{\infty}\frac{f_k(x^*)\exp(-s_kt^*)}{s_k}, & \text{for } x^*<x_0^*,\end{cases}
\tag{3.95}
$$

$$M_{ld}(x^*,t^*) = \int_0^{t^*} m_{ld}(x^*,\tau)\mathrm{d}\tau = \begin{cases} \dfrac{1}{\exp(P_e)-1} + \dfrac{\exp(P_e)\left(\exp(-P_e x_2^*) - \exp(-P_e x_1^*)\right)}{P_e(x_2^* - x_1^*)\left(\exp(P_e)-1\right)} \\ -\displaystyle\sum_{k=1}^{\infty} \dfrac{f_{1k}(x^*)}{s_k} \exp\left(-s_k t^*\right), \text{ for } 0 \le x^* < x_1^*, \\ \dfrac{\exp(P_e)\left(\exp(-P_e x_2^*) - \exp(-P_e x_1^*) + P_e(x^* - x_1^*)\right)}{P_e(x_2^* - x_1^*)\left(\exp(P_e)-1\right)} \\ \dfrac{x_2^* - x^*}{(x_2^* - x_1^*)\left(\exp(P_e)-1\right)} \\ -\displaystyle\sum_{k=1}^{\infty} \dfrac{f_{1k}(x^*)}{s_k} \exp\left(-s_k t^*\right), \text{ for } x_1^* \le x^* < x_2^*, \\ \dfrac{\exp(P_e)}{\exp(P_e)-1} + \dfrac{\exp(P_e)\left(\exp(-P_e x_2^*) - \exp(-P_e x_1^*)\right)}{P_e(x_2^* - x_1^*)\left(\exp(P_e)-1\right)} \\ -\displaystyle\sum_{k=1}^{\infty} \dfrac{f_{1k}(x^*)}{s_k} \exp\left(-s_k t^*\right), \text{ for } x_2^* \le x^* \le 1. \end{cases} \tag{3.96}$$

$$N_u(x^*,t^*) = \int_0^{t^*} n_u(x^*,\tau)\mathrm{d}\tau = \frac{1-\exp\left(P_e(x^*-1)\right)}{1-\exp\left(-P_e\right)} - \sum_{k=1}^{\infty} \frac{g_k(x^*)\exp\left(-s_k t^*\right)}{s_k}, \tag{3.97}$$

$$N_d(x^*,t^*) = \int_0^{t^*} n_d(x^*,\tau)\mathrm{d}\tau = \frac{1-\exp\left(P_e x^*\right)}{1-\exp\left(P_e\right)} - \sum_{k=1}^{\infty} \frac{i_k(x^*)\exp\left(-s_k t^*\right)}{s_k}, \tag{3.98}$$

$$N_l(x^*,t^*) = \int_0^{t^*} n_l(x^*,\tau)\mathrm{d}\tau = \begin{cases} \dfrac{\left(1-\exp\left(-P_e x_0^*\right)\right)\left(1-\exp\left(P_e(x^*-1)\right)\right)}{\beta\left(1-\exp\left(-P_e\right)\right)} \\ -\displaystyle\sum_{k=1}^{\infty} \dfrac{j_k(x^*)\exp\left(-s_k t^*\right)}{s_k}, & \text{for } x^* > x_0^*, \\ \dfrac{\left(\exp\left(P_e x^*\right)-1\right)\left(\exp\left(P_e(1-x_0^*)\right)-1\right)}{\beta\left(\exp\left(P_e\right)-1\right)} \\ -\displaystyle\sum_{k=1}^{\infty} \dfrac{j_k(x^*)\exp\left(-s_k t^*\right)}{s_k}, & \text{for } x^* < x_0^*, \end{cases} \tag{3.99}$$

$$N_{ld}(x^*,t^*) = \int_0^{t^*} n_{ld}(x^*,\tau)\mathrm{d}\tau$$

$$
= \begin{cases}
\dfrac{1-\exp(P_e x^*)}{\beta P_e (x_2^* - x_1^*)(\exp(P_e)-1)} \left(\exp(P_e)\left(\exp(-P_e x_2^*) - \exp(-P_e x_1^*)\right) + P_e(x_2^* - x_1^*)\right) \\
-\displaystyle\sum_{k=1}^{\infty} \frac{j_{1k}(x^*)}{s_k} \exp\left(-s_k t^*\right), \text{ for } 0 \le x^* < x_1^*, \\
\exp(P_e)\dfrac{\exp(-P_e x_2^*) - \exp(-P_e x_1^*) - \exp(P_e(x^* - x_2^*)) + P_e(x^* - x_1^*) + 1}{\beta P_e(x_2^* - x_1^*)\left(\exp(P_e)-1\right)} \\
+\dfrac{P_e(x_1^* - x_2^*)\exp(P_e x^*) + P_e(x_2^* - x^*) + \exp(P_e(x^* - x_1^*)) - 1}{\beta P_e(x_2^* - x_1^*)\left(\exp(P_e)-1\right)} \\
-\displaystyle\sum_{k=1}^{\infty} \frac{j_{1k}(x^*)}{s_k} \exp\left(-s_k t^*\right), \text{ for } x_1^* \le x^* < x_2^*, \\
\dfrac{\exp(P_e) - \exp(P_e x^*)}{\beta P_e (x_2^* - x_1^*)} \dfrac{\exp(-P_e x_2^*) - \exp(-P_e x_1^*) + P_e(x_2^* - x_1^*)}{\exp(P_e)-1} \\
-\displaystyle\sum_{k=1}^{\infty} \frac{j_{1k}(x^*)}{s_k} \exp\left(-s_k t^*\right), \text{ for } x_2^* \le x^* \le 1.
\end{cases} \tag{3.100}
$$

Tingsanchali and Manandhar [49] presented a solution for the flow depth with the lateral inflow considered as source and sink with the water depth given at both boundaries in its dimensional form. The unit-step responses for the flow depth corresponding to different inputs, i.e., Eqs. (3.97)−(3.99), are the non-dimensional forms of the responses given by Tingsanchali and Manandhar [49]. As a consequence, we deem it not necessary to explain the behavior of these responses any further to avoid repetition. However, it is to be noted that they did not provide any solution for the flow discharge subject to the same boundary conditions. These flow-discharge responses corresponding to different inputs are discussed in the next section and those are depicted through Figs. 3.8−3.12.

3.3 Results and discussion

The responses presented in the previous section are an extension to the work done by Cimorelli et al. [7]. Since the usefulness and accuracy of finite channel results to simulate the real flows was established by Cimorelli et al. [6], we show the results for different Péclet numbers and present comparisons with the corresponding semi-infinite channel responses. The main motivation behind these comparisons in our study is to check the appropriateness of semi-infinite channel responses when they are used to approximate finite channel results for the types of boundary conditions that are considered in this work. We present the comparisons with semi-infinite channel responses because of the unavailability of the analytical solutions for the considered types of boundary conditions. This section is divided in two parts. In the first part, the responses for the flow discharge and the flow depth corresponding to the concentrated lateral inflow, upstream boundary, and downstream boundary are discussed for two types of upstream boundaries. The second part discusses the behavior of the flow discharge and the flow depth corresponding to a uniformly distributed lateral inflow between the locations x_1^* and x_2^*.

3.3.1 Comparison of the unit-step responses for different values of the Péclet number

For the flow-discharge hydrograph at the upstream end

For the validation of the results presented in the previous section as well as to find the limitations of the semi-infinite channel responses when used to approximate the finite channel results, we compare the obtained finite channel unit-step responses with those of Fan and Li [19]. The dimensionless forms of the responses of the flow discharge to the concentrated unit-step input lateral inflow for a given flow discharge at the upstream end in a semi-infinite channel are expressed as

$$\begin{aligned} A_{l,\infty}(x^*,t^*) = &\frac{1}{2}\left(1-\operatorname{erf}\left(\frac{x^*-x_0^*-t^*}{\sqrt{4t^*}}\sqrt{P_e}\right)\right) \\ &+\frac{1}{2}\exp(P_e x^*)\left(1-\operatorname{erf}\left(\frac{x^*+x_0^*+t^*}{\sqrt{4t^*}}\sqrt{P_e}\right)\right), \text{ for } x^*>x_0^*, \end{aligned} \tag{3.101a}$$

$$\begin{aligned} A_{l,\infty}(x^*,t^*) = &\frac{1}{2}\left(\operatorname{erf}\left(\frac{|x^*-x_0^*|+t^*}{\sqrt{4t^*}}\sqrt{P_e}\right)-1\right) \\ &+\frac{1}{2}\exp(P_e x^*)\left(1-\operatorname{erf}\left(\frac{x^*+x_0^*+t^*}{\sqrt{4t^*}}\sqrt{P_e}\right)\right), \text{ for } x^*<x_0^*, \end{aligned} \tag{3.101b}$$

where erf(.) is the error function. The corresponding expression for the flow depth can be calculated, by using Eq. (3.9), as

$$B_{l,\infty}(x^*,t^*) = \frac{1}{\beta}\int_0^{t^*}\left(q_l^*(x^*,\tau)-\frac{\partial}{\partial x^*}A_{l,\infty}(x^*,\tau)\right)\mathrm{d}\tau. \tag{3.102}$$

Since the lateral inflow is concentrated at x_0^*, for $x^* \neq x_0^*$, $q_l^*(x^*,t^*) = 0$, and hence the above expression reduces to

$$B_{l,\infty}(x^*,t^*) = -\frac{1}{\beta}\int_0^{t^*}\frac{\partial}{\partial x^*}A_{l,\infty}(x^*,\tau)\mathrm{d}\tau, \quad \text{for } x^* \neq x_0^*. \tag{3.103}$$

It is difficult to solve this integral analytically, and consequently, we use numerical integration technique to evaluate it by using the inbuilt function *integral* in *MATLAB* which takes three arguments: $integral(fun, xmin, xmax)$; *fun* is used for the expression inside the integral of Eq. (3.103) with *xmin* as zero and *xmax* taking the value of t^*. β works only as a scaling factor, and hence its value is set as 1. Figures 3.3 and 3.6, respectively, present the comparison of the responses for flow discharge $A_l(x^*,t^*)$ and flow depth $B_l(x^*, t^*)$ in a finite channel with the responses for flow discharge $A_{l,\infty}(x^*, t^*)$ and flow depth $B_{l,\infty}(x^*, t^*)$ in a semi-infinite channel for different values of the Péclet number. In all the comparisons, the results of the finite channel are plotted with continuous curves, and those of the semi-infinite channel results are plotted with dashed curves. In Figs. 3.2−3.7, the flow-discharge and flow-depth responses to the unit-step lateral inflow input are plotted by taking the upstream and downstream boundary condition as zero, i.e., $Q^*(0, t^*) = 0$ and $h^*(1, t^*) = 0$. Physically, this means that there is no perturbation in the flow discharge at the upstream end to the uniform steady condition (Q_0) and also in the flow depth at the downstream end to the uniform steady condition (h_0).

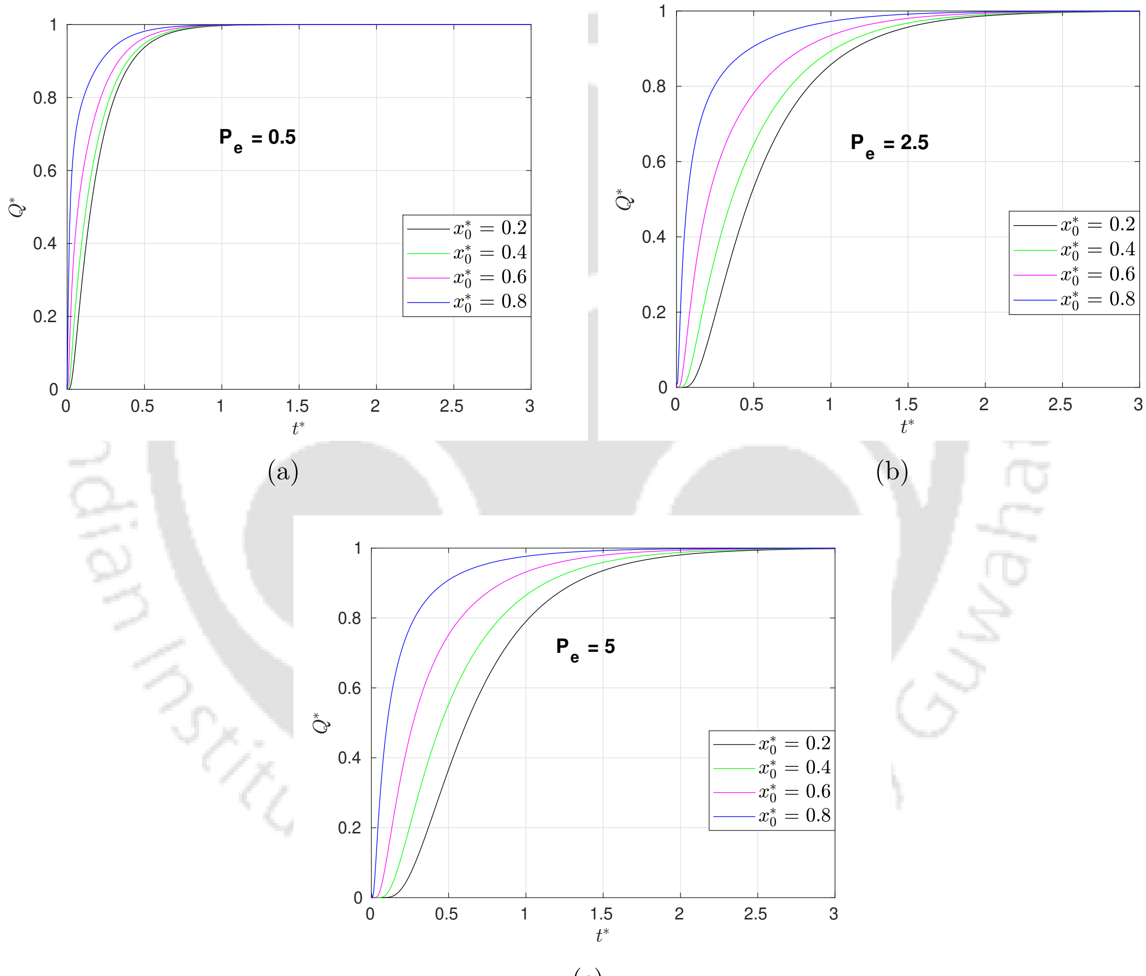

Figure 3.2: Flow-discharge response given in Eq. (3.55) at $x^* = 1$ to the unit-step lateral inflow concentrated at x_0^* with $Q^*(0, t^*) = 0$ and $h^*(1, t^*) = 0$: (a) $P_e = 0.5$, (b) $P_e = 2.5$, (c) $P_e = 5$

In Fig. 3.2, the flow-discharge responses to the unit-step lateral inflow input given at different x_0^* are plotted at the downstream end $(x^* = 1)$ for different values of P_e. As observed from this figure, the graphs converge to 1 for all the cases. The convergence

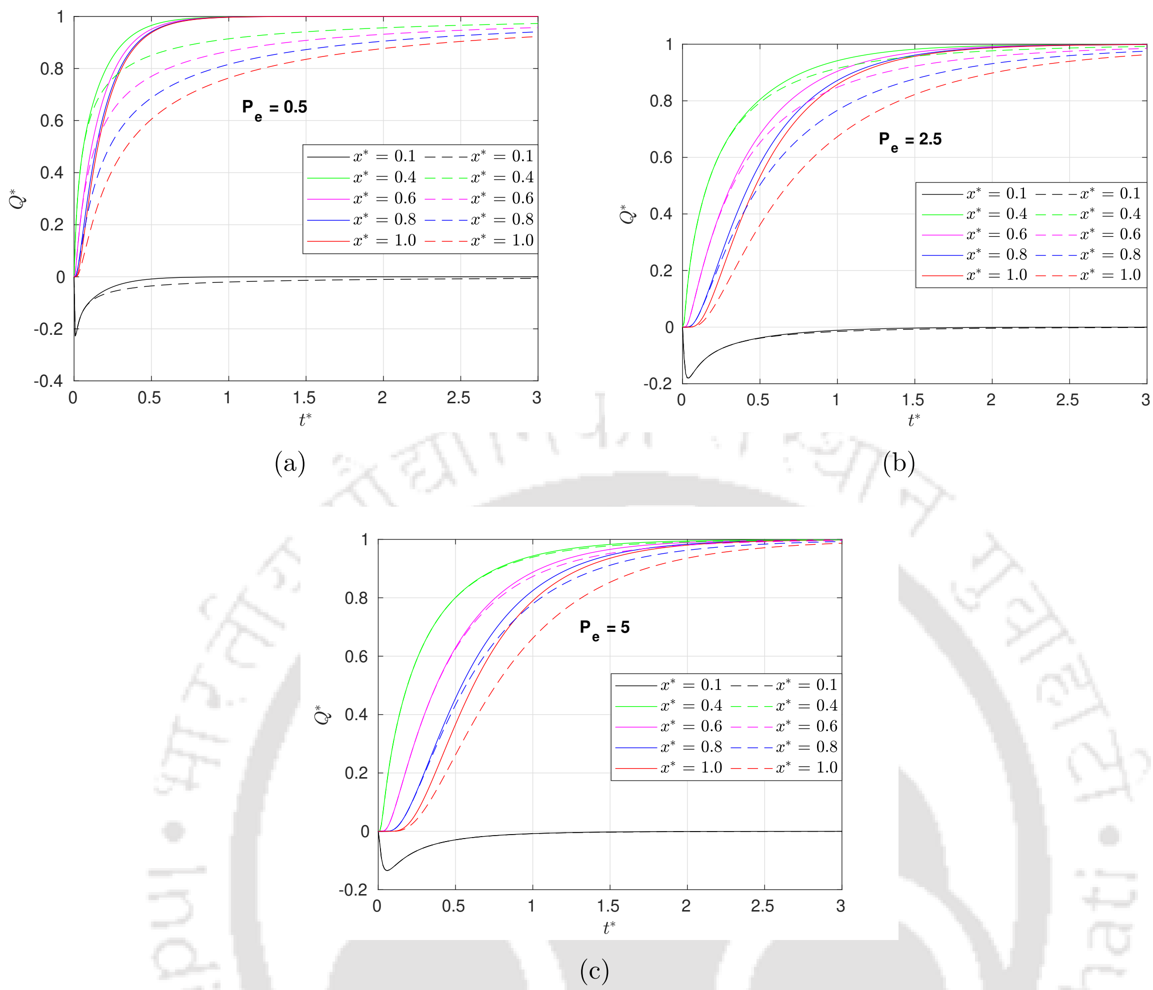

Figure 3.3: Comparison between flow-discharge response for finite channel given in Eq. (3.55) – continuous curves, and flow-discharge response for semi-infinite channel given in Eq. (3.101) – dashed curves, to a unit-step lateral inflow concentrated at $x_0^* = 0.2$ for different x^* with $Q^*(0,t^*) = 0$ and $h^*(1,t^*) = 0$: (a) $P_e = 0.5$, (b) $P_e = 2.5$, (c) $P_e = 5$

process takes longer for higher values of P_e. Larger the distance between the concentrated lateral input and downstream boundary, slower is the convergence of the graphs. This means that, when the distance between x_0^* and the downstream end is small, the effect of the unit-step lateral input can be observed more clearly, and the time lag between the input and output is observed to be small.

In Fig. 3.3, the effect of the unit-step lateral input given at $x_0^* = 0.2$ on the flow discharge at different locations of the channel is examined and compared with the corresponding semi-infinite channel results for different values of P_e. For $x^* < x_0^*$, a negative value of discharge is observed which is the result of the backwater effect induced by the lateral inflow. Since this lateral inflow response is derived by considering the upstream boundary condition as zero, this effect is much smaller and almost close to zero for the locations closer to the upstream end. However, it can be observed prominently on the upstream locations closer to the tributary. To get a positive value for the discharge, these responses should be combined with the appropriate upstream and downstream boundary conditions. This dip in the discharge values gets reduced as the value of P_e is increased which shows that the backwater effect of the lateral inflow and the downstream boundary is less effective for higher values of P_e. The sharpness in the dip is caused by the combined backwater effect of the downstream boundary and the lateral inflow which is more prominent for lower values of P_e as can be observed from Fig. 3.3(a). The sharpness in the dip also reduces as the value of P_e is increased. For the case $x^* > x_0^*$ in the finite channel results, the difference in the graph for the locations $x^* = 0.8$ and $x^* = 1$ is insignificant for $P_e = 0.5$ as can be observed from Fig. 3.3(a). This difference in these two responses increases as we increase the value of P_e. This is visible from Figs. 3.3(b) and 3.3(c). This means that the effect of the downstream boundary present in terms of a flow-depth hydrograph is clearly noticeable for lower values of the Péclet number. Due to this, the effect of the lateral input given at $x_0^* = 0.2$ is almost similar at the locations closer to the downstream end. The decay in the inputs is also prominent for the locations far from x_0^*. The convergence pattern for $x^* > x_0^*$ is similar to the one observed in Fig. 3.2. For $x^* < x_0^*$, the response predicted by the semi-infinite channel result is quite close to the finite channel response for $P_e = 0.5$, but it is not the case for $x^* > x_0^*$. Although the semi-infinite channel results do reciprocate the results well for the locations closer to the lateral inflow for $P_e = 5$, but as the distance between x_0^* and x^* increases in both directions, it is observed that the semi-infinite channel results underestimate the value of the discharge. The difference in the magnitude of the limiting value for $x^* > x_0^*$ and $x^* < x_0^*$ is exactly 1, giving a discontinuity in the discharge at x_0^*. This shows the direct effect of the concentrated lateral inflow located at the location x_0^* which gives rise to this discontinuity.

To study the effect of the lateral inflow along the entire channel, the behavior of the discharge response to the unit-step lateral inflow input given at different values of x_0^* is presented in Fig. 3.4 at different locations of the channel for $P_e = 1$. Here, for $x^* < x_0^*$, the reduction in the backwater effect of the lateral inflow is clearly visible as the distance between x^* and x_0^* is increased. The effect of the lateral inflow for $x^* > x_0^*$ approaches the value 1 as time progresses. But, for a particular value of x_0^*, its effect reduces as the distance between x^* and x_0^* is increased. This clearly shows the disturbance in the discharge caused by the lateral inflow. The discharge reduces for the upstream locations closer to x_0^*, and then a sudden jump is observed for the downstream locations closer to x_0^* due to the lateral inflow input. The sharpness in the dip in the discharge response for $x^* < x_0^*$ is more visible for x_0^* closer to the downstream end ($x^* = 1$). As the location of the concentrated lateral inflow is moved farther from the downstream end, the sharpness of the dip in the discharge responses decreases for $x^* < x_0^*$ which can be observed from Fig. 3.4(a). This might have happened because, for the locations closer to the downstream

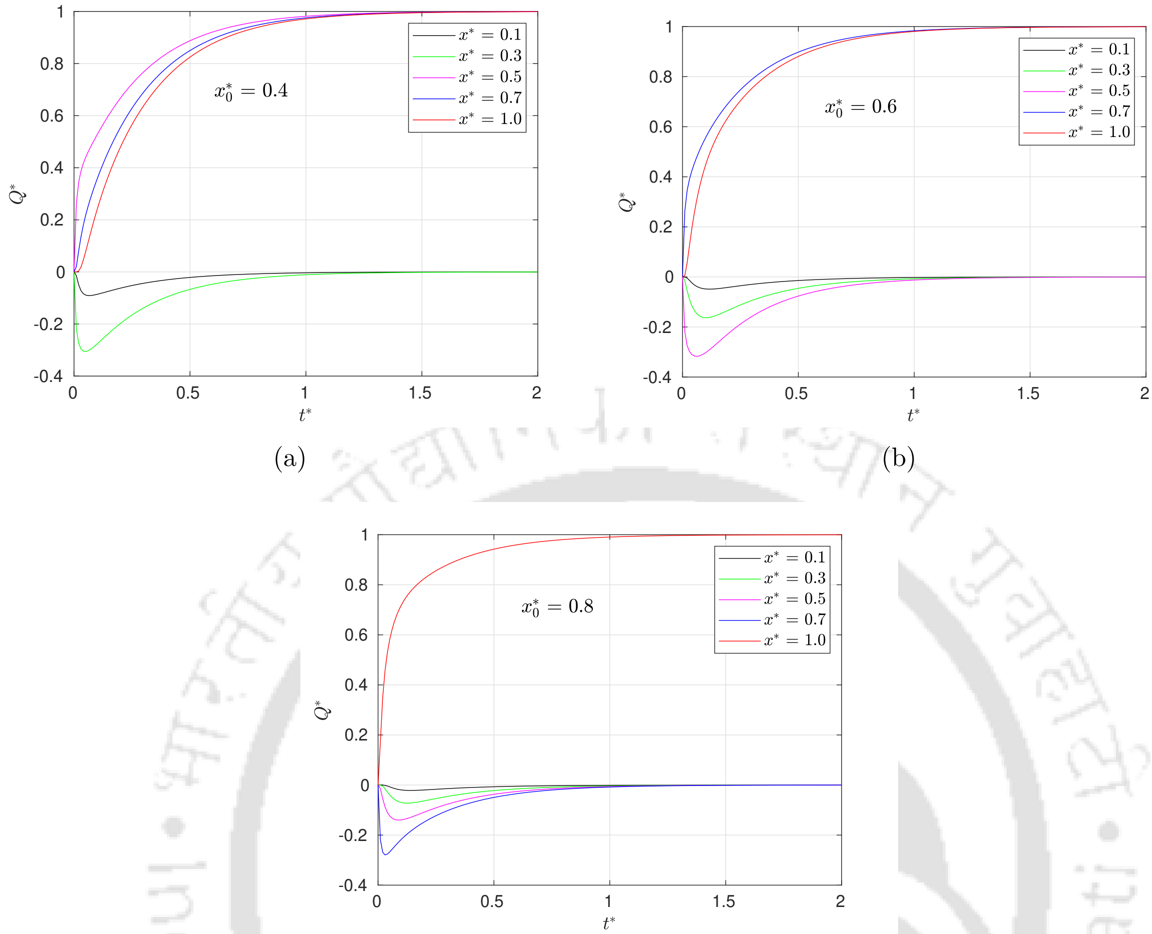

(a) (b)

(c)

Figure 3.4: Flow-discharge response given in Eq. (3.55) for different x^* to the unit-step lateral inflow concentrated at x_0^* for $P_e = 1$ with $Q^*(0, t^*) = 0$ and $h^*(1, t^*) = 0$: (a) $x_0^* = 0.4$, (b) $x_0^* = 0.6$, (c) $x_0^* = 0.8$

end, the combined backwater effect of the lateral inflow and the downstream boundary gives a sharper dip in the discharge. But for the locations closer to the upstream end, the backwater effect of the lateral inflow is more prominent compared with the backwater effect of the downstream boundary.

Figure 3.5 presents the behavior of the flow depth at a location closer to the downstream end, viz., $x^* = 0.9$, induced by the unit-step lateral input given at different locations of the lateral inflow for different values of P_e. We choose this location of observation because the downstream boundary is present in terms of the flow depth. The unit-step response given in Eq. (3.56) is derived under the assumption of flow depth as zero at the downstream end. The behavior of the effect of the lateral input on the flow depth is similar to the graphs in Fig. 3.2 except for the change in the convergence limits. The convergence value for each case is different, and it increases as the value of P_e increases.

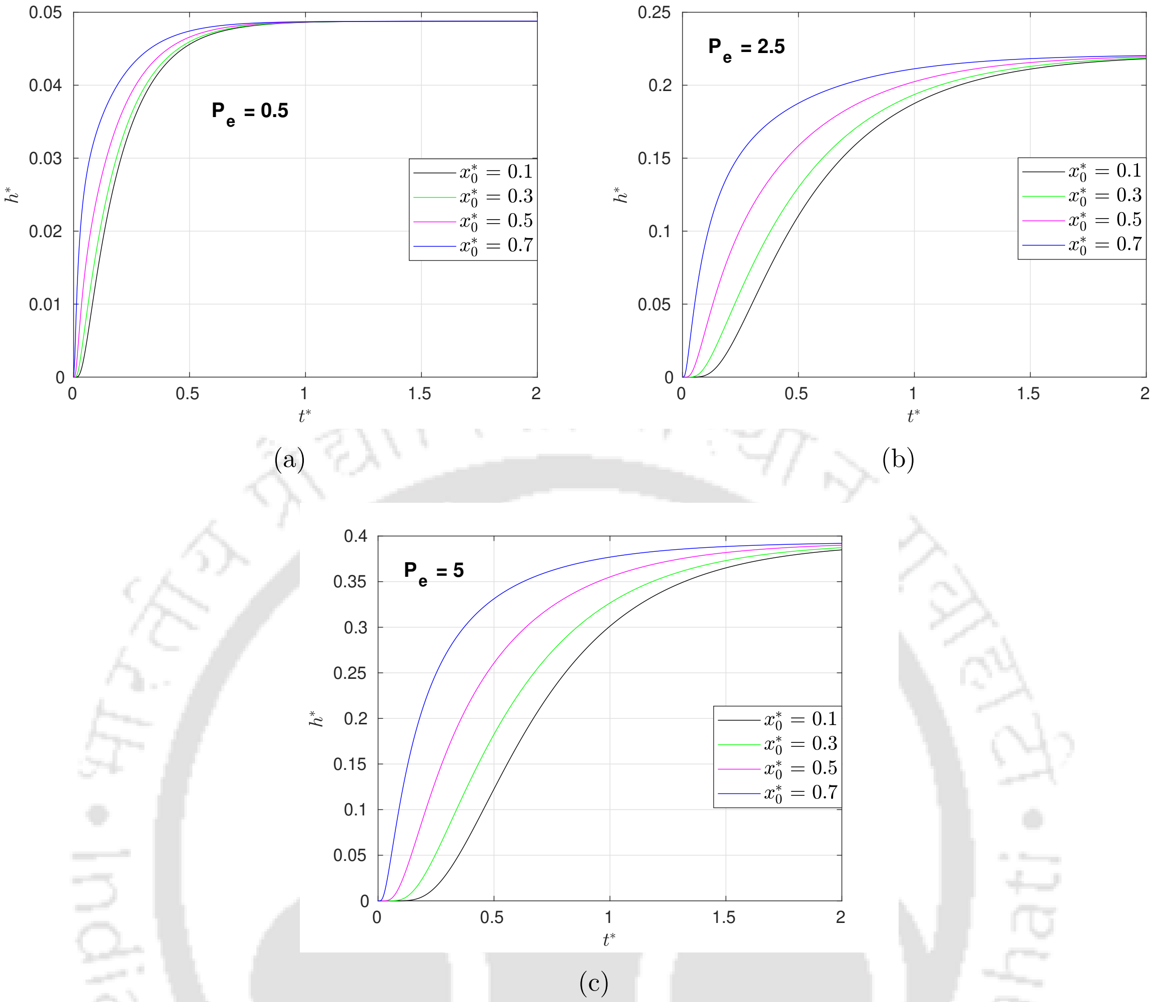

Figure 3.5: Flow-depth response given in Eq. (3.56) at $x^* = 0.9$ to the unit-step lateral inflow concentrated at x_0^* with $\beta = 1$, $Q^*(0, t^*) = 0$ and $h^*(1, t^*) = 0$: (a) $P_e = 0.5$, (b) $P_e = 2.5$, (c) $P_e = 5$

The responses for higher Péclet numbers take a longer time to converge as can be observed from Fig. 3.5(c). From Fig. 3.2 and Fig. 3.5, we can say that, for a given flow discharge at the upstream end, the flow discharge and flow depth are not sensitive to the lateral inflow location for large times for $x^* > x_0^*$, which is not the case for a flow-depth-based upstream boundary as shown later in Fig. 3.10.

Figure 3.6 presents the comparison of the effect of the unit-step lateral inflow concentrated at $x_0^* = 0.2$ on the flow depth at different locations of the channel with the corresponding semi-infinite channel response. For finite channels, although the value of the convergence limit increases as the value of P_e increases, it decreases with an increase in the value of x^* for the case $x^* > x_0^*$. The most interesting observation is for the case $P_e = 0.5$, for which higher values of the flow depth are observed for the location upstream to the location of the lateral inflow, i.e., $x^* = 0.1$. The convergence rate is also slower for higher values of x^* which can be clearly observed from Fig. 3.6(c). For $x^* > x_0^*$, the convergence limit is dependent on the point of observation but it is independent of the location of the lateral inflow. This means that, for any value of x_0^* with a given flow discharge at the upstream end, the convergence limit of the flow depth for $x^* > x_0^*$ is the same for all x^* in the case of a finite channel. But this limit is equal to 1 for the case of a semi-infinite channel. For $x^* < x_0^*$, the convergence limit is dependent on x_0^* as well. When x^* is closer to the upstream end, the responses estimated by the semi-infinite channel result is very close to the finite channel response for the case $P_e = 5$ as shown in Fig. 3.6(c). But, as the distance between x^* and the downstream end ($x^* = 1$) reduces, the semi-infinite channel response completely fails to estimate the finite channel response. The presence of the downstream plays a much dominant role in the behavior of the flow depth as compared with the presence of the concentrated lateral inflow.

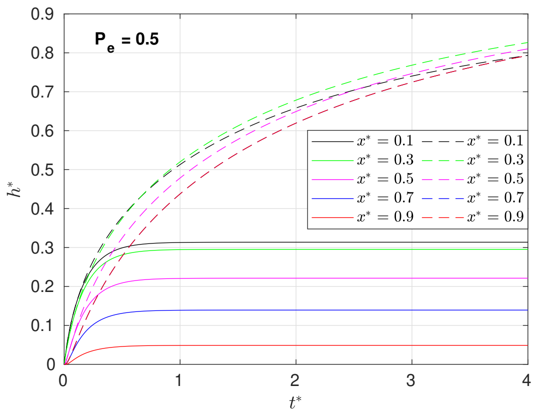

(a)

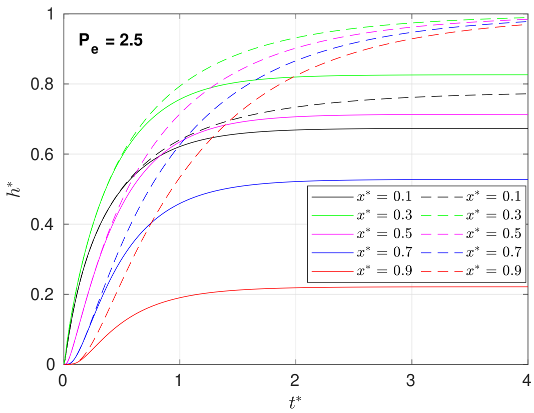

(b)

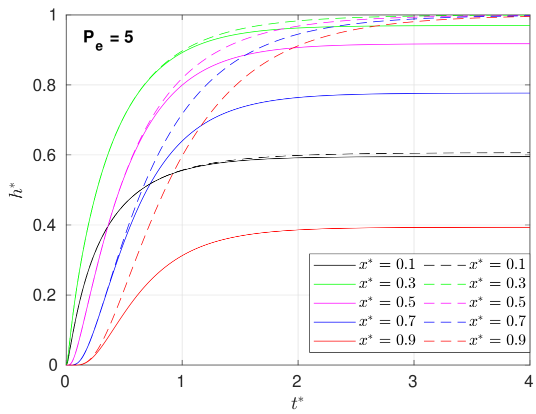

(c)

Figure 3.6: Comparison between flow-depth response for finite channel given in Eq. (3.56) – continuous curves, and flow-depth response for semi-infinite channel given in Eq. (3.103) – dashed curves, to the unit-step lateral inflow concentrated at $x_0^* = 0.2$ for different x^* with $\beta = 1$, $Q^*(0, t^*) = 0$ and $h^*(1, t^*) = 0$: (a) $P_e = 0.5$, (b) $P_e = 2.5$, (c) $P_e = 5$

The behavior of the flow-depth response to the unit-step lateral inflow input given at different x_0^* is presented in Fig. 3.7 for different locations of the channel and $P_e = 1$. The flow depth is continuous throughout the domain in contrast to the flow discharge which was shown in Fig. 3.4. Higher values of the flow depth are observed for the locations x^* closer to x_0^* with $x^* < x_0^*$ as is evident from Figs. 3.7(a)–3.7(c). This is the combined backwater effect of the lateral inflow and the downstream boundary which is more prominent here since we consider a lower value of P_e, viz., $P_e = 1$. The flow depth does decrease as the distance between x_0^* and the downstream end decreases. But the flow depth increases overall along the channel due to the lateral inflow and the downstream boundary. In a general sense, the flow depth slowly decreases as the distance between x^* and x_0^* is increased but higher values for the flow depth are observed at the locations closer to x_0^*.

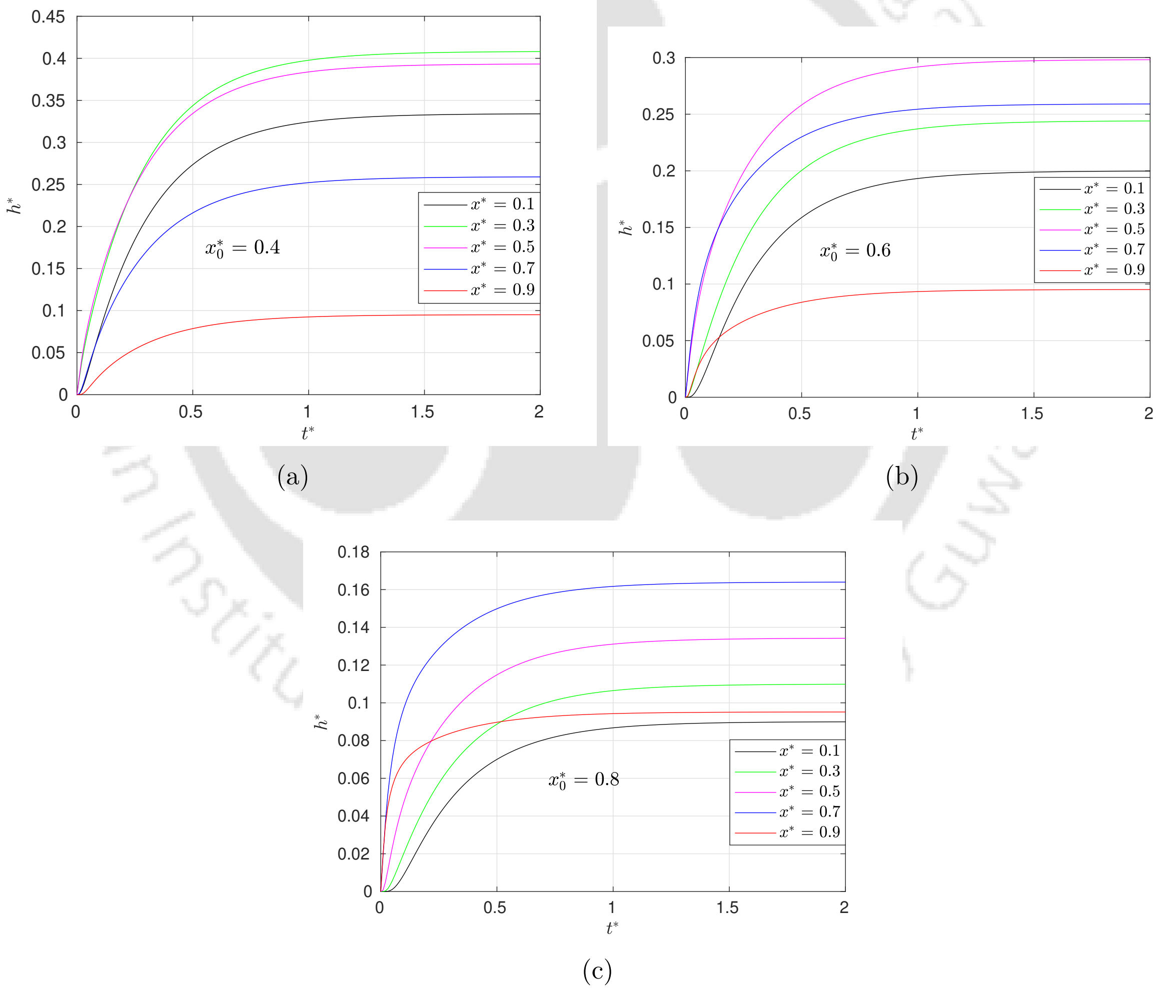

Figure 3.7: Flow-depth response given in Eq. (3.56) for different x^* to the unit-step lateral inflow concentrated at x_0^* for $P_e = 1$ with $\beta = 1$, $Q^*(0, t^*) = 0$ and $h^*(1, t^*) = 0$: (a) $x_0^* = 0.4$, (b) $x_0^* = 0.6$, (c) $x_0^* = 0.8$

Cimorelli et al. [7] presented the flow-discharge and the flow-depth responses to a flow discharge given at the upstream end, a flow depth given at the downstream end, and a uniformly distributed lateral inflow. It is observed that the behavior of the lateral response obtained here is quite different from the one in Cimorelli et al. [7]. However, the behavior of the lateral response presented for the case $x^* > x_0^*$ resembles the behavior of the corresponding upstream responses given in Cimorelli et al. [7].

For the flow-depth hydrograph at the upstream end

Here, we plan to compare the flow-discharge responses to a unit-step input as the flow-depth hydrograph imposed at the upstream end for a finite channel and semi-infinite channel for different values of the Péclet number. For this comparison, the semi-infinite channel result from Cimorelli et al. [6] is considered. The flow-discharge response derived by them is given as

$$Y_{u,\infty}(x^*, t^*) = \frac{\beta}{2}\operatorname{erfc}\left(\frac{x^* - t^*}{\sqrt{4t^*}}\sqrt{P_e}\right) + \frac{\beta}{\sqrt{\pi P_e t^*}}\exp\left(-\frac{(x^* - t^*)^2}{4t^*}P_e\right), \tag{3.104}$$

where erfc(.) denotes the complementary error function.

For this case, the downstream boundary condition and lateral inflow are taken as zero, i.e., $h^*(1, t^*) = 0$ and $T^*(t^*) = 0$. Physically, this means that there is no perturbation in the flow depth at the downstream end to the uniform steady condition (h_0) and there is no contribution of the lateral inflow to the channel. In Fig. 3.8, the flow discharge response $M_u(x^*, t^*)$ for a finite channel is compared with the flow discharge response $Y_{u,\infty}(x^*, t^*)$ for a semi-infinite channel, to a unit-step flow depth at the upstream end, for different values of P_e and x^*. Again, the value of β is kept as 1. One can clearly notice a peak of the response function which decays as one moves away from the upstream boundary. This peak is observed for both the finite channel and the semi-infinite channel. This peak reduces as the value of P_e is increased, and for large values of P_e, it completely vanishes. Cimorelli et al. [6] carried out this comparison with a stage-discharge relationship imposed at the downstream end at which the semi-infinite channel result mimics the finite channel result well for $P_e = 5$ except at $x^* = 1$. Graphs for $P_e = 5$ show a similar behavior as was mentioned in Cimorelli et al. [6], but the semi-infinite channel results do not match with the finite channel results at all the locations. Here, the difference is quite significant in the convergence limit when smaller values of the Péclet number are considered. This difference does decrease with an increase in the value of P_e but does not vanish completely. The convergence rate is also slower for the semi-infinite channel in comparison to the finite channel case.

Next, we consider that the upstream boundary condition and lateral inflow are zero, i.e., $h^*(0, t^*) = 0$ and $T^*(t^*) = 0$. Physically, this means that there is no perturbation in

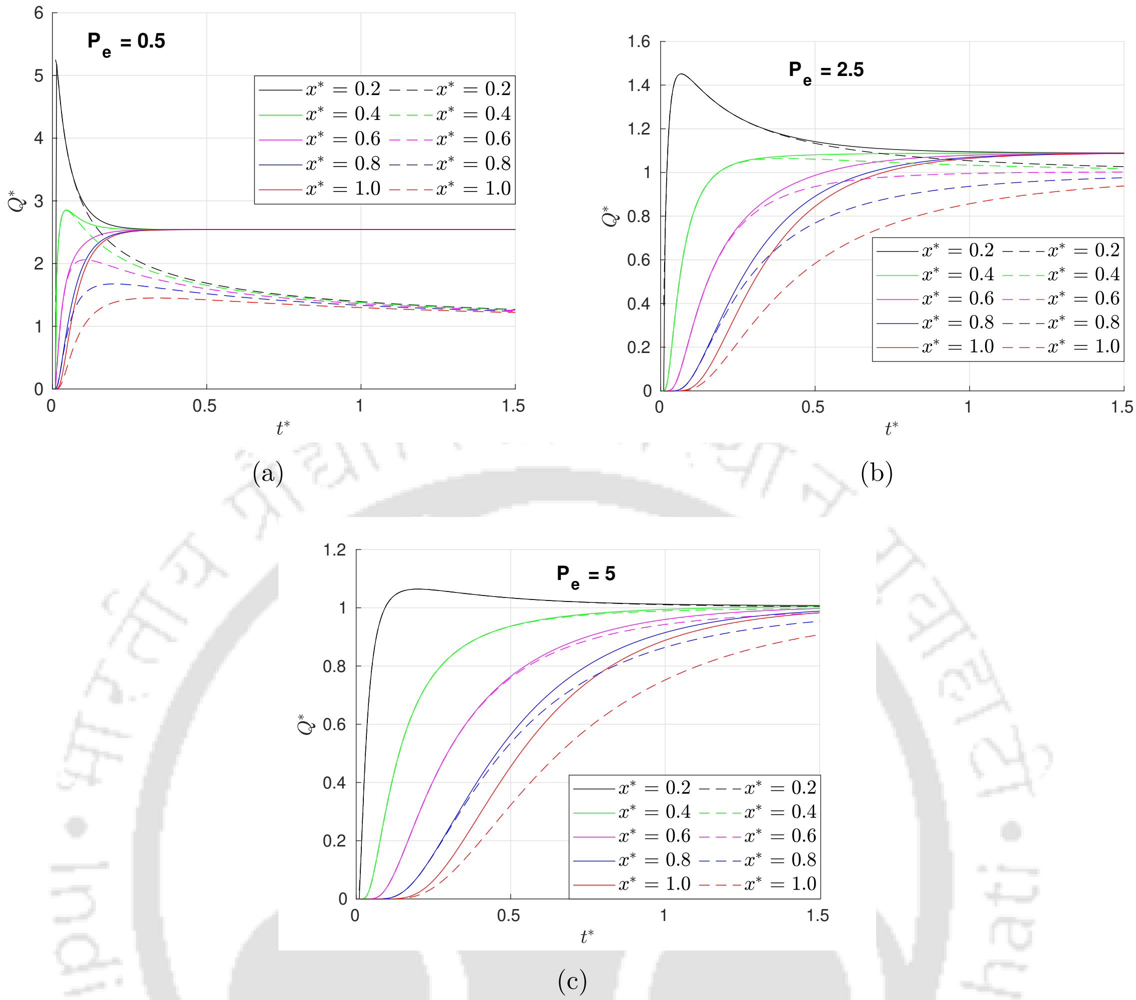

Figure 3.8: Comparison between flow-discharge response for finite channel given in Eq. (3.93) – continuous curves, and flow-discharge response for semi-infinite channel given in Eq. (3.104) – dashed curves, to the unit-step upstream flow depth at different x^* with $\beta = 1$, $h^*(1, t^*) = 0$ and $T^*(t^*) = 0$: (a) $P_e = 0.5$, (b) $P_e = 2.5$, (c) $P_e = 5$

the flow depth at the upstream end to the uniform steady condition (h_0) and there is no contribution of the lateral inflow to the channel. Figure 3.9 presents the flow discharge response $M_d(x^*, t^*)$ to a unit-step flow depth given at the downstream end for different values of P_e and x. Here, negative values of the flow discharge exist for all values of P_e. This dip corresponds to the effect of reduction in the flow discharge level in the upstream direction due to the downstream boundary which is the backwater effect. All values of the flow discharge are negative because the downstream response is derived under the assumption of zero upstream boundary condition. Therefore, this downstream response should be used with an upstream boundary, whether it is the flow discharge as given in Cimorelli et al. [7] or the flow depth which is presented above and shown in Fig. 3.8. For the locations very close to the downstream end (say, for $x^* = 0.8$), the dip in the flow discharge reduces as the Péclet number increases. This effect also reduces as the distance between x^* and the downstream boundary increases. For $P_e = 5$, the effect of the downstream boundary at the location $x^* = 0.2$ is almost negligible. The time taken to converge to the limiting value is longer for higher values of P_e.

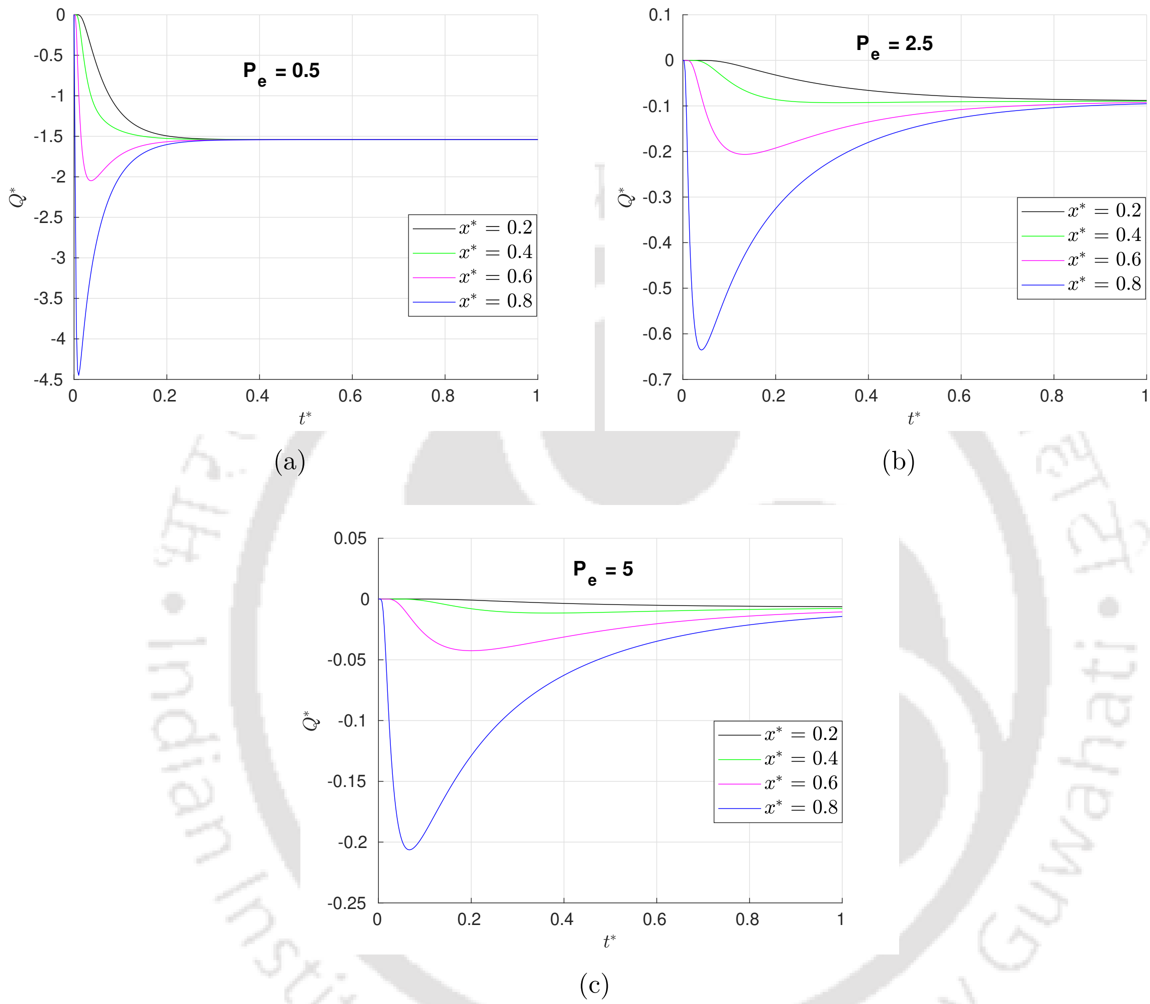

Figure 3.9: Flow-discharge response given in Eq. (3.94) to the unit-step downstream flow depth at different x^* with $\beta = 1$, $h^*(0, t^*) = 0$ and $T^*(t^*) = 0$: (a) $P_e = 0.5$, (b) $P_e = 2.5$, (c) $P_e = 5$

To compare the finite channel discharge response to a unit-step lateral inflow with a semi-infinite one, the method used in Fan and Li [19] is followed to derive the same. In order to obtain this form, we require a second-order partial differential equation for $h^*(x^*, t^*)$ which can be found from the system of equations given by Eqs. (3.9) and (3.10) as

$$-\frac{1}{P_e}\frac{\partial^2 h^*}{\partial x^{*2}} + \frac{\partial h^*}{\partial x^*} + \frac{\partial h^*}{\partial t^*} = \frac{q_l^*}{\beta}, \tag{3.105}$$

with $h^*(x^*, 0) = 0$ as the initial condition, and an upstream boundary given as a function of t^*, i.e., $h^*(0,t^*)$. The response to the unit-step lateral inflow is first solved for $h^*(x^*,t^*)$ by using the methodology followed by Fan and Li [19]. Then, the corresponding flow-discharge response is obtained by using Eq. (3.10). The flow-discharge response to the unit-step concentrated lateral inflow at x_0^*, for a given flow depth at the upstream end, can be written as

$$M_{l,\infty}(x^*,t^*) = \frac{1}{2P_e}\text{erfc}\left(\sqrt{\frac{P_e}{4t}}(x^* - x_0^* - t^*)\right) + \frac{\exp\left(-P_e x_0^*\right)}{2P_e}\text{erfc}\left(\sqrt{\frac{P_e}{4t}}(x^* + x_0^* - t^*)\right), \quad \text{for } x^* > x_0^*. \tag{3.106}$$

The flow-discharge responses to the unit-step lateral inflow are presented in Figs. 3.10−3.12 by taking the upstream and downstream boundary conditions as zero, i.e., $h^*(0,t^*) = 0$ and $h^*(1,t^*) = 0$. Physically, this means that there is no perturbation in the flow depth at the upstream and downstream ends to the uniform steady condition (h_0).

Figure 3.10 shows the behavior of the flow discharge at the downstream end ($x^* = 1$) induced by the unit-step lateral inflow given at different x_0^*. Here, higher values of the flow discharge at the downstream end are observed when the location of the concentrated lateral inflow is closer to it. Conforming to the behavior explained in the earlier cases, the asymptotic convergence takes more time for higher values of P_e. The steepness of the graph is also higher for the locations of the concentrated lateral inflow closer to the downstream boundary, which can be physically explained by the fact that the effect of a concentrated lateral inflow can be clearly observed at the locations nearer to the source. For $P_e = 0.5$, the effect of the lateral inflow at the downstream end from the farthest location, i.e., $x_0^* = 0.2$, is not prominent as observed from Fig. 3.10(a). As the limiting value is dependent on P_e as well as on x_0^*, there exists a higher convergence limit for higher values of x_0^*. Since the limiting value is dependent on x_0^*, it means that, if a flow-depth-based upstream boundary is considered, there will be a significant effect of the lateral inflow for large times as well. When higher values of P_e are considered, the difference in these limits is smaller for the locations of the concentrated inflow closer to the downstream end as can be observed from Fig. 3.10(c). When the product term $P_e x_0^*$ is very high for even the smallest value of x_0^*, all graphs seem to approach the same limit as can be observed from the expression given in Eq. (3.95).

Figure 3.11 shows a comparison between the discharge response $M_l(x^*,t^*)$ and the corresponding semi-infinite channel discharge response $M_{l,\infty}(x^*,t^*)$ to understand the effect of a concentrated lateral inflow at $x_0^* = 0.2$, for different values of P_e and x^*. Here, the semi-infinite channel result completely fails to reproduce the results of the finite channel responses. The behavior of the semi-infinite channel flow-discharge responses to the unit-step flow depth given at the upstream end is found satisfactory for higher Péclet numbers as shown in Fig. 3.8(c). However, this is not the case here which can be clearly observed

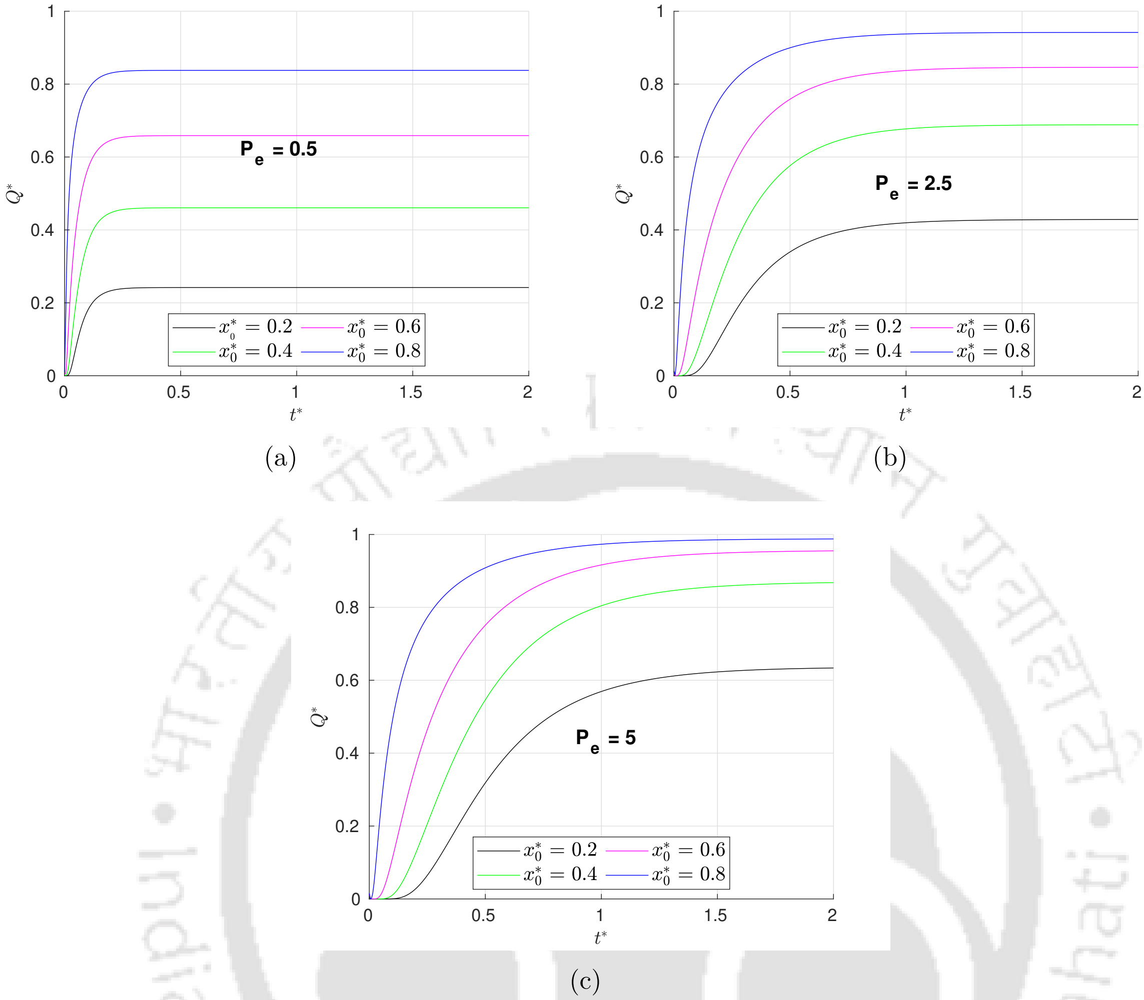

Figure 3.10: Flow-discharge response given in Eq. (3.95) at $x^* = 1$ to the unit-step lateral inflow concentrated at different x_0^* with $h^*(0, t^*) = 0$ and $h^*(1, t^*) = 0$: (a) $P_e = 0.5$, (b) $P_e = 2.5$, (c) $P_e = 5$

from Fig. 3.11(c). The convergence limits of the semi-infinite channel response decrease with an increase of the Péclet number, whereas the limiting values of the finite channel response are observed to be increasing with the Péclet number. The flow-discharge responses for the downstream end and the location closer to it, viz., $x^* = 0.8$, are almost similar. This behavior was also observed in the previous comparisons. This means that the effect of any type of input can be observed more clearly at the locations closer to the source, whether it be a concentrated lateral input or an upstream boundary input. In addition to this, the effect of different inputs on the flow discharge at the locations closer to the downstream end is overshadowed by the effect of a flow-depth-based downstream boundary due to which the difference in the responses at $x^* = 0.8$ and $x^* = 1$ is almost negligible for smaller values of P_e.

In Fig. 3.12, the behavior of the discharge response corresponding to the unit-step

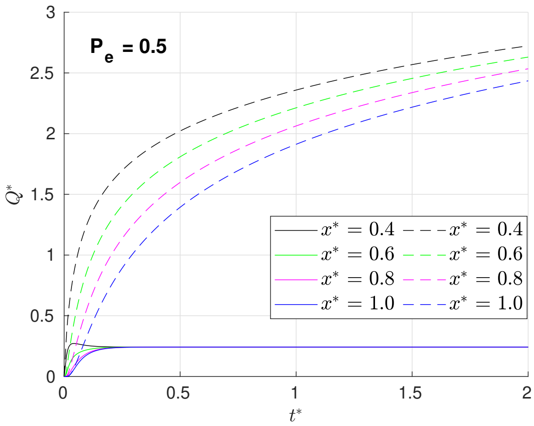

(a)

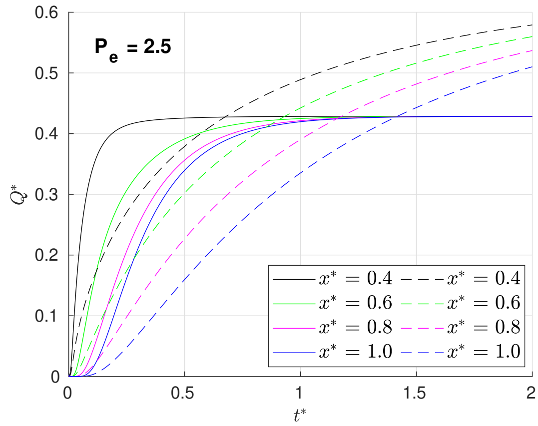

(b)

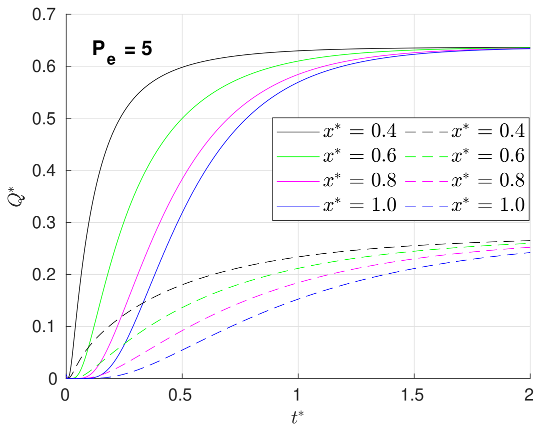

(c)

Figure 3.11: Comparison between flow-discharge response for finite channel given in Eq. (3.95) – continuous curves, and flow-discharge response for semi-infinite channel given in Eq. (3.106) – dashed curves, to the unit-step lateral inflow concentrated at $x_0^* = 0.2$ at different x^* with $h^*(0, t^*) = 0$ and $h^*(1, t^*) = 0$: (a) $P_e = 0.5$, (b) $P_e = 2.5$, (c) $P_e = 5$

lateral inflow concentrated at different x_0^* is presented at different locations of the channel for $P_e = 1$. Similar to the observation made from Fig. 3.4, in this case also, there is a discontinuity in the flow-discharge responses at $x^* = x_0^*$ which leads to distinct limiting values for the cases $x^* < x_0^*$ and $x^* > x_0^*$. The magnitude of the difference between these two limits is again 1 due to the unit-step input given for the concentrated lateral inflow at x_0^*. Furthermore, the values of the discharge are negative for the case $x^* < x_0^*$ which was also observed in Fig. 3.4. But, in contrast to that case, the limiting value for these cases does not reach 0 as the distance between x^* and the upstream boundary is decreased. This happens because the upstream boundary is present in terms of the flow depth here. The limiting values are dependent on the values of P_e and x_0^*, and they increase as the value of x_0^* is increased. As the distance between x_0^* and the downstream

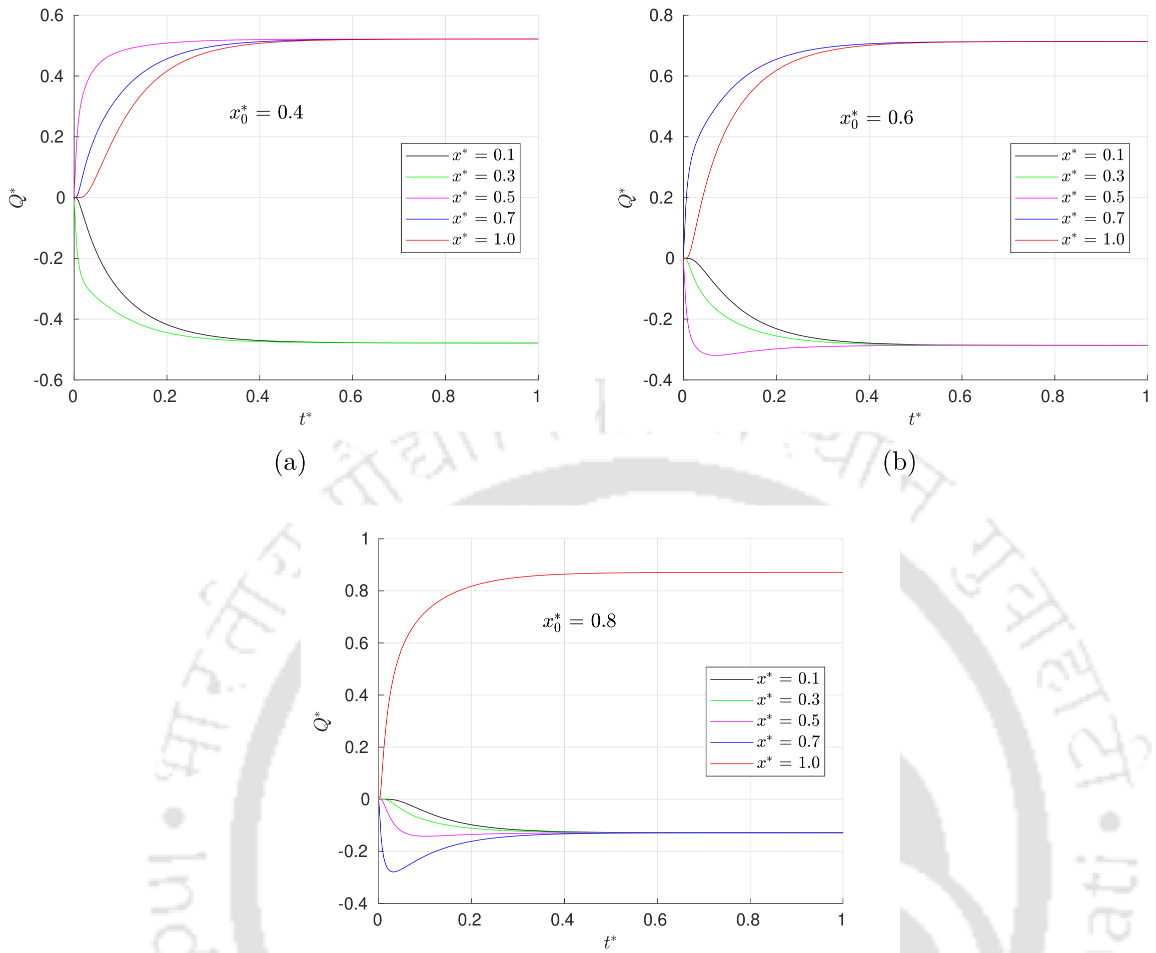

Figure 3.12: Flow-discharge response given in Eq. (3.95) at different x^* to the unit-step lateral inflow concentrated at x_0^* for $P_e = 1$ with $h^*(0,t^*) = 0$ and $h^*(1,t^*) = 0$: (a) $x_0^* = 0.4$, (b) $x_0^* = 0.6$, (c) $x_0^* = 0.8$

end is increased, there is a sharpness in the dip in the flow-discharge responses for the case $x^* < x_0^*$ and it is clearly visible from Fig. 3.12(c). This dip is expected to get sharper as the value of x_0^* is increased further; it appears for the locations closer to the downstream end. When x_0^* is moved closer to the downstream end ($x^* = 1$), the limiting values of the flow-discharge response $M_l(x^*, t^*)$ reach the value 1 for the case $x^* > x_0^*$ and 0 for the case $x^* < x_0^*$ which will be the same as the limiting values of the flow-discharge response $A_l(x^*, t^*)$. This means that, for large times, the response of the flow discharge to a unit-step lateral inflow concentrated at a location x_0^* is independent of P_e, x_0^*, and the type of the upstream boundary considered for the study. The behavior of the response functions given by Eqs. (3.97)$-$(3.99) will be the same as the ones presented by Tingsanchali and Manandhar [49].

After observing the behavior of the unit-step responses of the flow depth and flow discharge for different inputs, we can infer that the results are not the same for both types of boundary. The response for a flow-depth hydrograph imposed upstream presents an adequate impact of all the parameters in its limiting value in comparison with a flow-discharge hydrograph imposed upstream. When a unit-step input of the concentrated lateral inflow is given at x_0^* for a given flow discharge imposed upstream, the limiting value of the discharge response is 1 for the case $x^* > x_0^*$ irrespective of the location of the concentrated lateral inflow, and the limiting value is 0 for the case $x^* < x_0^*$. This is not the case for the discharge response for a given flow-depth hydrograph imposed upstream as can be observed from Eq. (3.95). Here, the limiting value does change with the change in the location of the lateral inflow and it has a positive value for the case $x^* > x_0^*$, but a negative one for $x^* < x_0^*$. The discharge responses for both types of upstream boundaries are found to be discontinuous at the location $x^* = x_0^*$ because this lateral inflow is concentrated at this location. However, the flow depth is found to be continuous along the channel length for both the cases, but its derivative $\partial h^*/\partial x^*$ is not continuous at this point which clearly agrees with Eq. (3.10). The limiting value of the flow-depth responses for both scenarios is dependent on the location of observation. The comparison shown above makes it clear that, for smaller values of P_e, the results for a semi-infinite channel cannot mimic the results of a finite channel for the flow-discharge responses. However, for higher values of P_e, the semi-infinite channel responses do agree with the finite channel responses at the locations closer to the concentrated lateral inflow locations. For the flow-depth responses, as the distance between x_0^* and the location of observation is increased, the semi-infinite channel results are not the same even for higher values of the Péclet number. This happens because the flow depth is found to be more sensitive to the effect of the downstream boundary and the concentrated lateral inflow. Although the semi-infinite channel response gives satisfactory results for higher values of the Péclet number in finding the effect of the lateral inflow on the flow discharge, they are not efficient enough in finding the flow depth for the locations closer to the downstream boundary.

3.3.2 Responses corresponding to a uniformly distributed lateral inflow between locations x_1^* and x_2^*

This part focuses on the difference in the responses of the flow discharge and the flow depth to a uniformly distributed lateral inflow for both types of upstream boundary conditions. An attempt is made to highlight the similarities and the differences in the behavior of the dependent variables for both types of upstream boundary conditions.

Behavior of the flow-discharge responses to distributed lateral inflow

In Fig. 3.13, the flow-discharge response $C_l(x^*, t^*)$ to a unit-step lateral inflow uniformly distributed between $x_1^* = 0.5$ and $x_2^* = 0.7$ is presented. For this case, $Q^*(0, t^*) = 0$ and $h^*(1, t^*) = 0$, which means that there is no perturbation in the flow discharge to the reference value Q_0 at the upstream boundary and no perturbation in the flow depth to the reference value h_0 at the downstream boundary. The backwater effect induced due to the lateral inflow can be observed for $x^* < x_1^*$, where a dip in the discharge is present for lower values of P_e. This dip reduces as the value of P_e increases, and for a particular value of P_e, it reduces as the distance between x^* and the upstream boundary decreases and the distance between x^* and x_1^* increases which is clearly visible from Fig. 3.13(a). For $x^* > x_2^*$, the limiting value is 1 while, for $x_1^* < x^* < x_2^*$, the limiting value linearly increases with an increase in x^*. However, for $x^* < x_1^*$, the limiting value diminishes to zero.

In Fig. 3.14, the flow-discharge response $M_{ld}(x^*, t^*)$ to a unit-step lateral inflow uniformly distributed between $x_1^* = 0.5$ and $x_2^* = 0.7$ is presented. For this case, $h^*(0, t^*) = 0$ and $h^*(1, t^*) = 0$, which means that there is no perturbation in the flow depth to the reference value h_0 at the upstream and the downstream boundaries. In this case, the limiting values for all the values of x^* are less than the respective values observed in Fig. 3.13. Due to the backwater effect induced due to the lateral inflow, for $x^* < x_1^*$, lower values for the discharge are observed for location close to x_1^*, but the limiting value does not reach zero because the upstream boundary is present in terms of flow depth. For a particular value of P_e, the limiting value of the flow discharge for $x_1^* < x^* < x_2^*$ linearly increases with x^*, and for $x^* > x_2^*$, it converges to some particular value. These limiting values increase with an increase in P_e, and for some higher values of P_e, the limiting values for the flow-discharge responses will be same as the one obtained for for a flow-discharge type upstream boundary which is presented in Fig. 3.13. Irrespective of the type of upstream boundary, higher values of the flow discharge are obtained for $x_2^* < x^* < 1$ which can be observed from Figs. 3.13 and 3.14.

For the case of a uniformly distributed lateral inflow along the channel length, the flow-discharge responses are compared with the corresponding semi-infinite channel responses taken from Cimorelli et al. [7, 6, 21]. When a flow-discharge hydrograph is imposed at the upstream end, the flow-discharge response to a unit-step lateral inflow uniformly distributed along the channel length for a semi-infinite channel can be expressed as [7, 21]

$$C_{l,\infty}(x^*, t^*) = t^* - \left\{ (t^* - x^*)\mathrm{N}\left(-(x^* - t^*)\sqrt{\frac{P_e}{2t^*}}\right) \right.$$
$$\left. + (t^* + x^*)\exp(P_e x^*)\mathrm{N}\left(-(x^* + t^*)\sqrt{\frac{P_e}{2t^*}}\right) \right\}, \tag{3.107}$$

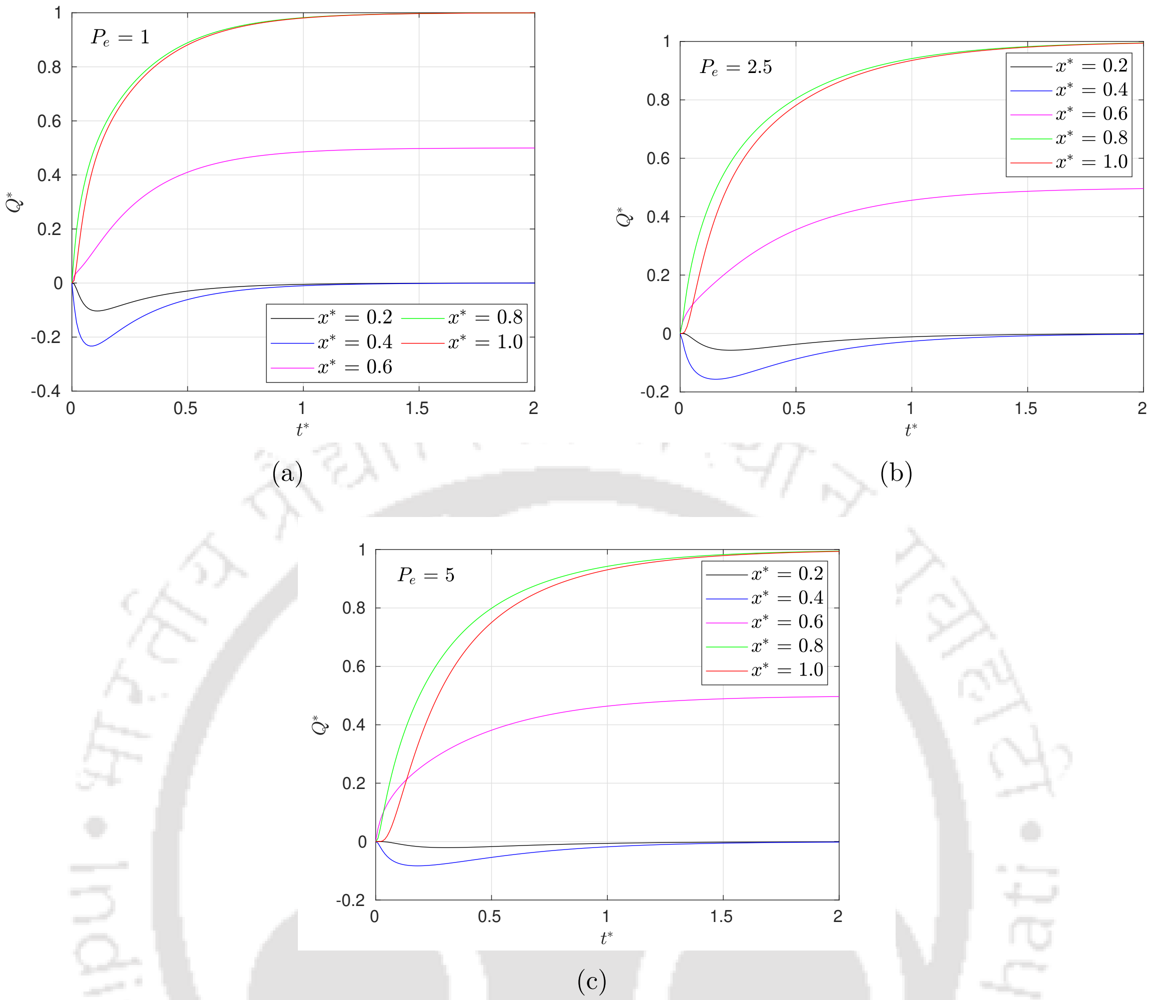

Figure 3.13: Flow-discharge response given in Eq. (3.57) at different x^* to a unit-step lateral inflow uniformly distributed between $x_1^* = 0.5$ and $x_2^* = 0.7$ with $Q^*(0,t^*) = 0$ and $h^*(1,t^*) = 0$: (a) $P_e = 1$, (b) $P_e = 2.5$, (c) $P_e = 5$

where N(.) is the standard normal distribution which can also be expressed in terms of the error function erf(.).

Similarly, when a flow-depth hydrograph is imposed at the upstream end, the flow-discharge response to a unit-step lateral inflow uniformly distributed along the channel length for a semi-infinite channel can be expressed as [7, 21]

$$M_{ld,\infty}(x^*,t^*) = \beta t^* - \frac{\beta}{2}\left(t^* - x^* + \frac{1}{P_e}\right)\mathrm{erfc}\left(\frac{x^*-t^*}{\sqrt{4t^*}}\sqrt{P_e}\right) + \frac{\beta}{2P_e}\exp(P_e x^*)\mathrm{erfc}\left(\frac{x^*+t^*}{\sqrt{4t^*}}\sqrt{P_e}\right) - \frac{\beta(t^*-x^*)}{\sqrt{4\pi P_e t^*}}\exp\left(-\frac{(x^*-t^*)^2}{4t^*}P_e\right) - \frac{\beta(t^*+x^*)}{\sqrt{4\pi P_e t^*}}\exp(P_e x^*)\exp\left(-\frac{(x^*+t^*)^2}{4t^*}P_e\right). \quad (3.108)$$

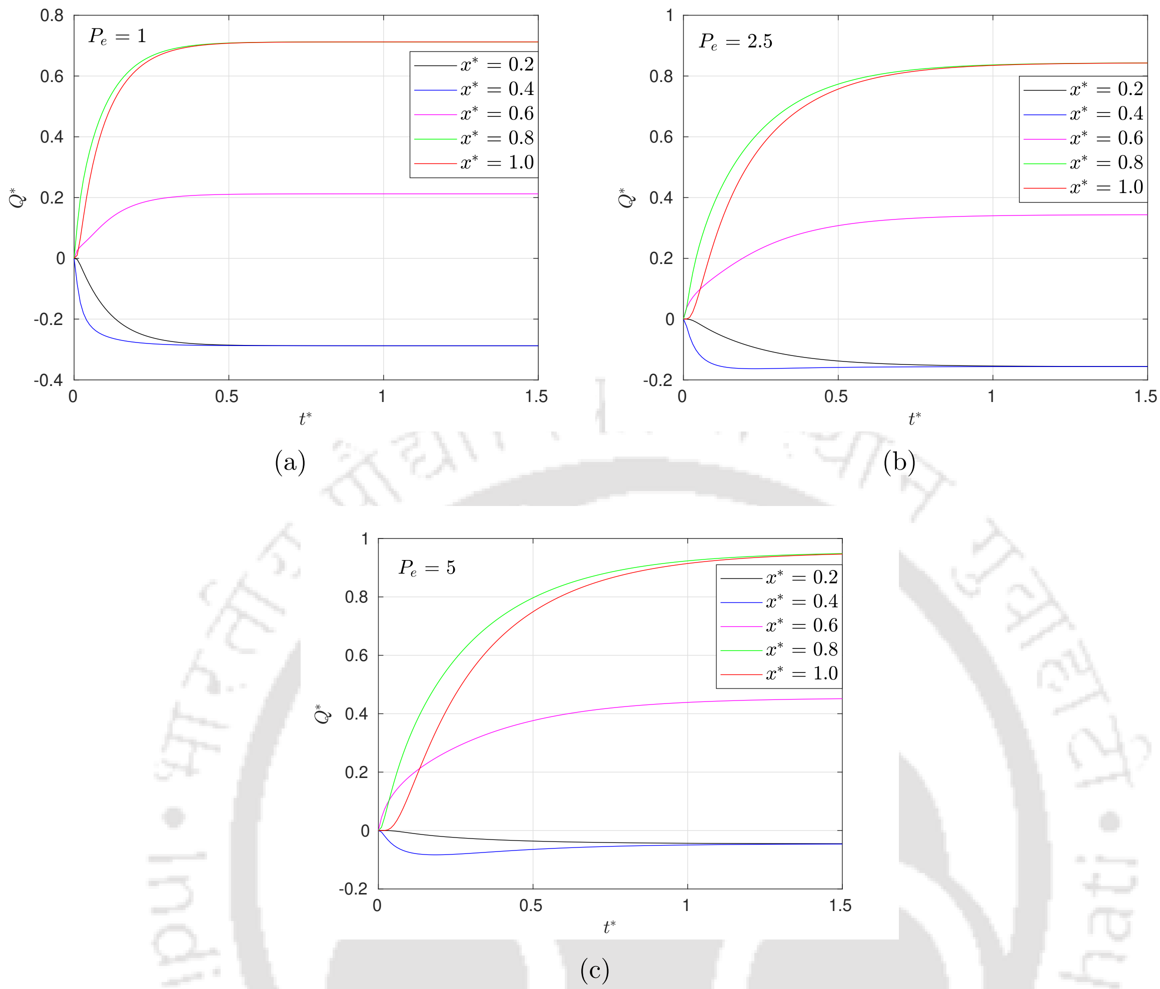

Figure 3.14: Flow-discharge response given in Eq. (3.96) at different x^* to a unit-step lateral inflow uniformly distributed between $x_1^* = 0.5$ and $x_2^* = 0.7$ with $h^*(0, t^*) = 0$ and $h^*(1, t^*) = 0$: (a) $P_e = 1$, (b) $P_e = 2.5$, (c) $P_e = 5$

In Fig. 3.15, a comparison of the flow-discharge response $C_l(x^*, t^*)$ for a finite channel given in Eq. (3.57) with the corresponding flow-discharge response for the semi-infinite channel given by Eq. (3.107), to a unit-step lateral inflow uniformly distributed along the channel length is presented. For this case, we again take $Q^*(0, t^*) = 0$ and $h^*(1, t^*) = 0$. The semi-infinite channel responses are observed to be very close to the finite channel responses. Responses for $P_e = 2.5$ plotted in Fig. 3.15(b) are quite close to each other up to $x^* = 0.4$. This agreement in these two responses further increases up to $x^* = 0.8$ as shown in Fig. 3.15(c). This means that, if a flow-discharge hydrograph is imposed at the upstream end, for $P_e > 2.5$, the semi-infinite channel flow-discharge response corresponding to a uniformly distributed lateral inflow is a good approximation of finite channel responses for the locations closer to the upstream end. But, for the locations closer to the downstream end, the semi-infinite channel results underestimate the flow discharge values even for $P_e = 5$. Following this observation, for the locations closer to the downstream end, the results presented here can be used to predict flow-discharge increase due to the lateral inflow in a finite length channel.

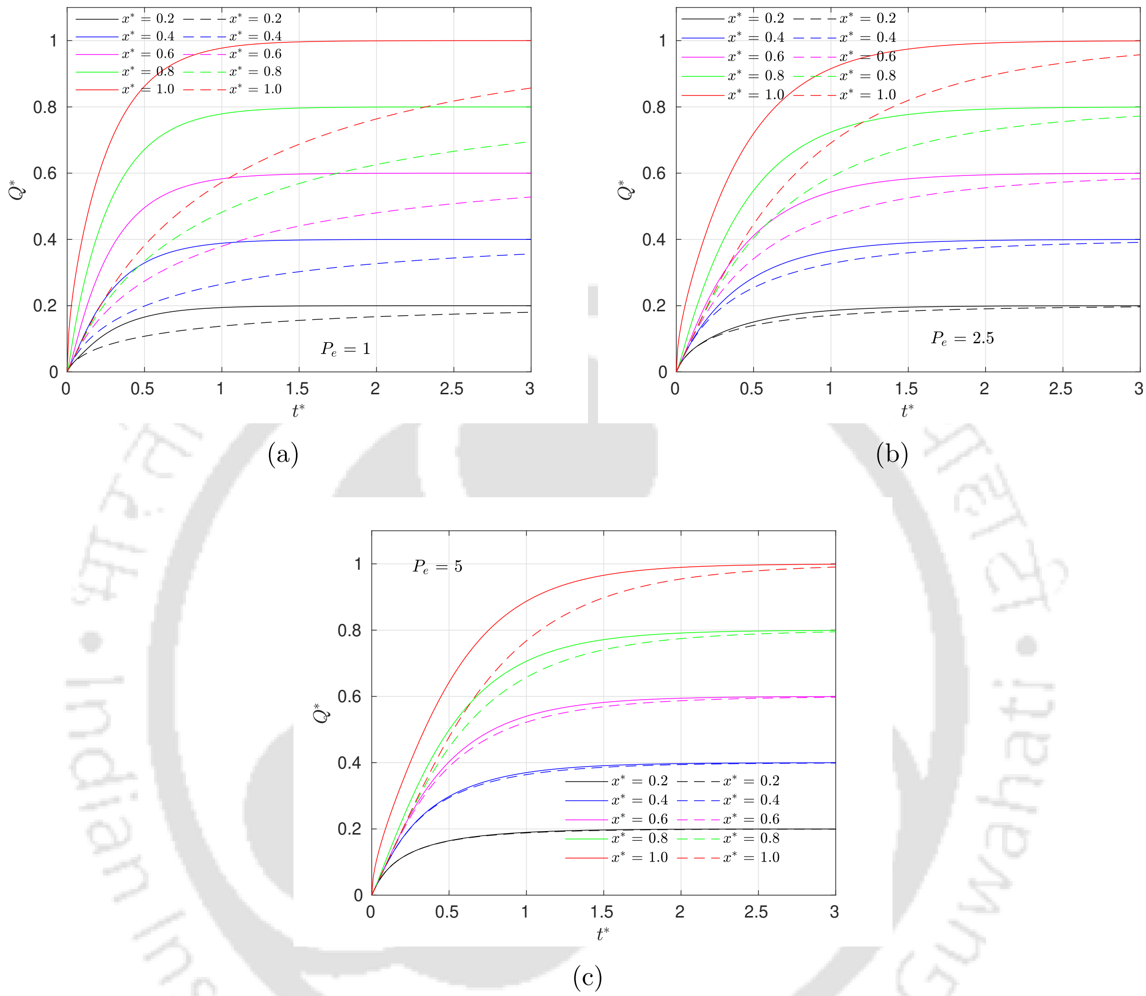

Figure 3.15: Comparison between flow-discharge response for finite channel given in Eq. (3.57) – continuous curves, and flow-discharge response for semi-infinite channel given in Eq. (3.107) – dashed curves, to the unit-step lateral inflow uniformly distributed between $x_1^* = 0$ and $x_2^* = 1$ for different x^* with $Q^*(0, t^*) = 0$ and $h^*(1, t^*) = 0$: (a) $P_e = 1$, (b) $P_e = 2.5$, (c) $P_e = 5$

In Fig. 3.16, a comparison of the flow-discharge response $M_{ld}(x^*, t^*)$ for a finite channel given by Eq. (3.96) with the corresponding flow-discharge response for the semi-infinite channel given in Eq. (3.108), to a unit-step lateral inflow uniformly distributed along the channel length is presented. For this case, we again take $h^*(0, t^*) = 0$ and $h^*(1, t^*) = 0$. It is observed that the semi-infinite channel response underestimates the values of the finite channel responses. Although these two responses do not agree in Figs. 3.16(a) and 3.16(b), they come very close to each other for $x^* \leq 0.8$ in Fig. 3.16(c). This shows that, for $P_e > 5$, the semi-infinite channel responses can be used to predict the flow discharge in a finite channel. In the finite channel responses, negative values of the flow discharge are observed at the locations closer to the upstream boundary corresponding to lower values of P_e. This effect is the result of the dominance of the downstream boundary for lower values of P_e. The behavior of these responses is different than the ones observed for a flow-discharge type upstream boundary in Fig. 3.15.

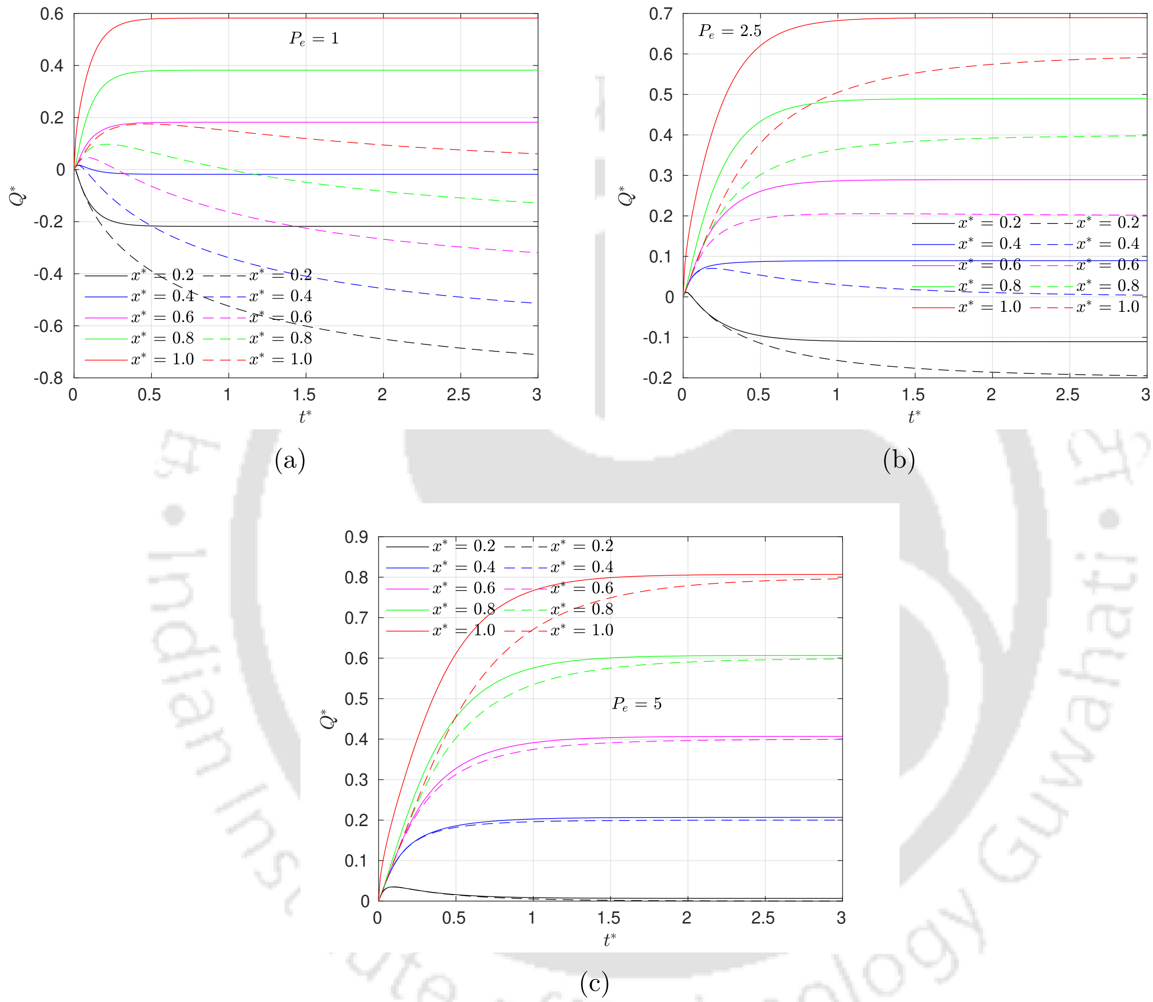

Figure 3.16: Comparison between flow-discharge response for finite channel given in Eq. (3.96) – continuous curves, and flow-discharge response for semi-infinite channel given in Eq. (3.108) – dashed curves, to the unit-step lateral inflow uniformly distributed between $x_1^* = 0$ and $x_2^* = 1$ for different x^* with $h^*(0, t^*) = 0$ and $h^*(1, t^*) = 0$: (a) $P_e = 1$, (b) $P_e = 2.5$, (c) $P_e = 5$

Behavior of the flow-depth responses to distributed lateral inflow

In Fig. 3.17, the flow-depth response $D_l(x^*, t^*)$ to a unit-step lateral inflow uniformly distributed between $x_1^* = 0.4$ and $x_2^* = 0.6$ is presented. For this case, $Q^*(0, t^*) = 0$

and $h^*(1,t^*) = 0$, which means that there is no perturbation in the flow discharge to the reference value Q_0 at the upstream boundary and no perturbation in the flow depth to the reference value h_0 at the downstream boundary. As opposed to the behavior observed for the flow discharge, the flow depth is dependent on the value of x^* along the whole channel length. The flow depth is observed to increase with an increase in P_e and the highest values are observed for the location $x^* = 0.5$, which is between the locations x_1^* and x_2^*. For a particular value of P_e, the flow depth slowly increases and achieves its highest value for some x^* between x_1^* and x_2^* and then decreases for $x^* > x_2^*$, to reach zero at the downstream end ($x^* = 1$).

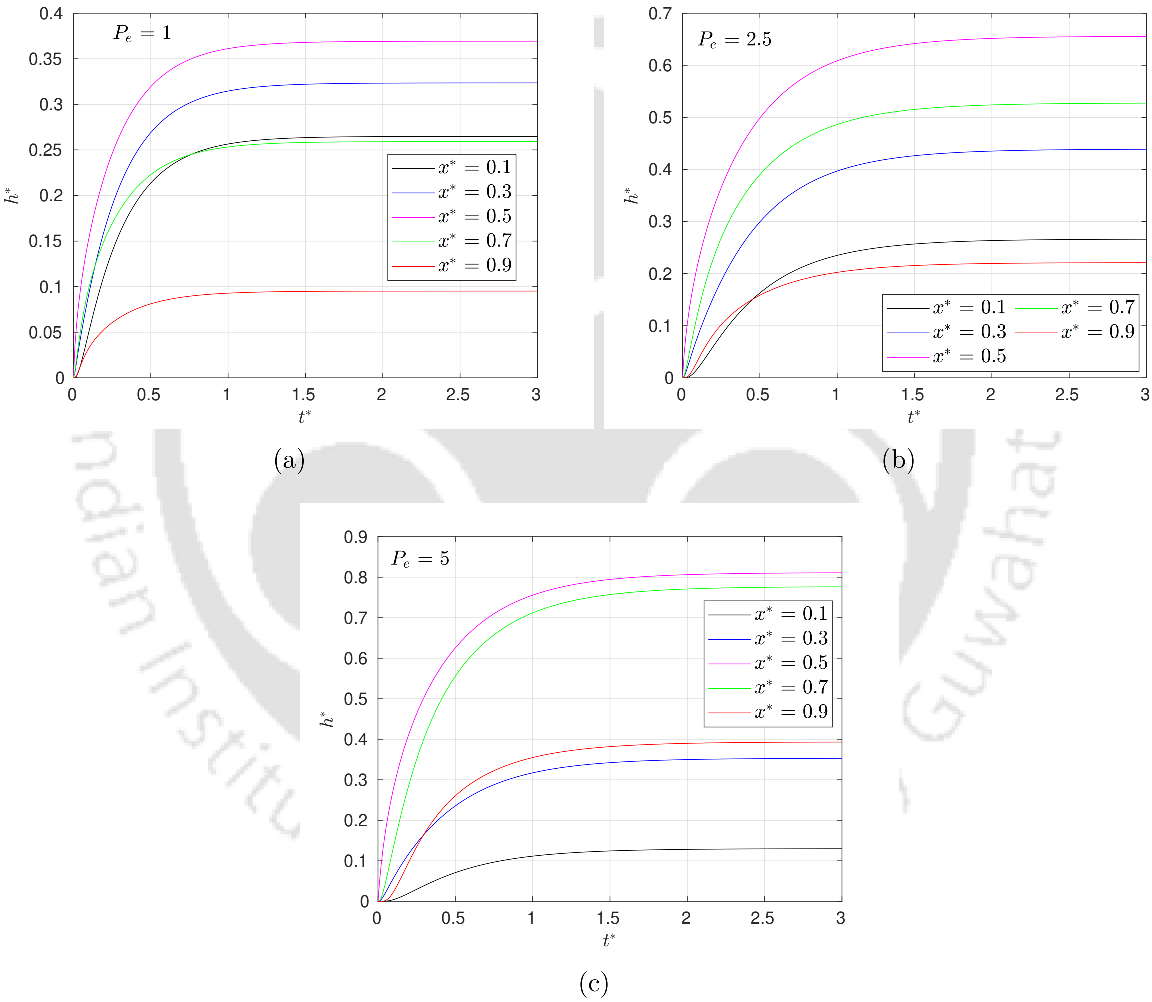

Figure 3.17: Flow-depth response given in Eq. (3.58) at different x^* to a unit-step lateral inflow uniformly distributed between $x_1^* = 0.4$ and $x_2^* = 0.6$ with $\beta = 1$, $Q^*(0,t^*) = 0$ and $h^*(1,t^*) = 0$: (a) $P_e = 1$, (b) $P_e = 2.5$, (c) $P_e = 5$

For Figs. 3.18 and 3.19, we take $h^*(0,t^*) = 0$ and $h^*(1,t^*) = 0$, which means that there is no perturbation in the flow depth to the reference value h_0 at the upstream and the downstream boundaries. In Fig. 3.18, the flow-depth response $N_{ld}(x^*,t^*)$ to a unit-step lateral inflow uniformly distributed between $x_1^* = 0.4$ and $x_2^* = 0.6$ is presented. The backwater effect due to the downstream boundary as well as the lateral inflow both influence the behavior of the flow depth along the channel. For the values of the Péclet number presented here, higher values of the flow depth are observed for locations between x_1^* and x_2^*, but this pattern does not stay the same if the value of the Péclet number or the values of x_1^* and x_2^* are changed. Even for higher values of P_e, higher values of the flow depth are present at the locations between the downstream end ($x^* = 1$) and x_2^*, because for higher values of P_e, the downstream boundary is less important and it cannot influence the flow depth to that extent which it can do for lower values of P_e. For lower values of P_e, the combined backwater effect of the downstream boundary and lateral inflow is forceful enough to obtain higher values of the flow depth between the locations x_1^* and x_2^*. The convergence rate is faster for the flow depths presented in Fig. 3.18 than the ones shown in Fig. 3.17 for all the cases of P_e. This means that the importance of the downstream boundary is also dependent on the type of the upstream boundary. To bring out the limitations as well as the efficacy of semi-infinite channel responses, the flow-depth responses to the uniformly distributed lateral inflow along the channel length are compared with the corresponding semi-infinite channel responses taken from Cimorelli et al. [6, 21]. When a flow-depth hydrograph is imposed at the upstream end, the flow-depth response to a unit-step lateral inflow uniformly distributed along the channel length for a semi-infinite channel can be expressed as [6, 21]

$$N_{ld,\infty}(x^*, t^*) = t^* - \frac{1}{2}(t^* - x^*)\text{erfc}\left((x^* - t^*)\sqrt{\frac{P_e}{4t^*}}\right) - \frac{1}{2}(t^* + x^*)\exp(P_e x^*)\text{erfc}\left((x^* + t^*)\sqrt{\frac{P_e}{4t^*}}\right). \tag{3.109}$$

In Fig. 3.19, a comparison of the flow-depth response $N_{ld}(x^*, t^*)$ for the finite channel given in Eq. (3.100) with the corresponding semi-infinite channel response given in Eq. (3.109), to a unit-step lateral inflow uniformly distributed along the channel length is presented. The semi-infinite channel responses completely fail to approximate the finite channel results for the cases of $P_e = 0.5$ and 2.5 as observed from Figs. 3.19(a) and 3.19(c). The values estimated by the semi-infinite channel response increase with an increase in x^*, which is not the case for the finite channel results. Due to the backwater effect of the downstream boundary, higher values of the flow-depth are observed at the location $x^* = 0.5$ in Figs. 3.19(a) and 3.19(c). However, for Fig. 3.19(c), the higher values for the finite channel results are obtained at $x^* = 0.7$. The semi-infinite channel results fail to predict this behavior of the flow depth. For $P_e = 5$, these two responses agree for the locations closer to the upstream end, but the difference between these two responses increases with an increase in x^*, i.e., moving closer to the downstream end. This shows that the semi-

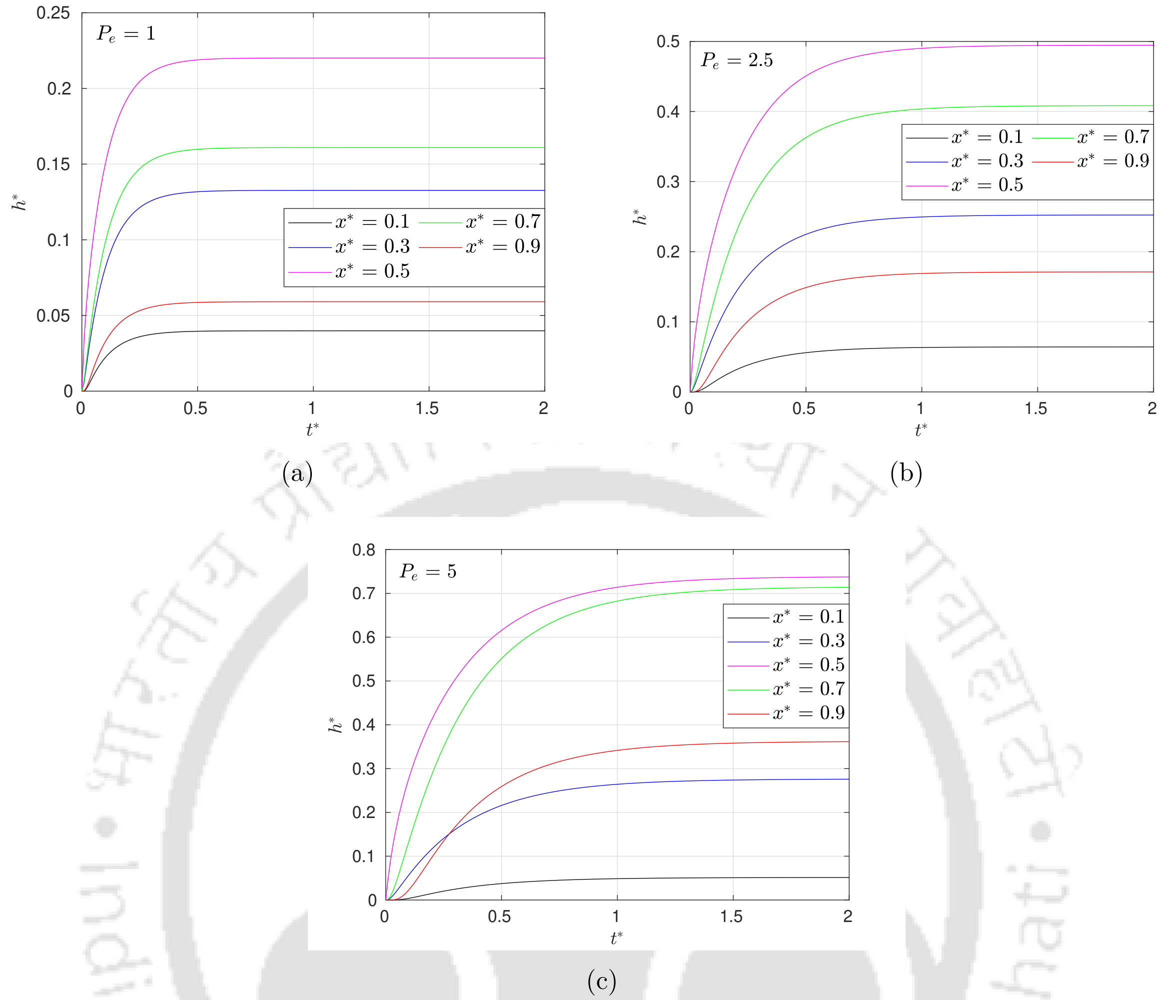

Figure 3.18: Flow-depth response given in Eq. (3.100) at different x^* to a unit-step lateral inflow uniformly distributed between $x_1^* = 0.4$ and $x_2^* = 0.6$ with $\beta = 1$, $h^*(0, t^*) = 0$ and $h^*(1, t^*) = 0$: (a) $P_e = 1$, (b) $P_e = 2.5$, (c) $P_e = 5$

infinite channel results can be used only to predict the flow-depth at locations far away from the downstream end and closer to the upstream end.

The flow-discharge and flow-depth responses to both types of lateral inflows can also be combined with the upstream and downstream responses to get the combined effect of the lateral inflows, upstream and downstream boundaries along the entire channel.

3.4 Conclusion

We have derived analytical solutions for the linearized diffusive wave model subject to two types of upstream boundary conditions: a concentrated lateral inflow, a uniformly distributed lateral inflow, and a flow-depth hydrograph imposed at the downstream boundary. The reason for considering a concentrated inflow is to include some special cases of

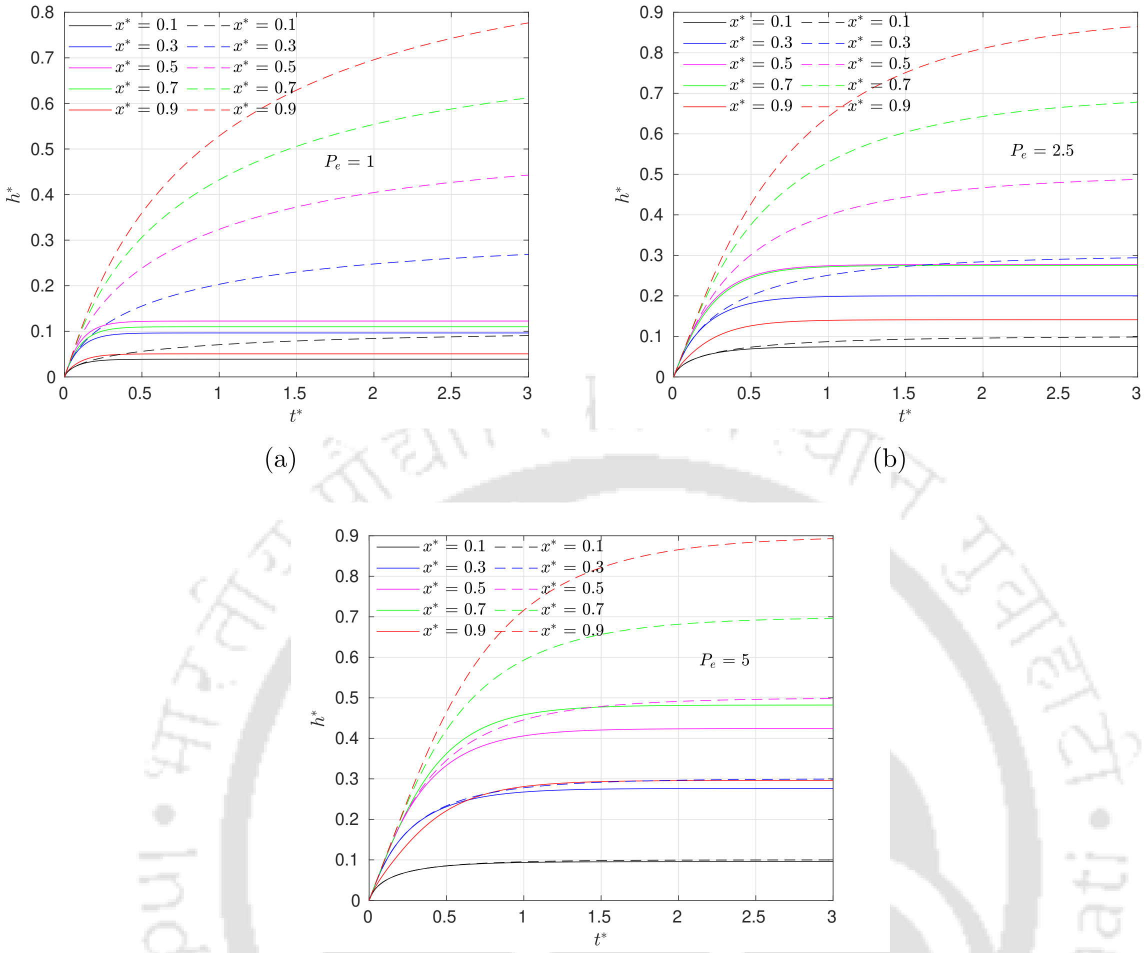

(a) (b)

(c)

Figure 3.19: Comparison between flow-depth response for finite channel given in Eq. (3.100) − continuous curves, and flow-depth response for semi-infinite channel given in Eq. (3.109) − dashed curves, to the unit-step lateral inflow uniformly distributed between $x^*_1 = 0$ and $x^*_2 = 1$ for different x^* with $\beta = 1$, $h^*(0, t^*) = 0$ and $h^*(1, t^*) = 0$: (a) $P_e = 1$, (b) $P_e = 2.5$, (c) $P_e = 5$

the spatial variation of the lateral inflow such as, when the width of the tributary joining the main channel is very small in comparison to the length of the main channel. On a point of note, a lateral inflow distributed between any two locations of a channel can include a wide range of lateral inflows. We can combine these results together and can also use them for more than one source of lateral inflow. The results presented in Cimorelli et al. [7, 6] did not take into account a space-dependent lateral inflow. As a consequence, the results presented by them for the lateral inflow cannot be used for such cases. We have presented the results for response functions of the concentrated lateral inflow as well as the uniformly distributed lateral inflow between any locations of the channel that can be combined with the upstream and downstream responses given by Cimorelli et al. [7].

We have obtained the unit-step response functions for all the inputs and shown the effect of the Péclet number on these responses.

The finite channel responses were compared with the corresponding semi-infinite channel responses to bring out the efficacy and limitations of the semi-infinite channel responses when used to approximate the finite channel results. These comparisons clearly establish the difference in the behavior of the responses for finite and semi-infinite channel cases. The comparison of the finite and semi-infinite channel results agrees with the fact that the downstream boundary cannot be ignored for lower values of the Péclet number (that is $P_e < 5$ in this case). Even for the highest value of the Péclet number that is considered here, the semi-infinite channel case cannot completely mimic the finite channel results. Although semi-infinite channel responses for a concentrated lateral inflow work satisfactorily in finding the flow discharge for higher Péclet numbers when a flow-discharge is given at the upstream end, they are not efficient in evaluating the flow depth at the locations closer to the downstream boundary. But if the flow depth is given at the upstream boundary, then the semi-infinite channel responses fail to simulate the behavior of the flow-discharge and the flow-depth responses.

In all the cases, the flow depth was observed to be more sensitive to the downstream boundary, the location of the lateral inflow, and the other parameters used in the study. For both types of lateral inflows, the response functions behaved differently depending on what type of upstream boundary was considered. The limiting value of the flow-depth responses corresponding to both types of lateral inflows were dependent on the Péclet number, channel width, location of observation, and location of lateral inflow for both types of upstream boundaries. For a given flow discharge at the upstream end, the limiting value for the flow discharge was independent of the channel parameters which was not the case for a given flow depth at the upstream boundary. In comparison to the flow depth, the flow discharge was found to be more robust to any change in the upstream boundary or the lateral inflow. This was also true for respective semi-infinite channel responses for both types of upstream boundaries. In fact, when a flow-discharge-based upstream boundary is present, for $P_e \geq 2.5$, the semi-infinite channel responses to a uniformly distributed lateral inflow were found to be good approximations for predicting the flow discharge in finite channel for the locations closer to the upstream end. But even for $P_e = 5$, the prediction of the flow discharge is not accurate at the locations closer to the downstream boundary. For $P_e > 5$, when a flow-depth hydrograph was taken at the upstream end, the semi-infinite channel flow-discharge responses to the upstream boundary and the uniformly distributed lateral inflow were found as appropriate approximation of the corresponding finite channel responses in comparison to the flow-discharge response to the concentrated lateral inflow. The results presented corresponding to the uniformly distributed lateral inflow between any two locations could include various types of lateral inflows including a lateral inflow uniformly distributed along the channel length.

CHAPTER 4

Diffusive wave approximation with different types of lateral inflow and a flow-discharge hydrograph imposed at the downstream end

In this chapter, an analytical solution for the diffusive model is presented for the flow discharge and the flow depth. The upstream boundary is considered as a flow-depth hydrograph while the downstream boundary is considered as a flow-discharge hydrograph. Two different types of lateral inflows are considered: a concentrated lateral inflow and a uniformly distributed lateral inflow between any two locations along the channel length. The analytical solution is derived by utilizing the Laplace transform through an extensive use of the *Laplace inversion theorem* and residue theorem. Some of the responses are compared with the corresponding semi-infinite channel responses.

4.1 Methodology

4.1.1 Governing equations and proposed method

The diffusive wave approximation of the Saint-Venant equations is derivable when the effect of the inertial forces is less in comparison to the other forces. The following equations depict the scenario [10]:

$$\frac{1}{b}\frac{\partial Q}{\partial x} + \frac{\partial h}{\partial t} = \frac{q_l}{b}, \tag{4.1}$$

$$\frac{\partial h}{\partial x} = S_0 - S_f, \tag{4.2}$$

A schematic diagram is given in Fig. 4.1.

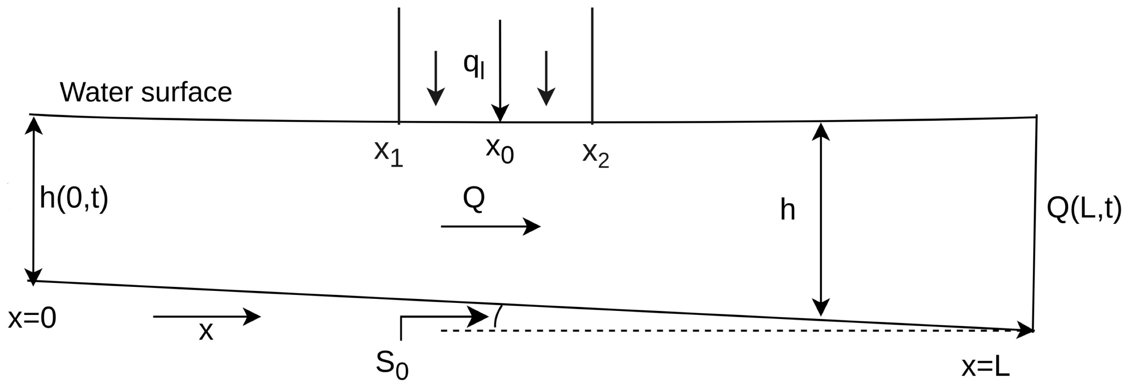

Figure 4.1: A schematic diagram for $1D$ flow structure in a prismatic channel

Our primary focus is to explore the contribution of the space- and time-dependent lateral inflow on the flow discharge and the flow depth at different locations of a finite channel of length L. Based on the concepts used in *Chapter 3*, the lateral inflow can be written as

$$q_l(x,t) = X(x)T(t), \tag{4.3}$$

where $X(x)$ and $T(t)$ represent the discharge distribution of lateral inflow in space and the total discharge of the lateral inflow, respectively [19]. Following the work of Cimorelli et al. [7], a prismatic channel is considered to linearize Eqs. (4.1) and (4.2). The perturbation technique is employed on two unknown variables h and Q. The perturbed quantities are $Q_1(x,t)$ and $h_1(x,t)$ with the higher-order terms being ignored with a reference condition of steady uniform flow represented by (Q_0, h_0). In order to simplify the discussion, dimensionless variables are used in this analysis. Here, the following transformations are considered [7]:

$$t^* = \frac{t}{L/C_0},\ x^* = x/L,\ h^* = h_1/h_0,\ Q^* = Q_1/Q_0,\ C_0 = -\frac{1}{b_0}\left(\frac{\partial S_f/\partial h}{\partial S_f/\partial Q}\right)_{(Q_0,h_0)},$$

where b_0 is the linearized water surface width and C_0 is the celerity of the linearized model.

Using the dimensionless quantities in Eqs. (4.1) and (4.2), the following system in h^* and Q^* is obtained:

$$\beta\frac{\partial h^*}{\partial t^*} + \frac{\partial Q^*}{\partial x^*} = X^*(x^*)T^*(t^*), \tag{4.4}$$

$$\frac{\partial h^*}{\partial x^*} + r_1 Q^* + r_2 h^* = 0, \tag{4.5}$$

with

$$X^*(x^*)T^*(t^*) = \frac{X(x)}{1/L}\frac{T(t)}{Q_0}. \tag{4.6}$$

The other parameters are as follows:

$$\beta = \frac{h_0}{Q_0}b_0C_0,\ r_1 = L\frac{Q_0}{h_0}\left(\frac{\partial S_f}{\partial Q}\right)_{(Q_0,h_0)},\ r_2 = L\left(\frac{\partial S_f}{\partial h}\right)_{(Q_0,h_0)},$$

where β is the dimensionless water surface width. It is assumed that there is no perturbation in flow discharge and flow depth before the application of any input, i.e., $Q^*(x^*,0) = 0$ and $h^*(x^*,0) = 0$. Then, applying the Laplace transform on the system comprising Eqs. (4.4) and (4.5), we get

$$\frac{\mathrm{d}\overline{Q^*}}{\mathrm{d}x^*} + \beta s\overline{h^*} = X(x^*)\overline{T^*}(s), \tag{4.7}$$

$$\frac{\mathrm{d}\overline{h^*}}{\mathrm{d}x^*} + r_1\overline{Q^*} + r_2\overline{h^*} = 0. \tag{4.8}$$

where $\overline{Q^*}(x^*,s)$, $\overline{h^*}(x^*,s)$, and $\overline{T^*}(s)$ are the Laplace transforms of $Q^*(x^*,t^*)$, $h^*(x^*,t^*)$, and $T^*(t^*)$, respectively. The above system can also be equivalently written in the following form:

$$\frac{\mathrm{d}\overline{U}(x^*,s)}{\mathrm{d}x^*} = M(s)\overline{U}(x^*,s) + R(x^*,s), \tag{4.9}$$

where

$$\overline{U}(x^*,s) = \begin{bmatrix}\overline{Q^*}(x^*,s)\\ \overline{h^*}(x^*,s)\end{bmatrix},\quad M(s) = \begin{bmatrix}0 & -\beta s\\ -r_1 & -r_2\end{bmatrix},\quad R(x^*,s) = \begin{bmatrix}X^*(x^*)\overline{T^*}(s)\\ 0\end{bmatrix}. \tag{4.10}$$

The solution to Eq. (4.9) is obtained as

$$\overline{U}(x^*,s) = \exp(M(s)x^*)\overline{U}(0,s) + \int_0^{x^*}\exp(M(s)(x^*-\phi))\,R(\phi,s)\mathrm{d}\phi, \tag{4.11}$$

where $\overline{U}(0,s) = \left(\overline{Q^*}(0,s)\ \overline{h^*}(0,s)\right)^T$ is the vector representing the upstream boundary condition. The entries α_{ij} of the matrix $\exp(M(s)x^*)$ have the following expressions as given by Cimorelli et al. [7]:

$$\alpha_{11}(x^*,s) = \exp\left(\frac{P_e x^*}{2}\right)\frac{\sqrt{Z}\cosh\left(\frac{x^*}{2}\sqrt{Z}\right) - P_e\sinh\left(\frac{x^*}{2}\sqrt{Z}\right)}{\sqrt{Z}}, \tag{4.12}$$

$$\alpha_{12}(x^*,s) = -2\beta s \exp\left(\frac{P_e x^*}{2}\right)\frac{\sinh\left(\frac{x^*}{2}\sqrt{Z}\right)}{\sqrt{Z}}, \tag{4.13}$$

$$\alpha_{21}(x^*,s) = -\frac{2P_e}{\beta}\exp\left(\frac{P_e x^*}{2}\right)\frac{\sinh\left(\frac{x^*}{2}\sqrt{Z}\right)}{\sqrt{Z}}, \tag{4.14}$$

$$\alpha_{22}(x^*,s) = \exp\left(\frac{P_e x^*}{2}\right)\frac{\sqrt{Z}\cosh\left(\frac{x^*}{2}\sqrt{Z}\right) + P_e \sinh\left(\frac{x^*}{2}\sqrt{Z}\right)}{\sqrt{Z}}, \tag{4.15}$$

with $Z = {P_e}^2 + 4P_e s$ where $P_e = C_0 L/D_0$ is the Péclet number; $D_0 = Q_0/(2b_0 S_0)$ is the linearized diffusivity coefficient. Now, we use two forms of $X^*(x^*)$ to study the effect of two different types of lateral inflow which are space-dependent in addition to being time-dependent.

4.1.2 Concentrated lateral inflow

The Dirac delta function can be used to represent the case of a lateral inflow concentrated at a location x_0 (with x_0^* as the non-dimensional form). It can represent the cases of a lateral inflow from a tributary of negligible width in comparison with the length of the channel under consideration. Using the property of the Dirac delta function, the integral of Eq. (4.11) can further be simplified as

$$\int_0^{x^*} \exp(M(s)\,(x^*-\phi))\,R(\phi,s)\mathrm{d}\phi = \overline{T^*}(s)\int_0^{x^*}\begin{bmatrix}\alpha_{11}(x^*-\phi,s)\delta(\phi-x_0^*)\\ \alpha_{21}(x^*-\phi,s)\delta(\phi-x_0^*)\end{bmatrix}\mathrm{d}\phi$$
$$= \begin{cases}\overline{T^*}(s)\begin{bmatrix}\alpha_{11}(x^*-x_0^*,s)\\ \alpha_{21}(x^*-x_0^*,s)\end{bmatrix}, & \text{for } x^* > x_0^*,\\ 0, & \text{for } x^* < x_0^*.\end{cases} \tag{4.16}$$

Finally, using Eqs. (4.11) and (4.16), we get the following form of the vector $\overline{U}(x^*,s)$:

$$\overline{U}(x^*,s) = \exp(M(s)x^*)\begin{bmatrix}\overline{Q^*}(0,s)\\ \overline{h^*}(0,s)\end{bmatrix} + \begin{bmatrix}\alpha_{11}(x^*-x_0^*,s)\overline{T^*}(s)\\ \alpha_{21}(x^*-x_0^*,s)\overline{T^*}(s)\end{bmatrix}, \quad \text{for } x^* > x_0^*, \tag{4.17a}$$

$$\overline{U}(x^*,s) = \exp(M(s)x^*)\begin{bmatrix}\overline{Q^*}(0,s)\\ \overline{h^*}(0,s)\end{bmatrix}, \quad \text{for } x^* < x_0^*. \tag{4.17b}$$

The system given in Eq. (4.17b) is valid for the locations upstream to the concentrated lateral inflow, whereas the system given in Eq. (4.17a) is valid for the subsequent locations downstream to the concentrated lateral inflow.

The upstream and downstream boundaries are considered as $h^*(0,t^*)$ and $Q^*(1,t^*)$, respectively. To utilize this fact effectively, we evaluate $\overline{Q^*}(x^*, s)$ at $x^* = 1$ from Eq. (4.17a) as

$$\overline{Q^*}(1, s) = \alpha_{11}(1, s)\overline{Q^*}(0, s) + \alpha_{12}(1, s)\overline{h^*}(0, s) + \alpha_{11}(1 - x_0^*, s)\overline{T^*}(s). \tag{4.18}$$

Using Eq. (4.18), the expression for $\overline{Q^*}(0, s)$ can be obtained as

$$\overline{Q^*}(0, s) = \frac{\overline{Q^*}(1, s)}{\alpha_{11}(1, s)} - \frac{\alpha_{12}(1, s)}{\alpha_{11}(1, s)}\overline{h^*}(0, s) - \frac{\alpha_{11}(1 - x_0^*, s)}{\alpha_{11}(1, s)}\overline{T^*}(s). \tag{4.19}$$

Subsequently, the system given in Eq. (4.17) gets converted to

$$\overline{Q^*}(x^*, s) = \overline{A}_u(x^*, s)\overline{h^*}(0, s) + \overline{A}_d(x^*, s)\overline{Q^*}(1, s) + \overline{A}_{lc}(x^*, s)\overline{T^*}(s), \tag{4.20}$$

$$\overline{h^*}(x^*, s) = \overline{B}_u(x^*, s)\overline{h^*}(0, s) + \overline{B}_d(x^*, s)\overline{Q^*}(1, s) + \overline{B}_{lc}(x^*, s)\overline{T^*}(s), \tag{4.21}$$

with

$$\overline{A}_u(x^*, s) = \exp\left(\frac{P_e x^*}{2}\right)\frac{2\beta s \sinh\left(\frac{1 - x^*}{2}\sqrt{Z}\right)}{\sqrt{Z}\cosh\left(\frac{\sqrt{Z}}{2}\right) - P_e \sinh\left(\frac{\sqrt{Z}}{2}\right)}, \tag{4.22}$$

$$\overline{A}_d(x^*, s) = \exp\left(\frac{x^* - 1}{2}P_e\right)\frac{\sqrt{Z}\cosh\left(\frac{x^*\sqrt{Z}}{2}\right) - P_e \sinh\left(\frac{x^*\sqrt{Z}}{2}\right)}{\sqrt{Z}\cosh\left(\frac{\sqrt{Z}}{2}\right) - P_e \sinh\left(\frac{\sqrt{Z}}{2}\right)}, \tag{4.23}$$

$$\overline{B}_u(x^*, s) = \exp\left(\frac{P_e x^*}{2}\right)\frac{\sqrt{Z}\cosh\left(\frac{x^* - 1}{2}\sqrt{Z}\right) + P_e \sinh\left(\frac{x^* - 1}{2}\sqrt{Z}\right)}{\sqrt{Z}\cosh\left(\frac{\sqrt{Z}}{2}\right) - P_e \sinh\left(\frac{\sqrt{Z}}{2}\right)}, \tag{4.24}$$

$$\overline{B}_d(x^*, s) = \frac{-2P_e}{\beta}\exp\left(\frac{x^* - 1}{2}P_e\right)\frac{\sinh\left(\frac{x^*\sqrt{Z}}{2}\right)}{\sqrt{Z}\cosh\left(\frac{\sqrt{Z}}{2}\right) - P_e \sinh\left(\frac{\sqrt{Z}}{2}\right)}, \tag{4.25}$$

$$\overline{A}_{lc}(x^*, s) = \exp\left(\frac{x^* - x_0^*}{2}P_e\right)\frac{4P_e s}{\sqrt{Z}}\frac{\sinh\left(\frac{x_0^*\sqrt{Z}}{2}\right)\sinh\left(\frac{1 - x^*}{2}\sqrt{Z}\right)}{\sqrt{Z}\cosh\left(\frac{\sqrt{Z}}{2}\right) - P_e \sinh\left(\frac{\sqrt{Z}}{2}\right)},$$

$$\text{for } x^* > x_0^*, \tag{4.26a}$$

$$\overline{A}_{lc}(x^*, s) = -\exp\left(\frac{x^* - x_0^*}{2}P_e\right)\frac{\sqrt{Z}\cosh\left(\frac{1-x_0^*}{2}\sqrt{Z}\right) - P_e\sinh\left(\frac{1-x_0^*}{2}\sqrt{Z}\right)}{\sqrt{Z}\left(\sqrt{Z}\cosh\left(\frac{\sqrt{Z}}{2}\right) - P_e\sinh\left(\frac{\sqrt{Z}}{2}\right)\right)}, \quad \text{for } x^* < x_0^*, \tag{4.26b}$$

and

$$\overline{B}_{lc}(x^*, s) = 2P_e\sinh\left(\frac{x_0^*\sqrt{Z}}{2}\right)\exp\left(\frac{P_e}{2}(x^* - x_0^*)\right) \times \frac{\sqrt{Z}\cosh\left(\frac{x^*-1}{2}\sqrt{Z}\right) + P_e\sinh\left(\frac{x^*-1}{2}\sqrt{Z}\right)}{\beta\sqrt{Z}\left(\sqrt{Z}\cosh\left(\frac{\sqrt{Z}}{2}\right) - P_e\sinh\left(\frac{\sqrt{Z}}{2}\right)\right)}, \quad \text{for } x^* > x_0^*, \tag{4.27a}$$

$$\overline{B}_{lc}(x^*, s) = 2P_e\sinh\left(\frac{x^*\sqrt{Z}}{2}\right)\exp\left(\frac{P_e}{2}(x^* - x_0^*)\right) \times \frac{\sqrt{Z}\cosh\left(\frac{1-x_0^*}{2}\sqrt{Z}\right) - P_e\sinh\left(\frac{1-x_0^*}{2}\sqrt{Z}\right)}{\beta\sqrt{Z}\left(\sqrt{Z}\cosh\left(\frac{\sqrt{Z}}{2}\right) - P_e\sinh\left(\frac{\sqrt{Z}}{2}\right)\right)}, \quad \text{for } x^* < x_0^*. \tag{4.27b}$$

The inverse of the system comprising Eqs. (4.20) and (4.21) is obtained as

$$Q^*(x^*, t^*) = A_u(x^*, t^*) \circledast h^*(0, t^*) + A_d(x^*, t^*) \circledast Q^*(1, t^*) + A_{lc}(x^*, t^*) \circledast T^*(t^*), \tag{4.28}$$
$$h^*(x^*, t^*) = B_u(x^*, t^*) \circledast h^*(0, t^*) + B_d(x^*, t^*) \circledast Q^*(1, t^*) + B_{lc}(x^*, t^*) \circledast T^*(t^*), \tag{4.29}$$

where $A_u(x^*, t^*)$, $A_d(x^*, t^*)$, $A_{lc}(x^*, t^*)$, $B_u(x^*, t^*)$, $B_d(x^*, t^*)$ and $B_{lc}(x^*, t^*)$ are the Laplace inverses of $\overline{A}_u(x^*, s)$, $\overline{A}_d(x^*, s)$, $\overline{A}_{lc}(x^*, s)$, $\overline{B}_u(x^*, s)$, $\overline{B}_d(x^*, s)$ and $\overline{B}_{lc}(x^*, s)$, respectively.

4.1.3 Uniformly distributed lateral inflow between two locations

In this case, the lateral inflow is considered to be uniformly distributed between two locations x_1 and x_2, with x_1^* and x_2^* as the non-dimensional forms of x_1 and x_2, respectively. This can be represented by using the unit-step function [19]. This case can handle the scenarios where the lateral inflow is from a tributary which is of significant width such that the width cannot be ignored, and x_1 and x_2 represent the two ends of the mouth of the tributary. Here, we write

$$X^*(x^*) = \frac{\mathrm{u}(x^* - x_1^*) - \mathrm{u}(x^* - x_2^*)}{x_2^* - x_1^*} = \begin{cases} \dfrac{1}{x_2^* - x_1^*}, & \text{for } x^* \in [x_1^*, x_2^*], \\ 0, & \text{for } x^* \notin [x_1^*, x_2^*], \end{cases} \tag{4.30}$$

where u(.) is the unit-step function with $x_2^* - x_1^* \neq 0$. Using Eq. (4.30), the integral in Eq. (4.11) can be simplified as

$$\int_0^{x^*} \exp(M(s)\,(x^* - \phi))\,R(\phi, s)\mathrm{d}\phi = \frac{\overline{T^*}(s)}{x_2^* - x_1^*} \begin{cases} 0, & \text{for } 0 \leq x^* < x_1^*, \\ \displaystyle\int_{x_1^*}^{x^*} \begin{pmatrix} \alpha_{11}(x^* - \phi, s) \\ \alpha_{21}(x^* - \phi, s) \end{pmatrix} \mathrm{d}\phi, & \text{for } x_1^* \leq x^* < x_2^*, \\ \displaystyle\int_{x_1^*}^{x_2^*} \begin{pmatrix} \alpha_{11}(x^* - \phi, s) \\ \alpha_{21}(x^* - \phi, s) \end{pmatrix} \mathrm{d}\phi, & \text{for } x_2^* \leq x^* \leq 1, \end{cases}$$

$$= \begin{cases} 0, & \text{for } 0 \leq x^* < x_1^* \\ \begin{pmatrix} \overline{T^*}(s) A_{11}(x^*, s) \\ \overline{T^*}(s) A_{21}(x^*, s) \end{pmatrix}, & \text{for } x^* \geq x_1^*. \end{cases} \tag{4.31}$$

Finally, using Eqs. (4.11) and (4.31), we get the following form of the vector $\overline{U}(x^*, s)$:

$$\overline{U}(x^*, s) = \exp(M(s)x^*) \begin{bmatrix} \overline{Q^*}(0, s) \\ \overline{h^*}(0, s) \end{bmatrix} + \begin{bmatrix} A_{11}(x^*, s)\overline{T^*}(s) \\ A_{21}(x^*, s)\overline{T^*}(s) \end{bmatrix}, \quad \text{for } x^* \geq x_1^* \tag{4.32a}$$

$$\overline{U}(x^*, s) = \exp(M(s)x^*) \begin{bmatrix} \overline{Q^*}(0, s) \\ \overline{h^*}(0, s) \end{bmatrix}, \quad \text{for } x^* < x_1^*, \tag{4.32b}$$

where

$$A_{11}(x^*, s) = \frac{1}{s(x_2^* - x_1^*)} \exp\left(\frac{x^* - x_1^*}{2} P_e\right) \left\{ \frac{P_e + 2s}{\sqrt{Z}} \sinh\left(\frac{x^* - x_1^*}{2}\sqrt{Z}\right) - \cosh\left(\frac{x^* - x_1^*}{2}\sqrt{Z}\right) \right\} + \frac{1}{s(x_2^* - x_1^*)}, \quad \text{for } x_1^* \leq x^* < x_2^*, \tag{4.33a}$$

$$A_{11}(x^*, s) = \frac{1}{s(x_2^* - x_1^*)} \exp\left(\frac{x^* - x_2^*}{2} P_e\right) \left\{ \cosh\left(\frac{x^* - x_2^*}{2}\sqrt{Z}\right) - \frac{P_e + 2s}{\sqrt{Z}} \sinh\left(\frac{x^* - x_2^*}{2}\sqrt{Z}\right) \right\} + \frac{1}{s(x_2^* - x_1^*)} \exp\left(\frac{x^* - x_1^*}{2} P_e\right) \left\{ \frac{P_e + 2s}{\sqrt{Z}} \sinh\left(\frac{x^* - x_1^*}{2}\sqrt{Z}\right) \right.$$

$$- \cosh\left(\frac{x^* - x_1^*}{2}\sqrt{Z}\right)\Bigg\}, \text{ for } x_2^* \leq x^* \leq 1, \tag{4.33b}$$

$$A_{21}(x^*, s) = \frac{1}{\beta s(x_2^* - x_1^*)}\exp\left(\frac{x^* - x_1^*}{2}P_e\right)\left\{\frac{P_e}{\sqrt{Z}}\sinh\left(\frac{x^* - x_1^*}{2}\sqrt{Z}\right)\right.$$
$$\left. - \cosh\left(\frac{x^* - x_1^*}{2}\sqrt{Z}\right)\right\} + \frac{1}{\beta s(x_2^* - x_1^*)}, \quad \text{for } x_1^* \leq x^* < x_2^*, \tag{4.34a}$$
$$A_{21}(x^*, s) = \frac{1}{\beta s(x_2^* - x_1^*)}\exp\left(\frac{x^* - x_2^*}{2}P_e\right)\left\{\cosh\left(\frac{x^* - x_2^*}{2}\sqrt{Z}\right)\right.$$
$$\left. - \frac{P_e}{\sqrt{Z}}\sinh\left(\frac{x^* - x_2^*}{2}\sqrt{Z}\right)\right\}$$
$$+ \frac{1}{\beta s(x_2^* - x_1^*)}\exp\left(\frac{x^* - x_1^*}{2}P_e\right)\left\{\frac{P_e}{\sqrt{Z}}\sinh\left(\frac{x^* - x_1^*}{2}\sqrt{Z}\right)\right.$$
$$\left. - \cosh\left(\frac{x^* - x_1^*}{2}\sqrt{Z}\right)\right\}, \text{ for } x_2^* \leq x^* \leq 1. \tag{4.34b}$$

The system given in Eq. (4.32b) is valid for the locations upstream to x_1^*, whereas the system given in Eq. (4.32a) is valid for the subsequent locations downstream to x_1^*. The expressions of $A_{11}(x^*, s)$ and $A_{21}(x^*, s)$ are the same as the ones obtained in *Chapter 3*.

It is known that $h^*(0, t^*)$ and $Q^*(1, t^*)$ are the upstream and downstream boundaries, respectively. By utilizing this information, we can evaluate $\overline{Q^*}(x^*, s)$ at $x^* = 1$ from Eq. (4.32a) as

$$\overline{Q^*}(1, s) = \alpha_{11}(1, s)\overline{Q^*}(0, s) + \alpha_{12}(1, s)\overline{h^*}(0, s) + A_{11}(1, s)\overline{T^*}(s). \tag{4.35}$$

Using Eq. (4.35), the expression for $\overline{Q^*}(0, s)$ can be obtained as

$$\overline{Q^*}(0, s) = \frac{\overline{Q^*}(1, s)}{\alpha_{11}(1, s)} - \frac{\alpha_{12}(1, s)}{\alpha_{11}(1, s)}\overline{h^*}(0, s) - \frac{A_{11}(1, s)}{\alpha_{11}(1, s)}\overline{T^*}(s). \tag{4.36}$$

Upon using Eqs. (4.33) and (4.34), the system given in Eq. (4.32) gets converted to

$$\overline{Q^*}(x^*, s) = \overline{A}_u(x^*, s)\overline{h^*}(0, s) + \overline{A}_d(x^*, s)\overline{Q^*}(1, s) + \overline{A}_{ld}(x^*, s)\overline{T^*}(s), \tag{4.37}$$
$$\overline{h^*}(x^*, s) = \overline{B}_u(x^*, s)\overline{h^*}(0, s) + \overline{B}_d(x^*, s)\overline{Q^*}(1, s) + \overline{B}_{ld}(x^*, s)\overline{T^*}(s), \tag{4.38}$$

where $\overline{A}_u(x^*, s)$, $\overline{A}_d(x^*, s)$, $\overline{B}_u(x^*, s)$ and $\overline{B}_d(x^*, s)$ are the same as the ones obtained in

Eqs. (4.20) and (4.21). The other two terms are obtained as follows:

$$\begin{aligned}
\overline{A}_{ld}(x^*,s) = {} & \frac{1}{s(x_2^*-x_1^*)}\frac{\sqrt{Z}\cosh\left(\dfrac{x^*}{2}\sqrt{Z}\right)-P_e\sinh\left(\dfrac{x^*}{2}\sqrt{Z}\right)}{\sqrt{Z}\left(\sqrt{Z}\cosh\left(\dfrac{\sqrt{Z}}{2}\right)-P_e\sinh\left(\dfrac{\sqrt{Z}}{2}\right)\right)} \\
& \times\left\{\exp\left(\frac{x^*-x_1^*}{2}P_e\right)\left(\sqrt{Z}\cosh\left(\frac{1-x_1^*}{2}\sqrt{Z}\right)-(P_e+2s)\sinh\left(\frac{1-x_1^*}{2}\sqrt{Z}\right)\right)\right. \\
& \left.-\exp\left(\frac{x^*-x_2^*}{2}P_e\right)\left(\sqrt{Z}\cosh\left(\frac{1-x_2^*}{2}\sqrt{Z}\right)-(P_e+2s)\sinh\left(\frac{1-x_2^*}{2}\sqrt{Z}\right)\right)\right\}, \\
& \text{for } 0\le x^*<x_1^*,
\end{aligned}\tag{4.39a}$$

$$\begin{aligned}
\overline{A}_{ld}(x^*,s) = {} & -\frac{\exp\left(\dfrac{x^*-x_2^*}{2}P_e\right)}{s(x_2^*-x_1^*)}\frac{\sqrt{Z}\cosh\left(\dfrac{1+x^*-x_2^*}{2}\sqrt{Z}\right)-P_e\sinh\left(\dfrac{1+x^*-x_2^*}{2}\sqrt{Z}\right)}{\sqrt{Z}\cosh\left(\dfrac{\sqrt{Z}}{2}\right)-P_e\sinh\left(\dfrac{\sqrt{Z}}{2}\right)} \\
& -\frac{2}{\sqrt{Z}}\frac{\exp\left(\dfrac{x^*-x_2^*}{2}P_e\right)}{x_2^*-x_1^*}\sinh\left(\frac{x_2^*-1}{2}\sqrt{Z}\right)\frac{\sqrt{Z}\cosh\left(\dfrac{x^*}{2}\sqrt{Z}\right)+P_e\sinh\left(\dfrac{x^*}{2}\sqrt{Z}\right)}{\sqrt{Z}\cosh\left(\dfrac{\sqrt{Z}}{2}\right)-P_e\sinh\left(\dfrac{\sqrt{Z}}{2}\right)} \\
& +\frac{2}{\sqrt{Z}}\frac{\exp\left(\dfrac{x^*-x_1^*}{2}P_e\right)}{x_2^*-x_1^*}\sinh\left(\frac{x^*-1}{2}\sqrt{Z}\right)\frac{\sqrt{Z}\cosh\left(\dfrac{x_1^*}{2}\sqrt{Z}\right)+P_e\sinh\left(\dfrac{x_1^*}{2}\sqrt{Z}\right)}{\sqrt{Z}\cosh\left(\dfrac{\sqrt{Z}}{2}\right)-P_e\sinh\left(\dfrac{\sqrt{Z}}{2}\right)}, \\
& +\frac{1}{s(x_2^*-x_1^*)}, \qquad \text{for } x_1^*\le x^*<x_2^*,
\end{aligned}\tag{4.39b}$$

$$\begin{aligned}
\overline{A}_{ld}(x^*,s) = {} & \frac{2}{\sqrt{Z}}\frac{\exp\left(\dfrac{x^*-x_1^*}{2}P_e\right)}{x_2^*-x_1^*}\sinh\left(\frac{x^*-1}{2}\sqrt{Z}\right)\frac{\sqrt{Z}\cosh\left(\dfrac{x_1^*}{2}\sqrt{Z}\right)+P_e\sinh\left(\dfrac{x_1^*}{2}\sqrt{Z}\right)}{\sqrt{Z}\cosh\left(\dfrac{\sqrt{Z}}{2}\right)-P_e\sinh\left(\dfrac{\sqrt{Z}}{2}\right)} \\
& -\frac{2}{\sqrt{Z}}\frac{\exp\left(\dfrac{x^*-x_2^*}{2}P_e\right)}{x_2^*-x_1^*}\sinh\left(\frac{x^*-1}{2}\sqrt{Z}\right)\frac{\sqrt{Z}\cosh\left(\dfrac{x_2^*}{2}\sqrt{Z}\right)+P_e\sinh\left(\dfrac{x_2^*}{2}\sqrt{Z}\right)}{\sqrt{Z}\cosh\left(\dfrac{\sqrt{Z}}{2}\right)-P_e\sinh\left(\dfrac{\sqrt{Z}}{2}\right)}, \\
& \text{for } x_2^*\le x^*\le 1,
\end{aligned}\tag{4.39c}$$

$$\overline{B}_{ld}(x^*, s) = \frac{-2P_e}{\beta s(x_2^* - x_1^*)} \frac{\sinh\left(\frac{x^*}{2}\sqrt{Z}\right)}{\sqrt{Z}\left(\sqrt{Z}\cosh\left(\frac{\sqrt{Z}}{2}\right) - P_e\sinh\left(\frac{\sqrt{Z}}{2}\right)\right)}$$
$$\times\left\{\exp\left(\frac{x^* - x_1^*}{2}P_e\right)\left(\sqrt{Z}\cosh\left(\frac{1 - x_1^*}{2}\sqrt{Z}\right) - (P_e + 2s)\sinh\left(\frac{1 - x_1^*}{2}\sqrt{Z}\right)\right)\right.$$
$$\left. - \exp\left(\frac{x^* - x_2^*}{2}P_e\right)\left(\sqrt{Z}\cosh\left(\frac{1 - x_2^*}{2}\sqrt{Z}\right) - (P_e + 2s)\sinh\left(\frac{1 - x_2^*}{2}\sqrt{Z}\right)\right)\right\},$$
$$\text{for } 0 \leq x^* < x_1^*, \qquad (4.40a)$$

$$\overline{B}_{ld}(x^*, s) = \frac{2P_e}{\beta s(x_2^* - x_1^*)}\exp\left(\frac{x^* - x_2^*}{2}P_e\right)\frac{\sinh\left(\frac{x^*}{2}\sqrt{Z}\right)}{\sqrt{Z}}$$
$$\times\frac{\sqrt{Z}\cosh\left(\frac{x_2^* - 1}{2}\sqrt{Z}\right) + (P_e + 2s)\sinh\left(\frac{x_2^* - 1}{2}\sqrt{Z}\right)}{\sqrt{Z}\cosh\left(\frac{\sqrt{Z}}{2}\right) - P_e\sinh\left(\frac{\sqrt{Z}}{2}\right)}$$
$$- \frac{1}{\beta s(x_2^* - x_1^*)}\exp\left(\frac{x^* - x_1^*}{2}P_e\right)\frac{\sqrt{Z}\cosh\left(\frac{x_1^*}{2}\sqrt{Z}\right) + P_e\sinh\left(\frac{x_1^*}{2}\sqrt{Z}\right)}{\sqrt{Z}}$$
$$\times\frac{\sqrt{Z}\cosh\left(\frac{x^* - 1}{2}\sqrt{Z}\right) + P_e\sinh\left(\frac{x^* - 1}{2}\sqrt{Z}\right)}{\sqrt{Z}\cosh\left(\frac{\sqrt{Z}}{2}\right) - P_e\sinh\left(\frac{\sqrt{Z}}{2}\right)} + \frac{1}{\beta s(x_2^* - x_1^*)},$$
$$\text{for } x_1^* \leq x^* < x_2^*, \qquad (4.40b)$$

$$\overline{B}_{ld}(x^*, s) = \frac{1}{\beta s(x_2^* - x_1^*)}\frac{\sqrt{Z}\cosh\left(\frac{x^* - 1}{2}\sqrt{Z}\right) + P_e\sinh\left(\frac{x^* - 1}{2}\sqrt{Z}\right)}{\sqrt{Z}\left(\sqrt{Z}\cosh\left(\frac{\sqrt{Z}}{2}\right) - P_e\sinh\left(\frac{\sqrt{Z}}{2}\right)\right)}$$
$$\times\left\{\exp\left(\frac{x^* - x_2^*}{2}P_e\right)\left(\sqrt{Z}\cosh\left(\frac{x_2^*}{2}\sqrt{Z}\right) + P_e\sinh\left(\frac{x_2^*}{2}\sqrt{Z}\right)\right)\right.$$
$$\left. - \exp\left(\frac{x^* - x_1^*}{2}P_e\right)\left(\sqrt{Z}\cosh\left(\frac{x_1^*}{2}\sqrt{Z}\right) + P_e\sinh\left(\frac{x_1^*}{2}\sqrt{Z}\right)\right)\right\},$$
$$\text{for } x_2^* \leq x^* \leq 1. \qquad (4.40c)$$

The inverse of the system comprising Eqs. (4.37) and (4.38) is obtained as

$$Q^*(x^*,t^*) = A_u(x^*,t^*) \circledast h^*(0,t^*) + A_d(x^*,t^*) \circledast Q^*(1,t^*) + A_{ld}(x^*,t^*) \circledast T^*(t^*), \quad (4.41)$$

$$h^*(x^*,t^*) = B_u(x^*,t^*) \circledast h^*(0,t^*) + B_d(x^*,t^*) \circledast Q^*(1,t^*) + B_{ld}(x^*,t^*) \circledast T^*(t^*), \quad (4.42)$$

where $A_u(x^*,t^*)$, $A_d(x^*,t^*)$, $B_u(x^*,t^*)$, and $B_d(x^*,t^*)$ are the same as the ones obtained in Eqs. (4.28) and (4.29) whereas $A_{ld}(x^*,t^*)$, $B_{ld}(x^*,t^*)$ are the Laplace inverses of $\overline{A}_{ld}(x^*,s)$ and $\overline{B}_{ld}(x^*,s)$, respectively.

4.2 Inverse transformations

To evaluate the time domain expressions, the *Laplace inversion theorem* is used. The functions in Eqs. (4.22)−(4.27), Eq. (4.39) and Eq. (4.40) appear to be two-valued in the neighborhood of the point s where $Z = 0$ but all of these give the same value for $Z = \exp(\mathrm{i}\pi)\,, \exp(-\mathrm{i}\pi)$. As a consequence, these functions are all single-valued with no branch points. The attribute of the Jordan's lemma given in *Chapter 1, Section 1.4* holds true for the functions in Eqs. (4.22)−(4.27), Eq. (4.39) and Eq. (4.40). Subsequently, the only singularities here are the zeros of the denominators of the functions given in these equations. We need to find the roots of the following equations to evaluate the integral in *Laplace inversion theorem*:

$$\sqrt{Z}\cosh\left(\frac{\sqrt{Z}}{2}\right) - P_e\sinh\left(\frac{\sqrt{Z}}{2}\right) = 0 \;\text{ and} \quad (4.43)$$

$$\sqrt{Z}\left(\sqrt{Z}\cosh\left(\frac{\sqrt{Z}}{2}\right) - P_e\sinh\left(\frac{\sqrt{Z}}{2}\right)\right) = 0. \quad (4.44)$$

Equations (4.43) and (4.44) can be simplified as

$$\sqrt{Z}\cosh\left(\frac{\sqrt{Z}}{2}\right)\left\{1 - \frac{P_e}{\sqrt{Z}}\tanh\left(\frac{\sqrt{Z}}{2}\right)\right\} = 0, \quad (4.45)$$

$$Z\cosh\left(\frac{\sqrt{Z}}{2}\right)\left\{1 - \frac{P_e}{\sqrt{Z}}\tanh\left(\frac{\sqrt{Z}}{2}\right)\right\} = 0. \quad (4.46)$$

The roots of these equations are the roots of the expression inside the braces, because the extra $\sqrt{Z}$ factor is non-zero except for $s = -P_e/4$, and this case is handled separately. Here, all roots exist only corresponding to the negative values of s. Using $\tanh\left(\sqrt{-x}\right) =$

$\mathrm{i}\tan(\sqrt{x})$, with s replaced by $-s$, leads to

$$1 - \frac{P_e}{\sqrt{4P_e s - P_e^2}} \tan\left(\frac{\sqrt{4P_e s - P_e^2}}{2}\right) = 0, \tag{4.47}$$

which can be written as

$$\sqrt{4P_e s - P_e^2} = P_e \tan\left(\frac{\sqrt{4P_e s - P_e^2}}{2}\right). \tag{4.48}$$

Now, the roots of Eq. (4.48) belong to I_k:

$$s_k \in I_k = \left(\frac{(2k-1)^2\pi^2}{4P_e} + \frac{P_e}{4}, \frac{(2k+1)^2\pi^2}{4P_e} + \frac{P_e}{4}\right) \text{ with } k \in \mathbb{N}. \tag{4.49}$$

However, there is an extra root in the following cases:
Case 1: If $0 < P_e < 2$, a root s_0 exists in the interval $I_0 = \left(\frac{P_e}{4}, \frac{\pi^2}{4P_e} + \frac{P_e}{4}\right)$, and only one root exists in each interval I_k as given in Eq. (4.49).
Case 2: If $P_e = 2$, a root $s_0 = P_e/4$ exists and there is only one root in the interval I_k for each k.
Case 3: If $P_e > 2$, a root s_0 exists in $\left(0, \frac{P_e}{4}\right)$ and only one root exists in each interval I_k.

Using the residue theorem, the integral present in the *Laplace inversion theorem* can be evaluated for the functions in Eqs. (4.22)–(4.27), Eq. (4.39) and Eq. (4.40) by obtaining the residues of these functions at the poles s_k. Since all the poles are simple ones, the evaluation of the residues can be performed by using the following standard formula:

$$\text{Res}\left(\exp(st)\overline{f}(s); s = -s_k\right) = \lim_{s\to -s_k} \exp(st)(s + s_k)\overline{f}(s) \tag{4.50}$$

to obtain $f(t)$ as

$$f(t) = \sum_{k=0}^{\infty} \text{Res}\left(\exp(st)\overline{f}(s); s = -s_k\right). \tag{4.51}$$

Using Eq. (4.51), we have

$$A_u(x^*, t^*) = \mathcal{L}^{-1}\left\{\overline{A}_u(x^*, s)\right\} = \sum_{k=0}^{\infty} a_{1k}(x^*) \exp(-s_k t^*), \tag{4.52}$$

with

$$a_{1k}(x^*) = \exp\left(\frac{P_e x^*}{2}\right)\frac{\beta s_k\sqrt{Z_k}\sin\left(\frac{x^*-1}{2}\sqrt{Z_k}\right)}{(2P_e s_k - P_e)\cos\left(\frac{\sqrt{Z_k}}{2}\right)}, \tag{4.53}$$

$$A_d(x^*,t^*) = \mathcal{L}^{-1}\left\{\overline{A}_d(x^*,s)\right\} = \sum_{k=0}^{\infty} a_{2k}(x^*)\exp\left(-s_k t^*\right), \tag{4.54}$$

with

$$a_{2k}(x^*) = \exp\left(\frac{x^*-1}{2}P_e\right)\frac{\sqrt{Z_k}\left(\sqrt{Z_k}\cos\left(\frac{x^*}{2}\sqrt{Z_k}\right) - P_e\sin\left(\frac{x^*}{2}\sqrt{Z_k}\right)\right)}{(4P_e s_k - 2P_e)\cos\left(\frac{\sqrt{Z_k}}{2}\right)}, \tag{4.55}$$

$$A_{lc}(x^*,t^*) = \mathcal{L}^{-1}\left\{\overline{A}_{lc}(x^*,s)\right\} = \sum_{k=0}^{\infty} a_{3k}(x^*)\exp\left(-s_k t^*\right), \tag{4.56}$$

with

$$a_{3k}(x^*) = \exp\left(\frac{x^*-x_0^*}{2}P_e\right)\frac{4P_e s_k\sin\left(\frac{x_0^*}{2}\sqrt{Z_k}\right)\sin\left(\frac{x^*-1}{2}\sqrt{Z_k}\right)}{(4P_e s_k - 2P_e)\cos\left(\frac{\sqrt{Z_k}}{2}\right)}, \text{ for } x^* > x_0^*, \tag{4.57a}$$

$$a_{3k}(x^*) = -\exp\left(\frac{x^*-x_0^*}{2}P_e\right)\left(\sqrt{Z_k}\cos\left(\frac{x^*}{2}\sqrt{Z_k}\right) - P_e\sin\left(\frac{x^*}{2}\sqrt{Z_k}\right)\right)$$
$$\times\frac{\sqrt{Z_k}\cos\left(\frac{1-x_0^*}{2}\sqrt{Z_k}\right) - P_e\sin\left(\frac{1-x_0^*}{2}\sqrt{Z_k}\right)}{(4P_e s_k - 2P_e)\cos\left(\frac{\sqrt{Z_k}}{2}\right)}, \text{ for } x^* < x_0^*, \tag{4.57b}$$

$$A_{ld}(x^*,t^*) = \mathcal{L}^{-1}\left\{\overline{A}_{ld}(x^*,s)\right\} = \sum_{k=0}^{\infty} a_{4k}(x^*)\exp\left(-s_k t^*\right), \tag{4.58}$$

with

$$a_{4k}(x^*) = -\frac{1}{s_k(x_2^*-x_1^*)}\frac{\sqrt{Z_k}\cos\left(\frac{x^*}{2}\sqrt{Z_k}\right) - P_e\sin\left(\frac{x^*}{2}\sqrt{Z_k}\right)}{(4P_e s_k - 2P_e)\cos\left(\frac{\sqrt{Z_k}}{2}\right)}$$

$$\times\left\{\exp\left(\frac{x^*-x_1^*}{2}P_e\right)\left(\sqrt{Z_k}\cos\left(\frac{1-x_1^*}{2}\sqrt{Z_k}\right)-(P_e-2s_k)\sin\left(\frac{1-x_1^*}{2}\sqrt{Z_k}\right)\right)\right.$$
$$\left.-\exp\left(\frac{x^*-x_2^*}{2}P_e\right)\left(\sqrt{Z_k}\cos\left(\frac{1-x_2^*}{2}\sqrt{Z_k}\right)-(P_e-2s_k)\sin\left(\frac{1-x_2^*}{2}\sqrt{Z_k}\right)\right)\right\},$$
$$\text{for } 0\le x^*<x_1^*, \tag{4.59a}$$

$$a_{4k}(x^*)=\sqrt{Z_k}\frac{\exp\left(\frac{x^*-x_2^*}{2}P_e\right)}{s_k(x_2^*-x_1^*)}\frac{\sqrt{Z_k}\cos\left(\frac{1+x^*-x_2^*}{2}\sqrt{Z_k}\right)-P_e\sin\left(\frac{1+x^*-x_2^*}{2}\sqrt{Z_k}\right)}{(4P_es_k-2P_e)\cos\left(\frac{\sqrt{Z_k}}{2}\right)}$$
$$-\frac{\exp\left(\frac{x^*-x_2^*}{2}P_e\right)}{x_2^*-x_1^*}\sin\left(\frac{x_2^*-1}{2}\sqrt{Z_k}\right)\frac{\sqrt{Z_k}\cos\left(\frac{x^*}{2}\sqrt{Z_k}\right)+P_e\sin\left(\frac{x^*}{2}\sqrt{Z_k}\right)}{(2P_es_k-P_e)\cos\left(\frac{\sqrt{Z_k}}{2}\right)}$$
$$+\frac{\exp\left(\frac{x^*-x_1^*}{2}P_e\right)}{x_2^*-x_1^*}\sin\left(\frac{x^*-1}{2}\sqrt{Z_k}\right)\frac{\sqrt{Z_k}\cos\left(\frac{x_1^*}{2}\sqrt{Z_k}\right)+P_e\sin\left(\frac{x_1^*}{2}\sqrt{Z_k}\right)}{(2P_es_k-P_e)\cos\left(\frac{\sqrt{Z_k}}{2}\right)},$$
$$\text{for } x_1^*\le x^*<x_2^*, \tag{4.59b}$$

$$a_{4k}(x^*)=\frac{\exp\left(\frac{x^*-x_1^*}{2}P_e\right)}{x_2^*-x_1^*}\sin\left(\frac{x^*-1}{2}\sqrt{Z_k}\right)\frac{\sqrt{Z_k}\cos\left(\frac{x_1^*}{2}\sqrt{Z_k}\right)+P_e\sin\left(\frac{x_1^*}{2}\sqrt{Z_k}\right)}{(2P_es_k-P_e)\cos\left(\frac{\sqrt{Z_k}}{2}\right)}$$
$$-\frac{\exp\left(\frac{x^*-x_2^*}{2}P_e\right)}{x_2^*-x_1^*}\sin\left(\frac{x^*-1}{2}\sqrt{Z_k}\right)\frac{\sqrt{Z_k}\cos\left(\frac{x_2^*}{2}\sqrt{Z_k}\right)+P_e\sin\left(\frac{x_2^*}{2}\sqrt{Z_k}\right)}{(2P_es_k-P_e)\cos\left(\frac{\sqrt{Z_k}}{2}\right)},$$
$$\text{for } x_2^*\le x^*\le 1, \tag{4.59c}$$

$$B_u(x^*,t^*)=\mathcal{L}^{-1}\left\{\overline{B}_u(x^*,s)\right\}=\sum_{k=0}^{\infty}b_{1k}(x^*)\exp\left(-s_kt^*\right), \tag{4.60}$$

with

$$b_{1k}(x^*)=\exp\left(\frac{P_ex^*}{2}\right)\frac{\sqrt{Z_k}\left(\sqrt{Z_k}\cos\left(\frac{x^*-1}{2}\sqrt{Z_k}\right)+P_e\sin\left(\frac{x^*-1}{2}\sqrt{Z_k}\right)\right)}{(4P_es_k-2P_e)\cos\left(\frac{\sqrt{Z_k}}{2}\right)}, \tag{4.61}$$

$$B_d(x^*,t^*) = \mathcal{L}^{-1}\left\{\overline{B}_d(x^*,s)\right\} = \sum_{k=0}^{\infty} b_{2k}(x^*)\exp\left(-s_k t^*\right), \tag{4.62}$$

with

$$b_{2k}(x^*) = -\frac{2P_e}{\beta}\exp\left(\frac{x^*-1}{2}P_e\right)\frac{\sqrt{Z_k}\sin\left(\frac{x^*}{2}\sqrt{Z_k}\right)}{(4P_e s_k - 2P_e)\cos\left(\frac{\sqrt{Z_k}}{2}\right)}, \tag{4.63}$$

$$B_{lc}(x^*,t^*) = \mathcal{L}^{-1}\left\{\overline{B}_{lc}(x^*,s)\right\} = \sum_{k=0}^{\infty} b_{3k}(x^*)\exp\left(-s_k t^*\right), \tag{4.64}$$

with

$$b_{3k}(x^*) = \frac{2P_e}{\beta}\exp\left(\frac{x^*-x_0^*}{2}P_e\right)\sin\left(\frac{x_0^*}{2}\sqrt{Z_k}\right) \times \frac{\sqrt{Z_k}\cos\left(\frac{x^*-1}{2}\sqrt{Z_k}\right)+P_e\sin\left(\frac{x^*-1}{2}\sqrt{Z_k}\right)}{(4P_e s_k - 2P_e)\cos\left(\frac{\sqrt{Z_k}}{2}\right)}, \quad \text{for } x^* > x_0^*, \tag{4.65a}$$

$$b_{3k}(x^*) = \frac{2P_e}{\beta}\exp\left(\frac{x^*-x_0^*}{2}P_e\right)\sin\left(\frac{x^*}{2}\sqrt{Z_k}\right) \times \frac{\sqrt{Z_k}\cos\left(\frac{1-x_0^*}{2}\sqrt{Z_k}\right)-P_e\sin\left(\frac{1-x_0^*}{2}\sqrt{Z_k}\right)}{(4P_e s_k - 2P_e)\cos\left(\frac{\sqrt{Z_k}}{2}\right)}, \quad \text{for } x^* < x_0^*, \tag{4.65b}$$

$$B_{ld}(x^*,t^*) = \mathcal{L}^{-1}\left\{\overline{B}_{ld}(x^*,s)\right\} = \sum_{k=0}^{\infty} b_{4k}(x^*)\exp\left(-s_k t^*\right), \tag{4.66}$$

with

$$b_{4k}(x^*) = \frac{2P_e}{\beta s_k(x_2^*-x_1^*)}\frac{\sin\left(\frac{x^*}{2}\sqrt{Z_k}\right)}{(4P_e s_k - 2P_e)\cos\left(\frac{\sqrt{Z_k}}{2}\right)} \times \left\{\exp\left(\frac{x^*-x_1^*}{2}P_e\right)\left(\sqrt{Z_k}\cos\left(\frac{1-x_1^*}{2}\sqrt{Z_k}\right)-(P_e-2s_k)\sin\left(\frac{1-x_1^*}{2}\sqrt{Z_k}\right)\right)\right.$$

$$- \exp\left(\frac{x^* - x_2^*}{2} P_e\right) \left(\sqrt{Z_k} \cos\left(\frac{1 - x_2^*}{2} \sqrt{Z_k}\right) - (P_e - 2s_k) \sin\left(\frac{1 - x_2^*}{2} \sqrt{Z_k}\right)\right) \Bigg\},$$

$$\text{for } 0 \le x^* < x_1^*, \tag{4.67a}$$

$$b_{4k}(x^*) = -\frac{2P_e}{\beta s_k (x_2^* - x_1^*)} \exp\left(\frac{x^* - x_2^*}{2} P_e\right) \sin\left(\frac{x^*}{2} \sqrt{Z_k}\right)$$
$$\times \frac{\sqrt{Z_k} \cos\left(\frac{1 - x_2^*}{2} \sqrt{Z_k}\right) + (2s_k - P_e) \sin\left(\frac{1 - x_2^*}{2} \sqrt{Z_k}\right)}{(4P_e s_k - 2P_e) \cos\left(\frac{\sqrt{Z_k}}{2}\right)}$$
$$+ \frac{1}{\beta s_k (x_2^* - x_1^*)} \exp\left(\frac{x^* - x_1^*}{2} P_e\right) \left(\sqrt{Z_k} \cos\left(\frac{x_1^*}{2} \sqrt{Z_k}\right) + P_e \sin\left(\frac{x_1^*}{2} \sqrt{Z_k}\right)\right)$$
$$\times \frac{\sqrt{Z_k} \cos\left(\frac{x^* - 1}{2} \sqrt{Z}\right) + P_e \sin\left(\frac{x^* - 1}{2} \sqrt{Z_k}\right)}{(4P_e s_k - 2P_e) \cos\left(\frac{\sqrt{Z_k}}{2}\right)}, \text{ for } x_1^* \le x^* < x_2^*, \tag{4.67b}$$

$$b_{4k}(x^*) = -\frac{1}{\beta s_k (x_2^* - x_1^*)} \frac{\sqrt{Z_k} \cos\left(\frac{x^* - 1}{2} \sqrt{Z_k}\right) + P_e \sin\left(\frac{x^* - 1}{2} \sqrt{Z_k}\right)}{(4P_e s_k - 2P_e) \cos\left(\frac{\sqrt{Z_k}}{2}\right)}$$
$$\times \Bigg\{ \exp\left(\frac{x^* - x_2^*}{2} P_e\right) \left(\sqrt{Z_k} \cos\left(\frac{x_2^*}{2} \sqrt{Z_k}\right) + P_e \sin\left(\frac{x_2^*}{2} \sqrt{Z_k}\right)\right)$$
$$- \exp\left(\frac{x^* - x_1^*}{2} P_e\right) \left(\sqrt{Z_k} \cos\left(\frac{x_1^*}{2} \sqrt{Z_k}\right) + P_e \sin\left(\frac{x_1^*}{2} \sqrt{Z_k}\right)\right) \Bigg\}, \text{ for } x_2^* \le x^* \le 1, \tag{4.67c}$$

where $Z_k = 4P_e s_k - P_e^2$. For the exceptional cases, we obtain different coefficients.

Case 1: When there is a root s_0 in $\left(\frac{P_e}{4}, \frac{\pi^2}{4P_e} + \frac{P_e}{4}\right)$, the coefficients in Eqs. (4.53), (4.55), (4.57), (4.59), (4.61), (4.63), (4.65) and (4.67) remain unchanged for s_0.

Case 2: When $P_e = 2$, implying $s_0 = P_e/4$ as a simple pole, the coefficients for $k = 0$ are replaced by

$$a_{10}(x^*) = \frac{3\beta}{4}(x^* - 1) \exp(x^*), \tag{4.68}$$

$$a_{20}(x^*) = \frac{3}{2}(1 - x^*) \exp(x^* - 1), \tag{4.69}$$

$$a_{30}(x^*) = \frac{3x_0^*}{2}(x^* - 1) \exp(x^* - x_0^*), \tag{4.70}$$

$$a_{40}(x^*) = \frac{3(x^* - 1)}{2(x_2^* - x_1^*)} \left((x_1^* + 1) \exp(x^* - x_1^*) - (x_2^* + 1) \exp(x^* - x_2^*)\right), \tag{4.71}$$

$$b_{10}(x^*) = \frac{3x^*}{2}\exp(x^*), \tag{4.72}$$
$$b_{20}(x^*) = -\frac{3x^*}{\beta}\exp(x^*-1), \tag{4.73}$$
$$b_{30}(x^*) = \frac{3x_0^* x^*}{\beta}\exp(x^*-x_0^*), \tag{4.74}$$
$$b_{40}(x^*) = \frac{3x^*}{\beta(x_2^*-x_1^*)}\left((x_1^*+1)\exp(x^*-x_1^*) - (x_2^*+1)\exp(x^*-x_2^*)\right). \tag{4.75}$$

Case 3: When there is a root s_0 in $(0, P_e/4)$, then for $k=0$, the functions in Eqs. (4.53), (4.55), (4.57), (4.59), (4.61), (4.63), (4.65) and (4.67) will be replaced by the negative of the respective function, and the hyperbolic function replacing the corresponding trigonometric function, with $Z_0 = P_e^2 - 4P_e s_0$.

To study the physical behavior of these impulse responses, we derive the corresponding unit-step responses which have the following forms:

$$a_u(x^*,t^*) = -\sum_{k=0}^{\infty}\frac{a_{1k}(x^*)}{s_k}\exp(-s_k t^*), \tag{4.76}$$
$$a_d(x^*,t^*) = 1-\sum_{k=0}^{\infty}\frac{a_{2k}(x^*)}{s_k}\exp(-s_k t^*), \tag{4.77}$$
$$a_{lc}(x^*,t^*) = \begin{cases} -1-\sum_{k=0}^{\infty}\frac{a_{3k}(x^*)}{s_k}\exp(-s_k t^*), & \text{for } x^* < x_0^*, \\ -\sum_{k=0}^{\infty}\frac{a_{3k}(x^*)}{s_k}\exp(-s_k t^*), & \text{for } x^* > x_0^*, \end{cases} \tag{4.78}$$
$$a_{ld}(x^*,t^*) = \begin{cases} -1-\sum_{k=0}^{\infty}\frac{a_{4k}(x^*)}{s_k}\exp(-s_k t^*), & \text{for } 0 \le x^* < x_1^*, \\ \frac{x^*-x_2^*}{x_2^*-x_1^*}-\sum_{k=0}^{\infty}\frac{a_{4k}(x^*)}{s_k}\exp(-s_k t^*), & \text{for } x_1^* \le x^* < x_2^*, \\ -\sum_{k=0}^{\infty}\frac{a_{4k}(x^*)}{s_k}\exp(-s_k t^*), & \text{for } x_2^* \le x^* \le 1, \end{cases} \tag{4.79}$$
$$b_u(x^*,t^*) = \exp(P_e x^*) - \sum_{k=0}^{\infty}\frac{b_{1k}(x^*)}{s_k}\exp(-s_k t^*), \tag{4.80}$$
$$b_d(x^*,t^*) = \frac{1}{\beta}\left(1-\exp(P_e x^*)\right) - \sum_{k=0}^{\infty}\frac{b_{2k}(x^*)}{s_k}\exp(-s_k t^*), \tag{4.81}$$
$$b_{lc}(x^*,t^*) = \begin{cases} \frac{1}{\beta}(\exp(P_e x^*)-1) - \sum_{k=0}^{\infty}\frac{b_{3k}(x^*)}{s_k}\exp(-s_k t^*), & \text{for } x^* < x_0^*, \\ \frac{\exp(P_e x^*)}{\beta}(1-\exp(-P_e x_0^*)) - \sum_{k=0}^{\infty}\frac{b_{3k}(x^*)}{s_k}\exp(-s_k t^*), & \text{for } x^* > x_0^*, \end{cases} \tag{4.82}$$

$$b_{ld}(x^*,t^*)=\begin{cases}\dfrac{1}{\beta}(\exp(P_e x^*)-1)-\displaystyle\sum_{k=0}^{\infty}\frac{b_{4k}(x^*)}{s_k}\exp(-s_k t^*), & \text{for } 0\leq x^*<x_1^*,\\ \dfrac{x^*-x_2^*}{\beta(x_2^*-x_1^*)}+\dfrac{\exp(P_e x^*)}{\beta P_e(x_2^*-x_1^*)}\left(\exp(-P_e x^*)-\exp(-P_e x_1^*)+P_e(x_2^*-x_1^*)\right) & \\ -\displaystyle\sum_{k=0}^{\infty}\frac{b_{4k}(x^*)}{s_k}\exp(-s_k t^*), & \text{for } x_1^*\leq x^*<x_2^*,\\ \dfrac{\exp(P_e x^*)}{\beta P_e(x_2^*-x_1^*)}\left(\exp(-P_e x_2^*)-\exp(-P_e x_1^*)+P_e(x_2^*-x_1^*)\right) & \\ -\displaystyle\sum_{k=0}^{\infty}\frac{b_{4k}(x^*)}{s_k}\exp(-s_k t^*), & \text{for } x_2^*\leq x^*\leq 1.\end{cases} \tag{4.83}$$

4.3 Results and discussion

In this section, the finite channel responses are compared with the corresponding semi-infinite channel responses due to the lack of availability of the analytical solutions in the literature for the same. A comparison for the upstream and lateral responses for the flow discharge is presented. The upstream responses are compared with the semi-infinite channel responses used in Cimorelli et al. [6] for a given flow depth at the upstream end. The flow-discharge upstream response for the semi-infinite channel with a flow-depth-based upstream boundary is given as

$$a_{u,\infty}(x^*,t^*)=\frac{\beta}{2}\mathrm{erfc}\left(\frac{x^*-t^*}{\sqrt{4t^*}}\sqrt{P_e}\right)+\frac{\beta}{\sqrt{\pi P_e t^*}}\exp\left(-\frac{(x^*-t^*)^2}{4t^*}P_e\right). \tag{4.84}$$

Similarly, the flow discharge response to the uniformly distributed lateral inflow for the semi-infinite channel with a flow-depth type upstream boundary, based on [21, 6], is given as

$$\begin{aligned}a_{ld,\infty}(x^*,t^*)&=\beta t^*-\frac{\beta}{2}\left(t^*-x^*+\frac{1}{P_e}\right)\mathrm{erfc}\left(\frac{x^*-t^*}{\sqrt{4t^*}}\sqrt{P_e}\right)\\&+\frac{\beta}{2P_e}\exp(P_e x^*)\mathrm{erfc}\left(\frac{x^*+t^*}{\sqrt{4t^*}}\sqrt{P_e}\right)-\frac{\beta(t^*-x^*)}{\sqrt{4\pi P_e t^*}}\exp\left(-\frac{(x^*-t^*)^2}{4t^*}P_e\right)\\&-\frac{\beta(t^*+x^*)}{\sqrt{4\pi P_e t^*}}\exp(P_e x^*)\exp\left(-\frac{(x^*+t^*)^2}{4t^*}P_e\right).\end{aligned} \tag{4.85}$$

In Fig. 4.2, the upstream responses for the flow discharge $a_u(x^*,t^*)$ evaluated in the previous section are compared with the corresponding semi-infinite channel responses $a_{u,\infty}(x^*,t^*)$ given in Eq. (4.84). For this comparison, we take $Q^*(1,t^*)=0$ and $T^*(t^*)=0$, which physically means that there is no perturbation in the flow discharge to the reference value Q_0 at the downstream end, and there is no lateral inflow in the channel. The values of the Péclet number are considered between 0.5 and 8. For $P_e = 0.5$ and 2, the response at $x^* = 0.2$ gets an instant peak. As the observed location moves away from the upstream end, the peak of the response becomes smooth. This peak is the effect of the instant input given at the upstream end, whereas the fall of the peak is the effect of the downstream boundary. As one increases the Péclet number, the effect of the downstream boundary reduces and the response takes a longer time to reduce to zero. This can be observed from Figs. 4.2(b) and 4.2(c) for both of which the flow discharge does not reach zero for $t^* = 3$ corresponding to $P_e = 2$, 8. On the contrary, this does not happen for $P_e = 0.5$ as can be observed from Fig. 4.2(a) that every response goes to zero after $t^* = 1$. Cimorelli et al. [6] presented this comparison with similar conditions except that the downstream boundary was considered as a stage-discharge relationship. In their comparison, the semi-infinite channel responses were in decent agreement with the finite channel responses for $P_e = 5$. Here, even for $P_e = 8$, the semi-infinite channel responses overestimate the finite channel responses for the locations closer to the downstream boundary. Both types of responses agree upto $x^* = 0.4$, but after that, the semi-infinite channel responses fail to estimate the responses for the finite channel. From this comparison and the one provided in Cimorelli et al. [6], we can infer that the usability of the semi-infinite channel responses in place of the finite channel responses also depends on the type of the considered downstream boundary.

In Fig. 4.3, the downstream response for the flow discharge corresponding to a unit-step flow discharge provided at the downstream boundary is presented. Here, we take $h^*(0, t^*) = 0$ and $T^*(t^*) = 0$, which physically means that there is no perturbation in the flow depth to the reference value h_0 at the upstream end, and there is no lateral inflow in the channel. The responses take a longer time to converge as the value of the Péclet number is increased. The effect of the downstream boundary seems to dominate the behavior of the responses. Although the values of the discharge reduce significantly for $P_e = 8$, the effect of the downstream boundary is still visible at $x^* = 0.8$. From the expression in Eq. (4.77), these responses are expected to reach 1 for large times, which also agrees with the condition of unit-step flow discharge imposed at the downstream boundary. Based on the pattern observed here, we can infer that these responses will take a long time to reach that stage. Even for lower values of P_e, the responses for $x^* = 0.8$ show a different pattern in initial times. These responses are very different from the ones obtained for a flow depth given at the downstream end which was discussed in *Chapter 3*. For all the considered values of P_e, the discharge increases and hence, always has positive values. This shows that the flow-discharge-based downstream boundary is responsible for the increase in the value of the flow discharge along the channel, and its effect gets reduced as one moves toward the upstream end, which is not the case for a flow-depth-based downstream boundary.

In Fig. 4.4, the flow-discharge response at $x^* = 0.9$ to the unit-step lateral inflow con-

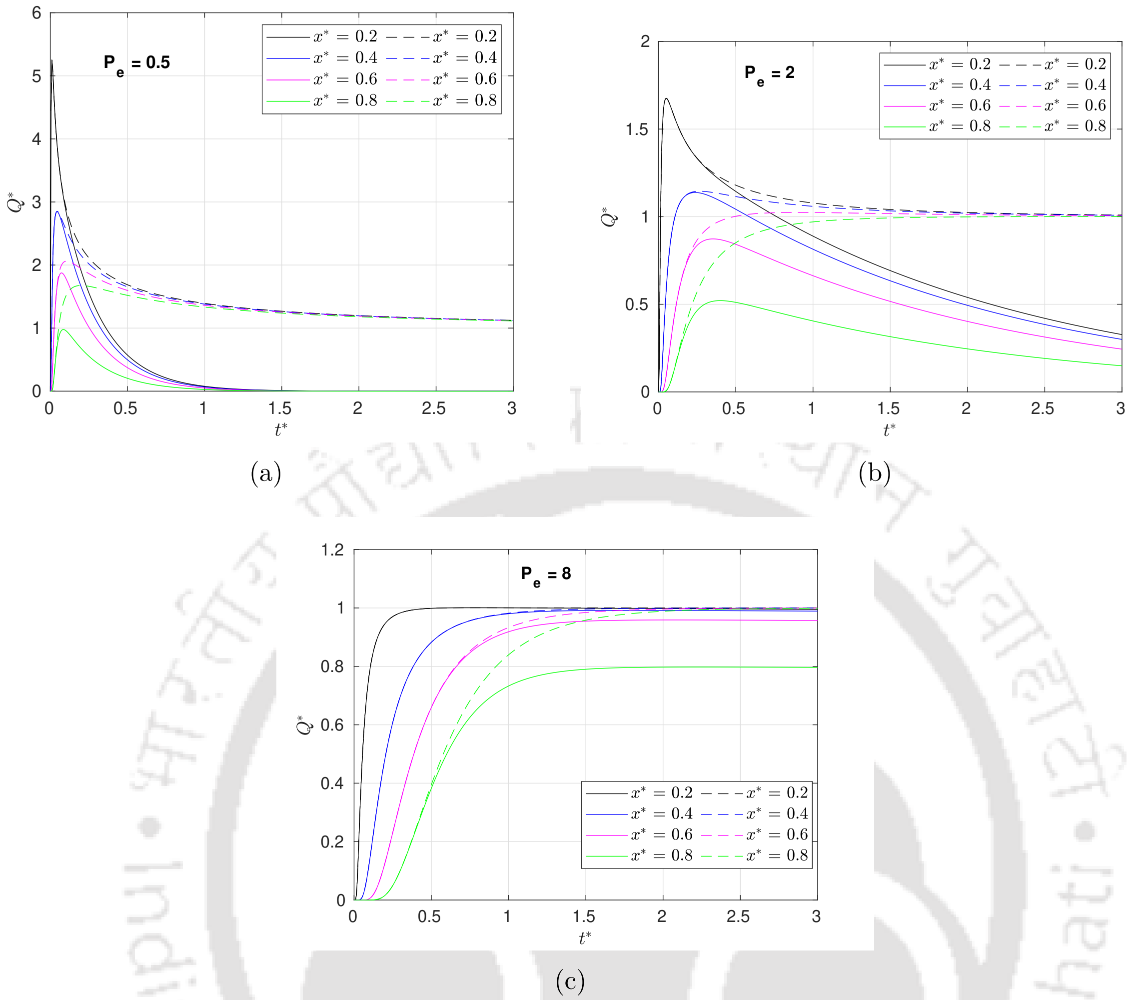

Figure 4.2: Comparison between flow-discharge response for finite channel given in Eq. (4.76) – continuous curves, and flow-discharge response for semi-infinite channel given in Eq. (4.84) – dashed curves, to the unit-step flow depth at the upstream end for different x^* with $Q^*(1,t^*) = 0$ and $T^*(t^*) = 0$: (a) $P_e = 0.5$, (b) $P_e = 2$, (c) $P_e = 8$

centrated at different x_0^* is plotted corresponding to different values of P_e. Here, we take $h^*(0,t^*) = 0$ and $Q^*(1,t^*) = 0$, which physically means that there is no perturbation in the flow depth to the reference value h_0 at the upstream end, and there is no perturbation in the flow discharge to the reference value Q_0 at the downstream end. The behavior of the concentrated lateral inflow responses is very similar to the upstream responses plotted in Fig. 4.2 except that the difference in the convergence limit is very significant. The convergence pattern agrees with the fact that, for higher Péclet numbers, the dominance of the downstream boundary reduces which is the reason behind the values of the discharge diminishing to zero for lower Péclet numbers.

In Fig. 4.5, the combined effect of unit-step flow-depth-based upstream boundary and unit-step flow-discharge-based downstream boundary on the flow depth is presented at

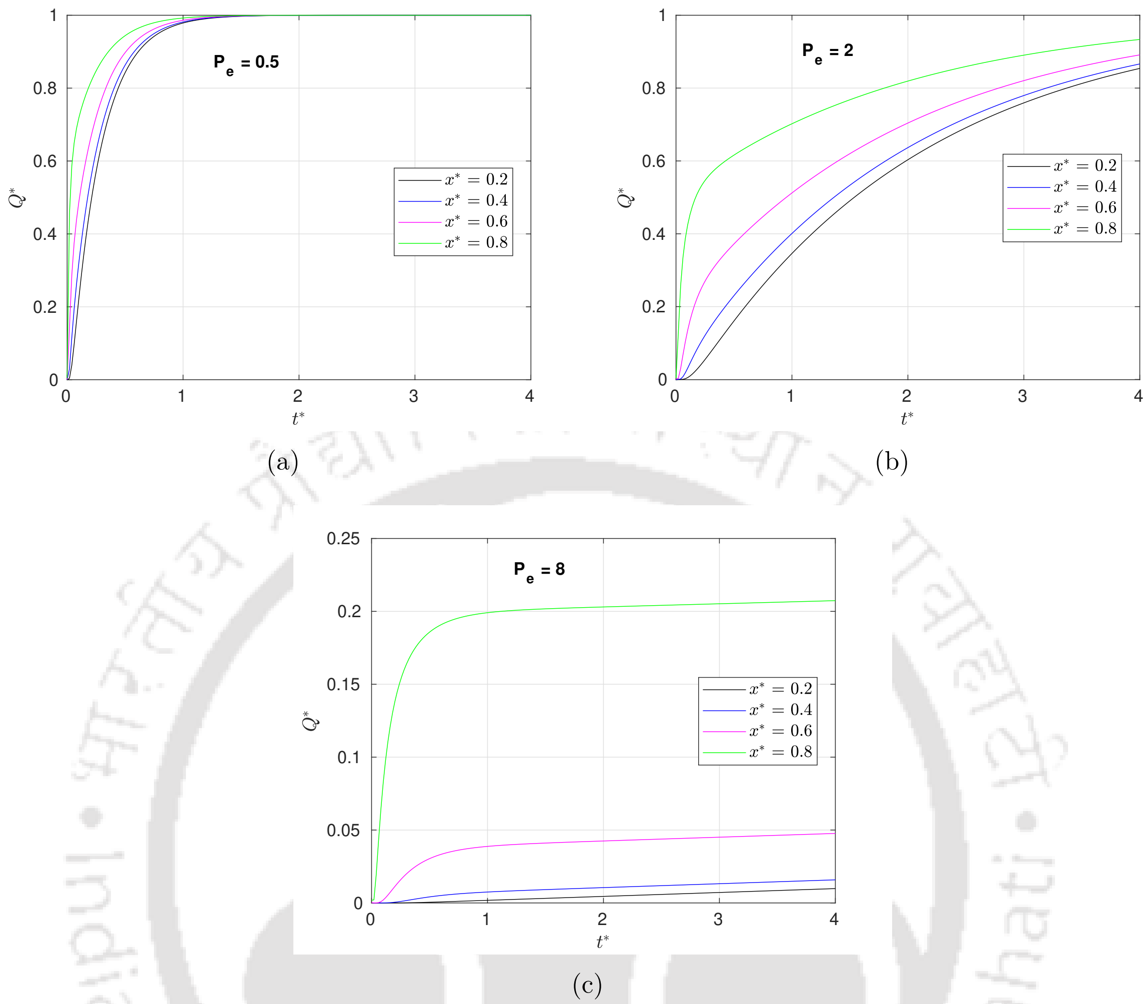

Figure 4.3: Flow-discharge response for finite channel given in Eq. (4.77) to the unit-step flow discharge at the downstream end for different x^* with $h^*(0, t^*) = 0$ and $T^*(t^*) = 0$: (a) $P_e = 0.5$, (b) $P_e = 2$, (c) $P_e = 4$

different locations of the channel. To plot this, no lateral inflow is considered in the channel which means $T^*(t^*) = 0$. As can be observed from Figs. 4.5(a)–4.5(b), the flow depth takes negative values initially, and then slowly increases to reach the value 1; this convergence limit is dependent on β which is kept at 1. These negative values are observed only for the locations closer to the downstream boundary. This means that a flow-discharge-based downstream boundary reduces the flow depth, and its effect reduces as one moves toward the upstream end, where the flow depth seems to increase from the starting time due to the presence of a unit-step flow depth imposed at the upstream end. The clear difference of the dominance of the downstream boundary is visible for the cases $x^* = 0.6$ and $x^* = 0.8$ for all cases of P_e that are plotted here. When considered separately, the convergence limit of these responses is dependent on all the parameters, i.e., P_e, β, and x. However, it can be observed from Fig. 4.5(c) that, although initial negative values

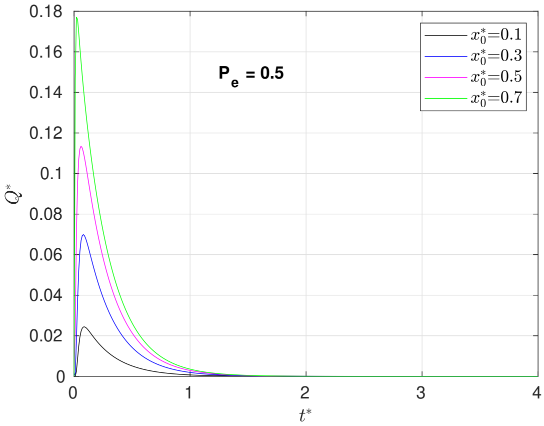

(a)

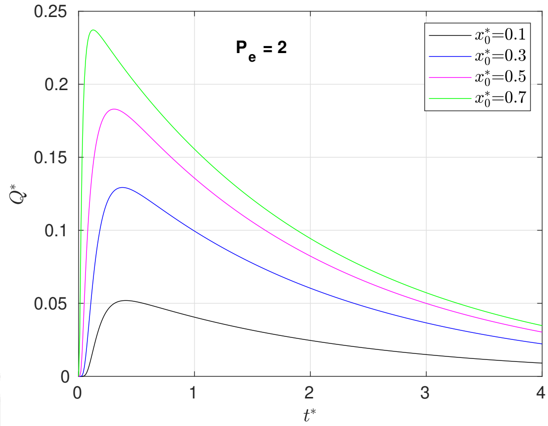

(b)

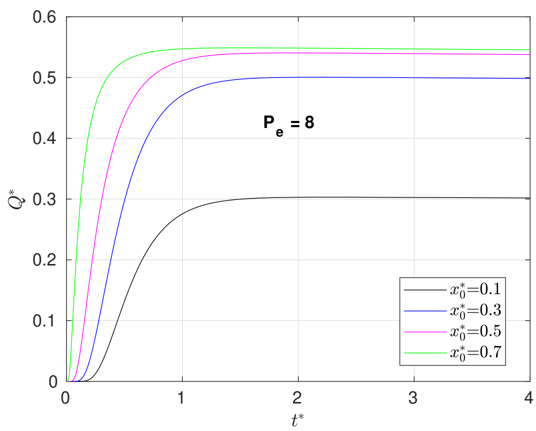

(c)

Figure 4.4: Flow-discharge response at $x^* = 0.9$ to the unit-step lateral inflow concentrated at different x_0^* for finite channel given in Eq. (4.78) with $h^*(0, t^*) = 0$ and $Q^*(1, t^*) = 0$: (a) $P_e = 0.5$, (b) $P_e = 2$, (c) $P_e = 8$

exist for the flow depth, the combined responses reach the value 1 for some large time. As the value of P_e increases, the responses take a longer time to converge. To show that this response takes a longer time to converge, results for $P_e = 4$ are plotted for a larger time scale. This convergence time increases rapidly as one considers increasing values of the Péclet number. If the value of β is increased, the effect of the downstream end is observed to reduce and the effect of the upstream boundary dominates the behavior of the flow-depth responses. Although the dimensionless channel width is dependent on various parameters, it is directly proportional to the linearized channel width b_0 and celerity C_0. This may mean that, for channels with large widths or with high celerity, the effect of the upstream boundary is more dominant than the effect of the downstream boundary. The value of β also increases with an increase in the reference value h_0 of the flow depth and with a decrease in reference value Q_0 of the flow discharge.

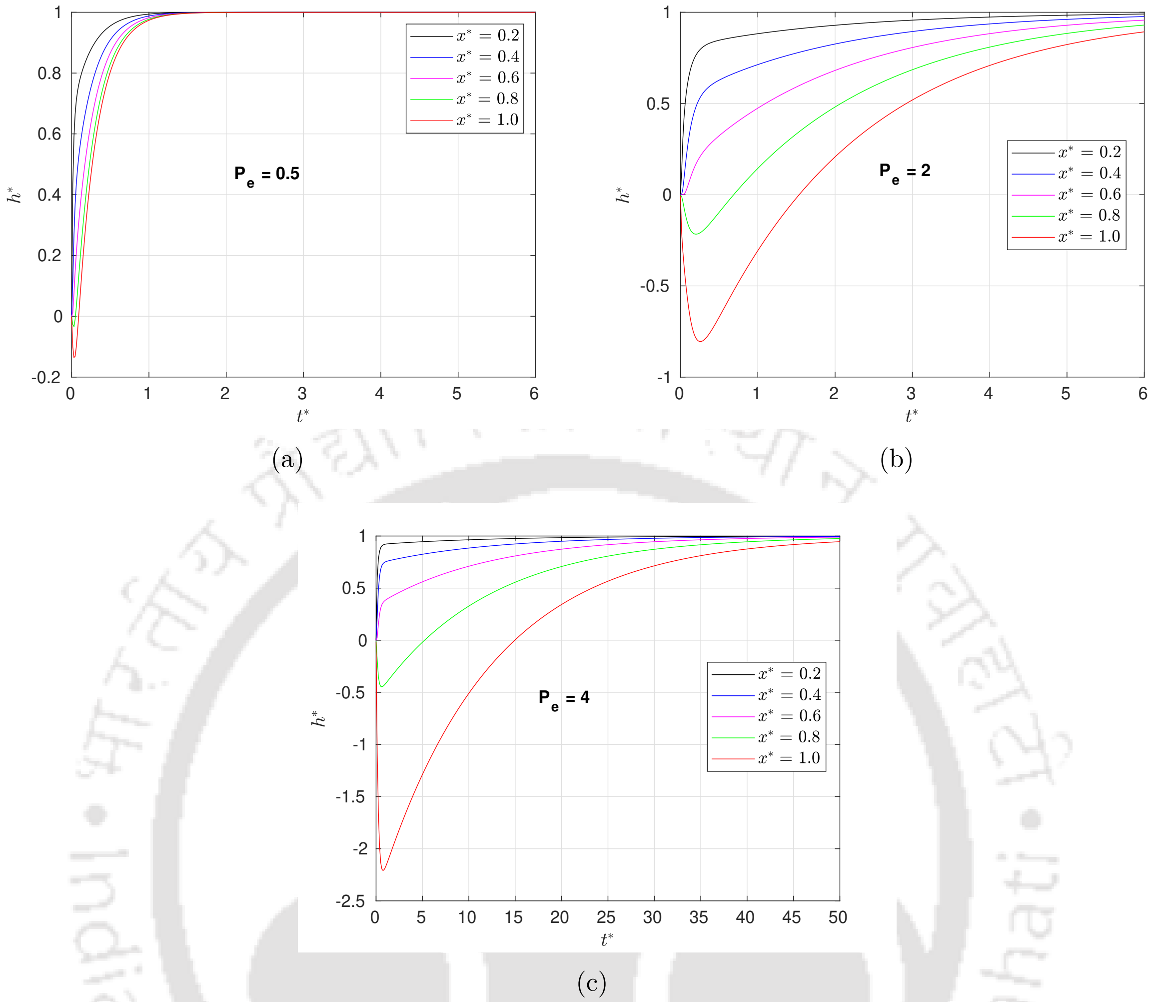

Figure 4.5: Combined flow-depth response to the unit-step flow depth at the upstream end given in Eq. (4.80) and unit-step flow discharge at the downstream end given in Eq. (4.81) at different x^* with $T^*(t^*) = 0$, $\beta = 1$: (a) $P_e = 0.5$, (b) $P_e = 2$, (c) $P_e = 4$

For Figs. 4.6–4.9, we consider $h^*(0, t^*) = 0$ and $Q^*(1, t^*) = 0$. This physically means that there is no perturbation in the flow depth to the reference value h_0 at the upstream end, and there is no perturbation in the flow discharge to the reference value Q_0 at the downstream end.

In Fig. 4.6, the effect of a uniformly distributed unit-step lateral inflow on the flow discharge is shown at different locations of the channel. The lateral inflow is uniformly distributed between the locations $x_1^* = 0.2$ and $x_2^* = 0.5$. The responses for $x^* < x_1^*$ converge to the value -1, and then the convergence limit increases as the distance between x^* and the downstream end decreases. The backwater effect for $x^* < x_1^*$ is almost similar for the cases $x^* = 0.1, 0.2$. However, the responses for x^* with $x_1^* \leq x^* < x_2^*$ shows a different pattern as compared to the responses for $x^* > x_2^*$ and $x^* < x_1^*$. For large times, the responses for $x_1^* \leq x^* \leq x_2^*$ are dependent on x^*, but for locations downstream to

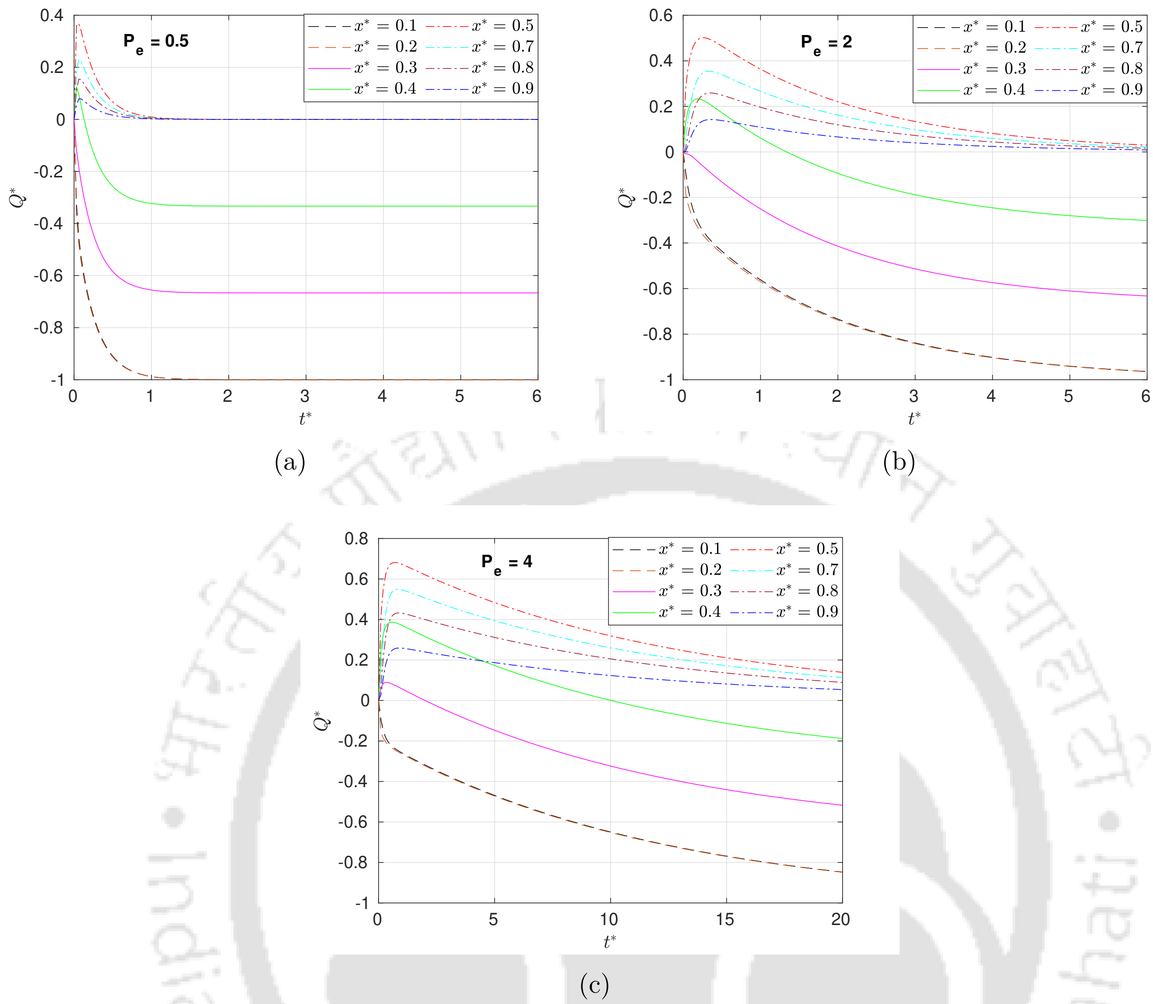

Figure 4.6: Flow-discharge response to the unit-step lateral inflow uniformly distributed between locations $x_1^* = 0.2$ and $x_2^* = 0.5$ given in Eq. (4.79) at different x^* with $h^*(0, t^*) = 0$ and $Q^*(1, t^*) = 0$: (a) $P_e = 0.5$, (b) $P_e = 2$, (c) $P_e = 4$

location x_2^*, all the responses approach zero as time progresses. This convergence process slows down as the Péclet number increases. To illustrate this slow convergence, a different time scale is taken while considering $P_e = 4$ as shown in Fig. 4.6(c). For $x^* \leq x_2^*$, due to the combined backwater effect of the downstream boundary and the lateral inflow, the flow discharge reduces in the upstream direction. Higher values of the flow discharge are observed for the locations closer to x_2^*. Beyond this, the flow discharge reduces as the observed location moves toward the downstream boundary. It ultimately reaches zero in agreement with the condition of zero flow discharge at the downstream end which was taken into account to derive the unit-step responses of the distributed lateral inflow.

The response of the flow depth to the unit-step lateral inflow distributed between the locations $x_1^* = 0.1$ and $x_2^* = 0.7$ is shown in Fig. 4.7. The limiting value increases with an increase in the value of x^* or P_e. Here, we take the value of P_e up to 2.5. A slight variation

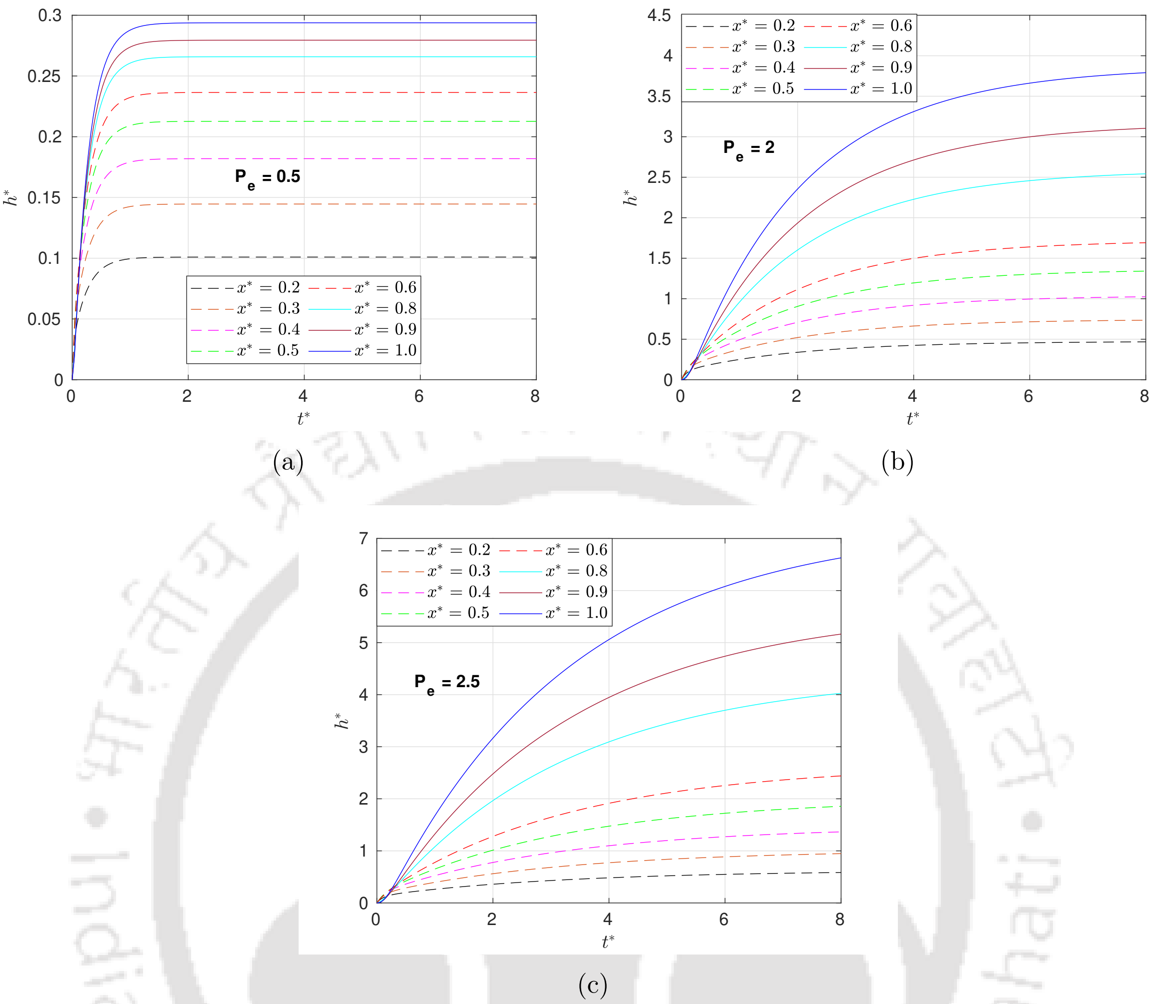

Figure 4.7: Flow-depth response to the unit-step lateral inflow uniformly distributed between locations $x_1^* = 0.1$ and $x_2^* = 0.7$ given in Eq. (4.83) at different x^* with $\beta = 1$, $h^*(0, t^*) = 0$ and $Q^*(1, t^*) = 0$: (a) $P_e = 0.5$, (b) $P_e = 2$, (c) $P_e = 2.5$

in the discharge due to the lateral inflow shows a significant impact on the flow depth. Even for $x^* > x_2^*$, the flow-depth response increases further as the value of the Péclet number is increased. The difference between the responses at the locations upstream and downstream to x_2^* increases as the value of P_e is increased further. This happens because of the downstream boundary present as a flow-discharge hydrograph. The effect of the downstream boundary appears to dominate up to $x^* = 0.8$ which is very close to the location $x_2^* = 0.7$. As one moves in the upstream direction, this effect reduces.

The responses of the flow depth to a uniformly distributed lateral inflow between locations x_1^* and x_2^* presented in the previous section can be used to find the flow-depth response corresponding to a lateral inflow uniformly distributed along the channel length. These responses are shown in Fig. 4.8. The flow depth increases as the value of x^* increases, and for higher Péclet numbers, an exponential growth is visible. This may

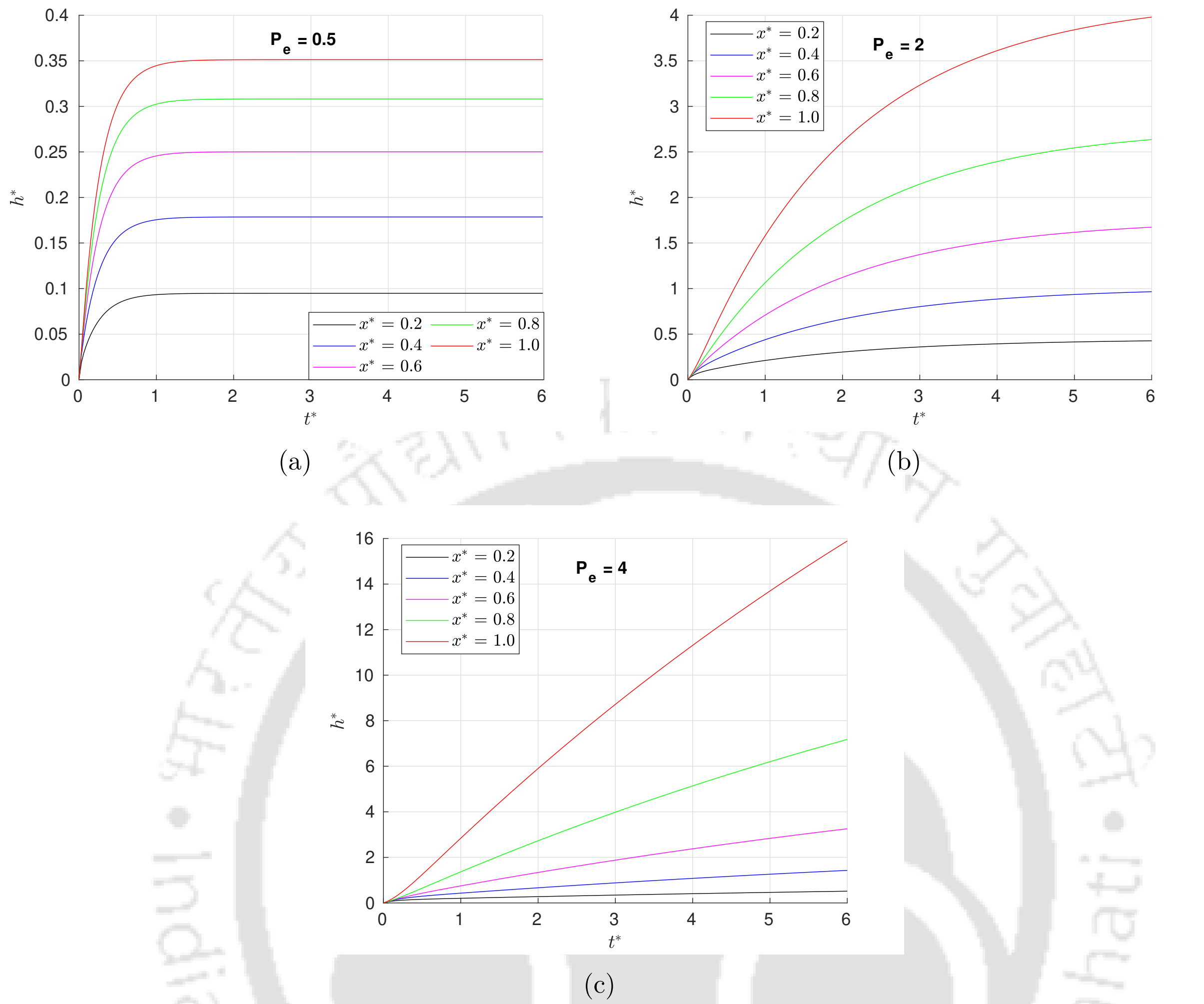

Figure 4.8: Flow-depth response to the unit-step lateral inflow uniformly distributed along the channel length given in Eq. (4.83) for $x_1^* = 0$, $x_2^* = 1$ at different x^* with $\beta = 1$, $h^*(0,t^*) = 0$ and $Q^*(1,t^*) = 0$: (a) $P_e = 0.5$, (b) $P_e = 2$, (c) $P_e = 4$

mean that even the slightest change in the flow-discharge distribution along the channel has a huge impact on the flow depth, and the exponential increase for the locations closer to the downstream boundary shows the sensitivity of the flow depth to the discharge-type downstream boundary. This is not the case for the flow discharge as can be observed from Fig. 4.9 presented next.

In Fig. 4.9, the flow-discharge response to the unit-step lateral inflow uniformly distributed along the channel length, i.e., $x_1^* = 0$ and $x_2^* = 1$ is compared with the corresponding semi-infinite channel response. For $P_e = 10$, the responses are in complete agreement upto $x^* = 0.4$, but the semi-infinite channel response overestimates the response for $x^* = 0.8$. Since the finite channel lateral response is derived by taking a zero downstream boundary, its effect brings down the flow discharge values as one moves toward the downstream end. For lower values of P_e, the semi-infinite channel response does

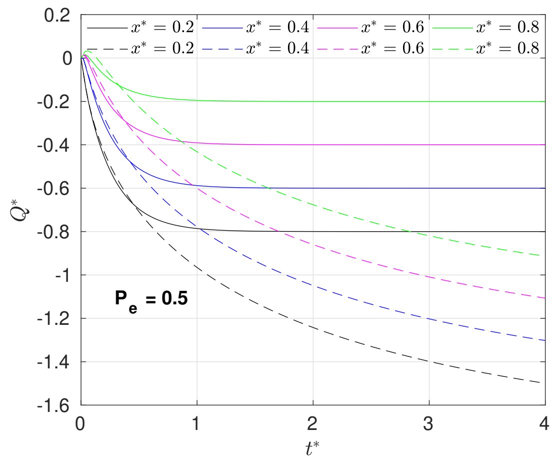

(a)

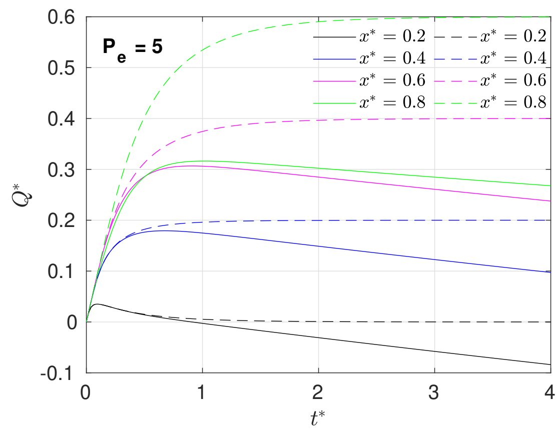

(b)

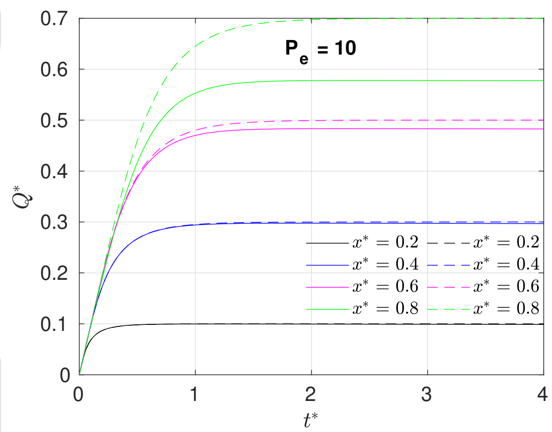

(c)

Figure 4.9: Comparison between flow discharge response for finite channel given in Eq. (4.79) – continuous curves, and flow discharge response for semi-infinite channel given in Eq. (4.85) – dashed curves, to the unit-step lateral inflow uniformly distributed along the channel length for $x_1^* = 0$, $x_2^* = 1$ at different x^* with $h^*(0,t^*) = 0$ and $Q^*(1,t^*) = 0$: (a) $P_e = 0.5$, (b) $P_e = 5$, (c) $P_e = 10$

not provide a satisfactory match with the finite channel responses. This shows that, for higher values of the Péclet number, the semi-infinite channel responses can be used to estimate the discharge for locations away from the downstream end.

4.4 Conclusion

Focusing on the simplified models of the Saint-Venant equations, we have derived an analytical solution for the linearized diffusive wave model in a finite length channel with a flow-depth-based upstream boundary and a flow-discharge-based downstream boundary.

Two types of lateral inflows were considered: a concentrated lateral inflow, and a uniformly distributed lateral inflow. The solutions for the flow discharge and the flow depth were presented. The system of equations was solved by using the Laplace transform, where the time domain solution was derived by using the *Laplace inversion theorem*.

For some cases, the unit-step responses were compared with the semi-infinite channel results subject to the same upstream condition and lateral inflows without considering the downstream boundary. To represent the case of a lateral inflow where the width of the segment with the lateral inflow is negligible in comparison to the length of the channel under consideration, a concentrated source was considered at x_0^*. For the second case, the lateral inflow was uniformly distributed between the locations x_1^* and x_2^* with $0 \leq x_1^* < x_2^* \leq 1$ which holds true for the case of a lateral inflow uniformly distributed throughout the channel. For all the unit responses corresponding to different inputs, the limiting value of the flow-depth responses is dependent on all the parameters, i.e., P_e, β, x^*, x_0^*, x_1^* and x_2^*. But the flow-discharge responses were independent of these parameters except for the response to the uniformly distributed lateral inflow. This may mean that a flow-depth-based upstream boundary and a flow-discharge-based downstream boundary could bring out prominently the sensitivity of the flow depth; however they cannot display the same for the flow discharge. Cimorelli et al. [6] presented these solutions by considering a stage-discharge relationship at the downstream end. Considering a flow-discharge hydrograph in place of the stage-discharge relationship changes the dynamics significantly. The stage-discharge relationship was reflected in the solution by using a feedback parameter which ranges between 0.6 to 1.3 for most of the downstream boundary presented in river application [6]. But a downstream boundary in terms of a flow-discharge hydrograph needs a separate solution to show the effect of the downstream boundary explicitly on the flow discharge and the flow depth. The semi-infinite channel response completely failed to approximate the results for the finite channel for lower values of the Péclet number. In all the responses presented, the flow-depth responses were affected by the flow-discharge-based downstream boundary as compared to the flow-discharge responses. For lower value of the Péclet number, the solutions presented could be used for predicting flow discharge and flow depth if a flow-discharge type downstream boundary and a flow-depth type upstream boundary were considered. Even for $P_e = 10$, the prediction of the flow discharge by the semi-infinite channel result was not accurate for the locations closer to the downstream boundary. Since the value of the Péclet number is directly related to the importance of the downstream boundary, this showed that the effect of a flow-discharge-based downstream boundary was more influential than a flow-depth-based downstream boundary which was discussed in *Chapter 3*. For the problems with a flow-discharge type downstream boundary imposed, the solutions presented here will be a better alternative to the semi-infinite channel solutions available in the literature.

CHAPTER 5

Impact of different types of lateral inflow and stage-discharge relation imposed at the downstream end of a finite channel for the diffusive wave model

In this chapter, an analytical solution for the diffusive wave model with a concentrated and a uniformly distributed lateral inflow for a finite channel is presented. The upstream boundary is taken as a flow-discharge hydrograph or a flow-depth hydrograph whereas the downstream end is subject to a stage-discharge relationship. The focus is on analyzing the impact of the lateral inflow concentrated at different locations or uniformly distributed between any two locations along the channel length on the flow discharge and the flow depth. The unit-step responses corresponding to the impulse responses for the lateral inflow are presented and the responses corresponding to the concentrated lateral inflow are also compared with the corresponding results of a semi-infinite channel where the downstream boundary is ignored.

5.1 Governing equations and proposed method

Under suitable assumptions for the Saint-Venant equations, a prismatic channel of length L for which the cross-sectional shape of the channel is fixed is considered and the bottom slope is taken as constant. The diffusive wave approximation of the Saint-Venant equations can be derived when the effect of the inertial forces is small in comparison with the other forces, which is described by the following equations [10]:

$$\frac{1}{b}\frac{\partial Q}{\partial x} + \frac{\partial h}{\partial t} = \frac{q_l}{b}, \tag{5.1a}$$

$$\frac{\partial h}{\partial x} = S_0 - S_f, \tag{5.1b}$$

and the notations involved in these equations are the same as the ones described in *Chapters 3* and *4*. A schematic diagram for the flow problem is presented in Fig. 5.1.

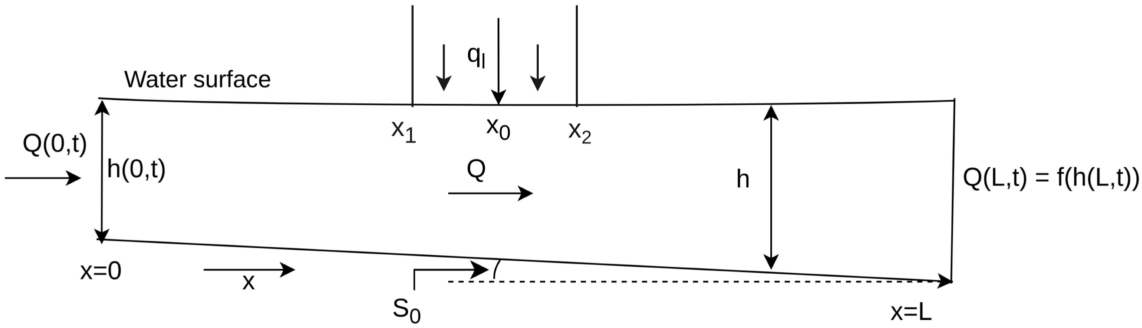

Figure 5.1: A schematic diagram for $1D$ flow structure in a prismatic channel

Our primary focus is to study the effect of different types of lateral inflow on the flow discharge and the flow depth at different locations of the channel of length L. Based on the concepts used in *Chapters 3* and *4*, it is possible to express $q_l(x,t)$ as a product of two functions as follows [19]:

$$q_l(x,t) = X(x)T(t), \tag{5.2}$$

where $X(x)$ represents the discharge distribution in space and $T(t)$ is the total discharge of the lateral inflow. The work of Cimorelli et al. [7] is followed to linearize Eq. (5.1). We use the perturbation technique on the unknown variables Q and h. The flow is perturbed around a steady uniform reference condition represented by (Q_0, h_0) with $Q_1(x,t)$ and $h_1(x,t)$ as the first-order increments in the flow discharge and the flow depth where higher-order terms are ignored. In order to simplify the formulation, we use dimensionless variables in this analysis. The following transformations are considered [7]:

$$t^* = \frac{t}{L/C_0}, \; x^* = \frac{x}{L}, \; h^* = \frac{h_1}{h_0}, \; Q^* = \frac{Q_1}{Q_0}, \tag{5.3}$$

where C_0 is the celerity of the linearized model given by

$$C_0 = -\frac{1}{b_0}\left(\frac{\partial S_f/\partial h}{\partial S_f/\partial Q}\right)_{(Q_0,h_0)}, \tag{5.4}$$

with b_0 as the water surface width corresponding to the reference condition.

Using the dimensionless quantities in Eq. (5.1), we get the following system:

$$\beta\frac{\partial h^*}{\partial t^*} + \frac{\partial Q^*}{\partial x^*} = X^*(x^*)T^*(t^*), \tag{5.5a}$$

$$\frac{\partial h^*}{\partial x^*} + r_1 Q^* + r_2 h^* = 0, \tag{5.5b}$$

with

$$X^*(x^*)T^*(t^*) = \frac{X(x)}{1/L}\frac{T(t)}{Q_0}. \tag{5.6}$$

The other parameters are

$$\beta = \frac{h_0}{Q_0} b_0 C_0,\ r_1 = L\left(\frac{\partial S_f}{\partial Q}\right)_{(Q_0,h_0)} \frac{Q_0}{h_0},\ r_2 = L\left(\frac{\partial S_f}{\partial h}\right)_{(Q_0,h_0)},$$

where β is the dimensionless water surface width.

We assume that there is no perturbation in the flow discharge and the flow depth before the application of any input, i.e., $Q^*(x^*,0) = 0$ and $h^*(x^*,0) = 0$. Then, applying Laplace transform on the system given by Eq. (5.5), we get

$$\frac{\mathrm{d}\overline{Q^*}}{\mathrm{d}x^*} + \beta s \overline{h^*} = X(x^*)\overline{T^*}(s), \tag{5.7a}$$

$$\frac{\mathrm{d}\overline{h^*}}{\mathrm{d}x^*} + r_1 \overline{Q^*} + r_2 \overline{h^*} = 0, \tag{5.7b}$$

where $\overline{Q^*}(x^*,s)$, $\overline{h^*}(x^*,s)$ and $\overline{T^*}(s)$ are the Laplace transforms of $Q^*(x^*,t^*)$, $h^*(x^*,t^*)$ and $T^*(t^*)$, respectively. This system can also be written in the following form:

$$\frac{\mathrm{d}\overline{U}(x^*,s)}{\mathrm{d}x^*} = M(s)\overline{U}(x^*,s) + R(x^*,s), \tag{5.8}$$

where

$$\overline{U}(x^*,s) = \begin{bmatrix} \overline{Q^*}(x^*,s) \\ \overline{h^*}(x^*,s) \end{bmatrix}, \qquad M(s) = \begin{bmatrix} 0 & -\beta s \\ -r_1 & -r_2 \end{bmatrix}, \qquad R(x^*,s) = \begin{bmatrix} X^*(x^*)\overline{T^*}(s) \\ 0 \end{bmatrix}. \tag{5.9}$$

The solution of Eq. (5.8) has the form (Cimorelli et al. [7])

$$\overline{U}(x^*,s) = \exp(M(s)x^*)\overline{U}(0,s) + \int_0^{x^*} \exp(M(s)(x^*-\phi))\, R(\phi,s)\mathrm{d}\phi, \tag{5.10}$$

where $\overline{U}(0,s) = \left(\overline{Q^*}(0,s)\ \overline{h^*}(0,s)\right)^T$ is the vector representing the upstream boundary condition. The entries α_{ij} of the matrix $\exp(M(s)x^*)$ can be written as

$$\alpha_{11}(x^*,s) = \exp\left(\frac{P_e x^*}{2}\right)\frac{\sqrt{Z}\cosh\left(\frac{x^*}{2}\sqrt{Z}\right) - P_e \sinh\left(\frac{x^*}{2}\sqrt{Z}\right)}{\sqrt{Z}}, \tag{5.11}$$

$$\alpha_{12}(x^*, s) = -2\beta s \exp\left(\frac{P_e x^*}{2}\right) \frac{\sinh\left(\frac{x^*}{2}\sqrt{Z}\right)}{\sqrt{Z}}, \tag{5.12}$$

$$\alpha_{21}(x^*, s) = -\frac{2P_e}{\beta} \exp\left(\frac{P_e x^*}{2}\right) \frac{\sinh\left(\frac{x^*}{2}\sqrt{Z}\right)}{\sqrt{Z}}, \tag{5.13}$$

$$\alpha_{22}(x^*, s) = \exp\left(\frac{P_e x^*}{2}\right) \frac{\sqrt{Z}\cosh\left(\frac{x^*}{2}\sqrt{Z}\right) + P_e \sinh\left(\frac{x^*}{2}\sqrt{Z}\right)}{\sqrt{Z}}, \tag{5.14}$$

with $Z = {P_e}^2 + 4P_e s$ where $P_e = C_0 L/D_0$ is the Péclet number; $D_0 = Q_0/(2b_0 S_0)$ is the linearized diffusivity coefficient. Cimorelli et al. [7, 6] presented the solution for the diffusive wave model by considering a uniformly distributed lateral inflow along the channel length and a stage-discharge relationship at the downstream end. We use the similar methodology to study the effect of space- and time-dependent lateral inflows.

In this work, two different types of upstream boundary condition are considered: a flow-discharge hydrograph or a flow-depth hydrograph. The downstream boundary is given by a rating curve or stage-discharge relationship, i.e., $Q(L, t) = F(h(L, t))$. Following Cimorelli et al. [7], after the linearization of the downstream boundary condition around the reference condition with $Q_0 = F(h_0)$, we get

$$Q_1(L, t) = \frac{\mathrm{d}F}{\mathrm{d}h}\bigg|_{h_0} h_1(L, t) \implies Q^*(1, t^*) = \frac{\beta}{a} h^*(1, t^*). \tag{5.15}$$

Here $a = \dfrac{b_0 C_0}{k}$ is known as the feedback parameter with $k = \dfrac{\mathrm{d}F}{\mathrm{d}h}\bigg|_{h_{0,L}}$. The feedback parameter now takes the form

$$a = \frac{\left.\frac{\mathrm{d}Q}{\mathrm{d}h}\right|_{h_0}}{\left.\frac{\mathrm{d}Q}{\mathrm{d}h}\right|_{h_{0,L}}}. \tag{5.16}$$

When the uniform steady condition is given at the downstream end, we get $a = 1$, but any deviation of a from 1 means that the downstream boundary moves away from the steady uniform flow condition. Application of the Laplace transform to Eq. (5.15) gives

$$\overline{Q^*}(1, s) = \frac{\beta}{a}\overline{h^*}(1, s). \tag{5.17}$$

5.1.1 Concentrated lateral inflow

In the first problem of this chapter, a concentrated lateral inflow is considered. For a concentrated lateral inflow at a point x_0 (with x_0^* as the dimensionless form), $X^*(x^*)$ can be represented by using the Dirac delta function. The integral of Eq. (5.10) can further be simplified, by using the Dirac delta function property provided in *Chapter 3, Section 3.1*, as

$$\int_0^{x^*} \exp(M(s)\,(x^* - \phi))\,R(\phi, s)\mathrm{d}\phi = \overline{T^*}(s)\int_0^{x^*} \begin{bmatrix} \alpha_{11}(x^* - \phi, s)\delta(\phi - x_0^*) \\ \alpha_{21}(x^* - \phi, s)\delta(\phi - x_0^*) \end{bmatrix} \mathrm{d}\phi$$

$$= \begin{cases} \overline{T^*}(s)\begin{bmatrix} \alpha_{11}(x^* - x_0^*, s) \\ \alpha_{21}(x^* - x_0^*, s) \end{bmatrix}, & \text{for } x^* > x_0^*, \\ 0, & \text{for } x^* < x_0^*. \end{cases} \tag{5.18}$$

Finally, using Eqs. (5.10) and (5.18), we get the following form of the vector $\overline{U}(x^*, s)$:

$$\overline{U}(x^*, s) = \begin{bmatrix} \alpha_{11}(x^*, s)\overline{Q^*}(0, s) + \alpha_{12}(x^*, s)\overline{h^*}(0, s) + \alpha_{11}(x^* - x_0^*, s)\overline{T^*}(s) \\ \alpha_{21}(x^*, s)\overline{Q^*}(0, s) + \alpha_{22}(x^*, s)\overline{h^*}(0, s) + \alpha_{21}(x^* - x_0^*, s)\overline{T^*}(s) \end{bmatrix}, \quad \text{for } x^* > x_0^*, \tag{5.19a}$$

$$\overline{U}(x^*, s) = \begin{bmatrix} \alpha_{11}(x^*, s)\overline{Q^*}(0, s) + \alpha_{12}(x^*, s)\overline{h^*}(0, s) \\ \alpha_{21}(x^*, s)\overline{Q^*}(0, s) + \alpha_{22}(x^*, s)\overline{h^*}(0, s) \end{bmatrix}, \quad \text{for } x^* < x_0^*, \tag{5.19b}$$

where Eq. (5.19a) represents the effect of the lateral inflow on the subsequent downstream locations while Eq. (5.19b) represents the effect on the locations upstream to the location of the concentrated lateral inflow.

5.1.2 Uniformly distributed lateral inflow

For the second problem in this chapter, a lateral inflow is considered to be uniformly distributed between two locations x_1 and x_2. Here, we write

$$X^*(x^*) = \frac{\mathrm{u}(x^* - x_1^*) - \mathrm{u}(x^* - x_2^*)}{x_2^* - x_1^*} = \begin{cases} \dfrac{1}{x_2^* - x_1^*} & \text{for } x^* \in [x_1^*, x_2^*], \\ 0 & \text{for } x^* \notin [x_1^*, x_2^*], \end{cases} \tag{5.20}$$

where u(.) is the unit-step function, x_1^* and x_2^* are the non-dimensional forms of x_1 and x_2, respectively, with $x_2^* - x_1^* \neq 0$. This definition is the same as the one used in *Chapter 3*. Using Eq. (5.20), the integral in Eq. (5.10) can be simplified as

$$\int_0^{x^*} \exp(M(s)\,(x^* - \phi))\,R(\phi, s)\mathrm{d}\phi = \begin{cases} 0, & \text{for } x^* < x_1^*, \\ \overline{T^*}(s)\begin{pmatrix} A_{11}(x^*, s) \\ A_{21}(x^*, s) \end{pmatrix} & \text{for } x^* \geq x_1^*, \end{cases} \tag{5.21}$$

Using this in the system given in Eq.(5.10), we get

$$\overline{U}(x^*,s) = \begin{bmatrix} \alpha_{11}(x^*,s)\overline{Q^*}(0,s) + \alpha_{12}(x^*,s)\overline{h^*}(0,s) + A_{11}(x^*,s)\overline{T^*}(s) \\ \alpha_{21}(x^*,s)\overline{Q^*}(0,s) + \alpha_{22}(x^*,s)\overline{h^*}(0,s) + A_{21}(x^*,s)\overline{T^*}(s) \end{bmatrix}, \quad \text{for } x^* \geq x_1^*, \tag{5.22a}$$

$$\overline{U}(x^*,s) = \begin{bmatrix} \alpha_{11}(x^*,s)\overline{Q^*}(0,s) + \alpha_{12}(x^*,s)\overline{h^*}(0,s) \\ \alpha_{21}(x^*,s)\overline{Q^*}(0,s) + \alpha_{22}(x^*,s)\overline{h^*}(0,s) \end{bmatrix}, \quad \text{for } x^* < x_1^*, \tag{5.22b}$$

where

$$\begin{aligned} A_{11}(x^*,s) = &\frac{1}{s(x_2^*-x_1^*)}\exp\left(\frac{x^*-x_1^*}{2}P_e\right)\left\{\frac{P_e+2s}{\sqrt{Z}}\sinh\left(\frac{x^*-x_1^*}{2}\sqrt{Z}\right)\right. \\ &\left.-\cosh\left(\frac{x^*-x_1^*}{2}\sqrt{Z}\right)\right\} + \frac{1}{s(x_2^*-x_1^*)}, \quad \text{for } x_1^* \leq x^* < x_2^*, \end{aligned} \tag{5.23a}$$

$$\begin{aligned} A_{11}(x^*,s) = &\frac{1}{s(x_2^*-x_1^*)}\exp\left(\frac{x^*-x_2^*}{2}P_e\right)\left\{\cosh\left(\frac{x^*-x_2^*}{2}\sqrt{Z}\right)\right. \\ &\left.-\frac{P_e+2s}{\sqrt{Z}}\sinh\left(\frac{x^*-x_2^*}{2}\sqrt{Z}\right)\right\} \\ &+\frac{1}{s(x_2^*-x_1^*)}\exp\left(\frac{x^*-x_1^*}{2}P_e\right)\left\{\frac{P_e+2s}{\sqrt{Z}}\sinh\left(\frac{x^*-x_1^*}{2}\sqrt{Z}\right)\right. \\ &\left.-\cosh\left(\frac{x^*-x_1^*}{2}\sqrt{Z}\right)\right\}, \quad \text{for } x_2^* \leq x^* \leq 1, \end{aligned} \tag{5.23b}$$

$$\begin{aligned} A_{21}(x^*,s) = &\frac{1}{\beta s(x_2^*-x_1^*)}\exp\left(\frac{x^*-x_1^*}{2}P_e\right)\left\{\frac{P_e}{\sqrt{Z}}\sinh\left(\frac{x^*-x_1^*}{2}\sqrt{Z}\right)\right. \\ &\left.-\cosh\left(\frac{x^*-x_1^*}{2}\sqrt{Z}\right)\right\} + \frac{1}{\beta s(x_2^*-x_1^*)}, \quad \text{for } x_1^* \leq x^* < x_2^*, \end{aligned} \tag{5.24a}$$

$$\begin{aligned} A_{21}(x^*,s) = &\frac{1}{\beta s(x_2^*-x_1^*)}\exp\left(\frac{x^*-x_2^*}{2}P_e\right)\left\{\cosh\left(\frac{x^*-x_2^*}{2}\sqrt{Z}\right)\right. \\ &\left.-\frac{P_e}{\sqrt{Z}}\sinh\left(\frac{x^*-x_2^*}{2}\sqrt{Z}\right)\right\} \\ &+\frac{1}{\beta s(x_2^*-x_1^*)}\exp\left(\frac{x^*-x_1^*}{2}P_e\right)\left\{\frac{P_e}{\sqrt{Z}}\sinh\left(\frac{x^*-x_1^*}{2}\sqrt{Z}\right)\right. \\ &\left.-\cosh\left(\frac{x^*-x_1^*}{2}\sqrt{Z}\right)\right\}, \quad \text{for } x_2^* \leq x^* \leq 1. \end{aligned} \tag{5.24b}$$

Here, Eq. (5.22a) represents the effect of the lateral inflow on the locations downstream to x_1^* while Eq. (5.22b) represents the effect on the locations upstream to x_1^*. The expressions of $A_{11}(x^*, s)$ and $A_{21}(x^*, s)$ are the same as the ones obtained in *Chapters 3*.

5.2 Analytical solutions for two types of upstream boundaries

We discuss the solutions with respect to two types of lateral inflow in the form of a concentrated one and a uniformly distributed one subject to two types of upstream boundaries as detailed below.

5.2.1 Flow-discharge hydrograph imposed at the upstream end

First, the case of concentrated lateral inflow is discussed. The upstream boundary is considered as $Q^*(0, t^*)$. Taking this into account, we evaluate the system in Eq. (5.19a) at $x^* = 1$ as

$$\overline{Q^*}(1, s) = \alpha_{11}(1, s)\overline{Q^*}(0, s) + \alpha_{12}(1, s)\overline{h^*}(0, s) + \alpha_{11}(1 - x_0^*, s)\overline{T^*}(s), \quad (5.25a)$$

$$\overline{h^*}(1, s) = \alpha_{21}(1, s)\overline{Q^*}(0, s) + \alpha_{22}(1, s)\overline{h^*}(0, s) + \alpha_{21}(1 - x_0^*, s)\overline{T^*}(s). \quad (5.25b)$$

Now using Eqs. (5.17) and (5.25), we get $\overline{h^*}(0, s)$ as

$$\overline{h^*}(0, s) = -\frac{\alpha_{11}(1, s) - \dfrac{\beta}{a}\alpha_{21}(1, s)}{\alpha_{12}(1, s) - \dfrac{\beta}{a}\alpha_{22}(1, s)}\overline{Q^*}(0, s) - \frac{\alpha_{11}(1 - x_0^*, s) - \dfrac{\beta}{a}\alpha_{21}(1 - x_0^*, s)}{\alpha_{12}(1, s) - \dfrac{\beta}{a}\alpha_{22}(1, s)}\overline{T^*}(s). \quad (5.26)$$

Using this, the system given in Eq. (5.19) is obtained as

$$\overline{Q^*}(x^*, s) = \overline{R}_{u,a}(x^*, s)\overline{Q^*}(0, s) + \overline{R}_{l,a}(x^*, s)\overline{T^*}(s), \quad (5.27a)$$

$$\overline{h^*}(x^*, s) = \overline{S}_{u,a}(x^*, s)\overline{Q^*}(0, s) + \overline{S}_{l,a}(x^*, s)\overline{T^*}(s). \quad (5.27b)$$

The Laplace inverses of $\overline{R}_{u,a}(x^*, s)$ and $\overline{S}_{u,a}(x^*, s)$ are already provided by Cimorelli et al. [7]. We try to find the inverse for the other two new terms. We can write them as

$$\begin{aligned}\overline{R}_{l,a}(x^*, s) =& \Bigg\{\sqrt{Z}\left(P_e \sinh\left(\frac{1 + x_0^* - x^*}{2}\sqrt{Z}\right) + \sqrt{Z}\cosh\left(\frac{1 + x_0^* - x^*}{2}\sqrt{Z}\right)\right) \\ &+ 2s\sinh\left(\frac{1 - x^*}{2}\sqrt{Z}\right)\left(a\sqrt{Z}\cosh\left(\frac{x_0^*\sqrt{Z}}{2}\right) + P_e(a - 2)\sinh\left(\frac{x_0^*\sqrt{Z}}{2}\right)\right)\Bigg\}\end{aligned}$$

$$\times \frac{\exp\left(\dfrac{x^* - x_{0}^*}{2} P_e\right)}{\sqrt{Z}\left(\sqrt{Z}\cosh\left(\dfrac{\sqrt{Z}}{2}\right) + (P_e + 2as)\sinh\left(\dfrac{\sqrt{Z}}{2}\right)\right)}, \quad \text{for } x^* > x_{0}^*, \tag{5.28a}$$

$$\overline{R}_{l,a}(x^*, s) = -2s\exp\left(\frac{x^* - x_{0}^*}{2} P_e\right)\frac{\sinh\left(\dfrac{x^*\sqrt{Z}}{2}\right)}{\sqrt{Z}}$$
$$\times \frac{a\sqrt{Z}\cosh\left(\dfrac{1 - x_{0}^*}{2}\sqrt{Z}\right) + P_e(2-a)\sinh\left(\dfrac{1 - x_{0}^*}{2}\sqrt{Z}\right)}{\sqrt{Z}\cosh\left(\dfrac{\sqrt{Z}}{2}\right) + (P_e + 2as)\sinh\left(\dfrac{\sqrt{Z}}{2}\right)}, \quad \text{for } x^* < x_{0}^*, \tag{5.28b}$$

$$\overline{S}_{l,a}(x^*, s) = \frac{\exp\left(\dfrac{x^* - x_{0}^*}{2} P_e\right)}{\beta\sqrt{Z}\left(\sqrt{Z}\cosh\left(\dfrac{\sqrt{Z}}{2}\right) + (P_e + 2as)\sinh\left(\dfrac{\sqrt{Z}}{2}\right)\right)}$$
$$\times \left\{a\sqrt{Z}\left(\sqrt{Z}\cosh\left(\frac{1 - x_{0}^* - x^*}{2}\sqrt{Z}\right) - P_e\sinh\left(\frac{1 - x_{0}^* - x^*}{2}\sqrt{Z}\right)\right)\right.$$
$$\left. + 2P_e\sinh\left(\frac{1 - x^*}{2}\sqrt{Z}\right)\left(\sqrt{Z}\cosh\left(\frac{x_{0}^*\sqrt{Z}}{2}\right) + (P_e + 2as)\sinh\left(\frac{x_{0}^*\sqrt{Z}}{2}\right)\right)\right\},$$
$$\text{for } x^* > x_{0}^*, \tag{5.29a}$$

$$\overline{S}_{l,a}(x^*, s) = \exp\left(\frac{x^* - x_{0}^*}{2} P_e\right)\frac{\sqrt{Z}\cosh\left(\dfrac{x^*\sqrt{Z}}{2}\right) + P_e\sinh\left(\dfrac{x^*\sqrt{Z}}{2}\right)}{\beta\sqrt{Z}}$$
$$\times \frac{a\sqrt{Z}\cosh\left(\dfrac{1 - x_{0}^*}{2}\sqrt{Z}\right) + P_e(2-a)\sinh\left(\dfrac{1 - x_{0}^*}{2}\sqrt{Z}\right)}{\sqrt{Z}\cosh\left(\dfrac{\sqrt{Z}}{2}\right) + (P_e + 2as)\sinh\left(\dfrac{\sqrt{Z}}{2}\right)}, \quad \text{for } x^* < x_{0}^*. \tag{5.29b}$$

Similarly, for the case of a uniformly distributed lateral inflow between x_{1}^* and x_{2}^*, the system given in Eq. (5.22a) is evaluated at $x^* = 1$ as

$$\overline{Q^*}(1, s) = \alpha_{11}(1, s)\overline{Q^*}(0, s) + \alpha_{12}(1, s)\overline{h^*}(0, s) + A_{11}(1, s)\overline{T^*}(s), \tag{5.30a}$$
$$\overline{h^*}(1, s) = \alpha_{21}(1, s)\overline{Q^*}(0, s) + \alpha_{22}(1, s)\overline{h^*}(0, s) + A_{21}(1, s)\overline{T^*}(s). \tag{5.30b}$$

Now using Eqs. (5.17) and (5.30), we get $\overline{h^*}(0,s)$ as

$$\overline{h^*}(0,s) = -\frac{\alpha_{11}(1,s) - \dfrac{\beta}{a}\alpha_{21}(1,s)}{\alpha_{12}(1,s) - \dfrac{\beta}{a}\alpha_{22}(1,s)}\overline{Q^*}(0,s) - \frac{A_{11}(1,s) - \dfrac{\beta}{a}A_{21}(1,s)}{\alpha_{12}(1,s) - \dfrac{\beta}{a}\alpha_{22}(1,s)}\overline{T^*}(s). \tag{5.31}$$

Using this, the system given in Eq. (5.22) is obtained as

$$\overline{Q^*}(x^*,s) = \overline{R}_{u,a}(x^*,s)\overline{Q^*}(0,s) + \overline{R}_{ld,a}(x^*,s)\overline{T^*}(s), \tag{5.32a}$$
$$\overline{h^*}(x^*,s) = \overline{S}_{u,a}(x^*,s)\overline{Q^*}(0,s) + \overline{S}_{ld,a}(x^*,s)\overline{T^*}(s). \tag{5.32b}$$

The functions $\overline{R}_{u,a}$ and $\overline{S}_{u,a}$ are the same as the ones obtained in Eq. (5.27). The functions $\overline{R}_{ld,a}$ and $\overline{S}_{ld,a}$ have the following forms:

$$\overline{R}_{ld,a}(x^*,s) = -\alpha_{12}(x^*,s)\frac{A_{11}(1,s) - \beta a^{-1}A_{21}(1,s)}{\alpha_{12}(1,s) - \beta a^{-1}\alpha_{22}(1,s)}, \quad \text{for } x^* < x_1^*, \tag{5.33a}$$
$$\overline{R}_{ld,a}(x^*,s) = -\alpha_{12}(x^*,s)\frac{A_{11}(1,s) - \beta a^{-1}A_{21}(1,s)}{\alpha_{12}(1,s) - \beta a^{-1}\alpha_{22}(1,s)} + A_{11}(x^*,s), \quad \text{for } x^* \geq x_1^*, \tag{5.33b}$$

$$\overline{S}_{ld,a}(x^*,s) = -\alpha_{22}(x^*,s)\frac{A_{11}(1,s) - \beta a^{-1}A_{21}(1,s)}{\alpha_{12}(1,s) - \beta a^{-1}\alpha_{22}(1,s)}, \quad \text{for } x^* < x_1^*, \tag{5.34a}$$
$$\overline{S}_{ld,a}(x^*,s) = -\alpha_{22}(x^*,s)\frac{A_{11}(1,s) - \beta a^{-1}A_{21}(1,s)}{\alpha_{12}(1,s) - \beta a^{-1}\alpha_{22}(1,s)} + A_{21}(x^*,s), \quad \text{for } x^* \geq x_1^*, \tag{5.34b}$$

where

$$\begin{aligned}\overline{R}_{ld,a}(x^*,s) = {} & \frac{2\sinh\left(\dfrac{x^*\sqrt{Z}}{2}\right)}{\sqrt{Z}(x_2^* - x_1^*)\left(\sqrt{Z}\cosh\left(\dfrac{\sqrt{Z}}{2}\right) + (P_e + 2as)\sinh\left(\dfrac{\sqrt{Z}}{2}\right)\right)} \\ & \times \left\{\exp\left(\frac{x^* - x_2^*}{2}P_e\right)\left((P_e(a-1) + 2as)\sinh\left(\frac{1-x_2^*}{2}\sqrt{Z}\right)\right.\right. \\ & \left. - (a-1)\sqrt{Z}\cosh\left(\frac{1-x_2^*}{2}\sqrt{Z}\right)\right) \\ & - \exp\left(\frac{x^* - x_1^*}{2}P_e\right)\left((P_e(a-1) + 2as)\sinh\left(\frac{1-x_1^*}{2}\sqrt{Z}\right)\right. \\ & \left.\left. - (a-1)\sqrt{Z}\cosh\left(\frac{1-x_1^*}{2}\sqrt{Z}\right)\right)\right\}, \quad \text{for } 0 \leq x^* < x_1^*, \end{aligned} \tag{5.35a}$$

$$\begin{aligned}
\overline{R}_{ld,a}(x^*,s) ={}& \frac{1}{s(x_2^*-x_1^*)} + \frac{2}{x_2^*-x_1^*}\exp\left(\frac{x^*-x_2^*}{2}P_e\right)\frac{\sinh\left(\frac{x^*\sqrt{Z}}{2}\right)}{\sqrt{Z}} \\
&\times \frac{(P_e(a-1)+2as)\sinh\left(\frac{1-x_2^*}{2}\sqrt{Z}\right)+(1-a)\sqrt{Z}\cosh\left(\frac{1-x_2^*}{2}\sqrt{Z}\right)}{\sqrt{Z}\cosh\left(\frac{\sqrt{Z}}{2}\right)+(P_e+2as)\sinh\left(\frac{\sqrt{Z}}{2}\right)} \\
&+ \frac{1}{s(x_2^*-x_1^*)}\exp\left(\frac{x^*-x_1^*}{2}P_e\right)\frac{\sqrt{Z}\cosh\left(\frac{x_1^*}{2}\sqrt{Z}\right)+(P_e+2s)\sinh\left(\frac{x_1^*}{2}\sqrt{Z}\right)}{\sqrt{Z}\cosh\left(\frac{\sqrt{Z}}{2}\right)+(P_e+2as)\sinh\left(\frac{\sqrt{Z}}{2}\right)} \\
&\times \frac{(P_e+2as)\sinh\left(\frac{x^*-1}{2}\sqrt{Z}\right)-\sqrt{Z}\cosh\left(\frac{x^*-1}{2}\sqrt{Z}\right)}{\sqrt{Z}}, \qquad \text{for } x_1^*\le x^*<x_2^*,
\end{aligned} \tag{5.35b}$$

$$\begin{aligned}
\overline{R}_{ld,a}(x^*,s) ={}& \frac{(P_e+2as)\sinh\left(\frac{x^*-1}{2}\sqrt{Z}\right)-\sqrt{Z}\cosh\left(\frac{x^*-1}{2}\sqrt{Z}\right)}{s\sqrt{Z}(x_2^*-x_1^*)\left(\sqrt{Z}\cosh\left(\frac{\sqrt{Z}}{2}\right)+(P_e+2as)\sinh\left(\frac{\sqrt{Z}}{2}\right)\right)} \\
&\times \left\{\exp\left(\frac{x^*-x_1^*}{2}P_e\right)\left(\sqrt{Z}\cosh\left(\frac{x_1^*}{2}\sqrt{Z}\right)+(P_e+2s)\sinh\left(\frac{x_1^*}{2}\sqrt{Z}\right)\right)\right. \\
&\left. -\exp\left(\frac{x^*-x_2^*}{2}P_e\right)\left(\sqrt{Z}\cosh\left(\frac{x_2^*}{2}\sqrt{Z}\right)+(P_e+2s)\sinh\left(\frac{x_2^*}{2}\sqrt{Z}\right)\right)\right\}, \\
&\text{for } x_2^*\le x^*\le 1,
\end{aligned} \tag{5.35c}$$

and

$$\begin{aligned}
\overline{S}_{ld,a}(x^*,s) ={}& -\frac{\sqrt{Z}\cosh\left(\frac{x^*\sqrt{Z}}{2}\right)+P_e\sinh\left(\frac{x^*\sqrt{Z}}{2}\right)}{\beta s\sqrt{Z}(x_2^*-x_1^*)\left(\sqrt{Z}\cosh\left(\frac{\sqrt{Z}}{2}\right)+(P_e+2as)\sinh\left(\frac{\sqrt{Z}}{2}\right)\right)} \\
&\times \left\{\exp\left(\frac{x^*-x_2^*}{2}P_e\right)\left((P_e(a-1)+2as)\sinh\left(\frac{1-x_2^*}{2}\sqrt{Z}\right)\right.\right. \\
&\left. -(a-1)\sqrt{Z}\cosh\left(\frac{1-x_2^*}{2}\sqrt{Z}\right)\right) \\
&-\exp\left(\frac{x^*-x_1^*}{2}P_e\right)\left((P_e(a-1)+2as)\sinh\left(\frac{1-x_1^*}{2}\sqrt{Z}\right)\right.
\end{aligned}$$

$$-(a-1)\sqrt{Z}\cosh\left(\frac{1-x_1^*}{2}\sqrt{Z}\right)\Bigg)\Bigg\},\quad \text{for } 0 \le x^* < x_1^*, \tag{5.36a}$$

$$\overline{S}_{ld,a}(x^*,s) = \frac{1}{\beta s(x_2^*-x_1^*)} - \exp\left(\frac{x^*-x_2^*}{2}P_e\right)\frac{\sqrt{Z}\cosh\left(\frac{x^*\sqrt{Z}}{2}\right)+P_e\sinh\left(\frac{x^*\sqrt{Z}}{2}\right)}{\beta s\sqrt{Z}(x_2^*-x_1^*)}$$
$$\times\frac{(P_e(a-1)+2as)\sinh\left(\frac{1-x_2^*}{2}\sqrt{Z}\right)+(1-a)\sqrt{Z}\cosh\left(\frac{1-x_2^*}{2}\sqrt{Z}\right)}{\sqrt{Z}\cosh\left(\frac{\sqrt{Z}}{2}\right)+(P_e+2as)\sinh\left(\frac{\sqrt{Z}}{2}\right)}$$
$$+\frac{1}{\beta s(x_2^*-x_1^*)}\exp\left(\frac{x^*-x_1^*}{2}P_e\right)\frac{\sqrt{Z}\cosh\left(\frac{x_1^*}{2}\sqrt{Z}\right)+(P_e+2s)\sinh\left(\frac{x_1^*}{2}\sqrt{Z}\right)}{\sqrt{Z}\cosh\left(\frac{\sqrt{Z}}{2}\right)+(P_e+2as)\sinh\left(\frac{\sqrt{Z}}{2}\right)}$$
$$\times\frac{P_e(2-a)\sinh\left(\frac{x^*-1}{2}\sqrt{Z}\right)-a\sqrt{Z}\cosh\left(\frac{x^*-1}{2}\sqrt{Z}\right)}{\sqrt{Z}},\quad \text{for } x_1^* \le x^* < x_2^*, \tag{5.36b}$$

$$\overline{S}_{ld,a}(x^*,s) = \frac{P_e(2-a)\sinh\left(\frac{x^*-1}{2}\sqrt{Z}\right)-a\sqrt{Z}\cosh\left(\frac{x^*-1}{2}\sqrt{Z}\right)}{\beta s\sqrt{Z}(x_2^*-x_1^*)\left(\sqrt{Z}\cosh\left(\frac{\sqrt{Z}}{2}\right)+(P_e+2as)\sinh\left(\frac{\sqrt{Z}}{2}\right)\right)}$$
$$\times\Bigg\{\exp\left(\frac{x^*-x_1^*}{2}P_e\right)\left(\sqrt{Z}\cosh\left(\frac{x_1^*}{2}\sqrt{Z}\right)+(P_e+2s)\sinh\left(\frac{x_1^*}{2}\sqrt{Z}\right)\right)$$
$$-\exp\left(\frac{x^*-x_2^*}{2}P_e\right)\left(\sqrt{Z}\cosh\left(\frac{x_2^*}{2}\sqrt{Z}\right)+(P_e+2s)\sinh\left(\frac{x_2^*}{2}\sqrt{Z}\right)\right)\Bigg\},$$
$$\text{for } x_2^* \le x^* \le 1. \tag{5.36c}$$

For $x_1^* = 0$ and $x_2^* = 1$, these expressions will be the same as the one obtained by Cimorelli et al. [7].

The inverse of the system given by Eq. (5.27) can be written as

$$Q^*(x^*,t^*) = R_{u,a}(x^*,t^*) \circledast Q^*(0,t^*) + R_{l,a}(x^*,t^*) \circledast T^*(t^*), \tag{5.37a}$$
$$h^*(x^*,t^*) = S_{u,a}(x^*,t^*) \circledast Q^*(0,t^*) + S_{l,a}(x^*,t^*) \circledast T^*(t^*), \tag{5.37b}$$

while the inverse of the system given by Eq. (5.32) can be written as

$$Q^*(x^*,t^*) = R_{u,a}(x^*,t^*) \circledast Q^*(0,t^*) + R_{ld,a}(x^*,t^*) \circledast T^*(t^*), \tag{5.38a}$$

$$h^*(x^*,t^*) = S_{u,a}(x^*,t^*) \circledast Q^*(0,t^*) + S_{ld,a}(x^*,t^*) \circledast T^*(t^*), \tag{5.38b}$$

with

$$R_{l,a}(x^*,t^*) = \sum_{k=0}^{\infty} \left(p_{1,k}(x^*) + p_{2,k}(x^*)\right) \exp\left(-s_k t^*\right), \tag{5.39}$$

$$S_{l,a}(x^*,t^*) = \sum_{k=0}^{\infty} \left(q_{1,k}(x^*) + q_{2,k}(x^*)\right) \exp\left(-s_k t^*\right), \tag{5.40}$$

$$R_{ld,a}(x^*,t^*) = \sum_{k=0}^{\infty} p_{3,k}(x^*) \exp\left(-s_k t^*\right), \tag{5.41}$$

$$S_{ld,a}(x^*,t^*) = \sum_{k=0}^{\infty} q_{3,k}(x^*) \exp\left(-s_k t^*\right), \tag{5.42}$$

where s_k is the k-th pole for the corresponding functions in the Laplace domain. The pole finding process is elaborated in Appendix B.1. Here $\circledast$ is the convolution operator. The coefficients in Eqs. (5.39)–(5.42) are obtained in the following forms:

$$p_{1,k}(x^*) = -\frac{\exp\left(\dfrac{x^*-x_0^*}{2}P_e\right)}{\sqrt{Z_k}\cos\left(\dfrac{\sqrt{Z_k}}{2}\right)\left(\dfrac{2+P_e-2as_k}{4s_k-P_e} + \dfrac{P_e+2a}{P_e-2as_k}\right)}$$
$$\times\left(P_e\sin\left(\frac{1+x_0^*-x^*}{2}\sqrt{Z_k}\right) + \sqrt{Z_k}\cos\left(\frac{1+x_0^*-x^*}{2}\sqrt{Z_k}\right)\right), \quad \text{for } x^* > x_0^*, \tag{5.43a}$$

$$p_{1,k}(x^*) = 0, \qquad \text{for } x^* < x_0^*, \tag{5.43b}$$

$$p_{2,k}(x^*) = \frac{2s_k\exp\left(\dfrac{x^*-x_0^*}{2}P_e\right)\sin\left(\dfrac{1-x^*}{2}\sqrt{Z_k}\right)}{P_e\cos\left(\dfrac{\sqrt{Z_k}}{2}\right)\left(2+P_e-2as_k + \dfrac{(P_e+2a)(4s_k-P_e)}{P_e-2as_k}\right)}$$
$$\times\left(a\sqrt{Z_k}\cos\left(\frac{x_0^*\sqrt{Z_k}}{2}\right) + P_e(a-2)\sin\left(\frac{x_0^*\sqrt{Z_k}}{2}\right)\right), \quad \text{for } x^* > x_0^*, \tag{5.44a}$$

$$p_{2,k}(x^*) = \frac{-2s_k\exp\left(\dfrac{x^*-x_0^*}{2}P_e\right)\sin\left(\dfrac{x^*}{2}\sqrt{Z_k}\right)}{P_e\cos\left(\dfrac{\sqrt{Z_k}}{2}\right)\left(2+P_e-2as_k + \dfrac{(P_e+2a)(4s_k-P_e)}{P_e-2as_k}\right)}$$

$$\times\left(a\sqrt{Z_k}\cos\left(\frac{1-x_0^*}{2}\sqrt{Z_k}\right)+P_e(2-a)\sin\left(\frac{1-x_0^*}{2}\sqrt{Z_k}\right)\right),\quad \text{for } x^*<x_0^*, \tag{5.44b}$$

$$q_{1,k}(x^*)=-\frac{a\exp\left(\frac{x^*-x_0^*}{2}P_e\right)}{\beta\sqrt{Z_k}\cos\left(\frac{\sqrt{Z_k}}{2}\right)\left(\frac{2+P_e-2as_k}{4s_k-P_e}+\frac{P_e+2a}{P_e-2as_k}\right)}$$
$$\times\left(P_e\sin\left(\frac{x_0^*+x^*-1}{2}\sqrt{Z_k}\right)+\sqrt{Z_k}\cos\left(\frac{x_0^*+x^*-1}{2}\sqrt{Z_k}\right)\right),\quad \text{for } x^*>x_0^*, \tag{5.45a}$$

$$q_{1,k}(x^*)=0,\qquad \text{for } x^*<x_0^*, \tag{5.45b}$$

$$q_{2,k}(x^*)=-\frac{2\exp\left(\frac{x^*-x_0^*}{2}P_e\right)\sin\left(\frac{1-x^*}{2}\sqrt{Z_k}\right)}{\beta\cos\left(\frac{\sqrt{Z_k}}{2}\right)\left(2+P_e-2as_k+\frac{(P_e+2a)(4s_k-P_e)}{P_e-2as_k}\right)}$$
$$\times\left(\sqrt{Z_k}\cos\left(\frac{x_0^*\sqrt{Z_k}}{2}\right)+(P_e-2as_k)\sin\left(\frac{x_0^*\sqrt{Z_k}}{2}\right)\right),\quad \text{for } x^*>x_0^*, \tag{5.46a}$$
$$q_{2,k}(x^*)=-\exp\left(\frac{x^*-x_0^*}{2}P_e\right)\left(\sqrt{Z_k}\cos\left(\frac{1-x^*}{2}\sqrt{Z_k}\right)+P_e\sin\left(\frac{1-x^*}{2}\sqrt{Z_k}\right)\right)$$
$$\times\frac{a\sqrt{Z_k}\cos\left(\frac{1-x_0^*}{2}\sqrt{Z_k}\right)+P_e(2-a)\sin\left(\frac{1-x_0^*}{2}\sqrt{Z_k}\right)}{\beta P_e\cos\left(\frac{\sqrt{Z_k}}{2}\right)\left(2+P_e-2as_k+\frac{(P_e+2a)(4s_k-P_e)}{P_e-2as_k}\right)},\quad \text{for } x^*<x_0^*, \tag{5.46b}$$

$$p_{3,k}(x^*)=-\frac{2}{P_e}\frac{\sin\left(\frac{x^*\sqrt{Z_k}}{2}\right)}{(x_2^*-x_1^*)\cos\left(\frac{\sqrt{Z_k}}{2}\right)\left(2+P_e-2as_k+\frac{(P_e+2a)(4s_k-P_e)}{P_e-2as_k}\right)}$$
$$\times\left\{\exp\left(\frac{x^*-x_2^*}{2}P_e\right)\left((P_e(a-1)-2as_k)\sin\left(\frac{1-x_2^*}{2}\sqrt{Z_k}\right)\right.\right.$$
$$\left.-(a-1)\sqrt{Z_k}\cos\left(\frac{1-x_2^*}{2}\sqrt{Z_k}\right)\right)$$

$$- \exp\left(\frac{x^* - x_1^*}{2} P_e\right)\left((P_e(a-1) - 2as_k)\sin\left(\frac{1-x_1^*}{2}\sqrt{Z_k}\right)\right.$$

$$\left.\left. - (a-1)\sqrt{Z_k}\cos\left(\frac{1-x_1^*}{2}\sqrt{Z_k}\right)\right)\right\}, \qquad \text{for } 0 \le x^* < x_1^*, \tag{5.47a}$$

$$p_{3,k}(x^*) = -\frac{2}{P_e(x_2^* - x_1^*)}\exp\left(\frac{x^* - x_2^*}{2}P_e\right)\sin\left(\frac{x^*\sqrt{Z_k}}{2}\right)$$

$$\times \frac{(P_e(a-1) - 2as_k)\sin\left(\frac{1-x_2^*}{2}\sqrt{Z_k}\right) + (1-a)\sqrt{Z_k}\cos\left(\frac{1-x_2^*}{2}\sqrt{Z_k}\right)}{\cos\left(\frac{\sqrt{Z_k}}{2}\right)\left(2 + P_e - 2as_k + \frac{(P_e+2a)(4s_k - P_e)}{P_e - 2as_k}\right)}$$

$$+ \exp\left(\frac{x^* - x_1^*}{2}P_e\right)\frac{\sqrt{Z_k}\cos\left(\frac{x_1^*}{2}\sqrt{Z_k}\right) + (P_e - 2s_k)\sin\left(\frac{x_1^*}{2}\sqrt{Z_k}\right)}{P_e s_k (x_2^* - x_1^*)}$$

$$\times \frac{(P_e - 2as_k)\sin\left(\frac{x^*-1}{2}\sqrt{Z_k}\right) - \sqrt{Z_k}\cos\left(\frac{x^*-1}{2}\sqrt{Z_k}\right)}{\cos\left(\frac{\sqrt{Z_k}}{2}\right)\left(2 + P_e - 2as_k + \frac{(P_e+2a)(4s_k - P_e)}{P_e - 2as_k}\right)}, \text{ for } x_1^* \le x^* < x_2^*, \tag{5.47b}$$

$$p_{3,k}(x^*) = \frac{(P_e - 2as_k)\sin\left(\frac{x^*-1}{2}\sqrt{Z_k}\right) - \sqrt{Z_k}\cos\left(\frac{x^*-1}{2}\sqrt{Z_k}\right)}{P_e s_k (x_2^* - x_1^*)\cos\left(\frac{\sqrt{Z_k}}{2}\right)\left(2 + P_e - 2as_k + \frac{(P_e+2a)(4s_k - P_e)}{P_e - 2as_k}\right)}$$

$$\times \left\{\exp\left(\frac{x^* - x_1^*}{2}P_e\right)\left(\sqrt{Z_k}\cos\left(\frac{x_1^*}{2}\sqrt{Z_k}\right) + (P_e - 2s_k)\sin\left(\frac{x_1^*}{2}\sqrt{Z_k}\right)\right)\right.$$

$$\left. - \exp\left(\frac{x^* - x_2^*}{2}P_e\right)\left(\sqrt{Z_k}\cos\left(\frac{x_2^*}{2}\sqrt{Z_k}\right) + (P_e - 2s_k)\sin\left(\frac{x_2^*}{2}\sqrt{Z_k}\right)\right)\right\},$$

$$\text{for } x_2^* \le x^* \le 1, \tag{5.47c}$$

$$q_{3,k}(x^*) = -\frac{\sqrt{Z_k}\cos\left(\frac{x^*\sqrt{Z_k}}{2}\right) + P_e\sin\left(\frac{x^*\sqrt{Z_k}}{2}\right)}{\beta P_e s_k (x_2^* - x_1^*)\cos\left(\frac{\sqrt{Z_k}}{2}\right)\left(2 + P_e - 2as_k + \frac{(P_e+2a)(4s_k - P_e)}{P_e - 2as_k}\right)}$$

$$\times \left\{\exp\left(\frac{x^* - x_2^*}{2}P_e\right)\left((P_e(a-1) - 2as_k)\sin\left(\frac{1-x_2^*}{2}\sqrt{Z_k}\right)\right.\right.$$

$$- (a-1)\sqrt{Z_k}\cos\left(\frac{1-x_2^*}{2}\sqrt{Z_k}\right)\Bigg)$$

$$- \exp\left(\frac{x^*-x_1^*}{2}P_e\right)\Bigg((P_e(a-1)-2as_k)\sin\left(\frac{1-x_1^*}{2}\sqrt{Z_k}\right)$$

$$- (a-1)\sqrt{Z_k}\cos\left(\frac{1-x_1^*}{2}\sqrt{Z_k}\right)\Bigg)\Bigg\}, \qquad \text{for } 0 \le x^* < x_1^*, \quad (5.48a)$$

$$q_{3,k}(x^*) = -\exp\left(\frac{x^*-x_2^*}{2}P_e\right)\frac{\sqrt{Z_k}\cos\left(\frac{x^*\sqrt{Z_k}}{2}\right)+P_e\sin\left(\frac{x^*\sqrt{Z_k}}{2}\right)}{\beta P_e s_k(x_2^*-x_1^*)}$$
$$\times\frac{(P_e(a-1)-2as_k)\sin\left(\frac{1-x_2^*}{2}\sqrt{Z_k}\right)+(1-a)\sqrt{Z_k}\cos\left(\frac{1-x_2^*}{2}\sqrt{Z_k}\right)}{\cos\left(\frac{\sqrt{Z_k}}{2}\right)\left(2+P_e-2as_k+\frac{(P_e+2a)(4s_k-P_e)}{P_e-2as_k}\right)}$$
$$+\exp\left(\frac{x^*-x_1^*}{2}P_e\right)\frac{\sqrt{Z_k}\cos\left(\frac{x_1^*}{2}\sqrt{Z_k}\right)+(P_e-2s_k)\sin\left(\frac{x_1^*}{2}\sqrt{Z_k}\right)}{\beta P_e s_k(x_2^*-x_1^*)}$$
$$\times\frac{P_e(2-a)\sin\left(\frac{x^*-1}{2}\sqrt{Z_k}\right)-a\sqrt{Z_k}\cos\left(\frac{x^*-1}{2}\sqrt{Z_k}\right)}{\cos\left(\frac{\sqrt{Z_k}}{2}\right)\left(2+P_e-2as_k+\frac{(P_e+2a)(4s_k-P_e)}{P_e-2as_k}\right)}, \text{ for } x_1^* \le x^* < x_2^*, \quad (5.48b)$$

$$q_{3,k}(x^*) = \frac{P_e(2-a)\sin\left(\frac{x^*-1}{2}\sqrt{Z_k}\right)-a\sqrt{Z_k}\cos\left(\frac{x^*-1}{2}\sqrt{Z_k}\right)}{\beta P_e s_k(x_2^*-x_1^*)\cos\left(\frac{\sqrt{Z_k}}{2}\right)\left(2+P_e-2as_k+\frac{(P_e+2a)(4s_k-P_e)}{P_e-2as_k}\right)}$$
$$\times\Bigg\{\exp\left(\frac{x^*-x_1^*}{2}P_e\right)\left(\sqrt{Z_k}\cos\left(\frac{x_1^*}{2}\sqrt{Z_k}\right)+(P_e-2s_k)\sin\left(\frac{x_1^*}{2}\sqrt{Z_k}\right)\right)$$
$$-\exp\left(\frac{x^*-x_2^*}{2}P_e\right)\left(\sqrt{Z_k}\cos\left(\frac{x_2^*}{2}\sqrt{Z_k}\right)+(P_e-2s_k)\sin\left(\frac{x_2^*}{2}\sqrt{Z_k}\right)\right)\Bigg\},$$
$$\text{for } x_2^* \le x^* \le 1. \quad (5.48c)$$

where $Z_k = 4P_e s_k - P_e^2$.

There are some exceptional cases corresponding to the poles of $\overline{R}_{l,a}(x^*,s)$, $\overline{S}_{l,a}(x^*,s)$, $\overline{R}_{ld,a}(x^*,s)$, and $\overline{S}_{ld,a}(x^*,s)$ which are elaborated in Appendix B.1. The coefficients corresponding to these exceptional cases are as follows:

Case 1: When there is a root s_0 in $(0, P_e/4)$, then for $k=0$, the coefficients are negative of those given in Eqs. (5.43)−(5.48) with the trigonometric functions replaced by the corresponding hyperbolic functions and $Z_0 = P_e^2 - 4P_e s_0$.

Case 2: The case $P_e - 2as + 2 = 0$ gives $s_0 = P_e/4$ as a simple pole. The coefficients corresponding to $k = 0$ are to be replaced by

$$p_{1,0}(x^*) + p_{2,0}(x^*) = \exp\left(\frac{x^* - x_0^*}{2} P_e\right) \frac{3x^*(P_e x_0^* + 2)}{2(P_e + 3a)}, \tag{5.49}$$

$$q_{1,0}(x^*) + q_{2,0}(x^*) = \exp\left(\frac{x^* - x_0^*}{2} P_e\right) \frac{3(P_e x^* + 2)(P_e x_0^* + 2)}{\beta P_e(P_e + 3a)}, \tag{5.50}$$

$$\begin{aligned} p_{3,0}(x^*) = {} & \frac{3x^*}{P_e(P_e + 3a)(x_2^* - x_1^*)} \left\{ \exp\left(\frac{x^* - x_1^*}{2} P_e\right)(4 + P_e x_1^*) \right. \\ & \left. - \exp\left(\frac{x^* - x_2^*}{2} P_e\right)(4 + P_e x_2^*) \right\}, \end{aligned} \tag{5.51}$$

$$\begin{aligned} q_{3,0}(x^*) = {} & \frac{6(2 + P_e x^*)}{\beta P_e^2(P_e + 3a)(x_2^* - x_1^*)} \left\{ \exp\left(\frac{x^* - x_1^*}{2} P_e\right)(4 + P_e x_1^*) \right. \\ & \left. - \exp\left(\frac{x^* - x_2^*}{2} P_e\right)(4 + P_e x_2^*) \right\}. \end{aligned} \tag{5.52}$$

Case 3: When there is a root s_0 in $\left(\frac{P_e}{4}, \frac{\pi^2}{4P_e} + \frac{P_e}{4}\right)$, then the coefficients given in Eqs. (5.43)–(5.46) remain unchanged for s_0.

To understand the behavior of these impulse responses, the unit-step responses are obtained by taking the time integral of the impulse responses from 0 to t^*. Laplace transform is used to evaluate these integrals as

$$R_l(x^*, t^*) = \int_0^{t^*} R_{l,a}(x^*, \tau)\mathrm{d}\tau = \begin{cases} -\displaystyle\sum_{k=0}^{\infty} p_{2,k}(x^*) \frac{\exp(-s_k t^*)}{s_k}, & \text{for } x^* < x_0^*, \\ 1 - \displaystyle\sum_{k=0}^{\infty} \left(p_{1,k}(x^*) + p_{2,k}(x^*)\right) \frac{\exp(-s_k t^*)}{s_k}, & \text{for } x^* > x_0^*, \end{cases} \tag{5.53}$$

$$S_l(x^*, t^*) = \int_0^{t^*} S_{l,a}(x^*, \tau)\mathrm{d}\tau = \begin{cases} \dfrac{1}{\beta}\left((a-1)\exp\left(P_e(x^* - 1)\right) + \exp\left(P_e(x^* - x_0^*)\right)\right) \\ -\displaystyle\sum_{k=0}^{\infty} q_{2,k}(x^*) \frac{\exp(-s_k t^*)}{s_k}, & \text{for } x^* < x_0^*, \\ \dfrac{1}{\beta}\left((a-1)\exp\left(P_e(x^* - 1)\right) + 1\right) \\ -\displaystyle\sum_{k=0}^{\infty} \left(q_{1,k}(x^*) + q_{2,k}(x^*)\right) \frac{\exp(-s_k t^*)}{s_k}, & \text{for } x^* > x_0^*, \end{cases} \tag{5.54}$$

$$R_{ld}(x^*,t^*) = \int_0^{t^*} R_{ld,a}(x^*,\tau)\mathrm{d}\tau = \begin{cases} -\sum_{k=0}^{\infty}\frac{p_{3,k}(x^*)}{s_k}\exp(-s_k t^*), & \text{for } 0 \le x^* < x_1^*, \\ \frac{x^*-x_1^*}{x_2^*-x_1^*} - \sum_{k=0}^{\infty}\frac{p_{3,k}(x^*)}{s_k}\exp(-s_k t^*), & \text{for } x_1^* \le x^* < x_2^*, \\ 1 - \sum_{k=0}^{\infty}\frac{p_{3,k}(x^*)}{s_k}\exp(-s_k t^*), & \text{for } x_2^* \le x^* \le 1, \end{cases} \tag{5.55}$$

$$\begin{aligned} S_{ld}(x^*,t^*) &= \int_0^{t^*} S_{ld,a}(x^*,\tau)\mathrm{d}\tau \\ &= \begin{cases} \frac{(a-1)}{\beta}\exp\left((x^*-1)P_e\right) + \frac{\exp\left(x^*P_e\right)}{\beta P_e(x_2^*-x_1^*)}\left(\exp\left(-x_1^*P_e\right) - \exp\left(-x_2^*P_e\right)\right) \\ -\sum_{k=0}^{\infty}\frac{q_{3,k}(x^*)}{s_k}\exp(-s_k t^*), \quad \text{for } 0 \le x^* < x_1^*, \\ \frac{1}{\beta}\left(\frac{x^*-x_1^*}{x_2^*-x_1^*} + (a-1)\exp\left((x^*-1)P_e\right)\right) + \frac{1-\exp\left((x^*-x_2^*)P_e\right)}{\beta P_e(x_2^*-x_1^*)} \\ -\sum_{k=0}^{\infty}\frac{q_{3,k}(x^*)}{s_k}\exp(-s_k t^*), \quad \text{for } x_1^* \le x^* < x_2^*, \\ \frac{1}{\beta}\left(1 + (a-1)\exp\left((x^*-1)P_e\right)\right) - \sum_{k=0}^{\infty}\frac{q_{3,k}(x^*)}{s_k}\exp(-s_k t^*), \quad \text{for } x_2^* \le x^* \le 1. \end{cases} \end{aligned} \tag{5.56}$$

5.2.2 Flow-depth hydrograph imposed at the upstream end

In this case, the upstream boundary is considered as $h^*(0,t^*)$. Taking this into account in Eqs. (5.17) and (5.25), we get $\overline{Q^*}(0,s)$ as

$$\overline{Q^*}(0,s) = -\frac{\alpha_{12}(1,s) - \frac{\beta}{a}\alpha_{22}(1,s)}{\alpha_{11}(1,s) - \frac{\beta}{a}\alpha_{21}(1,s)}\overline{h^*}(0,s) - \frac{\alpha_{11}(1-x_0^*,s) - \frac{\beta}{a}\alpha_{21}(1-x_0^*,s)}{\alpha_{11}(1,s) - \frac{\beta}{a}\alpha_{21}(1,s)}\overline{T^*}(s). \tag{5.57}$$

Using this, the system given by Eq. (5.19) is obtained as

$$\overline{Q^*}(x^*,s) = \overline{M}_{u,a}(x^*,s)\overline{h^*}(0,s) + \overline{M}_{l,a}(x^*,s)\overline{T^*}(s), \tag{5.58a}$$
$$\overline{h^*}(x^*,s) = \overline{N}_{u,a}(x^*,s)\overline{h^*}(0,s) + \overline{N}_{l,a}(x^*,s)\overline{T^*}(s). \tag{5.58b}$$

The Laplace inverses of $\overline{M}_{u,a}(x^*, s)$ and $\overline{N}_{u,a}(x^*, s)$ are already provided by Cimorelli et al. [6]. We now proceed to find the inverses of $\overline{M}_{l,a}(x^*, s)$ and $\overline{N}_{l,a}(x^*, s)$ where

$$\overline{M}_{l,a}(x^*, s) = \frac{2P_e \exp\left(\frac{x^* - x_0^*}{2}P_e\right)\sinh\left(\frac{x_0^*\sqrt{Z}}{2}\right)}{\sqrt{Z}\left(a\sqrt{Z}\cosh\left(\frac{\sqrt{Z}}{2}\right) + P_e(2-a)\sinh\left(\frac{\sqrt{Z}}{2}\right)\right)} \times \left\{(P_e + 2as)\sinh\left(\frac{1-x^*}{2}\sqrt{Z}\right) + \sqrt{Z}\cosh\left(\frac{1-x^*}{2}\sqrt{Z}\right)\right\}, \quad \text{for } x^* > x_0^*, \tag{5.59a}$$

$$\overline{M}_{l,a}(x^*, s) = -\exp\left(\frac{x^* - x_0^*}{2}P_e\right)\frac{\sqrt{Z}\cosh\left(\frac{x^*\sqrt{Z}}{2}\right) - P_e\sinh\left(\frac{x^*\sqrt{Z}}{2}\right)}{\sqrt{Z}} \frac{P_e(2-a)\sinh\left(\frac{1-x_0^*}{2}\sqrt{Z}\right) + a\sqrt{Z}\cosh\left(\frac{1-x_0^*}{2}\sqrt{Z}\right)}{a\sqrt{Z}\cosh\left(\frac{\sqrt{Z}}{2}\right) + P_e(2-a)\sinh\left(\frac{\sqrt{Z}}{2}\right)}, \quad \text{for } x^* < x_0^*, \tag{5.59b}$$

$$\overline{N}_{l,a}(x^*, s) = \frac{2P_e \exp\left(\frac{x^* - x_0^*}{2}P_e\right)\sinh\left(\frac{x_0^*\sqrt{Z}}{2}\right)}{\beta\sqrt{Z}\left(a\sqrt{Z}\cosh\left(\frac{\sqrt{Z}}{2}\right) + P_e(2-a)\sinh\left(\frac{\sqrt{Z}}{2}\right)\right)} \times \left\{P_e(2-a)\sinh\left(\frac{1-x^*}{2}\sqrt{Z}\right) + a\sqrt{Z}\cosh\left(\frac{1-x^*}{2}\sqrt{Z}\right)\right\}, \quad \text{for } x^* > x_0^*, \tag{5.60a}$$

$$\overline{N}_{l,a}(x^*, s) = \frac{2P_e \exp\left(\frac{x^* - x_0^*}{2}P_e\right)\sinh\left(\frac{x^*\sqrt{Z}}{2}\right)}{\beta\sqrt{Z}\left(a\sqrt{Z}\cosh\left(\frac{\sqrt{Z}}{2}\right) + P_e(2-a)\sinh\left(\frac{\sqrt{Z}}{2}\right)\right)} \times \left\{P_e(2-a)\sinh\left(\frac{1-x_0^*}{2}\sqrt{Z}\right) + a\sqrt{Z}\cosh\left(\frac{1-x_0^*}{2}\sqrt{Z}\right)\right\}, \quad \text{for } x^* < x_0^*. \tag{5.60b}$$

Similarly, for a uniformly distributed lateral inflow between x_1^* and x_2^*, using Eqs. (5.17) and (5.30), we get $\overline{Q^*}(0,s)$ as

$$\overline{Q^*}(0,s) = -\frac{\alpha_{12}(1,s) - \dfrac{\beta}{a}\alpha_{22}(1,s)}{\alpha_{11}(1,s) - \dfrac{\beta}{a}\alpha_{21}(1,s)}\overline{h^*}(0,s) - \frac{A_{11}(1,s) - \dfrac{\beta}{a}A_{21}(1,s)}{\alpha_{11}(1,s) - \dfrac{\beta}{a}\alpha_{21}(1,s)}\overline{T^*}(s). \tag{5.61}$$

Using this, we get the system given by Eq. (5.19) as

$$\overline{Q^*}(x^*,s) = \overline{M}_{u,a}(x^*,s)\overline{h^*}(0,s) + \overline{M}_{ld,a}(x^*,s)\overline{T^*}(s), \tag{5.62a}$$
$$\overline{h^*}(x^*,s) = \overline{N}_{u,a}(x^*,s)\overline{h^*}(0,s) + \overline{N}_{ld,a}(x^*,s)\overline{T^*}(s), \tag{5.62b}$$

where the functions $\overline{M}_{u,a}$ and $\overline{N}_{u,a}$ are the same as the ones obtained in Eq. (5.58). The other two terms are expressed as

$$\begin{aligned}\overline{M}_{ld,a}(x^*,s) = {} & \frac{\sqrt{Z}\cosh\left(\dfrac{x^*\sqrt{Z}}{2}\right) - P_e\sinh\left(\dfrac{x^*\sqrt{Z}}{2}\right)}{s\sqrt{Z}(x_2^*-x_1^*)\left(a\sqrt{Z}\cosh\left(\dfrac{\sqrt{Z}}{2}\right) + P_e(2-a)\sinh\left(\dfrac{\sqrt{Z}}{2}\right)\right)} \\ & \times\left\{\exp\left(\frac{x^*-x_2^*}{2}P_e\right)\left((P_e(a-1)+2as)\sinh\left(\frac{1-x_2^*}{2}\sqrt{Z}\right)\right.\right. \\ & \left. - (a-1)\sqrt{Z}\cosh\left(\frac{1-x_2^*}{2}\sqrt{Z}\right)\right) \\ & - \exp\left(\frac{x^*-x_1^*}{2}P_e\right)\left((P_e(a-1)+2as)\sinh\left(\frac{1-x_1^*}{2}\sqrt{Z}\right)\right. \\ & \left.\left. - (a-1)\sqrt{Z}\cosh\left(\frac{1-x_1^*}{2}\sqrt{Z}\right)\right)\right\}, \qquad \text{for } 0 \le x^* < x_1^*,\end{aligned} \tag{5.63a}$$

$$\begin{aligned}\overline{M}_{ld,a}(x^*,s) = {} & \frac{1}{s(x_2^*-x_1^*)} + \exp\left(\frac{x^*-x_2^*}{2}P_e\right)\frac{\sqrt{Z}\cosh\left(\dfrac{x^*\sqrt{Z}}{2}\right) - P_e\sinh\left(\dfrac{x^*\sqrt{Z}}{2}\right)}{s\sqrt{Z}(x_2^*-x_1^*)} \\ & \times\frac{(P_e(a-1)+2as)\sinh\left(\dfrac{1-x_2^*}{2}\sqrt{Z}\right) - (a-1)\sqrt{Z}\cosh\left(\dfrac{1-x_2^*}{2}\sqrt{Z}\right)}{a\sqrt{Z}\cosh\left(\dfrac{\sqrt{Z}}{2}\right) + P_e(2-a)\sinh\left(\dfrac{\sqrt{Z}}{2}\right)}\end{aligned}$$

$$+\frac{\exp\left(\frac{x^*-x_1^*}{2}P_e\right)\left(\sqrt{Z}\cosh\left(\frac{x_1^*}{2}\sqrt{Z}\right)+P_e\sinh\left(\frac{x_1^*}{2}\sqrt{Z}\right)\right)}{s\sqrt{Z}(x_2^*-x_1^*)\left(a\sqrt{Z}\cosh\left(\frac{\sqrt{Z}}{2}\right)+P_e(2-a)\sinh\left(\frac{\sqrt{Z}}{2}\right)\right)}$$
$$\times\left((P_e+2as)\sinh\left(\frac{x^*-1}{2}\sqrt{Z}\right)-\sqrt{Z}\cosh\left(\frac{x^*-1}{2}\sqrt{Z}\right)\right),\ \text{for } x_1^*\le x^*<x_2^*, \tag{5.63b}$$

$$\overline{M}_{ld,a}(x^*,s)=\frac{(P_e+2as)\sinh\left(\frac{x^*-1}{2}\sqrt{Z}\right)-\sqrt{Z}\cosh\left(\frac{x^*-1}{2}\sqrt{Z}\right)}{s\sqrt{Z}(x_2^*-x_1^*)\left(a\sqrt{Z}\cosh\left(\frac{\sqrt{Z}}{2}\right)+P_e(2-a)\sinh\left(\frac{\sqrt{Z}}{2}\right)\right)}$$
$$\times\left\{\exp\left(\frac{x^*-x_1^*}{2}P_e\right)\left(\sqrt{Z}\cosh\left(\frac{x_1^*}{2}\sqrt{Z}\right)+P_e\sinh\left(\frac{x_1^*}{2}\sqrt{Z}\right)\right)\right.$$
$$\left.-\exp\left(\frac{x^*-x_2^*}{2}P_e\right)\left(\sqrt{Z}\cosh\left(\frac{x_2^*}{2}\sqrt{Z}\right)+P_e\sinh\left(\frac{x_2^*}{2}\sqrt{Z}\right)\right)\right\},$$
$$\text{for } x_2^*\le x^*\le 1, \tag{5.63c}$$

and

$$\overline{N}_{ld,a}(x^*,s)=\frac{-2P_e\sinh\left(\frac{x^*\sqrt{Z}}{2}\right)}{\beta s\sqrt{Z}(x_2^*-x_1^*)\left(a\sqrt{Z}\cosh\left(\frac{\sqrt{Z}}{2}\right)+P_e(2-a)\sinh\left(\frac{\sqrt{Z}}{2}\right)\right)}$$
$$\times\left\{\exp\left(\frac{x^*-x_2^*}{2}P_e\right)\left((P_e(a-1)+2as)\sinh\left(\frac{1-x_2^*}{2}\sqrt{Z}\right)\right.\right.$$
$$\left.-(a-1)\sqrt{Z}\cosh\left(\frac{1-x_2^*}{2}\sqrt{Z}\right)\right)$$
$$-\exp\left(\frac{x^*-x_1^*}{2}P_e\right)\left((P_e(a-1)+2as)\sinh\left(\frac{1-x_1^*}{2}\sqrt{Z}\right)\right.$$
$$\left.\left.-(a-1)\sqrt{Z}\cosh\left(\frac{1-x_1^*}{2}\sqrt{Z}\right)\right)\right\},\qquad \text{for } 0\le x^*<x_1^*, \tag{5.64a}$$

$$\overline{N}_{ld,a}(x^*,s)=\frac{1}{\beta s(x_2^*-x_1^*)}-\frac{2P_e}{\beta s\sqrt{Z}(x_2^*-x_1^*)}\exp\left(\frac{x^*-x_2^*}{2}P_e\right)\sinh\left(\frac{x^*\sqrt{Z}}{2}\right)$$

$$\times \frac{(P_e(a-1)+2as)\sinh\left(\frac{1-x_2^*}{2}\sqrt{Z}\right)-(a-1)\sqrt{Z}\cosh\left(\frac{1-x_2^*}{2}\sqrt{Z}\right)}{a\sqrt{Z}\cosh\left(\frac{\sqrt{Z}}{2}\right)+P_e(2-a)\sinh\left(\frac{\sqrt{Z}}{2}\right)}$$

$$+\frac{\exp\left(\frac{x^*-x_1^*}{2}P_e\right)\left(\sqrt{Z}\cosh\left(\frac{x_1^*}{2}\sqrt{Z}\right)+P_e\sinh\left(\frac{x_1^*}{2}\sqrt{Z}\right)\right)}{\beta s\sqrt{Z}(x_2^*-x_1^*)\left(a\sqrt{Z}\cosh\left(\frac{\sqrt{Z}}{2}\right)+P_e(2-a)\sinh\left(\frac{\sqrt{Z}}{2}\right)\right)}$$

$$\times\left(P_e(2-a)\sinh\left(\frac{x^*-1}{2}\sqrt{Z}\right)-a\sqrt{Z}\cosh\left(\frac{x^*-1}{2}\sqrt{Z}\right)\right),\ \text{for } x_1^*\leq x^*<x_2^*, \tag{5.64b}$$

$$\overline{N}_{ld,a}(x^*,s)=\frac{P_e(2-a)\sinh\left(\frac{x^*-1}{2}\sqrt{Z}\right)-a\sqrt{Z}\cosh\left(\frac{x^*-1}{2}\sqrt{Z}\right)}{\beta s\sqrt{Z}(x_2^*-x_1^*)\left(a\sqrt{Z}\cosh\left(\frac{\sqrt{Z}}{2}\right)+P_e(2-a)\sinh\left(\frac{\sqrt{Z}}{2}\right)\right)}$$

$$\times\left\{\exp\left(\frac{x^*-x_1^*}{2}P_e\right)\left(\sqrt{Z}\cosh\left(\frac{x_1^*}{2}\sqrt{Z}\right)+P_e\sinh\left(\frac{x_1^*}{2}\sqrt{Z}\right)\right)\right.$$

$$\left.-\exp\left(\frac{x^*-x_2^*}{2}P_e\right)\left(\sqrt{Z}\cosh\left(\frac{x_2^*}{2}\sqrt{Z}\right)+P_e\sinh\left(\frac{x_2^*}{2}\sqrt{Z}\right)\right)\right\},$$

$$\text{for } x_2^*\leq x^*\leq 1. \tag{5.64c}$$

The inverses of the system given by Eq. (5.58) can be written as

$$Q^*(x^*,t^*)=M_{u,a}(x^*,t^*)\circledast Q^*(0,t^*)+M_{l,a}(x^*,t^*)\circledast T^*(t^*), \tag{5.65a}$$

$$h^*(x^*,t^*)=N_{u,a}(x^*,t^*)\circledast Q^*(0,t^*)+N_{l,a}(x^*,t^*)\circledast T^*(t^*), \tag{5.65b}$$

while the inverses of the system given by Eq. (5.62) can be written as

$$Q^*(x^*,t^*)=M_{u,a}(x^*,t^*)\circledast Q^*(0,t^*)+M_{ld,a}(x^*,t^*)\circledast T^*(t^*), \tag{5.66a}$$

$$h^*(x^*,t^*)=N_{u,a}(x^*,t^*)\circledast Q^*(0,t^*)+N_{ld,a}(x^*,t^*)\circledast T^*(t^*), \tag{5.66b}$$

with

$$M_{l,a}(x^*,t^*)=\sum_{k=0}^{\infty}b_{1,k}(x^*)\exp\left(-s_k t^*\right), \tag{5.67}$$

$$N_{l,a}(x^*,t^*)=\sum_{k=0}^{\infty}b_{2,k}(x^*)\exp\left(-s_k t^*\right), \tag{5.68}$$

$$M_{ld,a}(x^*,t^*) = \sum_{k=0}^{\infty} b_{3,k}(x^*) \exp\left(-s_k t^*\right), \tag{5.69}$$

$$N_{ld,a}(x^*,t^*) = \sum_{k=0}^{\infty} b_{4,k}(x^*) \exp\left(-s_k t^*\right), \tag{5.70}$$

$$\tag{5.71}$$

where s_k is the k-th pole for the corresponding functions in the Laplace domain. The poles finding process is elaborated in Appendix B.2. The coefficients of the functions given in Eqs. (5.67)−(5.70) are obtained in the following form:

- When $\epsilon = P_e(2a^{-1} - 1) > 0$,

$$b_{1,k}(x^*) = -2\epsilon \exp\left(\frac{x^* - x_0^*}{2} P_e\right) \sin\left(\frac{x_0^* \sqrt{Z_k}}{2}\right) \times \frac{(P_e - 2as_k)\sin\left(\frac{1-x^*}{2}\sqrt{Z_k}\right) + \sqrt{Z_k}\cos\left(\frac{1-x^*}{2}\sqrt{Z_k}\right)}{a\left(Z_k + \epsilon(\epsilon+2)\right)\cos\left(\frac{\sqrt{Z_k}}{2}\right)}, \quad \text{for } x^* > x_0^*, \tag{5.72a}$$

$$b_{1,k}(x^*) = \frac{\epsilon}{P_e} \exp\left(\frac{x^* - x_0^*}{2} P_e\right) \left(\sqrt{Z}\cos\left(\frac{x^* \sqrt{Z_k}}{2}\right) - P_e \sin\left(\frac{x^* \sqrt{Z_k}}{2}\right)\right) \times \frac{\epsilon \sin\left(\frac{1-x_0^*}{2}\sqrt{Z_k}\right) + \sqrt{Z_k}\cos\left(\frac{1-x_0^*}{2}\sqrt{Z_k}\right)}{\left(Z_k + \epsilon(\epsilon+2)\right)\cos\left(\frac{\sqrt{Z_k}}{2}\right)}, \quad \text{for } x^* < x_0^*, \tag{5.72b}$$

$$b_{2,k}(x^*) = -2\epsilon \exp\left(\frac{x^* - x_0^*}{2} P_e\right) \sin\left(\frac{x_0^* \sqrt{Z_k}}{2}\right) \times \frac{\epsilon \sin\left(\frac{1-x^*}{2}\sqrt{Z_k}\right) + \sqrt{Z_k}\cos\left(\frac{1-x^*}{2}\sqrt{Z_k}\right)}{\beta\left(Z_k + \epsilon(\epsilon+2)\right)\cos\left(\frac{\sqrt{Z_k}}{2}\right)}, \quad \text{for } x^* > x_0^*, \tag{5.73a}$$

$$b_{2,k}(x^*) = -2\epsilon \exp\left(\frac{x^* - x_0^*}{2} P_e\right) \sin\left(\frac{x^* \sqrt{Z_k}}{2}\right)$$

$$\times \frac{\epsilon \sin\left(\frac{1-x_0^*}{2}\sqrt{Z_k}\right) + \sqrt{Z_k}\cos\left(\frac{1-x_0^*}{2}\sqrt{Z_k}\right)}{\beta\left(Z_k + \epsilon(\epsilon+2)\right)\cos\left(\frac{\sqrt{Z_k}}{2}\right)}, \quad \text{for } x^* < x_0^*, \tag{5.73b}$$

$$b_{3,k}(x^*) = \frac{\epsilon}{aP_e}\frac{\sqrt{Z_k}\cos\left(\frac{x^*\sqrt{Z_k}}{2}\right) - P_e\sin\left(\frac{x^*\sqrt{Z_k}}{2}\right)}{s_k(x_2^*-x_1^*)(\epsilon(\epsilon+2)+Z_k)\cos\left(\frac{\sqrt{Z_k}}{2}\right)}$$
$$\times\left\{\exp\left(\frac{x^*-x_2^*}{2}P_e\right)\left((P_e(a-1)-2as_k)\sin\left(\frac{1-x_2^*}{2}\sqrt{Z_k}\right)\right.\right.$$
$$\left.-(a-1)\sqrt{Z_k}\cos\left(\frac{1-x_2^*}{2}\sqrt{Z_k}\right)\right)$$
$$-\exp\left(\frac{x^*-x_1^*}{2}P_e\right)\left((P_e(a-1)-2as_k)\sin\left(\frac{1-x_1^*}{2}\sqrt{Z_k}\right)\right.$$
$$\left.\left.-(a-1)\sqrt{Z_k}\cos\left(\frac{1-x_1^*}{2}\sqrt{Z_k}\right)\right)\right\}, \quad \text{for } 0 \le x^* < x_1^*, \tag{5.74a}$$

$$b_{3,k}(x^*) = \frac{\epsilon}{aP_e}\exp\left(\frac{x^*-x_2^*}{2}P_e\right)\frac{\sqrt{Z_k}\cos\left(\frac{x^*\sqrt{Z_k}}{2}\right) - P_e\sin\left(\frac{x^*\sqrt{Z_k}}{2}\right)}{s_k(x_2^*-x_1^*)}$$
$$\times\frac{(P_e(a-1)-2as_k)\sin\left(\frac{1-x_2^*}{2}\sqrt{Z_k}\right) - (a-1)\sqrt{Z_k}\cos\left(\frac{1-x_2^*}{2}\sqrt{Z_k}\right)}{(\epsilon(\epsilon+2)+Z_k)\cos\left(\frac{\sqrt{Z_k}}{2}\right)}$$
$$+\frac{\epsilon}{aP_e}\exp\left(\frac{x^*-x_1^*}{2}P_e\right)\frac{\sqrt{Z_k}\cos\left(\frac{x_1^*}{2}\sqrt{Z_k}\right) + P_e\sin\left(\frac{x_1^*}{2}\sqrt{Z_k}\right)}{s_k(x_2^*-x_1^*)}$$
$$\times\frac{(P_e-2as_k)\sin\left(\frac{x^*-1}{2}\sqrt{Z_k}\right) - \sqrt{Z_k}\cos\left(\frac{x^*-1}{2}\sqrt{Z_k}\right)}{(\epsilon(\epsilon+2)+Z_k)\cos\left(\frac{\sqrt{Z_k}}{2}\right)}, \quad \text{for } x_1^* \le x^* < x_2^*, \tag{5.74b}$$

$$b_{3,k}(x^*) = \frac{\epsilon}{aP_e}\frac{(P_e-2as_k)\sin\left(\frac{x^*-1}{2}\sqrt{Z_k}\right) - \sqrt{Z_k}\cos\left(\frac{x^*-1}{2}\sqrt{Z_k}\right)}{s_k(x_2^*-x_1^*)(\epsilon(\epsilon+2)+Z_k)\cos\left(\frac{\sqrt{Z_k}}{2}\right)}$$

$$\times\left\{\exp\left(\frac{x^*-x_1^*}{2}P_e\right)\left(\sqrt{Z_k}\cos\left(\frac{x_1^*}{2}\sqrt{Z_k}\right)+P_e\sin\left(\frac{x_1^*}{2}\sqrt{Z_k}\right)\right)\right.$$
$$\left.-\exp\left(\frac{x^*-x_2^*}{2}P_e\right)\left(\sqrt{Z_k}\cos\left(\frac{x_2^*}{2}\sqrt{Z_k}\right)+P_e\sin\left(\frac{x_2^*}{2}\sqrt{Z_k}\right)\right)\right\},$$
$$\text{for } x_2^*\le x^*\le 1. \tag{5.74c}$$

$$b_{4,k}(x^*)=-\frac{2\epsilon}{a}\frac{\sin\left(\dfrac{x^*\sqrt{Z_k}}{2}\right)}{\beta s_k(x_2^*-x_1^*)(\epsilon(\epsilon+2)+Z_k)\cos\left(\dfrac{\sqrt{Z_k}}{2}\right)}$$
$$\times\left\{\exp\left(\frac{x^*-x_2^*}{2}P_e\right)\left((P_e(a-1)-2as_k)\sin\left(\frac{1-x_2^*}{2}\sqrt{Z_k}\right)\right.\right.$$
$$\left.-(a-1)\sqrt{Z_k}\cos\left(\frac{1-x_2^*}{2}\sqrt{Z_k}\right)\right)$$
$$-\exp\left(\frac{x^*-x_1^*}{2}P_e\right)\left((P_e(a-1)-2as_k)\sin\left(\frac{1-x_1^*}{2}\sqrt{Z_k}\right)\right.$$
$$\left.\left.-(a-1)\sqrt{Z_k}\cos\left(\frac{1-x_1^*}{2}\sqrt{Z_k}\right)\right)\right\},\qquad \text{for } 0\le x^*<x_1^*, \tag{5.75a}$$

$$b_{4,k}(x^*)=-\frac{2\epsilon}{a}\frac{\exp\left(\dfrac{x^*-x_2^*}{2}P_e\right)\sin\left(\dfrac{x^*\sqrt{Z_k}}{2}\right)}{\beta s_k(x_2^*-x_1^*)}$$
$$\times\frac{(P_e(a-1)-2as_k)\sin\left(\dfrac{1-x_2^*}{2}\sqrt{Z_k}\right)-(a-1)\sqrt{Z_k}\cos\left(\dfrac{1-x_2^*}{2}\sqrt{Z_k}\right)}{(\epsilon(\epsilon+2)+Z_k)\cos\left(\dfrac{\sqrt{Z_k}}{2}\right)}$$
$$+\frac{\epsilon}{aP_e}\frac{\exp\left(\dfrac{x^*-x_1^*}{2}P_e\right)}{\beta s_k(x_2^*-x_1^*)}\frac{\sqrt{Z_k}\cos\left(\dfrac{x_1^*}{2}\sqrt{Z_k}\right)+P_e\sin\left(\dfrac{x_1^*}{2}\sqrt{Z_k}\right)}{(\epsilon(\epsilon+2)+Z_k)\cos\left(\dfrac{\sqrt{Z_k}}{2}\right)}$$
$$\times\left(P_e(2-a)\sin\left(\frac{x^*-1}{2}\sqrt{Z_k}\right)-a\sqrt{Z_k}\cos\left(\frac{x^*-1}{2}\sqrt{Z_k}\right)\right),\ \text{for } x_1^*\le x^*<x_2^*, \tag{5.75b}$$

$$b_{4,k}(x^*) = \frac{\epsilon}{aP_e} \frac{P_e(2-a)\sin\left(\frac{x^*-1}{2}\sqrt{Z_k}\right) - a\sqrt{Z_k}\cos\left(\frac{x^*-1}{2}\sqrt{Z_k}\right)}{\beta s_k(x_2^*-x_1^*)(\epsilon(\epsilon+2)+Z_k)\cos\left(\frac{\sqrt{Z_k}}{2}\right)}$$
$$\times\left\{\exp\left(\frac{x^*-x_1^*}{2}P_e\right)\left(\sqrt{Z_k}\cos\left(\frac{x_1^*}{2}\sqrt{Z_k}\right)+P_e\sin\left(\frac{x_1^*}{2}\sqrt{Z_k}\right)\right)\right.$$
$$\left.-\exp\left(\frac{x^*-x_2^*}{2}P_e\right)\left(\sqrt{Z_k}\cos\left(\frac{x_2^*}{2}\sqrt{Z_k}\right)+P_e\sin\left(\frac{x_2^*}{2}\sqrt{Z_k}\right)\right)\right\},$$
$$\text{for } x_2^* \le x^* \le 1. \tag{5.75c}$$

- When $\epsilon = 0$,

$$b_{1,k}(x^*) = -\exp\left(\frac{x^*-x_0^*}{2}P_e\right)\sin\left(x_0^*\frac{(2k-1)\pi}{2}\right)$$
$$\times\left\{\frac{(2k-1)\pi}{P_e}\cos\left(x^*\frac{(2k-1)\pi}{2}\right)-\sin\left(x^*\frac{(2k-1)\pi}{2}\right)\right\}, \tag{5.76}$$

$$b_{2,k}(x^*) = \frac{2}{\beta}\exp\left(\frac{x^*-x_0^*}{2}P_e\right)\sin\left(x_0^*\frac{(2k-1)\pi}{2}\right)\sin\left(x^*\frac{(2k-1)\pi}{2}\right), \tag{5.77}$$

$$b_{3,k}(x^*) = 2\frac{\frac{(2k-1)\pi}{P_e}\cos\left(\frac{2k-1}{2}x^*\pi\right)-\sin\left(\frac{2k-1}{2}x^*\pi\right)}{((2k-1)^2\pi^2+P_e^2)(x_2^*-x_1^*)}$$
$$\times\left\{\exp\left(\frac{x^*-x_2^*}{2}P_e\right)\left((2k-1)\pi\cos\left(\frac{2k-1}{2}x_2^*\pi\right)+P_e\sin\left(\frac{2k-1}{2}x_2^*\pi\right)\right)\right.$$
$$\left.-\exp\left(\frac{x^*-x_1^*}{2}P_e\right)\left((2k-1)\pi\cos\left(\frac{2k-1}{2}x_1^*\pi\right)+P_e\sin\left(\frac{2k-1}{2}x_1^*\pi\right)\right)\right\}, \tag{5.78}$$

$$b_{4,k}(x^*) = \frac{4\sin\left(\frac{2k-1}{2}x^*\pi\right)}{\beta(x_2^*-x_1^*)((2k-1)^2\pi^2+P_e^2)}$$
$$\times\left\{\exp\left(\frac{x^*-x_2^*}{2}P_e\right)\left((2k-1)\pi\cos\left(\frac{2k-1}{2}x_2^*\pi\right)+P_e\sin\left(\frac{2k-1}{2}x_2^*\pi\right)\right)\right.$$
$$\left.-\exp\left(\frac{x^*-x_1^*}{2}P_e\right)\left((2k-1)\pi\cos\left(\frac{2k-1}{2}x_1^*\pi\right)+P_e\sin\left(\frac{2k-1}{2}x_1^*\pi\right)\right)\right\}. \tag{5.79}$$

- When $-2 < \epsilon < 0$, the coefficients $b_{1,0}(x^*)$, $b_{2,0}(x^*)$, $b_{3,0}(x^*)$, and $b_{4,0}(x^*)$ for the root s_0 are the same as the ones given in Eqs. (5.72)–(5.75), respectively.

- When $\epsilon = -2$, the coefficients corresponding to the pole $s_0 = P_e/4$ are

$$b_{1,0}(x^*) = \frac{3x_0^*}{2P_e} \exp\left(\frac{x^* - x_0^*}{2}P_e\right)(P_e x^* - 2), \tag{5.80}$$

$$b_{2,0}(x^*) = \frac{3x_0^* x^*}{\beta} \exp\left(\frac{x^* - x_0^*}{2}P_e\right), \tag{5.81}$$

$$b_{3,0}(x^*) = \frac{3(P_e x^* - 2)}{P_e^3}\left\{\exp\left(\frac{x^* - x_1^*}{2}P_e\right)\frac{2 + P_e x_1^*}{x_2^* - x_1^*} - \exp\left(\frac{x^* - x_2^*}{2}P_e\right)\frac{2 + P_e x_2^*}{x_2^* - x_1^*}\right\}, \tag{5.82}$$

$$b_{4,0}(x^*) = \frac{6x^*}{\beta P_e^2}\left\{\exp\left(\frac{x^* - x_1^*}{2}P_e\right)\frac{2 + P_e x_1^*}{x_2^* - x_1^*} - \exp\left(\frac{x^* - x_2^*}{2}P_e\right)\frac{2 + P_e x_2^*}{x_2^* - x_1^*}\right\}. \tag{5.83}$$

- When $\epsilon < -2$, the coefficients corresponding to the new pole s_0 are negative of those given in Eqs. (5.72)−(5.75) with the trigonometric functions replaced by the corresponding hyperbolic functions, and $Z_0 = P_e^2 - 4P_e s_0$.

The unit-step responses for these impulse responses are evaluated by using Laplace transform as follows:

$$M_l(x^*, t^*) = \int_0^{t^*} M_{l,a}(x^*, \tau)\mathrm{d}\tau = \begin{cases} -\dfrac{\exp(-x_0^* P_e) + (a-1)\exp(-P_e)}{(1 + (a-1)\exp(-P_e))} \\ -\displaystyle\sum_{k=0}^{\infty}\frac{b_{1,k}(x^*)}{s_k}\exp(-s_k t^*), \quad \text{for } x^* < x_0^*, \\ \dfrac{1 - \exp(-x_0^* P_e)}{(1 + (a-1)\exp(-P_e))} \\ -\displaystyle\sum_{k=0}^{\infty}\frac{b_{1,k}(x^*)}{s_k}\exp(-s_k t^*), \quad \text{for } x^* > x_0^*, \end{cases} \tag{5.84}$$

$$N_l(x^*, t^*) = \int_0^{t^*} N_{l,a}(x^*, \tau)\mathrm{d}\tau = \begin{cases} \dfrac{(a-1)\exp((x^*-1)P_e)(1 - \exp(-x^* P_e))}{\beta(1 + (a-1)\exp(-P_e))} \\ +\dfrac{\exp((x^* - x_0^*)P_e)(1 - \exp(-x^* P_e))}{\beta(1 + (a-1)\exp(-P_e))} \\ -\displaystyle\sum_{k=0}^{\infty}\frac{b_{2,k}(x^*)}{s_k}\exp(-s_k t^*), \quad \text{for } x^* < x_0^*, \\ \dfrac{(1 - \exp(-x_0^* P_e))(1 + (a-1)\exp(P_e(x^*-1)))}{\beta(1 + (a-1)\exp(-P_e))} \\ -\displaystyle\sum_{k=0}^{\infty}\frac{b_{2,k}(x^*)}{s_k}\exp(-s_k t^*), \quad \text{for } x^* > x_0^*, \end{cases} \tag{5.85}$$

$$M_{ld}(x^*, t^*) = \int_0^{t^*} M_{ld,a}(x^*, \tau)\mathrm{d}\tau$$

$$= \begin{cases} \dfrac{\exp(P_e)\left(\exp(-x_2^*P_e)-\exp(-x_1^*P_e)\right)-P_e(a-1)(x_2^*-x_1^*)}{P_e(x_2^*-x_1^*)(a-1+\exp(P_e))} \\ -\displaystyle\sum_{k=0}^{\infty}\frac{b_{3,k}(x^*)}{s_k}\exp(-s_kt^*), & \text{for } 0\le x^*<x_1^*, \\ \dfrac{\exp(P_e)\left(P_e(x^*-x_1^*)+\exp(-x_2^*P_e)-\exp(-x_1^*P_e)\right)+P_e(a-1)(x-x_2^*)}{P_e(x_2^*-x_1^*)(a-1+\exp(P_e))} \\ -\displaystyle\sum_{k=0}^{\infty}\frac{b_{3,k}(x^*)}{s_k}\exp(-s_kt^*), & \text{for } x_1^*\le x^*<x_2^*, \\ \dfrac{\exp(P_e)}{a-1+\exp(P_e)}+\dfrac{\exp((1-x_2^*)P_e)-\exp((1-x_1^*)P_e)}{P_e(x_2^*-x_1^*)(a-1+\exp(P_e))} \\ -\displaystyle\sum_{k=0}^{\infty}\frac{b_{3,k}(x^*)}{s_k}\exp(-s_kt^*), & \text{for } x_2^*\le x^*\le 1, \end{cases} \tag{5.86}$$

$$N_{ld}(x^*,t^*)=\int_0^{t^*}N_{ld,a}(x^*,\tau)\mathrm{d}\tau$$

$$= \begin{cases} (1-\exp(xP_e))\,\dfrac{\exp(P_e)\left(\exp(-x_2^*P_e)-\exp(-x_1^*P_e)\right)-P_e(a-1)(x_2^*-x_1^*)}{\beta P_e(x_2^*-x_1^*)(a-1+\exp(P_e))} \\ -\displaystyle\sum_{k=0}^{\infty}\frac{b_{4,k}(x^*)}{s_k}\exp(-s_kt^*), & \text{for } 0\le x^*<x_1^*, \\ (a-1)\dfrac{1+(x^*-x_2^*)P_e+P_e(x_2^*-x_1^*)\exp(x^*P_e)-\exp\left((x^*-x_1^*)P_e\right)}{\beta P_e(x_2^*-x_1^*)(a-1+\exp(P_e))} \\ +\exp(P_e)\dfrac{1+(x^*-x_1^*)P_e+\exp\left(-x_2^*P_e\right)-\exp\left(-x_1^*P_e\right)-\exp\left((x^*-x_2^*)P_e\right)}{\beta P_e(x_2^*-x_1^*)(a-1+\exp(P_e))} \\ -\displaystyle\sum_{k=0}^{\infty}\frac{b_{4,k}(x^*)}{s_k}\exp(-s_kt^*), & \text{for } x_1^*\le x^*<x_2^*, \\ \dfrac{\exp(P_e)+(a-1)\exp(x^*P_e)}{\beta P_e(x_2^*-x_1^*)(a-1+\exp(P_e))}\left(P_e(x_2^*-x_1^*)+\exp(-x_2^*P_e)-\exp(-x_1^*P_e)\right) \\ -\displaystyle\sum_{k=0}^{\infty}\frac{b_{4,k}(x^*)}{s_k}\exp(-s_kt^*), & \text{for } x_2^*\le x^*\le 1. \end{cases} \tag{5.87}$$

Equations (5.84)−(5.87) are valid under the condition $P_e(2a^{-1}-1)\neq 0$.

5.3 Results and discussion

First, the results corresponding to the concentrated lateral inflow are discussed thoroughly. The discussion is carried out in two parts depending on the type of the upstream boundary. Then for the results corresponding to the uniformly distributed lateral inflow, the discussion is carried out in two parts based on the flow-discharge responses and the flow-depth responses.

5.3.1 Flow-discharge hydrograph imposed at the upstream end

The results derived for the concentrated lateral inflow in the previous section are compared with those obtained by Fan and Li [19] to ascertain the similarity and differences with respect to the Péclet number and the feedback parameter. The dimensionless form of the flow-discharge response to the unit-step input lateral inflow concentrated at x_0^* for a given flow discharge at the upstream end in a semi-infinite channel can be expressed as (based on [19])

$$\begin{aligned} R_{l,\infty}(x^*,t^*) &= \frac{1}{2}\left(1-\operatorname{erf}\left(\frac{x^*-x_0^*-t^*}{\sqrt{4t^*}}\sqrt{P_e}\right)\right) \\ &+\frac{1}{2}\exp(P_e x^*)\left(1-\operatorname{erf}\left(\frac{x^*+x_0^*+t^*}{\sqrt{4t^*}}\sqrt{P_e}\right)\right) \quad \text{for } x^* > x_0^*. \end{aligned} \quad (5.88)$$

The corresponding response for the flow depth can be calculated, by using Eq. (5.5), as

$$S_{l,\infty}(x^*,t^*) = \frac{1}{\beta}\int_0^{t^*}\left(X^*(x^*)T^*(\tau) - \frac{\partial}{\partial x^*}R_{l,\infty}(x^*,\tau)\right)\mathrm{d}\tau. \quad (5.89)$$

Since the lateral inflow is concentrated at x_0^*, for $x^* \neq x_0^*$, we get $X^*(x^*)T^*(t^*) = 0$ and hence, Eq. (5.89) reduces to

$$S_{l,\infty}(x^*,t^*) = -\frac{1}{\beta}\int_0^{t^*}\frac{\partial}{\partial x^*}R_{l,\infty}(x^*,\tau)\mathrm{d}\tau \text{ for } x^* > x_0^*. \quad (5.90)$$

It is difficult to evaluate this integral analytically. Hence, we use the technique of numerical integration in *MATLAB*. The value of β is kept at 1 since it works only as a scaling factor.

Behavior of the flow-discharge responses for different values of the Péclet number and the feedback parameter

The behavior of the lateral responses of flow discharge in the finite channel, i.e., $R_l(x^*,t^*)$ given in Eq. (5.53) is discussed, and also compared with the response given in Eq. (5.88), for different values of the Péclet number and the feedback parameter. In these comparisons, the results of the finite channel are plotted by continuous curves, and of the semi-infinite channel are plotted by dashed curves. In Figs. 5.2–5.5, the upstream boundary is taken as $Q^*(0,t^*) = 0$, which means there is no perturbation in the flow discharge to the reference value Q_0 at the upstream end.

A comparison between the expressions in Eqs. (5.53) and (5.88) is presented in Fig. 5.2 for different values of the Péclet number and the feedback parameter. In all the comparisons presented, P_e varies from 0.5 to 5 and a varies from 0.5 to 1.5. The responses are

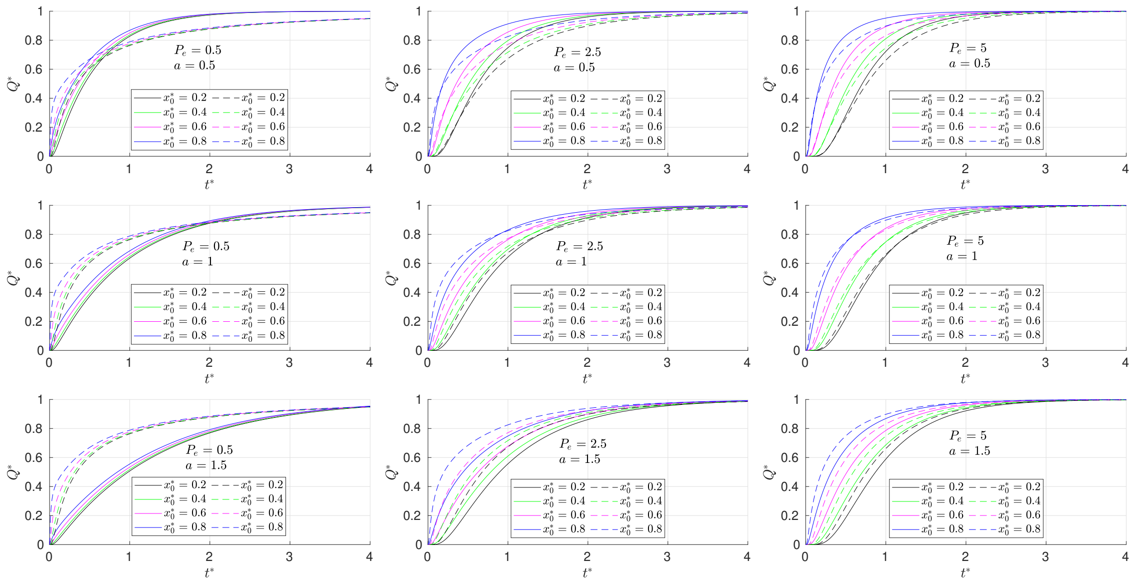

Figure 5.2: Comparison of the flow-discharge response for finite channel given in Eq. (5.53) – (continuous curves) with the flow discharge response for semi-infinite channel given in Eq. (5.88) – (dashed curves) at the downstream end ($x^* = 1$) to the unit-step lateral inflow concentrated at different x_0^* for different values of a and P_e with $Q^*(0, t^*) = 0$

compared at the downstream end ($x^* = 1$) for different lateral inflow locations, i.e., x_0^*. Here, the limiting value is independent of a and P_e, and is equal to 1 for finite channel response as well as for the semi-infinite one. For the finite channel case, the convergence of the flow discharge slows down as the value of a increase, and speeds up as the value of P_e is increased. It is observed here that the semi-infinite channel response can work as a substitute for the finite channel response corresponding to higher Péclet numbers, and when a steady uniform condition is applied at the downstream end, i.e., $a = 1$. In fact, as P_e is increased further for $a = 1$, the responses will be in complete agreement. The semi-infinite channel response does not agree with the finite channel response as a moves away from 1, or if smaller values of P_e are considered. The semi-infinite channel response underestimates the values of flow discharge for $a < 1$ and overestimates for $a > 1$. Here, $a < 1$ means that the coupling between the discharge and flow depth is smaller for $x^* < 1$ as compared to the coupling at $x^* = 1$. Physically, this happens for the cases of small bed slopes as mentioned in [7].

The function given in Eq. (5.53) is plotted in Fig. 5.3 to show the flow-discharge response to the lateral inflow concentrated at $x_0^* = 0.2$ for the subsequent locations of the channel. We observe that the responses corresponding to $P_e = 0.5$ increase suddenly for some time and then converge to the limiting value of 1. Due to this sudden jump in the value of flow discharge, a sharpness in the response is observed for the locations closer to

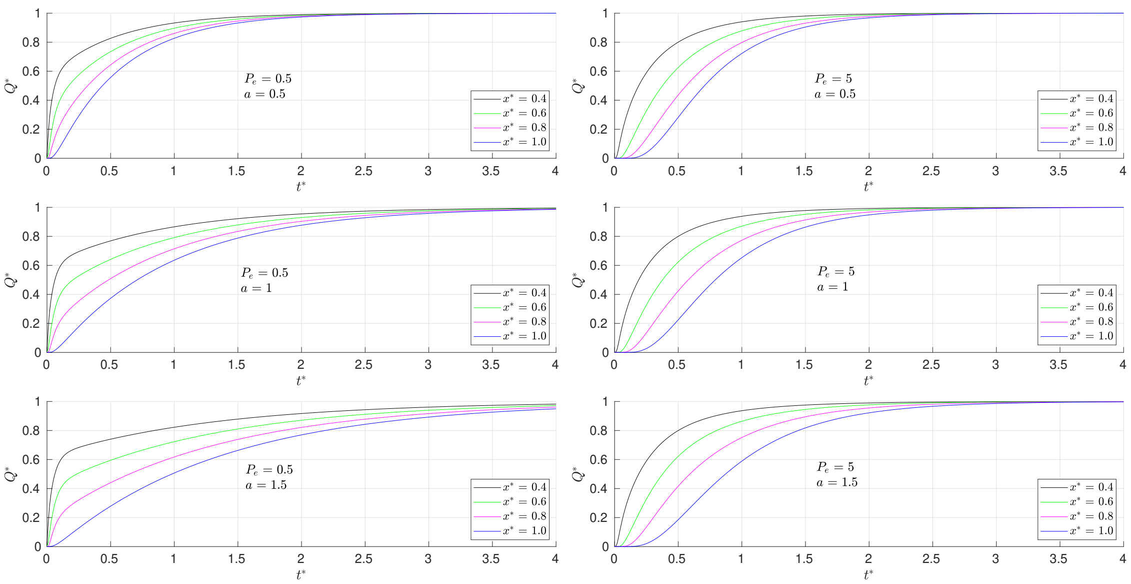

Figure 5.3: Flow-discharge response given in Eq. (5.53) at different locations of the channel to the lateral input given at $x_0^* = 0.2$ for different values of a and P_e with $Q^*(0, t^*) = 0$

the lateral input locations because of the instantaneous input given there. For $P_e = 5$, the responses are very smooth because the effect of the downstream boundary reduces as the Péclet number is increased. It is expected that the pattern will persist for any $P_e > 5$. The responses take more time to converge as the value of a is increased. For a particular case of a and P_e, it takes more time to converge for an observed location as its distance from the lateral input location is increased.

Behavior of the flow-depth responses for different values of the Péclet number and the feedback parameter

The behavior of the lateral responses of flow depth in the finite channel, i.e., $S_l(x^*, t^*)$ given in Eq. (5.54) is discussed, and also compared with the response given in Eq. (5.90), for different values of the Péclet number and the feedback parameter.

The expressions in Eqs. (5.54) and (5.90) are compared at the downstream end ($x^* = 1$) in Fig. 5.4 for different locations of lateral inflow. Here, the limiting value for the finite channel case is dependent on P_e, a, x^* and β. When we fit the expressions given in Eqs. (5.53) and (5.54) in the definition of a, we get $R_l(1, t^*) = \dfrac{\beta}{a} S_l(1, t^*)$ which implies that the flow depth converges to $\dfrac{a}{\beta}$ at the downstream end ($x^* = 1$) as $R_l(x^*, t^*)$ converges to 1 for all values of x. Since β acts as a scaling factor and its value is set to 1, the flow depth converges to a at the downstream end ($x^* = 1$). This is clearly visible from the limiting value of the function given in Eq. (5.54). This means that the flow-depth

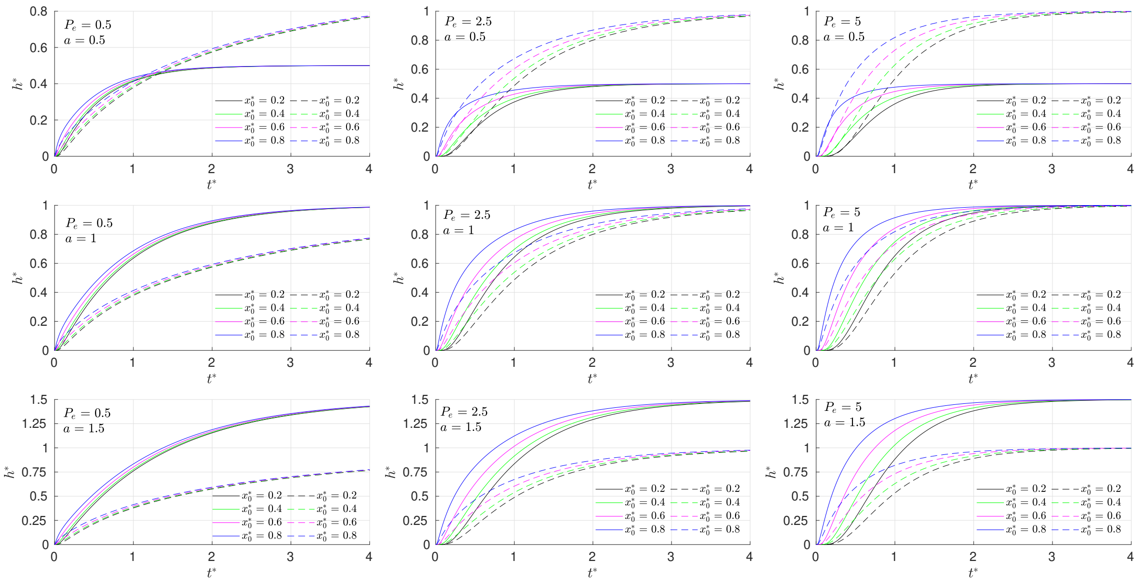

Figure 5.4: Comparison of the flow-depth response for finite channel given in Eq. (5.54) – (continuous curves) with the flow depth response for semi-infinite channel given in Eq. (5.90) – (dashed curves) at the downstream end ($x^* = 1$) to the unit-step lateral input given at different x_0^* for different values of a and P_e with $Q^*(0, t^*) = 0$

responses are more sensitive to the downstream boundary in comparison with the flow-discharge responses. For the semi-infinite channel case, the limit approaches 1 for all the values of P_e. This clearly means that the semi-infinite channel responses do not provide a suitable alternative for the finite channel responses. The closest resemblance between these two responses arises for $P_e = 5$ and $a = 1$, that too is not satisfactory. For $P_e = 0.5$, the responses at the downstream end ($x^* = 1$) for different lateral inputs are almost similar: the effect of the downstream boundary is dominant for smaller values of the Péclet number.

The flow-depth responses given in Eq. (5.54) are plotted in Fig. 5.5 to show the behavior of the responses to a unit-step lateral inflow concentrated at $x_0^* = 0.2$, at the subsequent locations. We observe that the limiting value depends on x^* and due to this, we have different limiting values for different observed locations except for the case $a = 1$ as shown in Fig. 5.5. For $P_e = 0.5$ and $a = 1$, the responses are almost identical, and for $P_e = 5$ and $a = 1$, the responses at $x^* = 0.8$, $x^* = 1$ are very close to each other. For $a = 0.5$, the limiting value slowly decreases along the channel to reach the limiting value 0.5 in contrast to the case $a = 1.5$, where the limiting value increases slowly to reach a.

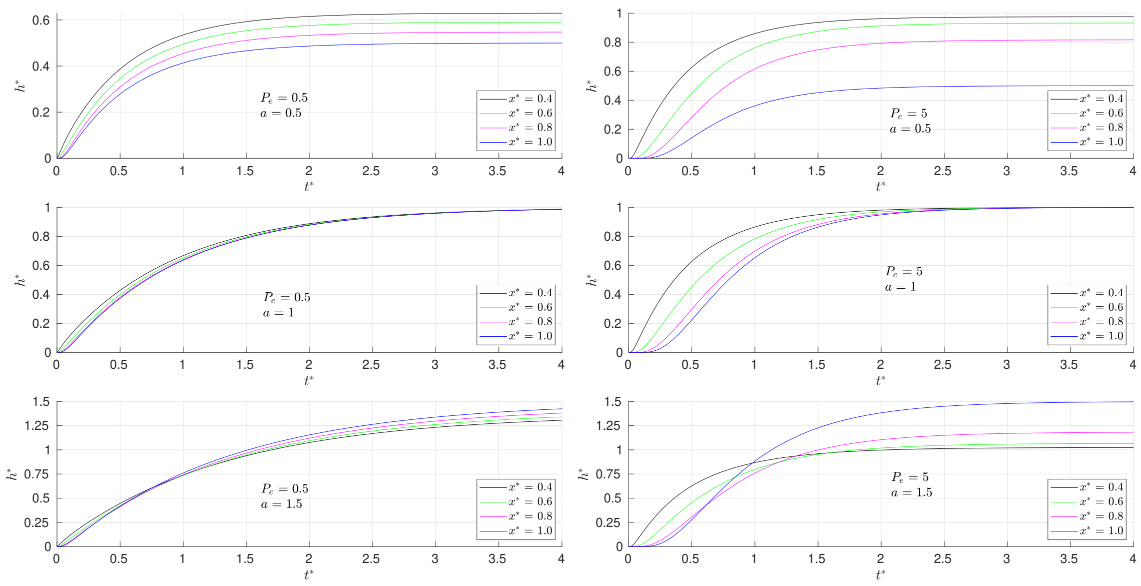

Figure 5.5: Flow-depth response given in Eq. (5.54) at different locations of the channel to the unit-step lateral inflow concentrated at $x_0^* = 0.2$ for different values of a and P_e with $Q^*(0, t^*) = 0$

5.3.2 Flow-depth hydrograph imposed at the upstream end

In this subsection, the results corresponding to the concentrated lateral inflow for a flow-depth-based upstream boundary are discussed. In Figs. 5.6–5.9, $h^*(0, t^*) = 0$, which means there is no perturbation in the flow depth to the reference value h_0 at the upstream end. The finite channel flow-depth responses are compared with the semi-infinite channel flow-depth responses at different locations of the channel with respect to the Péclet number and the feedback parameter. The semi-infinite channel response to the concentrated lateral inflow for a given flow depth at the upstream end can be obtained by solving the system given by Eq. (5.5). Its combined form can be written as

$$-\frac{1}{P_e}\frac{\partial^2 h^*}{\partial x^{*2}} + \frac{\partial h^*}{\partial x^*} + \frac{\partial h^*}{\partial t^*} = \frac{X^*(x^*)T^*(t^*)}{\beta}, \tag{5.91}$$

with $h^*(x^*, 0) = 0$ as the initial condition and $h^*(x^*, t^*)$ given at $x^* = 0$. Following the method used in [19], the flow-depth response to the unit-step lateral inflow concentrated at x_0^* for a given flow depth at the upstream end can be written as

$$N_{l,\infty}(x^*, t^*) = \frac{1}{2\beta P_e}\left\{\text{erfc}\left(\sqrt{\frac{P_e}{4t^*}}\,(x^* - x_0^* - t^*)\right) - \exp\left(P_e x^*\right)\text{erfc}\left(\sqrt{\frac{P_e}{4t^*}}\,(x^* + x_0^* + t^*)\right)\right.$$
$$+ \exp\left(-P_e x_0^*\right)\left\{\text{erfc}\left(\sqrt{\frac{P_e}{4t^*}}\,(x^* + x_0^* - t)\right)\right.$$

$$- \exp\left(P_e x^*\right)\text{erfc}\left(\sqrt{\frac{P_e}{4t^*}}\left(x^* - x_0^* + t^*\right)\right)\Bigg\}\Bigg\}, \quad \text{for} \quad x^* > x_0^*. \tag{5.92}$$

The response of the flow discharge to the unit-step lateral inflow concentrated at x_0^*, when the flow depth is given at the upstream end, can be obtained from

$$M_{l,\infty}(x^*, t^*) = \beta N_{l,\infty}(x^*, t^*) - \frac{\beta}{P_e}\frac{\partial N_{l,\infty}}{\partial x^*}. \tag{5.93}$$

Substituting Eq. (5.92) in Eq. (5.93), we get

$$M_{l,\infty}(x^*, t^*) = \frac{1}{2P_e}\text{erfc}\left(\sqrt{\frac{P_e}{4t^*}}(x^* - x_0^* - t^*)\right) + \frac{\exp\left(-P_e x_0^*\right)}{2P_e}\text{erfc}\left(\sqrt{\frac{P_e}{4t^*}}(x^* + x_0^* - t^*)\right). \tag{5.94}$$

Behavior of the flow-discharge responses for different values of the Péclet number and the feedback parameter

The behavior of the lateral responses of the flow discharge $M_l(x^*, t^*)$ given in Eq. (5.84) is discussed, and also compared with the response given in Eq. (5.94), for different values of the Péclet number and the feedback parameter.

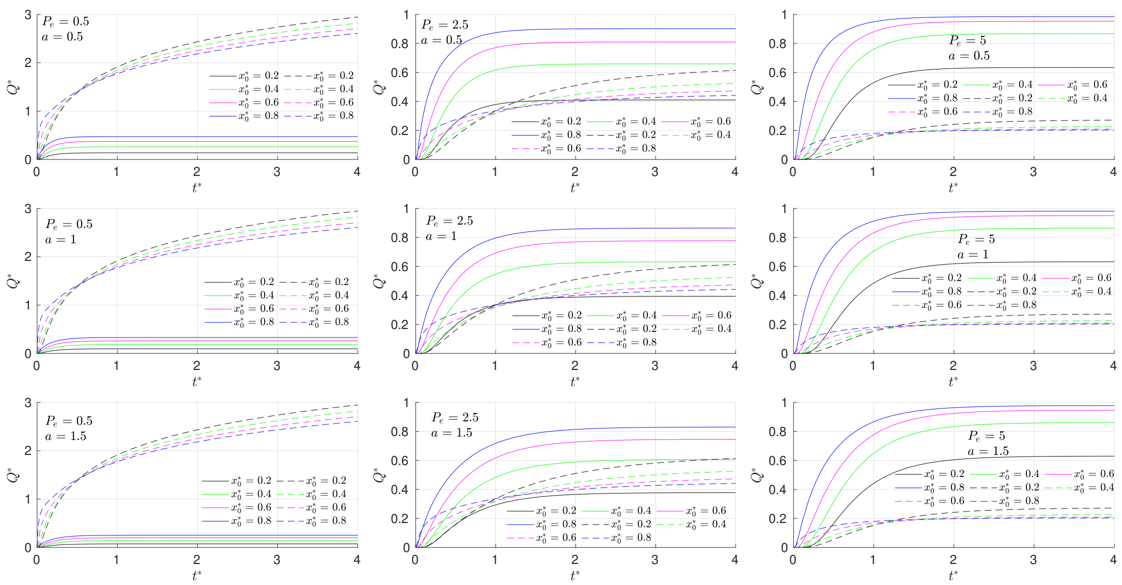

Figure 5.6: Comparison of the flow-discharge response for finite channel given in Eq. (5.84) – (continuous curves) with the flow discharge response for semi-infinite channel given in Eq. (5.94) – (dashed curves) at the downstream end ($x^* = 1$) to the unit-step lateral inflow concentrated at different x_0^* for different values of a and P_e with $h^*(0, t^*) = 0$

In Fig. 5.6, the flow-discharge responses given by Eqs. (5.84) and (5.94) are compared at the downstream end ($x^* = 1$) for different locations of lateral inflow. The limiting value for the finite length channel response is independent of x here, but it depends on P_e, a and x_0^*. The limiting value seems to increase with an increase in x_0^* for all values of a. The difference in the limiting values for different a can be observed by the rate of convergence of these graphs. For $a = 0.5$, the graphs converge faster to the limiting value as compared to the higher values of a. For the highest value of P_e considered, the responses for large values of x_0^* seem to come closer. It is expected that, for some large values of P_e, these responses will be identical to each other because higher values of P_e do not show the backwater effect of the downstream boundary due to which these responses come out almost the same. We can clearly observe that, for a given flow depth at the upstream end, the flow discharge is sensitive to different parameters as well as to the backwater effect induced by the downstream boundary which is not the case for a given flow discharge at the upstream end. The discharge responses for the semi-infinite channel fail to reciprocate the same behavior. In fact, the behavior is reversed for the semi-infinite channel response. Here, for smaller values of x_0^*, a higher limit is observed. But the limiting value does decrease with an increase in P_e whereas the convergence is slower for lower values of P_e. The convergence of the semi-infinite channel responses is slower compared to the finite channel responses in all the cases that are presented here.

In Fig. 5.7, the flow-discharge responses for a unit-step lateral inflow concentrated at $x_0^* = 0.2$ are plotted against time. When we observe these responses at the subsequent downstream locations, a spike appears in the responses for $P_e = 0.5$ corresponding to all values of a. This spike fades away as the observed location moves away from the lateral inflow location and moves toward the downstream boundary. This happens because the sudden rise of the input given at x_0^* is clearly visible on the location closer to it and the effect of the downstream boundary reduces the responses after a certain time. For $P_e = 5$, this behavior is not exhibited since the downstream boundary is not dominant for higher values of P_e. All responses converge to a particular value for different combinations of P_e and a. The convergence limit increases with an increase in P_e but decreases with an increase in a. The convergence also slows down as the value of a increases, and it also takes more time to converge as P_e increases.

Behavior of the flow-depth responses for different values of the Péclet number and the feedback parameter

The behavior of the lateral responses of the flow depth in the finite length channel $N_l(x^*, t^*)$ given in Eq. (5.85) is now discussed, and also compared with the response given in Eq. (5.92), for different values of the Péclet number and the feedback parameter. For studying the lateral responses of the flow depth for flow-depth hydrograph imposed at the upstream end, it is again required to look at the definition of the feedback parameter

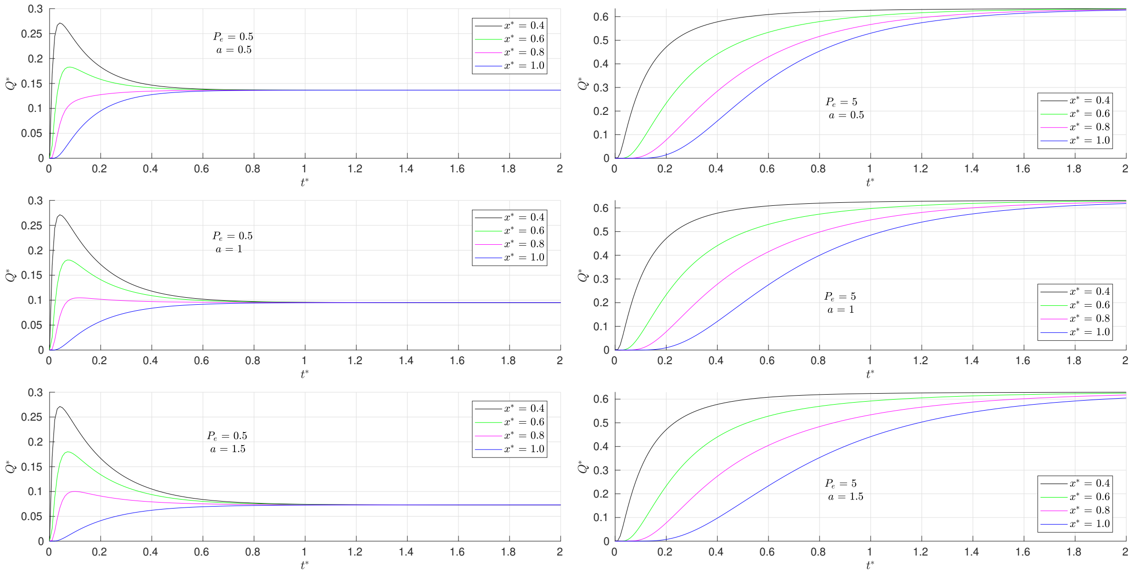

Figure 5.7: Flow-discharge response given in Eq. (5.84) at different locations of the channel to the unit-step lateral inflow concentrated at $x_0^* = 0.2$ for different values of a and P_e with $h^*(0, t^*) = 0$

a. As a consequence, we get $N_l(1, t^*) = \dfrac{a}{\beta} M_l(1, t^*)$. Since β is kept at 1 without loss of generality, the limiting value for the flow-depth response is a times the limiting value of the flow-discharge responses at the downstream end ($x^* = 1$). This is clear from Figs. 5.6 and 5.8.

The flow-depth response $N_l(x^*, t^*)$ given in Eq. (5.85), and the semi-infinite response given in Eq. (5.92), are compared at the downstream end ($x^* = 1$) in Fig. 5.8 for different lateral inflow locations. For the finite channel responses presented in Fig. 5.8, the limiting value slowly increases with an increase in the Péclet number for $a = 0.5$. For a particular value of P_e, the limiting value also increases with an increase in a. The convergence pattern agrees with the results presented earlier. The semi-infinite channel responses again fail to reproduce the results for the finite channel responses. Here, the limiting values decrease with an increase in the Péclet number. In the semi-infinite channel responses, the flow depth grows slowly for smaller values of x_0^* initially but after some time, it increases rapidly as compared to the responses of larger values of x_0^*.

To show the effect of a lateral inflow concentrated at $x_0^* = 0.2$, the flow-depth response given in Eq. (5.85) is plotted in Fig. 5.9 at the subsequent downstream locations. For this case, the flow depth changes with a change in x^* as can be verified from the limiting value of the function given in Eq. (5.85). For all the values of a considered here, the response at the location $x^* = 0.4$ is almost the same for a particular value of P_e. But the responses for the location closer to the downstream end increase with an increase in a and

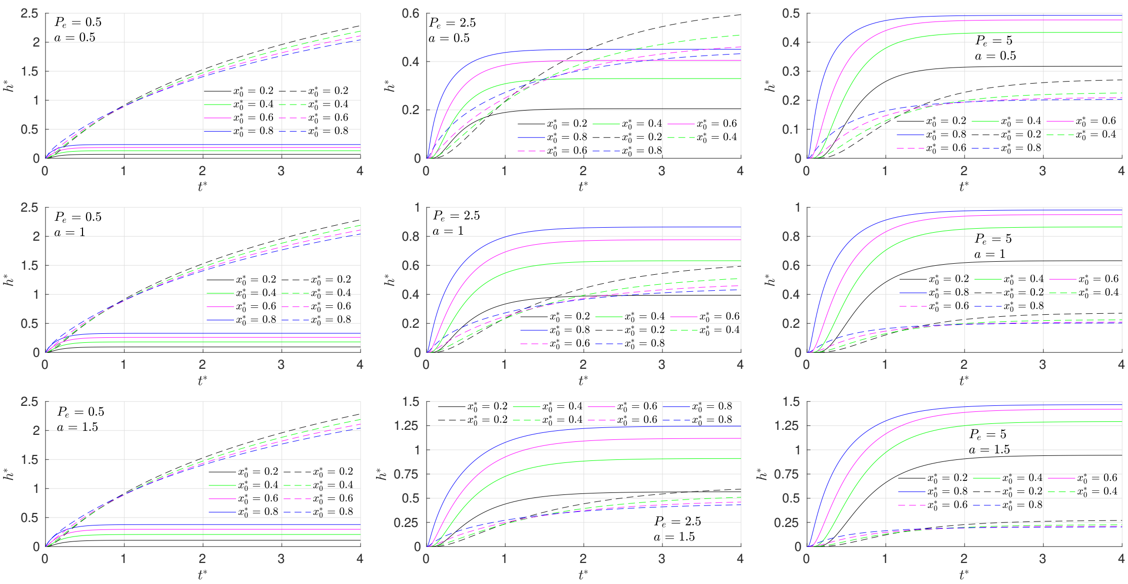

Figure 5.8: Comparison of flow-depth response for finite channel given in Eq. (5.85) − (continuous curves) with the flow depth response for semi-infinite channel given in Eq. (5.92) − (dashed curves) at the downstream end ($x^* = 1$) to the unit-step lateral inflow concentrated at different x_0^* for different values of a and P_e with $h^*(0, t^*) = 0$

converge to the same value for all values of x as a reaches 1. It surpasses the response for $x^* = 0.4$ when a crosses the value of 1. This happens because the effect of the downstream boundary can be felt for all the values of a; even for the highest value of P_e taken here.

For the case of uniformly distributed lateral inflow, the discussion is carried out on the basis of the type of unknown irrespective of the upstream boundary. The unit-step responses derived in the previous section for the case of an uniformly distributed lateral inflow are plotted for the flow discharge and flow depth against time for different values of the Péclet number and the feedback parameter at different channel locations. The lateral inflow is considered to be uniformly distributed between x_1^* and x_2^*. These graphs are plotted for $P_e = 1$, 2.5, 5 and $a = 0.5$, 1, 1.5. The dimensionless width β acts as a scaling factor, keeping its value at 1. The poles for the functions given in Eqs. (5.86), (5.87), (5.55), and (5.56) are evaluated in *MATLAB*, and the graphs are also plotted in *MATLAB*. The responses are not compared with any result since the special cases of the results presented here are already available. Cimorelli et al. [7, 6] have shown a thorough comparison with semi-infinite channel results for the case of a uniform distribution of the lateral inflow along the length of the channel, i.e., $x_1^* = 0$, $x_2^* = 1$.

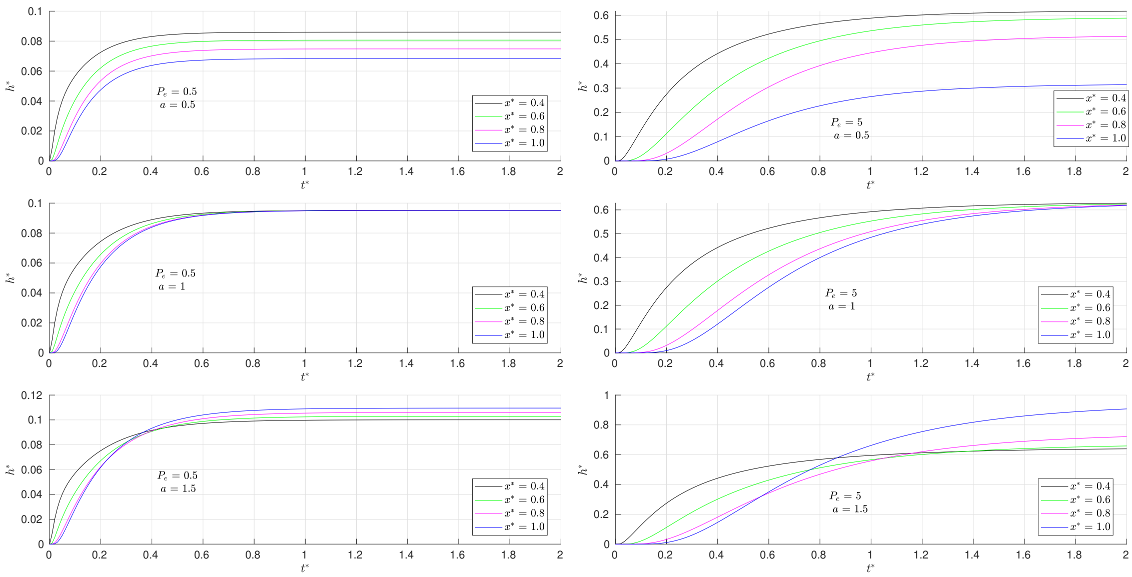

Figure 5.9: Flow-depth response given in Eq. (5.85) at different locations of the channel to the unit-step lateral inflow concentrated at $x_0^* = 0.2$ for different values of a and P_e with $h^*(0, t^*) = 0$

5.3.3 Flow-discharge response to a lateral inflow distributed between locations x_1^* and x_2^*

Here, the behavior of the flow-discharge response to the unit-step lateral inflow for a stage-discharge relationship imposed at the downstream end is discussed for the upstream boundary conditions: a flow-depth hydrograph and a flow-discharge hydrograph. The lateral inflow is uniformly distributed between the locations $x_1^* = 0.4$ and $x_2^* = 0.7$.

In Fig. 5.10, the flow-discharge response to the unit-step lateral inflow uniformly distributed between the locations x_1^* and x_2^* given in Eq. (5.86) is plotted against time at different locations of the channel for different values of P_e and a. For this case, the upstream boundary that is present in terms of a flow-depth hydrograph is considered as zero, i.e., $h^*(0, t^*) = 0$. This means that there is no perturbation in the flow depth at the upstream boundary to the uniform steady value of the flow depth (h_0). The backwater effect induced by the lateral inflow can be observed for the locations upstream to the location x_1^* and also for the locations between x_1^* and x_2^*. For $P_e = 1$, this backwater effect is prominent for the locations closer to x_1^* and slowly fades away as the value of x^* increases. The negative value of the discharge is due to the backwater effect. However, the negative limiting values for the locations closer to the upstream end are due to a flow-depth hydrograph imposed at the upstream end. The lateral inflow starts from the location $x_1^* = 0.4$, and the negative discharge is observed for the locations closer to it.

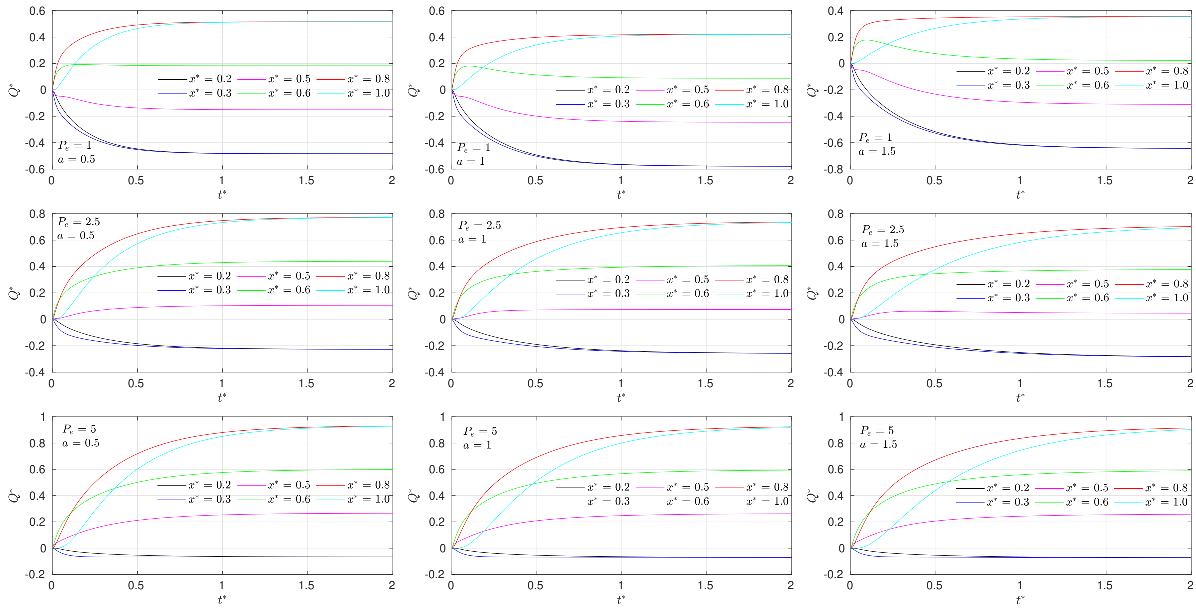

Figure 5.10: Flow-discharge response to the unit-step lateral inflow uniformly distributed between the locations $x_1^* = 0.4$ and $x_2^* = 0.7$, given in Eq. (5.86) at different locations x^* with $h^*(0, t^*) = 0$ and different values of P_e, a

This backwater effect reduces as the value of P_e increases. To get a positive discharge for all the locations in the channel, this response should be studied in combination with the upstream response to a non-zero value of $h^*(0, t^*)$. For the cases $0 \le x^* < x_1^*$ and $x_2^* < x^* \le 1$, the responses converge to a fixed value, increasing with an increase in P_e and decreasing with an increase in a. The change in the limiting values due to a change in the value of a is most visible for the cases with lower values of P_e since the effect of the downstream boundary is more prominent for lower values of P_e. The convergence rate slows down as the value of P_e is increased or the value of a is increased. For the case $x_1^* \le x^* \le x_2^*$, the limiting value for the response given in Eq. (5.86) is dependent on all the parameters, i.e., P_e, a, x^*, x_1^*, x_2^* and it linearly increases with an increase in x^*. But for the cases $0 \le x^* < x_1^*$ and $x_2^* \le x^* \le 1$, the limiting value is dependent on all other parameters except x^*.

In Fig. 5.11, the flow discharge response to the unit-step lateral inflow uniformly distributed between the locations x_1^* and x_2^* given in Eq. (5.55) is plotted against time at different locations of the channel for different values of P_e and a. For this unit-step response, the upstream boundary is taken as zero, which is present in terms of a flow-discharge hydrograph, i.e., $Q^*(0, t^*) = 0$. Physically, this means that there is no perturbation in the discharge at the upstream boundary to the uniform steady condition represented by Q_0. For the locations upstream to the location x_1^*, a dip in the discharge can be observed for

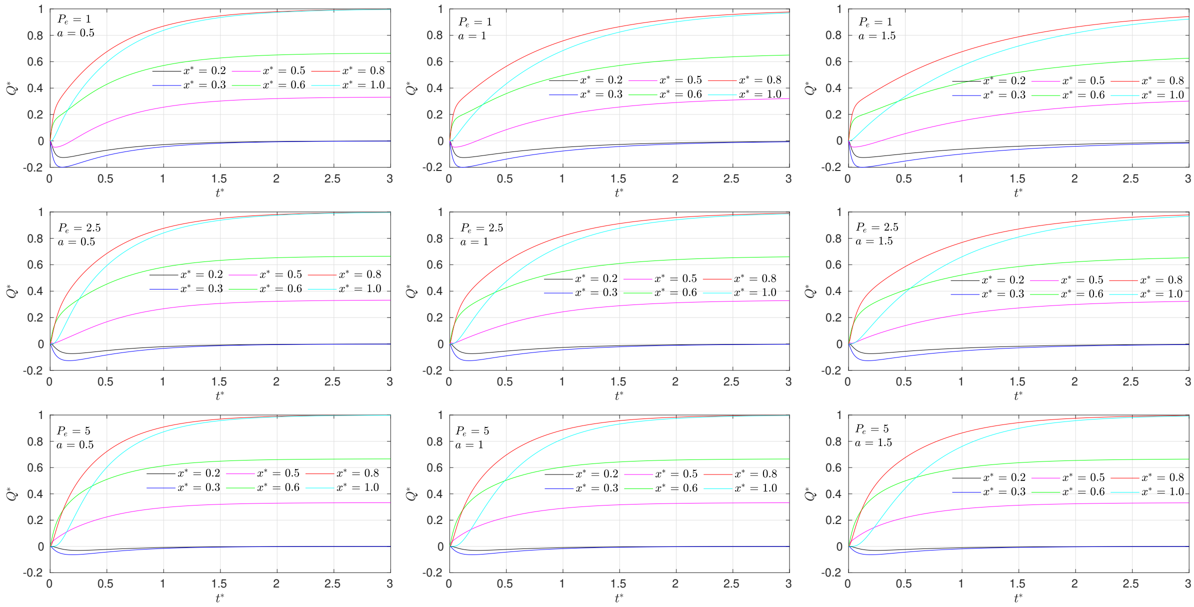

Figure 5.11: Flow-discharge response to the unit-step lateral inflow uniformly distributed between the locations $x_1^* = 0.4$ and $x_2^* = 0.7$, given in Eq. (5.55) at different locations x^* with $Q^*(0,t^*) = 0$ and different values of P_e, a

the initial time, and it slowly reaches zero. This dip is due to the backwater effect induced by the lateral inflow, which is most visible for the locations closer to x_1^*. However, the limiting values reach zero because the discharge at the upstream boundary is zero. This dip slowly fades away as the value of P_e increases, which means that the backwater effect induced by the lateral inflow is most prominent for smaller values of P_e. For $x_2^* < x^* \leq 1$ and lower values of P_e, the discharge increases sharply for some initial time and then slowly approaches the limiting value 1. The convergence rate slows down as the value of a is increased. For the case $0 \leq x^* < x_1^*$, the limiting value reduces to zero while for $x_1^* \leq x^* \leq x_2^*$, the limiting value linearly increases with an increase in x^*, and takes the value 1 for the case $x_2^* \leq x^* \leq 1$. By comparing with the responses presented in Fig. 5.10, it is found that the convergence value is not dependent on all the parameters under consideration. It mainly depends on the locations of the tributary and the observer. This may mean that, as the time approaches infinity, the discharge response for the case of a flow-discharge hydrograph imposed at the upstream end is more robust to the physical conditions of the channel under study in comparison with the flow-discharge response for the case of a flow-depth hydrograph imposed at the upstream end.

When the time variable approaches infinity ($t^* \to \infty$), a comparison between the limiting values of the flow-discharge responses given in Eqs. (5.86) and (5.55) is shown against x^* in Fig. 5.12 for different values of a and a lateral inflow distributed between

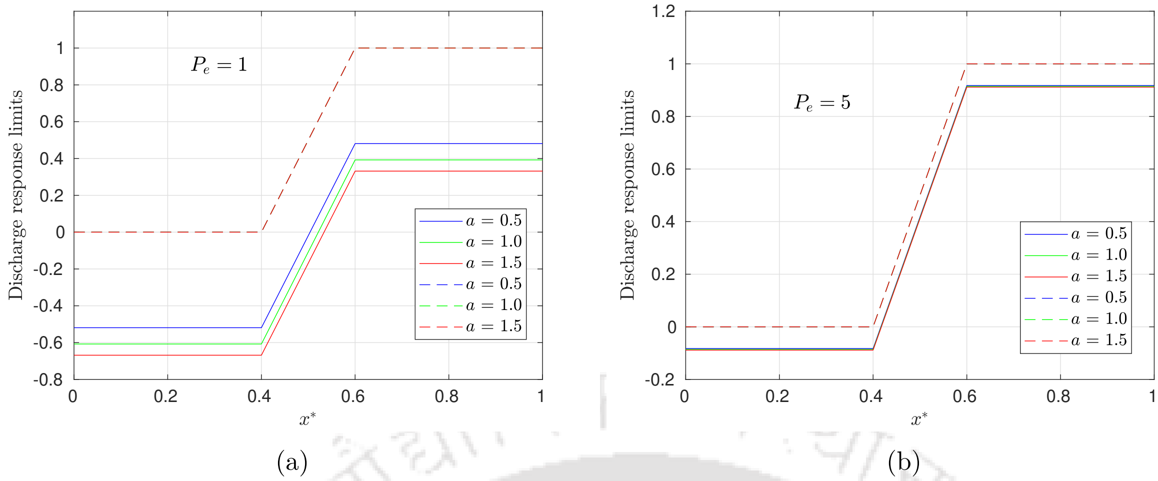

Figure 5.12: Comparison between $\lim\limits_{t^*\to\infty} M_{ld}(x^*, t^*)$ – (continuous curves) with $h^*(0, t^*) = 0$ and $\lim\limits_{t^*\to\infty} R_{ld}(x^*, t^*)$ – (dashed curves) with $Q^*(0, t^*) = 0$, $x_1^* = 0.4$ and $x_2^* = 0.6$ for different values of a: (a) $P_e = 1$, (b) $P_e = 5$

the locations $x_1^* = 0.4$ and $x_2^* = 0.6$. The comparison is shown for two cases: $P_e = 1$ and 5. For smaller values of P_e, a clear difference between the discharge limits for both types of upstream boundaries can be clearly observed. The limits of $M_{ld}(x^*, t^*)$ slowly decrease as the value of a is increased, which means that the discharge within the channel decreases as the feedback parameter increases. But the limits of $L_{ld}(x^*, t^*)$ are unaffected by any change in the downstream boundary condition. For larger values of P_e, the limits of $M_{ld}(x^*, t^*)$ are almost similar for all values of a, which means that the downstream boundary effect starts fading away for this case. For $P_e > 10$, the limits of the responses given in Eqs. (5.86) and (5.55) will be the same, which means that, for these cases, the type of upstream boundary does not matter for large times, i.e., whether it is a flow-depth hydrograph or a flow-discharge hydrograph.

5.3.4 Flow-depth response to a lateral inflow uniformly distributed between locations x_1^* and x_2^*

Here, the flow-depth response to the unit-step lateral inflow for a stage-discharge relationship imposed at the downstream end is discussed for the upstream boundary conditions: a flow-depth hydrograph and a flow-discharge hydrograph. The parameter values are set as the same as the ones described earlier. In Fig. 5.13, the flow depth response to the unit-step lateral inflow uniformly distributed between the locations x_1^* and x_2^* given in Eq. (5.87) is plotted against time at different locations of the channel for different values of P_e and a. For this case, the upstream boundary that is present in terms of a flow-depth hydrograph is considered as zero, i.e., $h^*(0, t^*) = 0$. This means that there is no

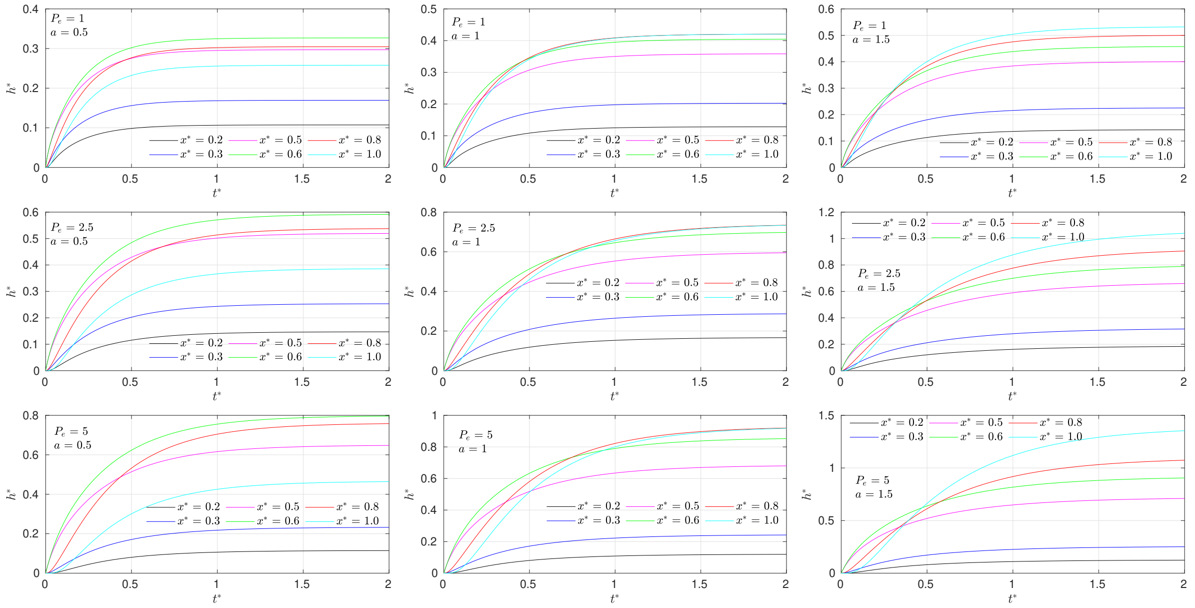

Figure 5.13: Flow-depth response to the unit-step lateral inflow uniformly distributed between the locations $x_1^* = 0.4$ and $x_2^* = 0.7$, given in Eq. (5.87) at different locations x^* with different values of P_e, a and $\beta = 1$, $h^*(0, t^*) = 0$

perturbation in the flow depth at the upstream boundary to the uniform steady value of the flow depth (h_0). At the downstream end ($x^* = 1$), the limiting value of the flow depth response given in Eq. (5.87) is $\dfrac{a}{\beta}$ times the limiting value of flow discharge response given in Eq. (5.86) which satisfies the linearized downstream boundary condition given in Eq. (5.15). The limiting value for the response given in Eq. (5.87) is dependent on all the parameters, i.e., β, P_e, a, x^*, x_1^*, x_2^* for $0 \leq x^* \leq 1$, which shows the sensitivity of the flow depth to all the parameters controlling the flow in the channel. Even for the cases $x^* < x_1^*$ and $x^* > x_2^*$, the limiting value is dependent on the location x^*, which is not the case for the flow-discharge response derived for similar boundary conditions and plotted in Fig. 5.10. As the value of a is increased, the backwater effect of the downstream boundary appears to dominate for $x^* > x_2^*$ due to which, for $a = 1.5$, the limiting value is the highest at the downstream end ($x^* = 1$) for all the values of P_e shown in Fig. 5.13. This is not true for the case $a = 0.5$. This shift in behavior happens as the value of a crosses 1. For $a = 1$, all the responses for $x^* > x_2^*$ converge to a single value, and the case $a = 1$ is a representation of a steady-uniform flow condition imposed at the downstream end. The converging pattern changes accordingly as the downstream boundary deviates from the steady-uniform condition. The backwater effect of the lateral inflow can be seen for the locations upstream to the location x_1^*, where the flow depth is increased despite the presence of a zero upstream boundary condition. The maximum value of the limiting

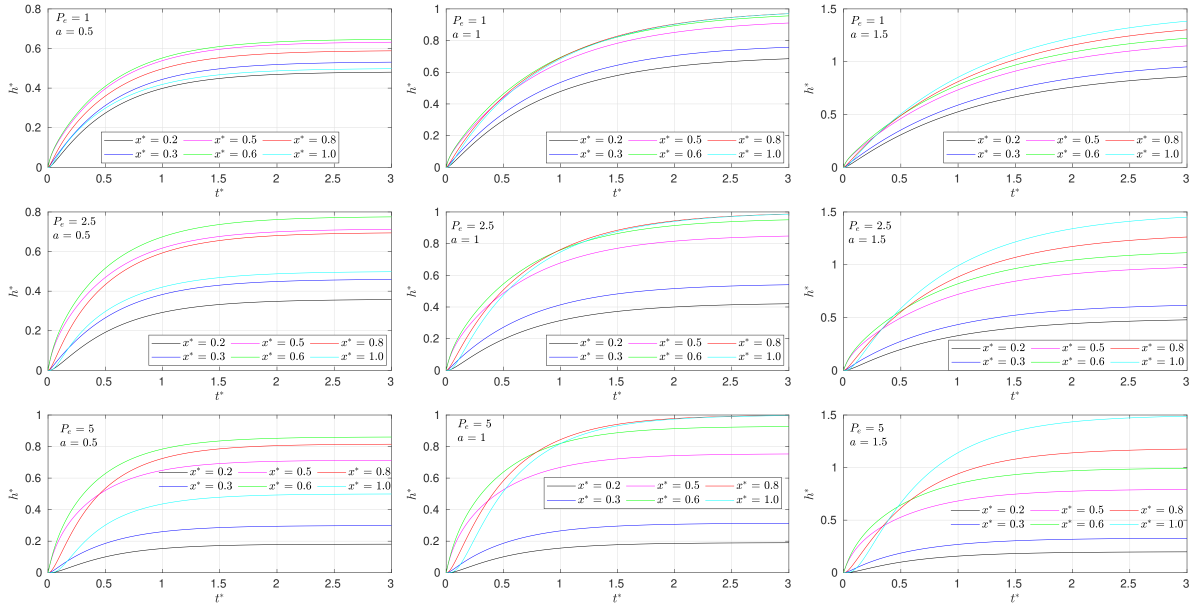

Figure 5.14: Flow-depth response to the unit-step lateral inflow uniformly distributed between the locations $x_1^* = 0.4$ and $x_2^* = 0.7$, given in Eq. (5.56) at different locations x^* with $Q^*(0,t^*) = 0$ and different values of P_e, a

value of the flow depth is different for different values of a. For $a = 0.5$, higher values for the flow depth are observed for the locations between x_1^* and x_2^*, viz., $x^* = 0.6$. As the value of a is increased, the backwater effect of the downstream boundary is dominant than the backwater effect of the lateral inflow. Due to this, the highest values for the flow depth are obtained at the downstream end.

In Fig. 5.14, the flow-depth response to the unit-step lateral inflow uniformly distributed between the locations x_1^* and x_2^* given in Eq. (5.56) is plotted against time at different locations of the channel for different values of P_e and a. For this case, no perturbation in the uniform steady reference condition Q_0 is considered at the upstream boundary. This means the upstream boundary is considered to be zero, i.e., $Q^*(0,t^*) = 0$. The convergence limit for the flow depth at the downstream end ($x^* = 1$) satisfies the downstream boundary condition given in Eq. (5.15) since it is a multiple of the limiting value of the flow-discharge response at $x^* = 1$ given in Eq. (5.55) by a factor of $\dfrac{a}{\beta}$. Since the value of β is kept at 1, the flow-depth responses at the downstream end ($x^* = 1$) approach a. Although the limiting value for the case $0 \leq x^* \leq x_2^*$ is dependent on all the parameters under consideration, but for $x_2^* \leq x^* \leq 1$, the limiting value is independent of the location of the lateral inflow. This is not the case for the flow-depth response obtained for a flow-depth hydrograph given at the upstream end. This means that, whether it is the flow discharge or the flow depth, the effect of the location of the lateral inflow cannot be observed for locations $x^* > x_2^*$ if a flow-discharge hydrograph is given at the upstream end. This shows the robustness of the models designed with a flow-discharge hydrograph imposed at the upstream end. The flow-depth responses slowly increase as the value of x^* is increased for $0 \leq x^* \leq x_2^*$, and then it decreases for $x^* > x_2^*$ corresponding to $a < 1$. However, for $a > 1$, the responses for $x^* > x_2^*$ slowly increase but for $a = 1$, these responses reach the limiting value 1. For $x^* > x_2^*$, the effect of the downstream boundary is more dominant than the effect of the lateral inflow. Due to this, the limiting values increase for higher values of a because the coupling between the flow discharge and the flow depth at the downstream end is more in comparison with the locations within the channel [7]. The increase in the flow depth at the locations upstream to the locations of the lateral inflow can be observed for all the cases plotted in Fig. 5.14. The magnitude of the flow depth is higher along the whole channel in comparison with the flow depth plotted in Fig. 5.13. Similar to the plot presented in Fig. 5.13, for $a = 0.5$, higher value of the flow depth is observed for a location between x_1^* and x_2^*. This is not true for $a \geq 1$ since, for these cases, the highest value of the flow depth is obtained at the downstream end ($x^* = 1$). This means that, for both types of upstream boundaries, the effect of the downstream boundary is prominent for the flow depth.

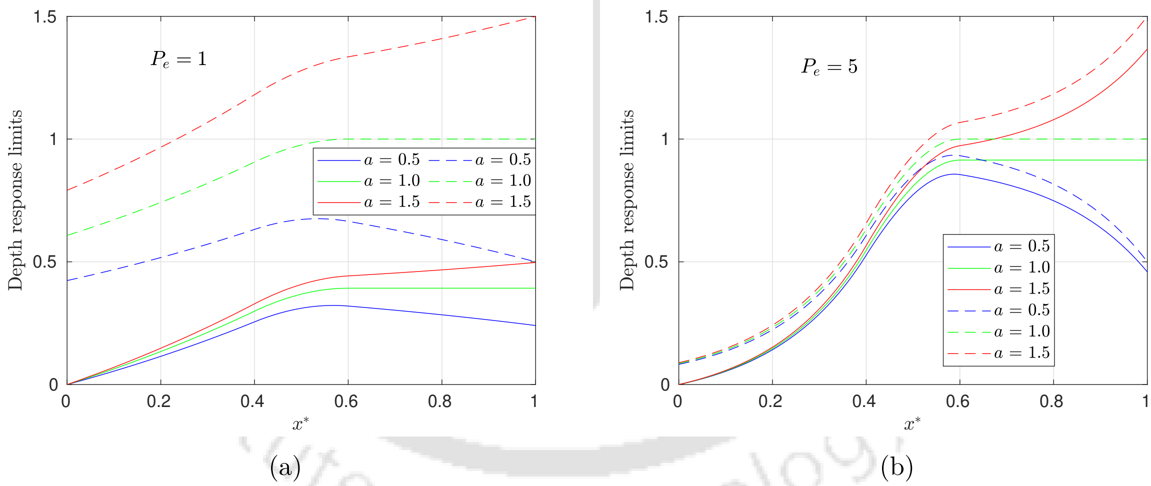

Figure 5.15: Comparison between $\lim_{t^* \to \infty} N_{ld}(x^*, t^*)$ – (continuous curves) with $h^*(0, t^*) = 0$ and $\lim_{t^* \to \infty} S_{ld}(x^*, t^*)$ – (dashed curves) with $Q^*(0, t^*) = 0$, $x_1^* = 0.4$ and $x_2^* = 0.6$, for different values of a: (a) $P_e = 1$, (b) $P_e = 5$

When the time variable approaches infinity ($t^* \to \infty$), a comparison between the limiting values of the depth responses given in Eqs. (5.87) and (5.56) is shown in Fig. 5.15 against x^* for different values of a and a lateral inflow distributed between the locations $x_1^* = 0.4$ and $x_2^* = 0.6$. The comparison is shown for two cases: $P_e = 1$ and 5. For $P_e = 1$, a clear difference between the depth limits for both types of upstream boundaries can be clearly observed. The limiting values for $S_{ld}(x^*, t^*)$ are much higher than those for

$N_{ld}(x^*, t^*)$ in the channel. The limits of both functions increase as the value of a increases. This shows the sensitivity of the flow depth to the presence of the downstream boundary irrespective of the type of the upstream boundary. For $P_e = 5$, these response limits come quite close to each other for $x_1^* \leq x^* \leq x_2^*$, and then slowly approach a for $x^* > x_2^*$. For these values of x_1^* and x_2^* and $P_e > 10$, these limits will coincide with each other, and the type of upstream boundary condition will not matter. But, the effect of the downstream boundary is visible on the flow depth even for higher values of P_e.

5.4 Conclusion

An analytical solution for the diffusive wave model with a concentrated lateral inflow and a uniformly distributed lateral inflow has been presented with a focus on studying the impact of the lateral inflow on the flow discharge and the flow depth in a finite length channel. The feedback parameter a controlling the downstream boundary with $0.6 \leq a \leq 1.3$ can represent most of the physically present downstream boundary conditions [6]. The upstream responses for both types of upstream boundary conditions are already presented by Cimorelli et al. [7, 6]. The lateral inflow given by them is found to be a particular case of the results presented in this work by considering $x_1^* = 0$ and $x_2^* = 1$. Results presented here can be used with the upstream responses given in [7, 6]. The concentrated lateral inflow can represent the case of lateral inflow from a tributary whose width is negligible in comparison with the length of the channel under study and it is mathematically represented by using the Dirac delta function, whereas the uniformly distributed lateral inflow between any locations x_1^* and x_2^* can represent the cases of fixed-width tributaries of a channel.

The responses of the flow discharge and the flow depth to the concentrated lateral inflow results were compared with the semi-infinite channel responses with the respective upstream boundaries imposed. The semi-infinite channel responses failed to reproduce satisfactory results for finite channel in many cases. The semi-infinite channel responses can be used to predict flow discharge in finite channels when a flow discharge is imposed at the upstream boundary and a steady uniform condition is applied at the downstream boundary, that too for higher Péclet numbers. If the flow depth is given at the upstream end or lower values of the Péclet number are considered, the semi-infinite channel responses are not appropriate approximations for finite channel responses. When the flow depth was applied at the upstream end, the finite channel responses were more sensitive to different parameters, viz., the location of the lateral inflow, the location of observation, the Péclet number and the backwater effect induced by the downstream boundary.

For the flow-discharge and the flow-depth responses corresponding to the uniformly distributed lateral inflow, for a given flow-depth hydrograph at the upstream end, the convergence rate for the flow discharge and the flow depth slows down if the value of P_e was increased as opposed to the case of a flow-discharge hydrograph given at the upstream end where the convergence rate increased if the value of P_e was increased. The responses for the case of a flow-depth hydrograph given at the upstream end were found to be more sensitive to the parameter controlling the channel flow. However, as time approached infinity, the flow-discharge responses for $x^* > x_2^*$ were independent of the location of the observation. This was not the case for a flow-discharge hydrograph given at the upstream end. For this case, the flow-discharge and flow-depth responses for $x^* > x_2^*$ were independent of the location of the lateral inflow, and in addition to that, the limiting value for the flow-discharge response was independent of all the parameters. For $0 \leq x^* \leq x_2^*$, the backwater effect induced by the lateral inflow could be observed for lower values of the Péclet number in the responses of the flow discharge as well as the responses of the flow depth. For a flow-depth hydrograph imposed at the upstream end, this backwater effect on locations close to x_1^* was more prominent. As the value of x^* was increased, the responses for the flow discharge slowly increased and then reduced for $x^* > x_2^*$ before it converged to a particular value. However, the responses for the flow depth showed a different type of behavior for $x^* > x_2^*$ as the value of a was increased. The responses for $x^* > x_2^*$ increased as the value of a crossed 1 and decreased for $a < 1$. This shows the sensitivity of the flow depth to the downstream boundary compared with the flow discharge. In addition to this, for P_e upto 5, and $a < 1$, higher values for the flow depth were observed for the locations between x_1^* and x_2^*, while for $a \geq 1$, the highest values for the flow depth were observed at the downstream end ($x^* = 1$). This is not true for the flow discharge for similar values of P_e, where higher values were observed for $x^* > x_2^*$ which was closer to the location x_2^*.

CHAPTER 6

Conclusion and future directions

This chapter provides a concise overview of the findings and contributions made by this thesis. Additionally, it offers a glance into the future research works and expansions of the current study.

6.1 Conclusion

In this thesis, the effect of different types of lateral inflow is studied in a finite length channel subject to different types of boundary conditions.

Chapter 2 is focused on the analytical solution for the complete linearized Saint-Venant equations for a uniformly distributed lateral inflow in a rectangular channel of finite length. The upstream and downstream boundaries are present in terms of a flow-discharge hydrograph. The flow is linearized around a steady-uniform reference condition and the series form solution is presented for the flow discharge. From the study of the behavior of the flow discharge for different physical parameters, it is observed that the flow discharge in the channel is highly sensitive to the consideration of the reference flow discharge. The selection of the reference flow discharge is dependent on the slope of the channel bed. The results are compared with the semi-infinite channel results which were found to be satisfactory for some cases. But the interpretation of the semi-infinite channel is also dependent on the slope of the channel. For different slopes, different channel lengths can be considered as semi-infinite channel. The results presented in this chapter may be preferred over semi-infinite channel results for the evaluation of the flow discharge for smaller values of the slopes.

In *Chapter 3*, an analytical solution for the diffusive wave model is derived for a prismatic channel. Two types of upstream boundaries are considered: a flow-discharge hydrograph and a flow-depth hydrograph. The downstream boundary is considered as a flow-depth hydrograph. The solution for the diffusive wave model is presented by considering two different types of lateral inflow: a concentrated lateral inflow and a uniformly distributed lateral inflow between any two locations of the channel. The results are discussed for different values of the Péclet number, and some of them are also compared with the corresponding semi-infinite channel responses to bring out the importance of the downstream boundary. From a thorough analysis, the flow depth is found to be more sensitive to the downstream boundary in comparison with the flow discharge. The backwater effect induced due to the downstream boundary and the lateral inflow is more dominant for lower values of the Péclet number. The semi-infinite channel also failed to approximate the finite channel results for lower values of the Péclet number. For Péclet number close to 5, the semi-infinite channel responses were found an appropriate approximation to estimate flow discharge in a finite length channel but that is not the case for the flow depth.

Chapter 4 focuses on the analytical solution of the diffusive wave model for a prismatic channel with a flow-depth hydrograph considered at the upstream end, and a flow-discharge hydrograph considered at the downstream end. Two different lateral inflows are considered: a concentrated lateral inflow and a uniformly distributed lateral inflow between any two locations along the channel length. The flow properties are analyzed for different values of the Péclet number and various locations of the lateral inflow. Some of the responses are compared with the corresponding semi-infinite channel responses wherever possible. In contrast to the result obtained in *Chapter 3*, the semi-infinite channel results did not give satisfactory approximation for the finite channel results. The flow depth is found to be highly sensitive to any change in the flow discharge at the downstream end. The backwater effect induced due to a flow-discharge-based downstream boundary shows different behavior than the one induced due to a flow-depth-based downstream boundary.

In *Chapter 5*, an analytical solution for the diffusive wave model is derived for a prismatic channel by considering two types of upstream boundaries: a flow-discharge hydrograph and a flow-depth hydrograph. The downstream boundary is considered as a stage-discharge relationship and it is controlled by a term called feedback parameter which, when in the range 0.6 to 1.3 can accommodate a wide range of downstream boundaries present in river flow. The solution for the diffusive wave model is presented by considering two different types of lateral inflows: a concentrated lateral inflow and a uniformly distributed lateral inflow between any two locations of the channel. This chapter is mainly focused on the effect of the lateral inflows on the flow discharge and the flow depth corresponding to both types of upstream boundaries. The results corresponding to the concentrated lateral inflow are also compared with the respective semi-infinite channel responses. Similar to the observation found in *Chapters 3* and *4*, the flow depth is more sensitive to the downstream boundary than the flow discharge. The convergence rate for the flow discharge and the flow depth is found to be dependent on the type of the upstream boundary. The behavior of the unit-step responses is shown for a steady state condition. This comparison shows that the flow discharge is insensitive to all the parameters for large times. The results corresponding to a flow-depth type upstream boundary bring out the sensitivity of the dependent variables to the physical parameters more clearly.

6.2 Future works

Here, we provide some ideas how the current research can be extended.

1. In all the problems considered in this thesis, the initial condition is taken as zero. A non-zero initial condition does contribute to change in the flow behavior upto some extent. Therefore, all these problems can be extended to combine the effect of the initial conditions in addition to the considered boundary conditions and lateral inflows.

2. For all the considered problems, the unknown variables are linearized around a steady uniform reference condition. In this study, we found that the flow depth is more often dependent on the location of observation than the flow discharge. So, a steady non-uniform condition, which includes a steady uniform flow discharge and a steady non-uniform flow depth as the reference value, may help in providing better approximation of the dependent variables.

3. To find the solution for a space- and time-dependent lateral inflow, we have used the diffusive wave model which exhibits less complexity than the complete Saint-Venant equations. The methodology followed in *Chapters 3–5* may be tried on the complete Saint-Venant equations. This will increase the mathematical complexity of the problem, but might provide solutions for a wider range of channel flows.

Bibliography

[1] M. Abramowitz and I. A. Stegun. *Handbook of Mathematical Functions with Formulas, Graphs, and Mathematical Tables*, volume 55. US Government Printing Office, Washington D.C., 1948.

[2] L. V. Ahlfors. *Complex Analysis: An Introduction to the Theory of Analytic Functions of One Complex Variable*, volume 331. McGraw-Hill, University of Minnesota, 1979.

[3] W. Brutsaert. Review of Green's functions for linear open channel. *Journal of the Engineering Mechanics Division*, 99(6):1247–1257, 1973. `https://doi.org/10.1061/JMCEA3.0001836`.

[4] H. Chanson. *Hydraulics of Open Channel Flow*. Elsevier, Oxford, 2004. `https://doi.org/10.1016/B978-0-7506-5978-9.X5000-4`.

[5] W.-H. Chung, A. A. Aldama, and J. A. Smith. On the effects of downstream boundary conditions on diffusive flood routing. *Advances in Water Resources*, 16(5):259–275, 1993. `https://doi.org/10.1016/0309-1708(93)90018-B`.

[6] L. Cimorelli, L. Cozzolino, A. D'Aniello, and D. Pianese. Exact solution of the Linear Parabolic Approximation for flow-depth based diffusive flow routing. *Journal of Hydrology*, 563:620–632, 2018. `https://doi.org/10.1016/j.jhydrol.2018.06.026`.

[7] L. Cimorelli, L. Cozzolino, R. Della Morte, and D. Pianese. Analytical solutions of the linearized parabolic wave accounting for downstream boundary condition and uniform lateral inflows. *Advances in Water Resources*, 63:57–76, 2014. `https://doi.org/10.1016/j.advwatres.2013.11.003`.

[8] L. Cimorelli, L. Cozzolino, R. Della Morte, D. Pianese, and V. P. Singh. A new frequency domain analytical solution of a cascade of diffusive channels for flood routing. *Water Resources Research*, 51(4):2393–2411, 2015. https://doi.org/10.1002/2014WR016192.

[9] A. Crosato. *Analysis and Modelling of River Meandering*. IOS Press, Amsterdam, 2008.

[10] J. A. Cunge, F. M. Holly, and A. Verwey. *Practical Aspects of Computational River Hydraulics*. Pitman, Boston, 1980.

[11] B. de Saint-Venant. Theory of unsteady water flow, with application to river floods and to propagation of tides in river channels. *French Academy of Science*, 73(99):148–154, 1871.

[12] C. Di Cristo, M. Iervolino, T. Moramarco, and A. Vacca. Applicability of diffusive model for mud-flows: An unsteady analysis. *Journal of Hydrology*, 600:126512, 2021. https://doi.org/10.1016/j.jhydrol.2021.126512.

[13] C. Di Cristo, M. Iervolino, and A. Vacca. Greens function of the linearized Saint-Venant equations in laminar and turbulent flows. *Acta Geophysica*, 60:173–190, 2012. https://doi.org/10.2478/s11600-011-0039-8.

[14] C. Di Cristo, M. Iervolino, and A. Vacca. Applicability of kinematic, diffusion, and quasi-steady dynamic wave models to shallow mud flows. *Journal of Hydrologic Engineering*, 19(5):956–965, 2014. https://doi.org/10.1061/(ASCE)HE.1943-5584.0000881.

[15] G. Doetsch. *Guide to the Applications of Laplace Transforms*. D. Van Nostrand, New York, 1961.

[16] J. Dooge and J. Napiórkowski. The effect of the downstream boundary conditions in the linearized St Venant equations. *The Quarterly Journal of Mechanics and Applied Mathematics*, 40(2):245–256, 1987. https://doi.org/10.1093/qjmam/40.2.245.

[17] J. Dooge, J. Napiórkowski, and W. Strupczewski. The linear downstream response of a generalized uniform channel. *Acta Geophysica Polonica*, 35(3):277–291, 1987.

[18] G. Duró, A. Crosato, and P. Tassi. Numerical study on river bar response to spatial variations of channel width. *Advances in Water Resources*, 93:21–38, 2016. https://doi.org/10.1016/j.advwatres.2015.10.003.

[19] P. Fan and J. Li. Diffusive wave solutions for open channel flows with uniform and concentrated lateral inflow. *Advances in Water Resources*, 29(7):1000–1019, 2006. `https://doi.org/10.1016/j.advwatres.2005.08.008`.

[20] J. D. Fenton. Flood routing methods. *Journal of Hydrology*, 570:251–264, 2019. `https://doi.org/10.1016/j.jhydrol.2019.01.006`.

[21] M. Franchini and E. Todini. PABL: a parabolic and backwater scheme with lateral inflow and outflow. In *Fifth IAHR International Symposium on Stochastic Hydraulics, Birmingham*, pages 1–12, 1988. Report No. 10.

[22] S. Hayami. On the propagation of flood waves. *Bulletins-Disaster Prevention Research Institute, Kyoto University*, 1:1–16, 1951.

[23] P.-C. Huang. Establishing a time-varying flood-wave impulse function combined with a dynamic machine-learning technique in response to the disturbance of boundary conditions. *Journal of Flood Risk Management*, 16(4):e12941, 2023. `https://doi.org/10.1111/jfr3.12941`.

[24] P.-C. Huang and K. T. Lee. Channel hydrological response function considering inflow conditions and hydraulic characteristics. *Journal of Hydrology*, 591:125546, 2020. `https://doi.org/10.1016/j.jhydrol.2020.125546`.

[25] P.-C. Huang and K. T. Lee. Channel-flow response function considering the downstream tidal effect and hydraulic characteristics. *Journal of Hydrology*, 603:126827, 2021. `https://doi.org/10.1016/j.jhydrol.2021.126827`.

[26] C. M. Kazezyilmaz-Alhan. An improved solution for diffusion waves to overland flow. *Applied Mathematical Modelling*, 36(9):4165–4172, 2012. `https://doi.org/10.1016/j.apm.2011.11.045`.

[27] C. M. Kazezyilmaz-Alhan and M. A. Medina. Kinematic and diffusion waves: Analytical and numerical solutions to overland and channel flow. *Journal of Hydraulic Engineering*, 133(2):217–228, 2007. `https://doi.org/10.1061/(ASCE)0733-9429(2007)133:2(217)`.

[28] G. Kefayati, A. Tolooiyan, and A. P. Dyson. Finite difference lattice Boltzmann method for modeling dam break debris flows. *Physics of Fluids*, 35(1):013102, 01 2023. `https://doi.org/10.1063/5.0130947`.

[29] S. LeRoy K. The relation of hydrographs of runoff to size and character of drainage-basins. *Eos, Transactions American Geophysical Union*, 13(1):332–339, 1932. `https://doi.org/10.1029/TR013i001p00332`.

[30] M. J. Lighthill and G. B. Whitham. On kinematic waves I. Flood movement in long rivers. *Proceedings of the Royal Society of London. Series A. Mathematical and Physical Sciences*, 229(1178):281–316, 1955. `https://doi.org/10.1098/rspa.1955.0088`.

[31] R. K. Linsley Jr, M. A. Kohler, and J. L. Paulhus. *Hydrology for Engineers*. McGraw-Hill, New York, 1975.

[32] X. Litrico and V. Fromion. Analytical approximation of open-channel flow for controller design. *Applied Mathematical Modelling*, 28(7):677–695, 2004. `https://doi.org/10.1016/j.apm.2003.10.014`.

[33] X. Litrico and V. Fromion. Frequency modeling of open-channel flow. *Journal of Hydraulic Engineering*, 130(8):806–815, 2004. `https://doi.org/10.1061/(ASCE)0733-9429(2004)130:8(806)`.

[34] X. Litrico and V. Fromion. Simplified modeling of irrigation canals for controller design. *Journal of Irrigation and Drainage Engineering*, 130(5):373–383, 2004. `https://doi.org/10.1061/(ASCE)0733-9437(2004)130:5(373)`.

[35] R. Mizanur Rashid and M. H. Hanif Chaudhry. Flood routing in channels with flood plains. *Journal of Hydrology*, 171(1):75–91, 1995. `https://doi.org/10.1016/0022-1694(95)02693-J`.

[36] K. Mizumura. Analytical solution of nonlinear diffusion wave model. *Journal of Hydrologic Engineering*, 17(7):782–789, 2012. `https://doi.org/10.1061/(ASCE)HE.1943-5584.0000511`.

[37] T. Moramarco, Y. Fan, and R. L. Bras. Analytical solution for channel routing with uniform lateral inflow. *Journal of Hydraulic Engineering, ASCE*, 125(7):707–713, 1999. `https://doi.org/10.1061/(ASCE)0733-9429(1999)125:7(707)`.

[38] R. Moussa. Analytical Hayami solution for the diffusive wave flood routing problem with lateral inflow. *Hydrological Processes*, 10(9):1209–1227, 1996. `https://doi.org/10.1002/(SICI)1099-1085(199609)10:9<1209::AID-HYP380>3.0.CO;2-2`.

[39] R. Moussa and C. Bocquillon. Algorithms for solving the diffusive wave flood routing equation. *Hydrological Processes*, 10(1):105–123, 1996. `https://doi.org/10.1002/(SICI)1099-1085(199601)10:1<105::AID-HYP304>3.0.CO;2-P`.

[40] S. Munier, X. Litrico, G. Belaud, and P. Malaterre. Distributed approximation of open-channel flow routing accounting for backwater effects. *Advances in Water Resources*, 31(12):1590–1602, 2008. `https://doi.org/10.1016/j.advwatres.2008.07.007`.

[41] J. J. Napiórkowski. Chapter 1 - Linear Theory of Open Channel Flow. In *Advances in Theoretical Hydrology*, European Geophysical Society Series on Hydrological Sciences, pages 3–15. Elsevier, Amsterdam, 1992. `https://doi.org/10.1016/B978-0-444-89831-9.50008-9`.

[42] B. Nazari and D.-J. Seo. Symbolic explicit solutions for 1-Dimensional linear diffusive wave equation with lateral inflow and their applications. *Water Resources Research*, 57(3):e2019WR026906, 2021. `https://doi.org/10.1029/2019WR026906`.

[43] L. Ridolfi, A. Porporato, and R. Revelli. Greens function of the linearized de Saint-Venant equations. *Journal of engineering mechanics*, 132(2):125–132, 2006. `https://doi.org/10.1061/(ASCE)0733-9399(2008)134:9(809.2)`.

[44] A. I. Saichev and W. A. Woyczynski. *Distributions in the Physical and Engineering Sciences, Volume 1, Distributional and Fractal Calculus, Integral Transforms and Wavelets*. Springer, 1997. `https://doi.org/10.1007/978-1-4612-4158-4`.

[45] P. Sarkhosh, A. Salama, and Y.-C. Jin. A one-dimensional semi-implicit finite volume modeling of non-inertia wave through rockfill dams. *Journal of Hydroinformatics*, 22(6):1485–1505, 2020. `https://doi.org/10.2166/hydro.2020.056`.

[46] G. Savant, C. J. Trahan, L. Pettey, T. O. McAlpin, G. L. Bell, and C. J. McKnight. Urban and overland flow modeling with dynamic adaptive mesh and implicit diffusive wave equation solver. *Journal of Hydrology*, 573:13–30, 2019. `https://doi.org/10.1016/j.jhydrol.2019.03.061`.

[47] V. P. Singh, G.-T. Wang, and D. D. Adrian. Flood routing based on diffusion wave equation using mixing cell method. *Hydrological Processes*, 11(14):1881–1894, 1997. `https://doi.org/10.1002/(SICI)1099-1085(199711)11:14%3C1881::AID-HYP536%3E3.0.CO;2-K`.

[48] V. Te Chow, D. R. Maidment, and L. W. Mays. *Applied Hydrology*. McGraw Hill Education, New York, 1988.

[49] T. Tingsanchali and S. K. Manandhar. Analytical diffusion model for flood routing. *Journal of Hydraulic Engineering, ASCE*, 111(3):435–454, 1985. `https://doi.org/10.1061/(ASCE)0733-9429(1985)111:3(435)`.

[50] C. W.-S. Tsai. Applicability of kinematic, noninertia, and quasi-steady dynamic wave models to unsteady flow routing. *Journal of Hydraulic Engineering, ASCE*, 129(8):613–627, 2003. `https://doi.org/10.1061/(ASCE)0733-9429(2003)129:8(613)`.

[51] C. W.-S. Tsai. Flood routing in mild-sloped riverswave characteristics and downstream backwater effect. *Journal of Hydrology*, 308(1):151–167, 2005. https://doi.org/10.1016/j.jhydrol.2004.10.027.

[52] C. W.-S. Tsai and B. Yen. Linear analysis of shallow water wave propagation in open channels. *Journal of Engineering Mechanics, ASCE*, 127(5):459–472, 2001. https://doi.org/10.1061/(ASCE)0733-9399(2001)127:5(459).

[53] G.-T. Wang, S. Chen, J. Boll, and V. P. Singh. Nonlinear convection-diffusion equation with mixing-cell method for channel flood routing. *Journal of Hydrologic Engineering*, 8(5):259–265, 2003. https://doi.org/10.1061/(ASCE)1084-0699(2003)8:5(259).

[54] L. Wang, J. Q. Wu, W. J. Elliot, F. R. Fiedler, and S. Lapin. Linear diffusion-wave channel routing using a discrete Hayami convolution method. *Journal of Hydrology*, 509:282–294, 2014. https://doi.org/10.1016/j.jhydrol.2013.11.046.

[55] B. Yen and C. W.-S. Tsai. On noninertia wave versus diffusion wave in flood routing. *Journal of Hydrology*, 244(1-2):97–104, 2001. https://doi.org/10.1016/S0022-1694(00)00422-4.

[56] S. Zhang and J. G. Duan. 1D finite volume model of unsteady flow over mobile bed. *Journal of Hydrology*, 405(1-2):57–68, 2011. https://doi.org/10.1016/j.jhydrol.2011.05.010.

Appendices

APPENDIX A

Explaining the Laplace inverse process

The Laplace inverse for one series is derived in full and this procedure works for all other series too. The inverse calculation process for $(\overline{h}_1)_m(x,s)$ is explored in the following way:

$$
\begin{aligned}
(\overline{h}_1)_m(x,s) &= \exp(-k_1(s)(L-x)) \exp\left(-(2mL+L+x)\sqrt{k_2(s)}\right) \frac{1}{s^2+\beta s} \\
&= \frac{\exp(-(a_1 s + a_2)(L-x))}{s^2+\beta s} \\
&\quad \times \exp\left(-(2mL+L+x)\sqrt{a_3}\sqrt{\left(s+\frac{a_4}{2a_3}\right)^2 - \gamma^2}\right) \\
\implies (\overline{h}_1)_m(x,s) &= \exp\left(-a_2(L-x) - a_1(L-x)\left(s+\frac{a_4}{2a_3} - \frac{a_4}{2a_3}\right)\right)\frac{1}{s^2+\beta s} \\
&\quad \times \left\{\exp\left(-\sqrt{a_3}(2mL+L+x)\sqrt{\left(s+\frac{a_4}{2a_3}\right)^2 - \gamma^2}\right)\right. \\
&\quad \left. - \exp\left(-\sqrt{a_3}(2mL+L+x)\left(s+\frac{a_4}{2a_3}\right)\right)\right\} \\
&\quad + \left\{\exp\big(-\sqrt{a_3}(2mL+L+x)s\big)\exp\left(-(2mL+L+x)\frac{a_4}{2\sqrt{a_3}}\right)\right\} \\
&\quad \times \exp\left(-(a_2+a_1 s)(L-x)\right)\frac{1}{s^2+\beta s}. \qquad \text{(A.1)}
\end{aligned}
$$

To find the inverse, breaking Eq. (A.1) into two parts and considering two constituent functions F_1 and F_2 for convenience, we have

$$\begin{aligned}F_1(x,s) = &\exp\left(-(L-x)\left(a_2-\frac{a_1a_4}{2a_3}\right)\right)\exp\left(-a_1(L-x)\left(s+\frac{a_4}{2a_3}\right)\right)\frac{1}{s^2+\beta s}\\ &\times\left\{\exp\left(-\sqrt{a_3}(2mL+L+x)\sqrt{\left(s+\frac{a_4}{2a_3}\right)^2-\gamma^2}\right)\right.\\ &\left.-\exp\left(-\sqrt{a_3}(2mL+L+x)\left(s+\frac{a_4}{2a_3}\right)\right)\right\},\end{aligned} \tag{A.2}$$

whose Laplace inverse is

$$\begin{aligned}\mathcal{L}^{-1}\{F_1(x,s)\} = &\frac{1}{\beta}(1-\exp(-\beta t))\circledast\left(\exp\left\{-(L-x)\left(a_2-\frac{a_1a_4}{2a_3}\right)-\frac{a_4t}{2a_3}\right\}\right.\\ &\times\frac{\gamma\sqrt{a_3}(2mL+L+x)}{\sqrt{(t-a_1(L-x))^2-a_3(2mL+L+x)^2}}\\ &\times \mathrm{I}_1\left(\gamma\sqrt{(t-a_1(L-x))^2-a_3(2mL+L+x)^2}\right)\\ &\left.\times\,\mathrm{u}\big[t-(a_1(L-x)+\sqrt{a_3}(2mL+L+x))\big]\right).\end{aligned} \tag{A.3}$$

Similarly, by considering

$$\begin{aligned}F_2(x,s) = &\exp\left(-a_2(L-x)-(2mL+L+x)\frac{a_4}{2\sqrt{a_3}}\right)\\ &\times\exp\Big(-\big(a_1(L-x)+\sqrt{a_3}(2mL+L+x)\big)s\Big)\frac{1}{s^2+\beta s},\end{aligned} \tag{A.4}$$

its Laplace inverse can be obtained as

$$\begin{aligned}\mathcal{L}^{-1}\{F_2(x,s)\} = &\frac{1}{\beta}\exp\left(-a_2(L-x)-(2mL+L+x)\frac{a_4}{2\sqrt{a_3}}\right)\\ &\times\mathrm{u}\big[t-(a_1(L-x)+\sqrt{a_3}(2mL+L+x))\big]\\ &\times\Big\{1-\exp\big\{-\beta(t-(a_1(L-x)+\sqrt{a_3}(2mL+L+x)))\big\}\Big\}.\end{aligned} \tag{A.5}$$

Now, using Eqs. (A.3) and (A.5), the Laplace inverse of $(\overline{h}_1)_m(x,s)$ can be written as

$$\mathcal{L}^{-1}\{(\overline{h}_1)_m(x,s)\} = \mathcal{L}^{-1}\{F_1(x,s)\}+\mathcal{L}^{-1}\{F_2(x,s)\}. \tag{A.6}$$

The same process is followed to find the inverse of each of all other series.

APPENDIX B

Poles finding method

B.1 The flow-discharge hydrograph imposed at the upstream end and the stage-discharge relation imposed at the downstream end

We already know that, the *Laplace inversion theorem* for a function $f : [0, \infty) \to \mathbb{R}$ with Laplace transform $\overline{f}$ is given by

$$f(t) = \frac{1}{2\pi \mathrm{i}} \int_{\gamma} \exp{(st)} \overline{f}(s) \mathrm{d}s, \tag{B.1}$$

where γ is a line parallel to the imaginary axis, and all singularities of the function $\overline{f}$ lie to the left of this line. The functions $\overline{R}_{l,a}$, $\overline{S}_{l,a}$, $\overline{R}_{ld,a}$, and $\overline{S}_{ld,a}$ given in Eqs. (5.28), (5.29), (5.35), and (5.36), respectively, appear to be two-valued in the neighborhood of the point s where $Z = 0$ but these functions give the same value for $Z = \exp(\mathrm{i}\pi)$, $\exp(-\mathrm{i}\pi)$. Therefore, all of them are single-valued with no branch points. Subsequently, the only singularities here are the zeros of the denominators of these functions. The attribute of the Jordan's lemma given in *Chapter 1, Section 1.4* holds true for all of these functions. We need to find the roots of the following equations to evaluate the integral given in Eq. (B.1) for these functions:

$$\sqrt{Z} \cosh\left(\frac{\sqrt{Z}}{2}\right) + (P_e + 2as) \sinh\left(\frac{\sqrt{Z}}{2}\right) = 0, \tag{B.2}$$

$$\sqrt{Z}\left(\sqrt{Z}\cosh\left(\frac{\sqrt{Z}}{2}\right)+(P_e+2as)\sinh\left(\frac{\sqrt{Z}}{2}\right)\right)=0. \tag{B.3}$$

Equations (B.2) and (B.3) can be simplified as

$$\sqrt{Z}\cosh\left(\frac{\sqrt{Z}}{2}\right)\left\{1+\frac{(P_e+2as)}{\sqrt{Z}}\tanh\left(\frac{\sqrt{Z}}{2}\right)\right\}=0, \tag{B.4}$$

$$Z\cosh\left(\frac{\sqrt{Z}}{2}\right)\left\{1+\frac{(P_e+2as)}{\sqrt{Z}}\tanh\left(\frac{\sqrt{Z}}{2}\right)\right\}=0. \tag{B.5}$$

The roots of these equations are the roots of the expression inside the braces, because the extra $\sqrt{Z}$ factor is non-zero except for $s=-P_e/4$, which is considered under exceptional cases. These roots exist only for negative values of s and are the same as the ones given in [7]. Using $\tanh(\sqrt{-x}) = \mathrm{i}\tan(\sqrt{x})$ and replacing s by $-s$, the equation gets converted to

$$1+\frac{(P_e-2as)}{\sqrt{4P_es-P_e^2}}\tan\left(\frac{\sqrt{4P_es-P_e^2}}{2}\right)=0, \tag{B.6}$$

which can be written as

$$-\sqrt{4P_es-P_e^2}=(P_e-2as)\tan\left(\frac{\sqrt{4P_es-P_e^2}}{2}\right). \tag{B.7}$$

Now, the roots of Eq. (B.7) belong to I_k, i.e.,

$$s_k\in I_k=\left(\frac{(2k-1)^2\pi^2}{4P_e}+\frac{P_e}{4},\frac{(2k+1)^2\pi^2}{4P_e}+\frac{P_e}{4}\right)\ \text{with}\ k\in\mathbb{N}. \tag{B.8}$$

However, there are few exceptions as follows:

1. If (P_e-2as) changes sign from positive to negative in some interval I_m among I_k, then Eq. (B.7) has two roots in that interval. We split this interval into two sub-intervals:

$$I_{m_1}=\left(\frac{(2m-1)^2\pi^2}{4P_e}+\frac{P_e}{4},\frac{P_e}{2a}\right)\ ;\ I_{m_2}=\left(\frac{P_e}{2a},\frac{(2m+1)^2\pi^2}{4P_e}+\frac{P_e}{4}\right). \tag{B.9}$$

   Other intervals will contain only one root each.

2. If (P_e-2as) changes sign in $\left(0,\frac{\pi^2}{4P_e}+\frac{P_e}{4}\right)$, then the following three cases arise:

   - If (P_e-2as) changes sign for $s<P_e/4$ and $a>2+4/P_e$, then a root s_0 exists in the interval $I_0=(0,P_e/4)$, and only one root exists in each interval I_k given in Eq. (B.8).

- If $(P_e - 2as)$ changes sign for $s < P_e/4$ and $P_e - 2as + 2 = 0$, then a root $s_0 = P_e/4$ exists and there is only one root in the interval I_k for each k.
- If $(P_e - 2as)$ takes negative value for $s \in \left(\frac{P_e}{4}, \frac{\pi^2}{4P_e} + \frac{P_e}{4}\right)$ and $a < 2 + 4/P_e$, then one root s_0 exists in $\left(\frac{P_e}{4}, \frac{\pi^2}{4P_e} + \frac{P_e}{4}\right)$ and only one root exists in each interval I_k.

Using the residue theorem, the integral in Eq. (B.1) can be evaluated for $\overline{R}_{l,a}(x^*, s)$, $\overline{S}_{l,a}(x^*, s)$, $\overline{R}_{ld,a}(x^*, s)$, and $\overline{S}_{ld,a}(x^*, s)$ by obtaining the residues of these functions at the poles s_k. Since all the poles are simple ones, then the residues can be evaluated by using the formula

$$\mathrm{Res}\left(\exp(st)\overline{f}(s); s = -s_k\right) = \lim_{s \to -s_k} \exp(st)(s + s_k)\overline{f}(s) \tag{B.10}$$

to obtain $f(t)$ as

$$f(t) = \sum_{k=0}^{\infty} \mathrm{Res}\left(\exp(st)\overline{f}(s); s = -s_k\right). \tag{B.11}$$

Upon using the above, the inverses of $\overline{R}_{l,a}(x^*, s)$, $\overline{S}_{l,a}(x^*, s)$, $\overline{R}_{ld,a}(x^*, s)$, and $\overline{S}_{ld,a}(x^*, s)$ are calculated.

B.2 The flow-depth hydrograph imposed at the upstream end and the stage-discharge relation imposed at the downstream end

The functions $\overline{M}_{l,a}$, $\overline{N}_{l,a}$, $\overline{M}_{ld,a}$, and $\overline{N}_{ld,a}$ given in Eqs. (5.59), (5.60), (5.63), and (5.64), respectively, appear to be two-valued in the neighborhood of the point s where $Z = 0$ but these functions give the same value for $Z = \exp(\mathrm{i}\pi)$, $\exp(-\mathrm{i}\pi)$. So, all of them are single-valued with no branch points. Subsequently, the only singularities here are the zeros of the denominators of these functions. The attribute of the Jordan's lemma also holds true. The functions $\overline{M}_{l,a}$, $\overline{N}_{l,a}$, $\overline{M}_{ld,a}$, and $\overline{N}_{ld,a}$ have the same expression in the denominator. We need to find the roots of the following equation to evaluate the integral given in Eq. (B.1) for these functions:

$$\sqrt{Z}\left(\sqrt{Z}\cosh\left(\frac{\sqrt{Z}}{2}\right) + \epsilon \sinh\left(\frac{\sqrt{Z}}{2}\right)\right) = 0, \tag{B.12}$$

where $\epsilon = P_e(2a^{-1} - 1)$. The roots of this equation are the same as the ones provided by Cimorelli et al. [6] because the extra $\sqrt{Z}$ factor is non-zero except for $s = -P_e/4$ which is considered under exceptional cases. The roots of this equation exist for negative values of s only, and they belong to the expression inside the braces. The above expression can be rearranged as

$$(4P_e s - P_e^2)\cos\left(\frac{\sqrt{4P_e s - P_e^2}}{2}\right)\left\{1 + \frac{\epsilon}{\sqrt{4P_e s - P_e^2}}\tan\left(\frac{\sqrt{4P_e s - P_e^2}}{2}\right)\right\} = 0.$$

Here onward, we write $Z = 4P_e s - P_e^2$. Now, the roots are classified as follows:

1. $\epsilon = 0$, which corresponds to $a = 2$. Here, the roots correspond to $Z\cos\left(\frac{\sqrt{Z}}{2}\right) = 0$ which are expressed as $s_k = \frac{(2k-1)^2\pi^2}{4P_e} + \frac{P_e}{4}$.
2. When $\epsilon > 0$, we need to find the roots of
$$\tan\left(\frac{\sqrt{Z}}{2}\right) = -\frac{\sqrt{Z}}{\epsilon}, \tag{B.13}$$
and they belong to I_k, i.e.,
$$s_k \in I_k = \left(\frac{(2k-1)^2\pi^2}{4P_e} + \frac{P_e}{4}, \frac{(2k+1)^2\pi^2}{4P_e} + \frac{P_e}{4}\right) \text{ with } k \in \mathbb{N}. \tag{B.14}$$
3. There are few exceptions for $\epsilon < 0$. When $-2 < \epsilon < 0$, there is a root $s_0 \in \left(\frac{P_e}{4}, \frac{\pi^2}{4P_e} + \frac{P_e}{4}\right)$ in addition to s_k given in Eq. (B.14).
4. When $\epsilon = -2$, we get $s_0 = P_e/4$ as a root, and the roots from Eq. (B.14) are retained as they are.
5. When $\epsilon < -2$, there is a root $s_0 \in \left(0, \frac{P_e}{4}\right)$ in addition to s_k given in Eq. (B.14).

Using Eq. (B.11), the inverses of $\overline{M}_{l,a}(x^*, s)$, $\overline{N}_{l,a}(x^*, s)$, $\overline{M}_{ld,a}(x^*, s)$, and $\overline{N}_{ld,a}(x^*, s)$ are calculated.

Status of manuscripts out of the thesis

A. **Published:**

1. Shiva Kandpal and Swaroop Nandan Bora, "Analytical solution for linearized Saint-Venant equations with a uniformly distributed lateral inflow in a finite rectangular channel", *Water Resources Management*, 37(14), 5655−5676, (2023), doi: `https://doi.org/10.1007/s11269-023-03623-9`.

2. Shiva Kandpal and Swaroop Nandan Bora, "Impact of a concentrated lateral inflow and stage–discharge relation imposed at the downstream end of a finite channel for a diffusive wave model", *Acta Geophysica*, 72, 3683−3701 (2024), doi: `https://doi.org/10.1007/s11600-024-01303-9`.

3. Shiva Kandpal and Swaroop Nandan Bora, "Diffusive wave model in a finite length channel with a concentrated lateral inflow subject to different types of boundary conditions", *Physics of Fluids*, 36 (4): 045158, doi: `https://doi.org/10.1063/5.0186831`.

B. **Communicated:**

1. Shiva Kandpal and Swaroop Nandan Bora, "Non-inertia wave approximation in a finite length channel with different types of lateral inflow by using Laplace transform".

2. Shiva Kandpal and Swaroop Nandan Bora, "Non-inertia wave model approximation with stage-discharge relationship imposed at the downstream end and a space- and time-dependent lateral inflow".

3. Shiva Kandpal and Swaroop Nandan Bora, “Influence of space- and time-dependent lateral inflow for a non-inertia wave model in a finite length channel with a stage hydrograph imposed at the downstream end”.